U.PORTO

INSTITUTO DE CIÊNCIAS BIOMÉDICAS ABEL SALAZAR
UNIVERSIDADE DO PORTO

U.PORTO

FMUP FACULDADE DE MEDICINA
UNIVERSIDADE DO PORTO

THE MOLECULAR BASIS OF PROGRAMMED CELL DEATH IN *Neurospora crassa*

António Pedro da Rocha Cardoso Gonçalves

Tese de doutoramento em Patologia e Genética Molecular

2014

António Pedro da Rocha Cardoso Gonçalves

The molecular basis of programmed cell death in *Neurospora crassa*

Tese de Candidatura ao grau de Doutor em Patologia e Genética Molecular submetida ao Instituto de Ciências Biomédicas Abel Salazar da Universidade do Porto.

Orientador: Professor Doutor Arnaldo António de Moura Silvestre Videira

Categoria: Professor catedrático

Afiliação: ICBAS-Instituto de Ciências Biomédicas Abel Salazar da Universidade do Porto e IBMC-Instituto de Biologia Molecular e Celular da Universidade do Porto.

HOW DO I LOVE YOU, THESIS?
LET ME COUNT THE WAYS...

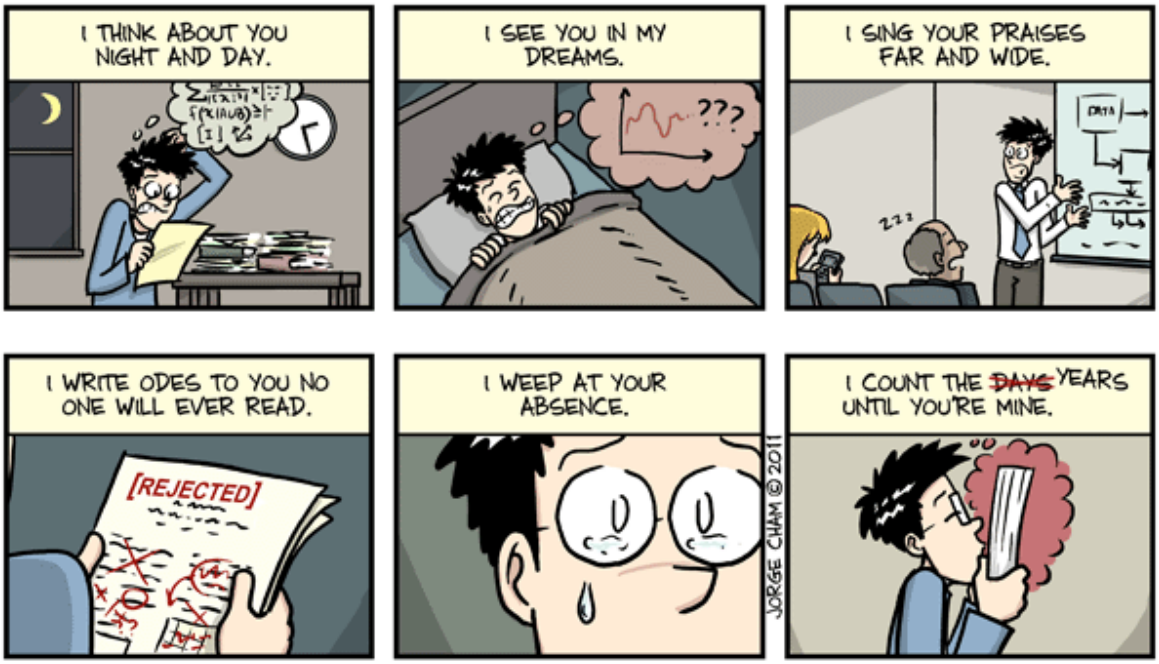

WWW.PHDCOMICS.COM

"O heróico num ser humano é não pertencer a um rebanho."
José Saramago

Dedicada ao meu Pai.

Table of contents

List of publications

* Gonçalves AP, Videira A. Programmed cell death in *Neurospora crassa*. New Journal of Science 2014; Article ID 479015.

* Fernandes AS, Gonçalves AP, Castro A, Lopes TA, Gardner R, Glass NL, Videira A. Modulation of fungal sensitivity to staurosporine by targeting proteins identified by transcriptional profiling. Fungal Genet Biol 2011;48(12):1130-8.

** Gonçalves AP, Videira A, Máximo V, Soares P. Synergistic growth inhibition of cancer cells harboring the *RET/PTC1* oncogene by staurosporine and rotenone involves enhanced cell death. J Biosci 2011;36(4):639-48.

** Gonçalves AP, Videira A, Soares P, Máximo V. Orthovanadate-induced cell death in RET/PTC1-harboring cancer cells involves the activation of caspases and altered signaling through PI3K/Akt/mTOR. Life Sci 2011;89(11-12):371-7.

** Gonçalves AP, Máximo V, Lima J, Singh KK, Soares P, Videira A. Involvement of p53 in cell death following cell cycle arrest and mitotic catastrophe induced by rotenone. Biochim Biophys Acta – Mol Cell Res 2011;1813(3):492-9.

Gonçalves AP, Hall C, Kowbel DJ, Glass NL, Videira A. CZT-1 is a novel transcription factor controlling cell death and natural drug resistance in *Neurospora crassa*. *[submitted for publication]*

Gonçalves AP, Cordeiro JM, Monteiro J, Muñoz A, Correia-de-Sá P, Read ND, Videira A. Activation of a TRP-like channel and intracellular calcium dynamics during phospholipase C-mediated cell death. *[submitted for publication]*

Gonçalves AP, Cordeiro JM, Monteiro J, Lucchi C, Kowbel DJ, Correia-de-Sá P, Glass NL, Videira A. Extracellular calcium triggers unique transcriptional programs and modulates staurosporine-induced cell death in *Neurospora crassa*. *[in preparation]*

Gonçalves AP, Cordeiro JM, Monteiro J, Lucchi C, Lobo-da-Cunha A, Correia-de-Sá P, Videira A. A link between Ca^{2+} dynamics and bioenergetics during fungal cell death. *[in preparation]*

* presented in the “Appendix” section of this thesis;
** presented as part of the second chapter of this thesis, “Mechanisms of cell death-inducing drugs in thyroid cancer cells”.

Agradecimentos

Em primeiro lugar, uma palavra de agradecimento ao meu “chefe”, Professor Arnaldo Videira. Agradeço-lhe os ensinamentos e conversas sobre ciência e não só. Agradeço-lhe também por me ter concedido a autonomia necessária para converter a minha criatividade em experiências no laboratório. Foi “Good!”.

Um agradecimento particular para os meus co-supervisores durante os meus períodos de visita a outros laboratórios: Paula Soares, Valdemar Máximo, Louise Glass e Nick Read.

Quero agradecer a todos que de alguma forma estiveram envolvidos neste trabalho. Entre eles:

IBMC/ICBAS: Alexandre, Ana, Andreia, Ângela, Bruno, Carla, Catarina, Chiara, Elsa, João, Laura, Margarida, Maria, Maria do Carmo, Mariana, Marisa, Nuno, Olímpia, Patrícia, Paulo, Ricardo, Rosa.

IPATIMUP: Adélia, Adriana, André, Dina, Helena, Hugo Prazeres, Hugo Seca, Joana Nunes, Joana Santos, Joana Silva, Joana Torres, João, Jorge, Maria Inês, Mariline, Patrícia, Paula, Raquel, Ricardo, Rute, Xana.

Berkeley: Blanca, Bob, Carlos, Charles, Christy, David, Hillary, James, Jason, Javi, Jens, Jiuhai, Joanna, Julie, Marie e Ray, Marta, Mike, Monika, Moritz, Morgann, Raquel, Richard, Sam, Timo, Trevor, Wilfried, Yi.

Edinburgh: Adokiye, Adriana, Alberto, Jean, Karen, Kathryn, Meiling, Parvathy, Patricia, Saskia, Smija.

Fundação Calouste Gulbenkian: Cristina, Teresa.

Do fundo do coração, um agradecimento aos meus pais por me terem proporcionado uma boa educação e por me terem transmitidos bons princípios, espírito de trabalho e gosto pela aprendizagem. Um beijo especial para a minha mãe, Judite.

Para a minha princesa Raquel, pela ternura, apoio, bons conselhos e amor ao longo destes anos. Espero poder retribuir.

Este trabalho é principalmente meu, mas é também um bocadinho de todos que neste texto referi. Por isso, a todos, o meu “Muito obrigado”!

Funding

The author was recipient of a PhD research fellowship from Fundação Calouste Gulbenkian (ref.: 104210), a research fellowship from COMPETE - Programa Operacional Factores de Competitividade (Pest-LA051301-BTI) and a short-term fellowship from the European Molecular Biology Organization (329-2012).

The work presented here was supported by Fundação para a Ciência e a Tecnologia of Portugal (PEst-C/SAU/LA0002/2013, FCOMP-01-0124-FEDER-037277), the European POCI program of QCAIII co-participated by FEDER (NORTE-07-0124-FEDER-000003), the University of Porto (PP_IJUP2011-20) and the National Institutes of Health (NIH R24 GM081597).

Institutions involved in the project

The research presented here was conducted at the following institutions:

Instituto de Biologia Molecular e Celular da Universidade do Porto, Portugal
Instituto de Ciências Biomédicas Abel Salazar da Universidade do Porto, Portugal
Instituto de Patologia e Imunologia Molecular da Universidade do Porto, Portugal
University of California, Berkeley, United States
University of Edinburgh, United Kingdom

FUNDAÇÃO CALOUSTE GULBENKIAN

EMBO

FCT
Fundação para a Ciência e a Tecnologia
MINISTÉRIO DA CIÊNCIA, TECNOLOGIA E ENSINO SUPERIOR

U.PORTO

Ciência.Inovação 2010

Programa Operacional Ciência e Inovação 2010
MINISTÉRIO DA CIÊNCIA, TECNOLOGIA E ENSINO SUPERIOR

COMPETE
PROGRAMA OPERACIONAL FACTORES DE COMPETITIVIDADE

QREN
QUADRO DE REFERÊNCIA ESTRATÉGICO NACIONAL

UNIÃO EUROPEIA
Fundo Europeu de Desenvolvimento Regional

NIH National Institutes of Health
Turning Discovery Into Health

IBMC
INSTITUTO DE BIOLOGIA MOLECULAR E CELULAR
INSTITUTE FOR MOLECULAR AND CELL BIOLOGY

U.PORTO

INSTITUTO DE CIÊNCIAS BIOMÉDICAS ABEL SALAZAR
UNIVERSIDADE DO PORTO

IPATIMUP

Figure index

Table index

List of abbreviations

$[Ca^{2+}]_c$	Cytosolic free calcium
2-APB	2-aminoethoxydiphenyl borate
ABC	ATP-binding cassette
AOX	Alternative oxidase
ATP	Adenosine triphosphate
BAPTA	1,2-bis(ortho-aminophenoxy)ethane-N,N,N’,N’-tetrasodium
BCL-2	B cell lymphoma 2
BN-PAGE	Blue native polyacrylamide gel electrophoresis
bp	Base pairs
BrdU	Bromodeoxyuridine
Ca^{2+}	Calcium
$CaCl_2$	Calcium chloride
CARD	Caspase recruitment domain
CCCP	Carbonyl cyanide m-chlorophenylhydrazone
cDNA	Complementary deoxyribonucleic acid
CI	Combination index
CRAC	Calcium release-activated calcium channel
DAG	1,2-diacylglycerol
DAPI	4',6-diamidino-2-phenylindole
DED	Death effector domain
$_dH_2O$	Distilled water
DHE	Dihydroethidium
DHR123	Dihydrorhodamine 123
DISC	Death-inducing signaling complex
DMSO	Dimethyl sulfoxide
DNA	Deoxyribonucleic acid
DPI	Diphenyleneiodonium
DRI	Dose reduction index
ER	Endoplasmic reticulum
FAD	Flavin adenine dinucleiotide
FADD	FAS-associated death domain protein
FDA	Fluorescein diacetate
FeS	Iron-sulfur clusters
FITC	Fluorescein isothiocyanate
FMN	Flavin mononucleotide
FPKM	Fragments per kilobase of transcript per million mapped reads
GFS	Glucose-fructose-sorbose
GSH	Reduced glutathione
GWAS	Genome-wide association study

HACS	High-affinity calcium uptake system
IP_3	Inositol-1,4,5-triphosphate
K^+	Potassium
LACS	Low-affinity calcium uptake system
$LiCl_2$	Lithium chloride
MCU	Mitochondrial calcium uniporter
mitoAeq	Mitochondrial aequorin
MM	Minimal medium
mPTP	Mitochondrial permeability transition pore
mRNA	Messenger ribonucleic acid
mtDNA	Mitochondrial deoxyribonucleic acid
NAC	N-acetyl-cysteine
PAF	Penicillium antifungal protein
PBS	Phosphate-buffered saline
PCD	Programmed cell death
PDT	Population doubling time
PI	Propidium iodide
PIP_2	Phosphatidylinositol-4,5-bisphosphate
PKC	Protein kinase C
qRT-PCR	Semi-quantitative real time polymerase chain reaction
RIP	Repeat-induced point mutation
RLU	Relative light units
RNA	Ribonucleic acid
RNA-seq	High-throughput ribonucleic acid sequencing
ROS	Reactive oxygen species
RPKM	Reads per kilobase of transcript per million mapped reads
SDS-PAGE	Sodium dodecyl sulfate polyacrylamide gel electrophoresis
SNP	Single nucleotide polymorphism
SOCE	Store-operated calcium entry
TRP	Transient receptor potential
TUNEL	Terminal deoxynucleotidyl transferase-mediated deoxyuridine triphosphate biotin nick-labelling
U-73122	1-[6-((17β-3-methoxyestra-1,3,5(10)-trien-17-yl)amino)hexyl]-1H-pyrrole-2,5-dione
VDAC	Voltage-dependent anion-selective channel
X-gal	5-bromo-4-chloro-3-indolyl-β-D-galactopyranoside
YM-58483	4-methyl-4'-[3,5-bis(trifluoromethyl)-1H-pyrazol-1-yl]-1,2,3-thiadiazole-5-carboxanilide
ΔΨm	Mitochondrial membrane potential

Outline

This thesis is divided in two main chapters. In the first chapter, “Mediators of cell death in *Neurospora crassa*”, the model organism *N. crassa* and an overview of its major genetic and biological features are initially reported. A thorough review on the current knowledge on the mechanisms of programmed cell death (PCD) with emphasis on filamentous fungi is then presented and will form the basis of a review manuscript for a future publication. The Introduction also reviews other subjects relevant for this work, namely mitochondrial bioenergetics and calcium signaling. After the Material and Methods, the Results concerning the use of *N. crassa* as a model to study fundamental aspects of cell death signaling and execution, more specifically the mechanisms of staurosporine-induced cell death, are shown. The Results and the Discussion were subdivided in sections that correspond to different areas of the work. The experiments, results and discussion described in the first chapter of this thesis covered most of the duration of the PhD work and are therefore particularly focused. The work was primarily accomplished at the Mitochondria Lab of the IBMC-Institute of Molecular and Cellular Biology and ICBAS-Institute of Biomedical Sciences Abel Salazar of the University of Porto, Portugal, under the supervision of Dr. Arnaldo Videira. Data were also obtained thanks to collaborations and work visits to the Glass Lab at the Department of Plant and Microbial Biology of the University of California, Berkeley, United States (5 months under the supervision of Dr. Louise Glass) and the Fungal Cell Biology Group of the Institute of Cell Biology of the University of Edinburgh, United Kingdom (1 month under the supervision of Dr. Nick Read).

The second chapter of this thesis, “Mechanisms of cell death-inducing drugs in thyroid cancer cells”, includes three publications that resulted from work performed with human cells. This part of the PhD project was conducted at the Cancer Biology Group of the Institute of Molecular Pathology and Immunology of the University of Porto (IPATIMUP), Portugal, under the supervision of Dr. Paula Soares and Dr. Valdemar Máximo. There, thyroid carcinoma cell lines were used to study the mechanisms of three different cell death-inducing drugs. Furthermore, these cell lines were used to mimic some of the results previously obtained in *N. crassa*, namely the synergistic cell death effect of drug combinations.

Aims

The general aim of this project was to unravel novel mechanisms of programmed cell death. We aimed to establish *N. crassa* as a model organism for the study of cell death, as the current knowledge regarding programmed cell death in fungi is somewhat scarce. In order to fill that gap, we intended to identify novel mediators of cell death in *N. crassa*. In addition to this, cancer cell lines were used to understand the effects of some cell death-inducing agents. More specific objectives of this work are presented below:

- to comprehend the influence of calcium dynamics during staurosporine-induced cell death;
- to understand the role of cellular bioenergetics components, such as the mitochondrial respiratory chain complex I and alternative NAD(P)H dehydrogenases, during cell death;
- to know how the novel *N. crassa* transcription factor CZT-1 modulates cell death;
- to characterize the transcriptional response of *N. crassa* to cell death stimuli;
- to mimic experiments and results obtained in *N. crassa*, namely the synergistic activity of combinations of cell death-inducing agents, in cancer cell lines;
- to characterize the mechanisms of cell death-inducing drugs, such as staurosporine, rotenone or sodium orthovanadate.

In summary, we aimed to provide novel insights into the molecular basis of programmed cell death and hope that the scientific findings reported here represent an useful source of information for future investigations.

Summary

Programmed cell death (PCD) represents one of the most basic aspects of cell biology and its importance for cell and tissue homeostasis is well illustrated by the fact that deregulated cell death is a common feature of several human pathologies. From an evolutionary point of view, the relevance of cell death is corroborated by the fact that the process occurs in all kingdoms, from bacteria to higher eukaryotes. Indeed, although only recognized in recent years, microbes such as fungi undergo controlled forms of cell death. This circumstance, allied to the fact that fungi are genetically tractable and easy to manipulate, prompted several research groups to use these organisms to investigate the mechanisms of PCD. In this context, we have been establishing the filamentous fungus *Neurospora crassa* as a model organism for the study of PCD, taking advantage of being part of a scientific community that enjoys a large number of genetic and biochemical research tools.

The protein kinase inhibitor staurosporine induces PCD in *N. crassa* as deduced from morphological and biochemicals alterations such as loss of viability, permeability to the early apoptosis and late apoptosis/necrosis markers YOPRO-1 and propidium iodide, respectively, increased reactive oxygen species (ROS) production, loss of mitochondrial membrane potential, DNA fragmentation, glutathione export, activation of multidrug resistance proteins and altered intracellular calcium (Ca^{2+}) signaling. Transcriptional profiling of staurosporine-induced cell death by high-throughput RNA sequencing (RNA-seq) illustrates a very dynamic response to the drug.

We were particularly interested in understanding the role of Ca^{2+} during staurosporine-induced cell death. Using cells expressing the cytosolic free Ca^{2+}-reporter aequorin, we observed that the drug promotes well defined alterations in the cytosolic levels of Ca^{2+} that we defined as the staurosporine Ca^{2+} signature. Upon exposure to staurosporine, cells move Ca^{2+} to and from internal storage organelles like the endoplasmic reticulum, vacuoles and mitochondria. Addition of the membrane-impermeant Ca^{2+} chelator BAPTA at different time points obliterates the Ca^{2+} signature, indicating that a continuous Ca^{2+} influx from the

extracellular medium also occurs upon addition of staurosporine. This Ca^{2+} influx involves specific mechanisms and is not due to cell membrane damage.

The fungal response to staurosporine is affected by the concentration of Ca^{2+} in the culture medium, highlighting the importance of extracellular Ca^{2+} uptake for staurosporine-induced cell death. Limitation of Ca^{2+} ions sensitizes cells to staurosporine and results in increased accumulation of ROS. Conversely, an approximately 30-fold excess of Ca^{2+} leads to increased drug tolerance and decreased ROS accumulation. In line with these results, RNA-seq of staurosporine-induced cell death shows distinct transcriptional programs in cells deprived or with excessive availability of Ca^{2+} and allowed the identification of two novel putative Ca^{2+}-binding proteins. Using Δ*cch-1*, Δ*fig-1*, Δ*yvc-1* mutants and a set of inhibitors, we show that extracellular Ca^{2+} entry does not occur through the hitherto described high- and low-affinity Ca^{2+} uptake systems, but through the opening of plasma membrane channels with properties resembling the transient receptor potential (TRP) family.

Inhibition of phospholipase C and downstream effectors blocks the staurosporine Ca^{2+} signature, implicating the phospholipase C signaling pathway as an orchestrator of *N. crassa* cell death. In addition, deletion of *plc-2*, one of the four phospholipase C genes in *N. crassa*, not only abolishes the development of the cytosolic Ca^{2+} response, but also renders the cells highly resistant to staurosporine. Partial blockage of the response to staurosporine after inhibition of a putative inositol-1,4,5-trisphosphate (IP_3) receptor suggests that Ca^{2+} release from internal stores following IP_3 formation combines with the extracellular Ca^{2+} influx.

We found that both the respiratory chain and the generation of ROS are required for the staurosporine-induced Ca^{2+} signature and cell death. At the molecular level, our results indicate that cells devoid of certain subunits of the mitochondrial complex I like the 51 kDa and 14 kDa proteins, termed NUO51 and NUO14, or lacking the alternative Ca^{2+}-binding NAD(P)H dehydrogenase NDE-1 are hypersensitive to staurosporine and incapable of setting up a proper Ca^{2+} response to the drug. NDE-1 seems to protect from excessive ROS accumulation induced by staurosporine. Abnormal cytosolic Ca^{2+} dynamics and increased tolerance to staurosporine are observed in cells expressing disease-related mutations in *nuo51*, the fungal homologue of the human *NDUFV1* gene. Thus, the

results further support previous indications that mitochondrial bioenergetics are an important component of the fungal response to staurosporine.

The role of a novel transcription factor, encoded by NCU09974, during staurosporine-induced cell death was characterized. This protein contains a conserved DNA-binding domain that positions it in a family of zinc cluster transcription factors, found exclusively in fungi, and was termed CZT-1 (Cell death-activated Zinc cluster Transcription factor). The lack of CZT-1 results in hypersensitivity, increased ROS accumulation and altered cytosolic Ca^{2+} dynamics in the presence of staurosporine. Transcriptional profiling by RNA-seq shows that, in contrast to wild type, staurosporine-treated Δ*czt-1* cells are unable to repress certain genes for the mitochondrial respiratory chain and to induce genes related with the endoplasmic reticulum, suggesting a role for CZT-1 in the regulation of the activity of these organelles. These studies also indicate that CZT-1 regulates the expression of multiple ATP-binding cassette (ABC) transporters, including ABC-3, which has been shown to extrude staurosporine to the extracellular medium. Additionally, the expression of *czt-1* (and consequently *abc-3*) is variable in a wild subtropical population of *N. crassa* and this is associated with altered tolerance to staurosporine. A genome-wide association study on this wild population pointed out genes likely associated with the cell death role of CZT-1, including catalase-1 (*cat-1*) and the apoptosis-inducing factor-homologous mitochondrion-associated inducer of death 2 (*amid-2*).

Because deregulation of the physiological occurrence of PCD is an hallmark of tumorigenesis, investigations on the mechanisms of the cell death-inducing agents staurosporine, sodium orthovanadate and rotenone were extended to cancer cells models. Staurosporine causes a cell cycle arrest in G_1 and cell death in a thyroid papillary carcinoma-derived cell line. Treatment with sodium orthovanadate above certain concentrations induces typical features of cell death including DNA fragmentation, loss of mitochondrial membrane potential, ROS production and caspase-3 activation. We also showed that the PI3K/Akt/mTOR signaling pathway mediates the effects of sodium orthovanadate. Rotenone triggers a G_2/M cell cycle arrest associated with mitotic catastrophe and slippage, followed by cell death and senescence. We showed that while rotenone-induced cell cycle arrest and cell death involves the activity of the transcription factor p53, these effects are largely independent of the classical role of the drug as a

mitochondrial complex I inhibitor and ROS-promoting agent, as deduced from experiments using cells devoid of mitochondrial DNA and consequently lacking a functional respiratory chain. The combinatorial use of staurosporine and rotenone in human cancer cells results in a synergistic interaction, mimicking previous observations in *N. crassa*.

Altogether, our data supports the usefulness of the filamentous fungus *N. crassa* as a model for the study of PCD mechanisms induced by exogenous compounds and establishes a basis for future research.

Sumário

A morte celular programada (PCD, do inglês *Programmed Cell Death*) representa um dos aspectos mais básicos da biologia celular. A sua importância na homeostasia de células e tecidos está bem patente na evidência de que a desregulação do processo de morte celular é uma característica comum de diversas patologias humanas. Do ponto de vista evolutivo, a relevância da morte celular é corroborada pelo facto desta ocorrer em espécies de todos os reinos, desde bactérias até eucariotas superiores. Dados recentes demonstram que a PCD ocorre em microorganismos como fungos, o que, aliado à facilidade no manuseamento laboratorial e manipulação genética destes organismos, levou vários grupos a usá-los para compreender os mecanismos de morte celular. Neste contexto, temos vindo a estabelecer *Neurospora crassa* como um modelo para o estudo de PCD, usufruindo do grande número de ferramentas genéticas e bioquímicas disponíveis para este fungo filamentoso.

O inibidor de proteínas quinase estaurosporina induz PCD em *N. crassa* com base no aparecimento de alterações morfológicas e bioquímicas tais como perda de viabilidade, permeabilidade aos marcadores de apoptose precoce e apoptose tardia/necrose YOPRO-1 e iodeto de propídeo, respectivamente, aumento da produção de espécies reactivas de oxigénio (ROS), perda do potencial de membrana mitocondrial, fragmentação de DNA, efluxo de glutationa, activação de proteínas de resistência a fármacos e alteração da sinalização intracelular por cálcio (Ca^{2+}). A análise da expressão genética global após tratamento com estaurosporina por sequenciação de RNA (RNA-seq) demonstra uma resposta genética ao fármaco bastante dinâmica.

O nosso grupo está particularmente interessado em compreender o papel do Ca^{2+} durante a morte celular induzida pela estaurosporina. Neste estudo foram usadas células com expressão do gene repórter de Ca^{2+} aequorina. Observámos que o fármaco leva a alterações bem definidas dos níveis citosólicos de Ca^{2+}, que definimos como a assinatura de Ca^{2+} induzida pela estaurosporina. Na presença de estaurosporina, as células movem Ca^{2+} de e para organelos de armazenamento, como o retículo endoplasmático, vacúolo e mitocôndria. A

adição do quelante de Ca^{2+} extracelular BAPTA em diferentes tempos oblitera a assinatura de Ca^{2+}, indicando assim a ocorrência dum influxo contínuo de Ca^{2+} do meio extracelular após tratamento com estaurosporina. Este influxo de Ca^{2+} envolve mecanismos específicos, não ocorrendo devido a danos inespecíficos na membrana celular.

A resposta de *N. crassa* à estaurosporina é afectada pela concentração de Ca^{2+} no meio de cultura, reforçando a importância da captação de Ca^{2+} extracelular durante a morte celular induzida pela estaurosporina. A limitação de iões de Ca^{2+} aumenta a sensibilidade das células ao fármaco e causa um aumento na acumulação de ROS. Por outro lado, a presença duma concentração de Ca^{2+} 30 vezes maior em relação à concentração padrão torna as células mais resistentes à estaurosporina e diminui a acumulação de ROS. Em linha com estes resultados, análises por RNA-seq da morte celular induzida pela estaurosporina em condições de défice ou excesso de Ca^{2+} no meio de cultura indicam a ocorrência de programas de transcrição distintos e permitiram a identificação de duas novas proteínas com potencial para ligarem Ca^{2+}. Fazendo uso dos mutantes Δ*cch-1*, Δ*fig-1* e Δ*yvc-1* e de um conjunto de inibidores, demonstrámos que a entrada de Ca^{2+} do meio extracelular causada pela estaurosporina é desempenhada não pelos sistemas de captação de Ca^{2+} de alta e baixa afinidade actualmente conhecidos, mas sim pela abertura de canais na membrana celular com propriedades semelhantes aos canais da família dos receptores de potencial transitório (TRP, do inglês *Transient Receptor Potential*).

A inibição da fosfolipase C e efectores a jusante leva a supressão da assinatura de Ca^{2+} induzida pela estaurosporina, implicando a cascata de sinalização da fosfolipase C como um interveniente pivô durante a morte celular em *N. crassa*. Adicionalmente, a deleção do gene *plc-2*, um dos quatro genes que codificam fosfolipases C em *N. crassa*, não só impediu o desenvolvimento de resposta de Ca^{2+} à estaurosporina, como também tornou as células hiperresistentes ao fármaco. Verificámos também que a inibição do receptor do inositol-1,4,5-trisfosfato (IP_3) leva a um bloqueio parcial da resposta à estaurosporina, sugerindo que a libertação de Ca^{2+} de reservatórios intracelulares que respondem a IP_3 acumula com a captação do ião a partir do meio extracelular.

O nosso trabalho demonstrou que tanto a cadeia respiratória da mitocôndria como a produção de ROS são imprescindíveis para o desenvolvimento da assinatura de Ca^{2+} e morte celular induzida pela estaurosporina. A nível molecular, os resultados indicam que células às quais foram removidos certas subunidades do complexo I da cadeia respiratória como as proteínas 51 kDa e 14 kDa (designadas NUO51 e NUO14) ou a desidrogenase alternativa NDE-1 são hipersensíveis à estaurosporina e incapazes de promover uma resposta intracelular apropriada em termos de sinalização por Ca^{2+}. A enzima NDE-1 parece proteger as células da acumulação excessivas de ROS induzida pela estaurosporina. Também verificámos que células com expressão de formas mutadas e relacionadas com doenças do gene *nuo51*, homólogo do gene humano *NDUFV1*, apresentam uma desregulação na resposta de Ca^{2+} à estaurosporina e um aumento na tolerância ao fármaco. Todos estes dados reforçam indicações prévias de que a bioenergética mitocondrial é um componente importante da resposta do fungo durante o processo de morte celular induzido pela estaurosporina.

O papel dum novo factor de transcrição, codificado pelo gene NCU09974, durante a morte celular induzida pela estaurosporina, foi também estudado. Esta proteína possui um domínio de ligação ao DNA conservado, que a posiciona na família dos factores de transcrição *zinc cluster* e, por isso, foi designada de CZT-1 (*Cell death-activated Zinc cluster Transcription factor*). A ausência de CZT-1 resulta em aumento de sensibilidade, maior acumulação de ROS e diferente resposta de Ca^{2+} intracelular na presença de estaurosporina. A análise de alterações transcriptómicas por RNA-seq revela que, ao contrário da estirpe selvagem, o mutante Δ*czt-1* é incapaz de reprimir a expressão de genes que codificam componentes da cadeia respiratória e de induzir genes relacionados com funções do retículo endoplasmático, o que sugere que o CZT-1 controla algumas das actividades destes organelos. Os dados obtidos por RNA-seq também indicam que o CZT-1 regula a expressão de vários transportadores da família *ATP-binding cassette* (transportadores ABC), incluindo o ABC-3, cujo papel na extrusão da estaurosporina foi previamente demonstrado pelo nosso grupo. A expressão do gene *czt-1* (e consequentemente do gene *abc-3*) é variável numa população natural subtropical de *N. crassa* e relaciona-se com alterações na resistência a estaurosporina. Um estudo de associação genómica nesta

população indicou genes possivelmente relacionados com a função do CZT-1 durante a morte celular, nomeadamente os que codificam a *catalase-1* (*cat-1*) e o *apoptosis-inducing factor-homologous mitochondrion-associated inducer of death 2* (*amid-2*).

Decidimos estender a investigação sobre os mecanismos dos compostos que induzem morte celular estaurosporina, ortovanadato de sódio e rotenona, a modelos de cancro, uma vez que a desregulação da ocorrência fisiológica da PCD é um marco da tumorigénese. A estaurosporina causa uma paragem no ciclo celular em G_1 e morte celular numa linha celular obtida dum carcinoma papilar da tiróide. O tratamento com ortovanadato de sódio acima de certas concentrações leva ao aparecimento de marcadores de morte celular como fragmentação de DNA, perda do potencial de membrana mitocondrial, produção de ROS e activação de caspase-3. Também mostrámos que os efeitos do ortovanadato de sódio são mediados pela via de sinalização PI3K/Akt/mTOR. A rotenona despoleta uma paragem no ciclo celular em G_2/M associada a catástrofe mitótica, seguida de morte celular e senescência. Os nossos dados indicam que a indução de paragem do ciclo celular e morte causadas pela rotenona envolvem o factor de transcrição p53. Usando células sem DNA mitocondrial, e consequentemente sem uma cadeia respiratória funcional, verificámos que estes efeitos são amplamente independentes da actividade clássica da rotenona como um inibidor do complexo I da mitocôndria e um agente promotor de ROS. O uso combinado de estaurosporina e rotenona em células tumorais resulta num efeito sinérgico na inibição do crescimento e indução de morte celular, o que mimetiza observações anteriores em *N. crassa*.

Em conjunto, os dados obtidos realçam a utilidade do fungo filamentoso *N. crassa* como um modelo de estudo dos mecanismos de PCD e estabelece uma base para trabalhos futuros.

CHAPTER I

MEDIATORS OF CELL DEATH IN *Neurospora crassa*

1. Introduction

1.1) The biology of *Neurospora crassa*

An historical overview

Neurospora crassa is a multicellular ascomycete initially documented in 1843 (Fig. 1), when several parisian bakeries were infested by cultures of an orange sporulating mould (1). The fungus was then designated *Monilia sitophila* and found in diverse carbohydrate-rich food and sugar cane processing waste.

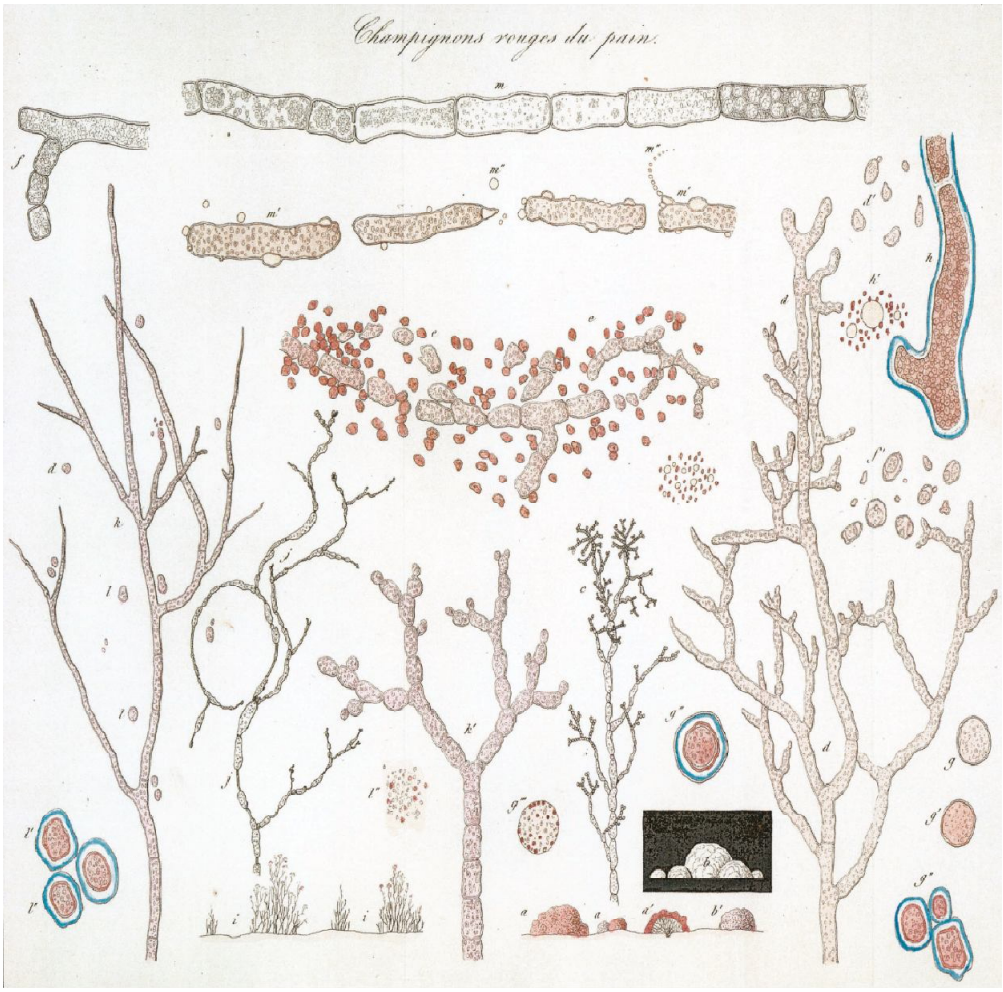

Figure 1 - Plate 1, with the title “Champignons rouges du pain”, from the first ever report of *Neurospora*.
Adapted from reference (2) with permission (American Society for Microbiology).

A century later, mycologists Cornelius Shear and Bernard Dodge, in 1927, moved it to the Neurospora genus, based on the discovery that this fungus possesses a sexual morphological structure called perithecia (3). Literally translated, “Neurospora” means “nerve” plus “spore” and the explanation for this name resides in the fact that the spores of the fungus display longitudinal striations resembling animal axons, which belong to the nervous system. In 1958, the Nobel Prize in Physiology and Medicine was awarded to George Wells Beadle and Edward Lawrie Tatum because of their “one gene-one enzyme” pioneering hypothesis. The theory, that conceived the idea that particular portions of genetic material lead to the synthesis of specific proteins, was described in 1941 (4). This work allowed the comprehension of one the most basic aspects of Biology and provoked the explosion of Molecular Genetics. In their research, Beadle and Tatum used essentially *N. crassa*. In another breakthrough work using *N. crassa* during the 1940s, Norman Horowitz showed that metabolic pathways comprise a series of steps each of them catalysed by an enzyme (5). The aforementioned works of renowned geneticists represent only a few of the examples of successful applications of Neurospora to the study of the molecular basis of biological processes. The fungus has also been used to study circadian rhythms, gene silencing, DNA repair, cell differentiation and mitochondrial biology (6).

Taxonomy

The Neurospora genus belongs to the Ascomycota phylum, Pezizomycotina subphylum, Sordariomycetes class, Sordariales order, Sordariaceae family (7). Other closely related fungi within the Sordariomycetes class include *Podospora anserina*, *Chaetomium globosum*, *Magnaporthe grisea*, *Trichoderma reesei* and *Fusarium verticillioides* (Fig. 2) (8).

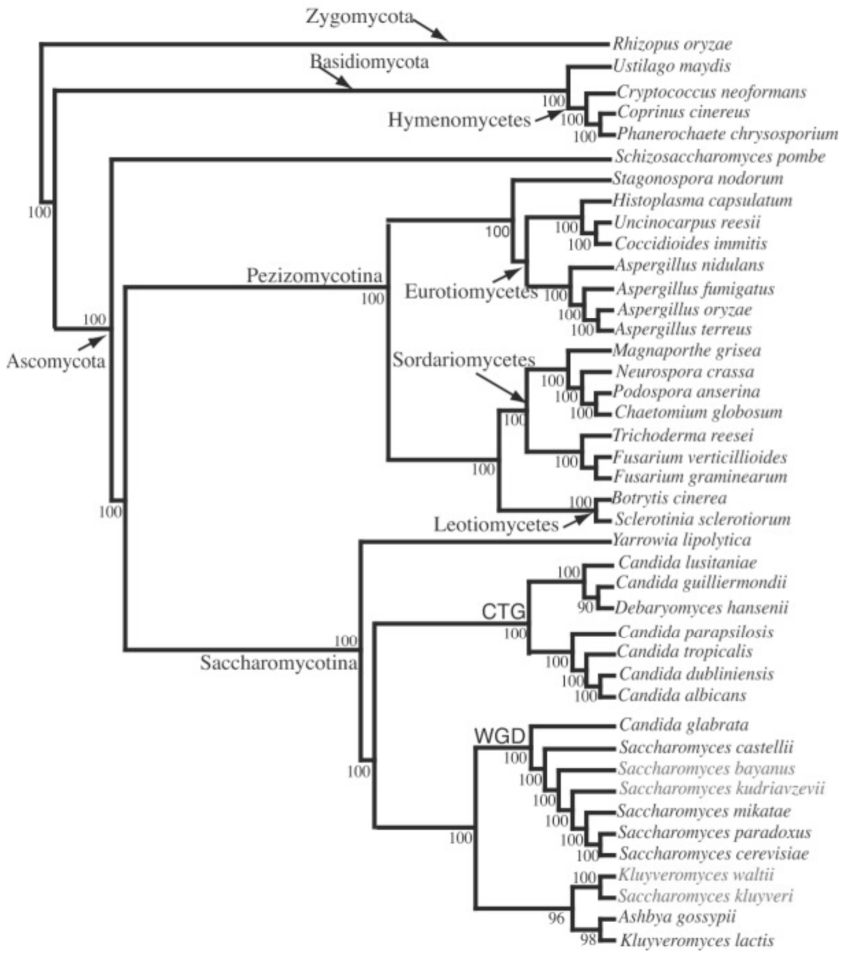

Figure 2 - MRP supertree derived from 4805 fungal gene families.
Bootstrap scores for all nodes are displayed. *Rhizopus oryzae* has been selected as an outrgroup. Subphyla and class clades are highlighted. Adapted from reference (8) with permission (BioMed Central).

Cell biology, physiology and habitat

N. crassa is a multicellular organism. Tubular, branched hyphae (Fig. 3) grow by extension in a process that seems to involve a tip-high calcium (Ca^{2+}) gradient (9-11) and incomplete septa form between cells. The septa contain pores, allowing the flow of cytoplasmic and nuclear elements. The cell wall is made mainly of β-glucans, chitin, polygalactosamine and protein (12). A classic eukaryote plasma membrane lies beneath the cell wall. The cytoplasm contains typical eukaryotic organelles. Cells (except microconidia) contain more than one nuclei and their division in a single hypha is asynchronous.

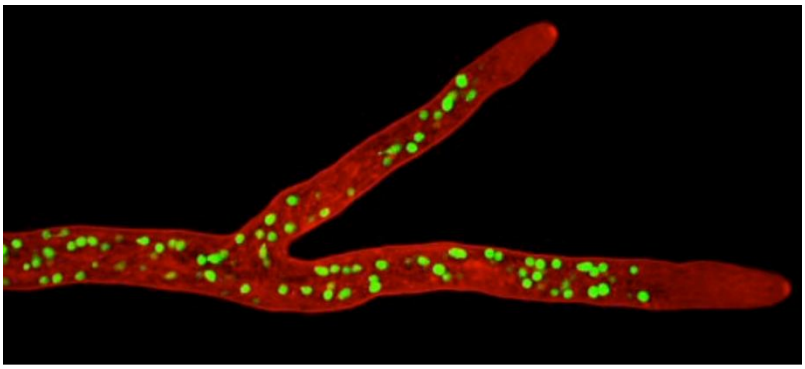

Figure 3 - Confocal imaging of *N. crassa* after co-labeling with FM4-64 (red) and the nuclei with histone H1-GFP (green).
Courtesy of Patrick C. Hickey and Nick D. Read.

Neurospora enjoys modest nutritional requirements: the common minimal medium (Vogel's minimal medium (MM)) includes a sugar, a nitrogen source (ammonium and nitrate), phosphate, sulfate, potassium, magnesium, calcium, trace metals and a small amount of the vitamin biotin (13). Nonetheless, the fungus can grow with several other nutritional regimes. *N. crassa* is an obligate aerobe and possesses typical glycolytic, hexose monophosphate shunt, Krebs cycle and oxidative phosphorylation enzymes. *N. crassa* mitochondria possess a branched respiratory chain with alternative NAD(P)H dehydrogenases (14, 15) and one alternative oxidase (16, 17).

The genus Neurospora is conspicuous in nature, as individuals are found in all moist tropical and subtropical areas, penetrating also in many temperate zones, especially in connection with human agriculture and commercial activity (18-20). These fungi are among the first colonists of burned vegetation (Fig. 4) which is probably related to the fact that ascospores, the products of the sexual cycle, require heat for activation. This aspect is also related to the well-developed capacity to use cellulosic materials, particularly in moist and hot areas. The extension of the habitat of *N. crassa* to bakeries and sugar cane processing plants is understandable on the same basis (21).

Figure 4 - *N. crassa* growing on a burned tree in Portugal.
Note the presence of the orange mould throughout the trunk. Courtesy of Arnaldo Videira.

Genetics and life cycle

N. crassa has an asexual and a sexual life cycle. The asexual life cycle is characterized by the development of macroconidia on aerial hyphae (Fig. 5). The conidia are the unicellular stage of the fungus (5-8 µm diameter) and germinate in an appropriate environment. A germ tube extends and hyphae form (8-15 µm diameter). Growth continues by tip extension, branching and cell fusion until the development of a typical mycelium. In a laboratory setting, a conidial inoculum on the centre of a culture medium-containing Petri dish leads to rapid radial extension (Fig. 6A) followed by a more copious branching and growth into the medium. *N. crassa* achieves linear growth rates of approximately 3-5 mm per hour at 25-35ºC, perhaps the fastest growth of any fungus. In liquid aerated medium, the doubling time of *N. crassa* is about 2.2 to 2.7 hours at 25ºC (21).

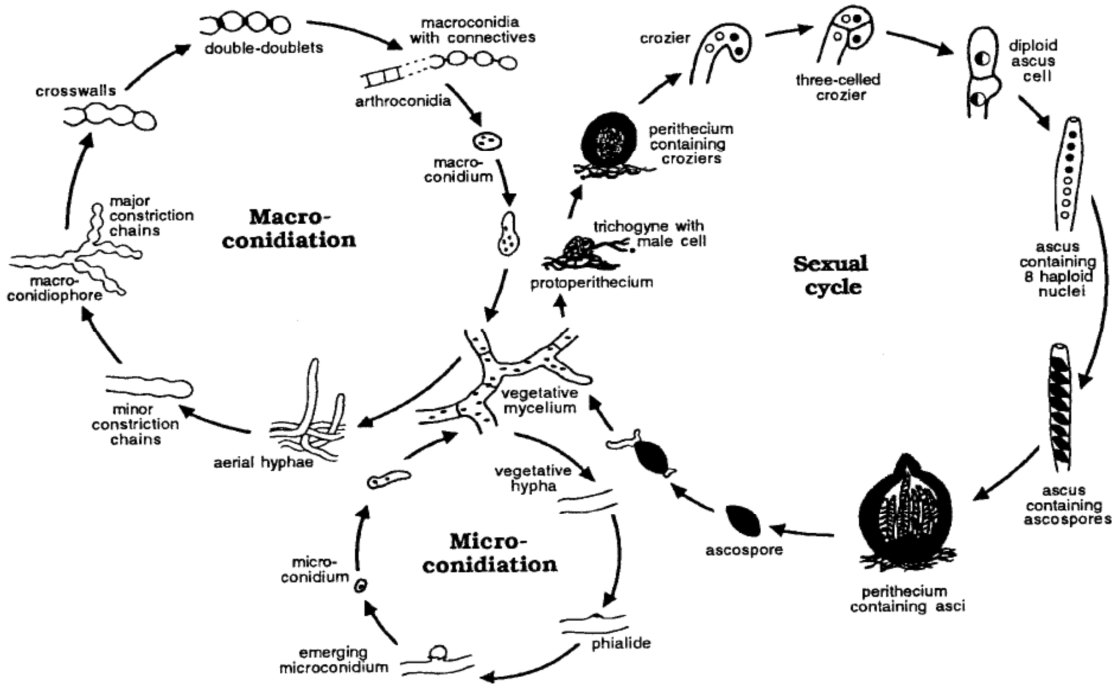

Figure 5 - *A*sexual (macroconidiation and microconidiation) and sexual life cycles of *N. crassa*.
See text for details. Adapted from reference (22) with permission (John Wiley and Sons).

Upon exhaustion of nutrients, phototropic aerial hyphae form, branch and yield a profusion of macroconidia (Fig. 6B) by budding and segmentation. The conidia develop an intense orange, carotenoid pigment and the surface possesses a loosely adhering and hydrophobic protein coat which maintains the dryness, making light air movements enough for dispersion. Though haploid, macroconidia and hyphae are coenocytic, meaning that they have multiple nuclei (Fig. 3). Homokaryotic mycelia, that is, with multiple but genetically identical nuclei is the most frequent form of *N. crassa*, because normally cells derive from a single ascospore which contains a single nucleus (19). However, genetically different haploid nuclei may coexist in the same cell or mycelia (heterokaryons) and this can be readily achieved in the laboratory by mixing strains of the same mating type. Heterothallic species also produce microconidia. These are smaller, uninucleate cells which are extruded directly and serially from microconidiophores. In the laboratory, the production of microconidia can be stimulated (23), but these cells germinate with lower efficiency than macroconidia.

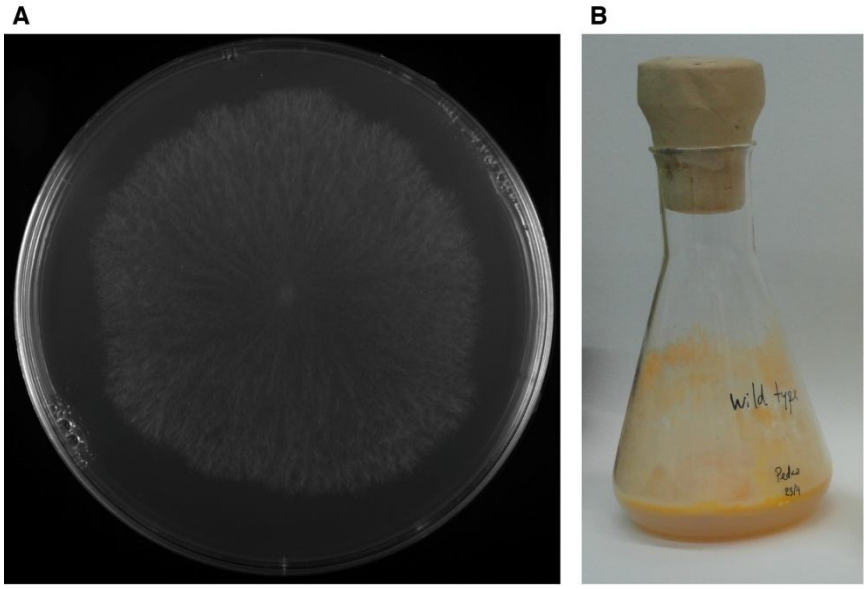

Figure 6 - *N. crassa* growing in Vogel's minimal medium with agar on a Petri dish (A) or flask (B).
Pictures were taken after 32 hours (A) and 7 days (B) of growth at 26º C, respectively.

The sexual life cycle of the heterothallic *N. crassa* is also depicted on Fig. 5. It requires two strains of opposite mating type, which is determined by the genetic regions *mat-A* and *mat-a*. Under determined conditions such as reduced nitrogen and carbon (24), the female parent strain forms a multicellular structure designated protoperithecium which begins to develop as a small knot of hyphae that surrounds a few special cells. These cells differentiate as an ascogonium and one of them acts as the female gamete. The outer hyphae of the protoperithecium form a dense and protective layer through which several filamentous trichogynes emerge from the gametic cell. The fertilizing agents are conidia from the male parent strain with the opposite mating type. They secrete a pheromone stimulus which is sensed by the trichogynes of the female parent and results in growth of the latter until both elements contact and fuse (25). Upon fusion, a nucleus of the conidium travels through the trichogyne to the ascogonial cell in the protoperithecium. The nuclei of opposite mating types divide 10 or more times in an enlarging mass of ascogenous hyphae now designated perithecium (26). Nuclei of opposite mating type pair and undergo simultaneous divisions at the tips of the ascogenous hyphae, whereas in the sub-apical cell of the crozier, pre-meiotic DNA replication takes place (27). Nuclear fusion occurs and completes the fertilization process, yielding the only diploid stage of the life cycle. Two meiotic

divisions immediately follow as the ascus grows into a long and tubular sac. Each of the four meiotic products undergoes one mitotic division and the resulting eight nuclei are enclosed by hard and melanized spore walls (Fig. 7). Individual perithecia may form 200-400 asci, all of which are usually derived from a single pair of haploid parental nuclei. If the parents have different alleles at one gene, asci will contain four of one parental type and four of the other.

Figure 7 - A squashed perithecium of *N. crassa*.
The image is reproduced from the Fungal Genetics Stock Center website (www.fgsc.net) with permission.

A beaklike structure with a pore (the ostiole) forms at the top of the perithecium and the tips of mature asci insert themselves one at a time into it. Because of the osmotic pressure within the asci, they explode at the tip, shooting the ascospores from the ostiole. A gluey material on the ascospores promotes adhesion to the landing spot. Two or three days after being shot the ascospores are fully mature and germinate upon heat activation (60ºC for 30 minutes in the laboratory).

The genome and collection of knockout strains

N. crassa was the first filamentous fungus to have its genome fully sequenced (28). The publication of the genome acted as an extremely important boost for studies involving this organism. Many genes implicated in diverse biological processes such as metabolism, signaling, cell cycle, cell death,

epigenetics, gene silencing and growth have been unravelled since then. The main features of the genome are depicted in Table 1 (2).

Table 1 - The main features of the *N. crassa* genome.

Feature	Value
General	
Size (bp)	38044345
Number of chromosomes / Linkage groups	7
% G+C	50
Protein-coding genes	10082
Protein-coding genes (> 100 amino acids)	9200
Introns	17118
tRNA genes	424
5S rRNA	74
Percent coding	44
Average gene size (bp)	1673 (481 aa)
Average intron size (bp)	135.4
Average intergenic distance (bp)	1953
Predicted protein-coding sequences	
Identified by similarity to known sequences	1336 (13%)
Conserved hypothetical proteins	4606 (46%)
Predicted proteins (no similarity to known sequences)	4140 (41%)

aa: amino acids

With around 10000 protein-coding genes, *N. crassa* possesses nearly twice as many genes as *Saccharomyces cerevisiae* (~6300) and *Schizosaccharomyces pombe* (~4800), consistently with its higher biological complexity. More than a half of the *N. crassa* proteins do not have significant matches in either *S. cerevisiae* and *S. pombe*, two classical yeast models (28). Importantly, a considerable fraction of *N. crassa* genes (~15%) display best homology matches to either plants or animals, which is consistent with the complex biology of filamentous fungi.

Another interesting characteristic of the *N. crassa* genome is the unusually low proportion of highly similar genes in opposition to other sequenced organisms (28). Thus, the degree of gene redundancy is reduced and this is particularly useful when analysing the behavior of knockout cells. Limited redundancy results from the presence of a very sophisticated mechanism of defence called repeat-induced point-mutation (RIP) through which cells detect and mutate both copies of a sequence duplication. Not only the high number of mutations likely lead to lack

of expression of the sequence but also RIPped sequences are targets of silencing by DNA methylation (28). This indicates that most, if not all, paralogous genes in *N. crassa* duplicated and diverged before the emergence of RIP and that gene duplication has been arrested since then (28). RIP has been used for several years in the laboratory as a strategy to disrupt genes. However, in recent years a gene replacement and homologous recombination-based approach has been used to generate deletion strains (29). Using this strategy, the *Neurospora Genome Project*, currently underway, has enabled the construction of thousands of deletion strains that are available for the Neurospora community (30, 31).

1.2) Programmed cell death (PCD)

PCD in mammalian cells

Balance between cell division and cell death is of supreme importance for the development and maintenance of multicellular organisms. Deregulation of this equilibrium can lead to pathological conditions, namely cancer and neurodegenerative disorders. Therefore, the balance between life and death is tightly controlled and abnormal elements can be effectively eliminated by a process called ”PCD” (32). Decades ago, PCD was held synonymous with apoptosis, and the concepts of apoptosis and necrosis were the only used to explain the death of cells. However, in recent years, it has become evident that this is an oversimplification of the highly sophisticated mechanisms guarding the organism against potentially harmful situations. Many reports have been published and many terms have been proposed to define dissimilar pathways of cell death. However, some of these distinct ways of dying might not be really different, because there are many overlapping features and the precise biochemical mechanisms are often unclear. To overcome these issues, the Nomenclature Committee on Cell Death has recently proposed unified criteria for the definition of cell death and its different morphologies and molecular signals (33). According to these guidelines, cell death can be classified in anoikis, autophagic cell death, caspase-dependent apoptosis, caspase-independent apoptosis, cornification, entosis, extrinsic apoptosis by death receptors, extrinsic apoptosis by dependence

receptors, mitotic catastrophe, necroptosis, netosis, parthanatos and pyroptosis (33).

Since PCD has been mostly studied in mammalian models, a summary of the most important facts and mechanisms related to this subject are present in the next paragraphs. For simplification purposes, this overview of the different cell death modalities will focus on three concepts: apoptosis, necrosis and autophagy. Classically, necrosis was considered an accidental and uncontrolled type of cell death. However, recent data has shown clearly that specific pathways and mediators like RIP1 and RIP3 are activated during necrotic cell death and that it has a physiological role rather than being accidental (34). Autophagy is employed by cells in order to degrade or recycle cellular components such as proteins and organelles. Autophagy leads to the breakdown of the cytoplasm within double-membrane specialized vesicles called autophagosomes which eventually fuse with the lysosome (35). It is still somewhat controversial whether autophagy is a cell death or survival mechanism. A plausible view is that, due to its recycling nature, autophagy can be initially a protective mechanism operated by the cells to cope with demanding conditions or lifestyle adaptation. However, this can derive to an autophagic death mode if the stress pressure is unbearable. The core molecular machinery of autophagy, initially identified in *S. cerevisiae*, consists in a group of proteins involved in the formation of the autophagosome, termed “ATG” (36). At the signaling level, autophagy is controlled by the target of rapamycin (TOR) kinase (35, 36).

The term “apoptosis” (*apo*-from, *ptosis*-falling, meaning “dropping off” of petals or leaves from plants or trees) was coined in 1972 by Kerr and colleagues to designate a well-ordered suicide genre of cell death (Fig. 8) (37). Apoptosis is morphologically characterized by cell rounding and reduction of volume, chromatin condensation, nuclear fragmentation and persistence of an intact plasma membrane until the late stages of the process (38).

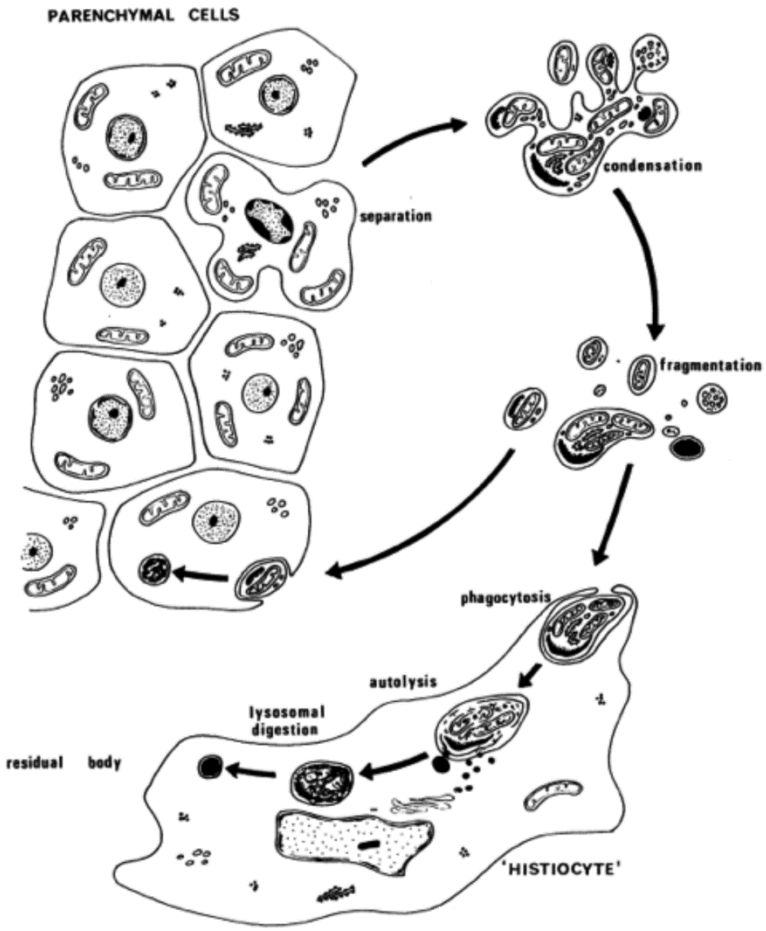

Figure 8 - Morphological aspects of apoptosis.
Adapted from the original publication that coined the term “apoptosis” (37) with permission (Nature Publishing Group).

Molecularly, apoptosis presents different forms. Depending on the apoptotic stimulus, a group of aspartate-specific proteases called caspases may be activated (caspase-dependent apoptosis). Caspases are the ultimate executioners of cell death and cleave regulatory and structural elements of the cell such as cytoskeletal proteins like actin or nuclear proteins such as the poly ADP-ribose polymerase-1 (PARP-1) and the transcription factor p53 (39). Apoptosis can also develop without the involvement of caspases (caspase-independent apoptosis). Although maybe in a too simplistic way, apoptosis can be divided in two pathways: the extrinsic and the intrinsic pathways. The extrinsic pathway is triggered by the binding of extracellular ligands to cell surface receptors, such as FAS/CD95L, tumor necrosis factor α (TNFα) and TNF ligand superfamily, member 10 (TNF-related apoptosis inducing ligand, TRAIL) bind to their death receptors (FAS/CD95, TNFα receptor 1 (TNFR1) and TRAIL receptor (TRAILR)1-2,

respectively) (33). Ligation to these receptors induces the formation of a multiprotein death-inducing signaling complex (DISC) that recruits adaptor proteins like the FAS-associated death domain protein (FADD) and activates the initiator caspase-8 which begins the cell death process (38, 39). The intrinsic pathway (or the mitochondrial pathway) of apoptosis is activated when intracellular sensors indicate over-the-threshold cell damage or when a developmental program is underway. The key event of the intrinsic pathway of apoptosis is the permeabilization of the mitochondrial outer membrane and consequent release of apoptogenic molecules from the mitochondrial intermembrane space to the cytosol (39). These include second mitochondria-derived activator of caspase (SMAC/DIABLO), OMI/HtrA2, the apoptosis-inducing factor (AIF), endonuclease G (EndoG) and cytochrome *c*. SMAC/DIABLO and OMI/HtrA2 bind the X-linked inhibitor of apoptosis protein (XIAP) and antagonize its ability to inhibit caspases. AIF and EndoG are two DNA nucleases that migrate to the nucleus *en route* to cell death. In the cytosol, cytochrome *c* binds and induces a conformational change and oligomerization of the apoptotic protease-activating factor 1 (APAF1). This results in the formation of the apoptosome, which also includes the initiator caspase-9, which in turn cleaves and activates the executioners caspase-3 and caspase-7. Actually, both the extrinsic and intrinsic pathways converge in the activation of caspase-3 and caspase-7. The permeabilization of the mitochondrial outer membrane, the critical parameter during mitochondrial-mediated apoptosis is finely controlled through interactions between members of the B cell lymphoma 2 (BCL-2) family, characterized by the presence of a BCL-2 homology (BH) domain which, depending on the specific protein, is differently organized (40). This group of proteins comprises both anti-apoptotic (BCL-2, BCL-W, BCL-XL, A1 and MCL-1) as well as pro-apoptotic members. The pro-apoptotic proteins are subdivided in effectors (BAK, BAX and BOK) and BH3-only proteins that transmit the apoptotic signal to the effectors (BID, BIM, BAD, BIK, BMF, BNIP3, HRK, NOXA and PUMA).

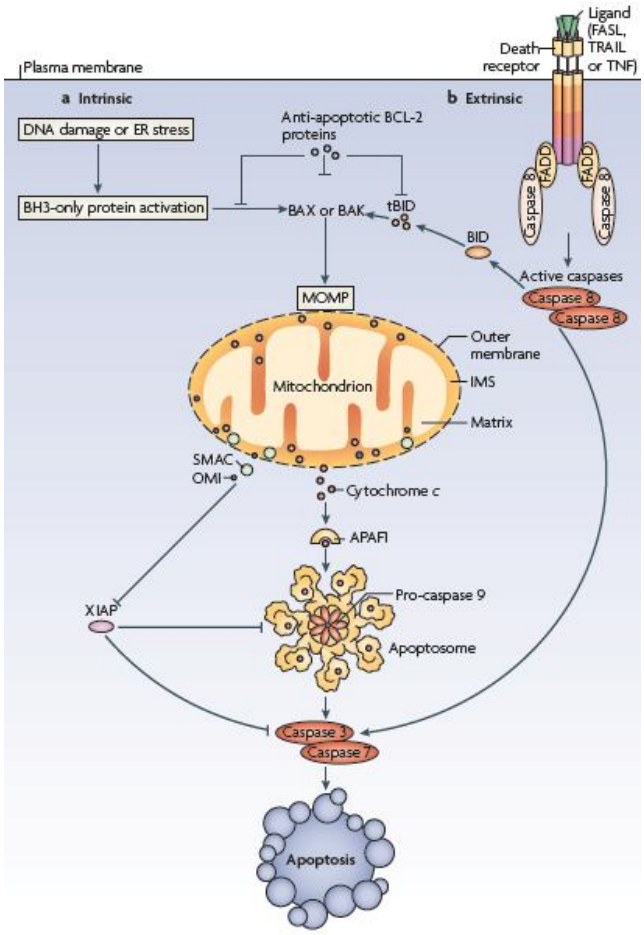

Figure 9 - Intrinsic and extrinsic pathways of apoptosis.
See text for details. Adapted from reference (39) with permission (Nature Publishing Group).

Despite the advances made in the comprehension of the cell death subject, several mechanisms are still a matter of debate and new approaches might unravel new pathways and mediators.

PCD in fungi

It has become increasingly clear that simpler organisms, including prokaryotes, plants and fungi, also undergo regulated forms of cell death. In the fungal kingdom, PCD was initially pinpointed in the second half of the 1990s in *S. cerevisiae*. In a work with the endoplasmic reticulum (ER)-localized ATPase Cdc48, an AAA family member required for retrotranslocation of ubiquitinated proteins to the cytosol, Madeo *et al* observed that the expression of the *cdc48*^{S565G} temperature-sensitive mutant under non-permissive temperatures results in the appearance of hallmarks of apoptosis (see below) (41). *S. cerevisiae* also serves as a “clean” model for the study of mammalian molecules involved in cell death,

since the heterologous expression of human proteins like BCL-2 family members promotes and suppresses apoptosis in yeast (42-45). These data acted as a breakthrough in PCD research because they challenged other scientists to conduct studies in phylogenetically lower organisms that are normally more genetically tractable and easier to manipulate.

There is still some controversy regarding the degree of similarity between fungal and metazoan cell death and whether the metazoan terminology can be applied to fungi. Thus, a cautious choice is to employ the designation “apoptotic-like cell death”, although these concepts will not be substantially discriminated in this dissertation, for simplification purposes. Similarly to mammals, fungal cells undergoing apoptotic-like cell death generally exhibit morphological and biochemical features that can be detected in the laboratory. This includes DNA fragmentation and condensation, cell shrinkage, phosphatidylserine exposure, reactive oxygen species (ROS) production, mitochondrial membrane depolarization, reduced glutathione (GSH) efflux and caspase-like activities (46-49). However, due to the biological characteristics of fungi, some technical aspects of the detection of PCD in fungi must be considered.

An early biochemical alteration of cells undergoing cell death is the externalization of phosphatidylserine, a phospholipid that is normally in the internal leaflet, to the external leaflet of the cell membrane. In the original mammalian-optimized methodology, phosphatidylserine, when at the external leaflet of the cell membrane, can be readily detected using recombinant annexin V conjugated with a fluorochrome. However, fungal cells possess a cell wall, hampering the direct staining with annexin V. This represents a good example of the current limitations of standard techniques to detect apoptotic-like cell death in fungi. In such situations, cell wall-degrading enzymes must be applied although this is a harsh procedure and signifies an additional stress that should be ideally avoided. Cell wall removal must also be performed when DNA fragmentation is to be analysed with the terminal deoxynucleotidyl transferase-mediated deoxyuridine triphosphate biotin nick-labelling (TUNEL) method. There are, however, some alternative available fluorescent probes that may be employed to detect cell death without the need of removing the cell wall. Our laboratory has been using YO-PRO1 to detect cell death in *N. crassa*. YO-PRO1 is a small cyanine cation dye that is only permeable in cells undergoing apoptosis (50). Another drawback resides in the

fact that filamentous fungi are unicellular during a limited time-window of their life cycle and highly quantitative methodologies like flow cytometry can only be applied during the unicellular stage. As an alternative for the multicellular stages of the life cycle, microscopy can be performed. Apoptotic markers like the production of ROS, mitochondrial membrane depolarization or caspase-like activities may be detected using comercially available fluorescent probes that are able to penetrate fungal cells or can be used in isolated organelles.

Why would fungal cells execute PCD?

In animals, it is well established that PCD is associated with developmental processes like the deletion of certain macrostructures, modeling of organs, regulation of cell number or removal of defective and potentially harmful cells (32). In fungi, early evidences of the occurrence of PCD were challenged by the scientific community partly because the molecular identity of the intervenients was completely unknown. Though, the growing availability of sequenced fungal genomes has pushed this forward. Another topic of discussion that accompanied the initial reports of cell death in fungi was the uncertain relevance of such a process in microbial cells. Namely, why would unicellular organisms like yeast be programmed to die? This is particularly pertinent in yeast, where cell death means organismal death (or “phenoptosis”, as coined by Skulachev (51)). These interesting but rather hard questions have been addressed by some works.

Possible explanations can be obtained from an evolutionary perspective. It is known that yeasts, despite being unicellular, prefer to live as colonies (52) and these social communities undergo a differentiation-like program involving the apoptotic death of the centre of the colony only (53). There is evidence showing that if the dead zone (colony centre) is removed, there is a reduction in the growth in the periphery, suggesting an altruistic nature of cell death and an advantageous outcome, that is, the maintenance of the whole colony at the expense of death of a part of it (53). Thus, natural yeast cell death may be related to a kin selection evolutionary mechanism - an aging programme in which within a population some unwanted organisms die to benefit related ones regulating life span (54, 55).

It has been hypothesized that cell density is the threshold factor that determines that certain parameters such as DNA mutations and the nutritional

environment are at a critical value and lead to cell death of part of the population (54, 56). Importantly, both types of aging (chronological and replicative) result in the appearance of apoptotic markers (57-59). In chronological aging yeast, after more than 90% of a population dies, a small subpopulation of cells that survive are able to regrow (60). This might be because of the release of substances from dying cells that alter the composition of the growth medium and promote the growth of the small subpopulation of surviving individuals (54). Indeed, an ammonia concentration gradient in aged colonies guarantees that cells at the centre die while the ones at the periphery proliferate (61). Treatment with high concentrations of α-factor pheromone, which is normally secreted to activate mating, results in apoptotic-like cell death signaled by the Ste20 kinase, suggesting that yeast cell death may be triggered in response to unsuccessful mating (62). Thus, quorum sensing may play a role in natural death of unicellular organisms.

A recent report showed the coordinated involvement of the apoptotic and autophagic cell death on yeast gametogenesis, more specifically during a spore number control mechanism when cells develop aborted meiotic products (63). Interestingly, this process, termed “programmed nuclear destruction”, was broadly observed in wild yeast isolates and apparently to the benefit of sibling cells, indicating its physiological relevance. Another report linked the apoptotic machinery of the *Cryptococcus neoformans* yeast with the development of drug resistance phenotypes. More specifically, the authors showed that Aif1-mediated cell death is required to eliminate aneuploid cells and in the absence of the protein, the accumulation of such cells leads to resistance to the antifungal fluconazole (64).

Programmmed cell death might be a key evolutionary event during unicellular to multicellular transition. When yeast cells face an environmental set-up that promotes multicellularity (through a sedimentation strategy), there is a development of clustering snowflake-type genotypes which spread through multicellular propagules (65). This adaptive yeast subpopulations exhibit high rates of cell death, decreasing the size of propagules but also increasing their production (65).

Involvement of PCD during developmental, differentiation and host interaction processes in filamentous fungi

The multicellular nature and higher complexity of filamentous fungi makes the perception of fungal PCD even more conceivable (46-48). PCD in filamentous fungi is well documented, though available literature is not as extensive as for *S. cerevisiae*. Table 2 summarizes work demonstrating the involvement of PCD during developmental or differentiation processes in filamentous fungi.

Table 2 - PCD in filamentous fungi during differentiation or developmental processes.

Stimulus	Organism	Molecules	ROS	MC	Reference(s)
Heterokaryon incompatibility	*Neurospora crassa*, *Podospora anserina*, Aspergillus niger	HET-C1/2, PIN-C1/2, TOL, MAT-A/a, HET-6, UN-24, VIB-1, IME-2	yes	no	(66-80)
Senescent cultures	*Podospora anserina*, *Botrytis cinerea*	Mitochondrial complex IV (cytochrome *c* oxidase)	yes	yes	(81-85)
Appressorium morphogenesis	*Magnaporthe grisea*	Several autophagy-related genes	NA	NA	(86-89)
Protoperithecia formation	*Podospora anserina*	PaATG1, PaATG8	NA	NA	(90)
Asci maturation and ascospore formation	*Coniochaete tetrasperma*, *Podospora anserina*	-	NA	NA	(91, 92)
Meiotic defects	*Coprinopsis cinereus*	-	NA	NA	(93)
Basidial differentiation	*Agaricus bisporus*	-	NA	NA	(94)
Conidiation	*Aspergillus nidulans*	PrpA	NA	yes	(95)

Columns “ROS” and “MC” denote, for the effect of each stimulus, the involvement of ROS or metacaspases, respectively. NA: not assessed.

P. anserina has been used since the 1950s as a model for studying aging (96), which is phenotypically associated with a senescence-type form of cell death characterized by a reorganization of the mitochondrial DNA and a decrease in mycelium growth rate, reflected in the formation of aerial hyphae as well as increase in pigmentation and death of peripheral hyphae (83). This process seems to be related to the activity of cytochrome *c* oxidase (complex IV) of the mitochondrial respiratory chain (81, 82, 84).

PCD has been also implicated in reproduction-related functions. In *Aspergillus nidulans*, sporulation was associated with apoptotic-like death including caspase activity and degradation of a PARP-like protein (95). In *P.*

anserina, disruption of the two metacaspases (putative homologues of caspases) leads to defects in ascospore formation (91). In *Coniochaete tetrasperma*, during the asci maturation process, the initial number of 8 is reduced to 4 ascospores per ascus by means of cell death (92). In *Coprinopsis cinereus*, cytological indicators of cell death were observed in immature basidiospores of meiotic mutants whose nuclei were arrested after meiotic metaphase I (93). Cell death was also evidenced prior to the basidial differentiation in *Agaricus bisporus* (94).

In the rice blast pathogen *M. grisea* autophagic cell death is involved in several steps of differentiation and plant infection. The deletion of the autophagy-mediator genes *MgATG1* and *MgATG8* affects the fungus ability to survive, conidiate, germinate, form mature perithecia and cause infection (87). Magnaporthe develop a specialized type of cells called appressorium which is required to penetrate the outer cuticle of leaves and stems of rice plants (89). Its morphogenesis requires the completion of mitosis, nuclear migration, and death of the conidium originating the infection (88). Interestingly, this spore death is mediated by autophagy since disruption of *MgATG8* prevented the cell death step. Although appressoria were formed, they lacked pathogenicity due to an inability to penetrate the plant tissues. This defect was further confirmed by a genome-wide functional analysis that revealed that disruption of 16 genes necessary for non-selective macroautophagy in Magnaporthe causes lack of virulence due to impairment of both conidial PCD and appressorium maturation (86). In *P. anserina*, mutation or deletion of *PaATG1* and *PaATG8* also leads to defects in the formation of sexual structures such as protoperithecia (90).

Another specialized phenomenon called “heterokaryon incompatibility”, involving nonself recognition and PCD, occurs in fungi. Nonself recognition is an essential process to distinguish oneself from another. It is ubiquitous and relies on the major histocompatibility complex in humans (97). The analogous nonself recognition system of filamentous fungi (heterokaryon incompatibility) is important during vegetative growth. Hyphal fusion can occur between cells of the same fungal colony but also between hyphae of different strains. The latter results in the formation of an heterokaryon in which cells possess nuclei with different genetic backgrounds (67, 69). If individuals originating the heterokaryon are genetically dissimilar at the *het* loci, a cell death program on the fusion compartment and surrounding cells is triggered and leads to the rejection of heterokaryon formation

(Fig. 10) (67, 69). This equips cells with a competent barrier to undesired heterokaryon formation and has been shown to restrict viral transfer between fungal individuals and to prevent resource appropriation (98-101).

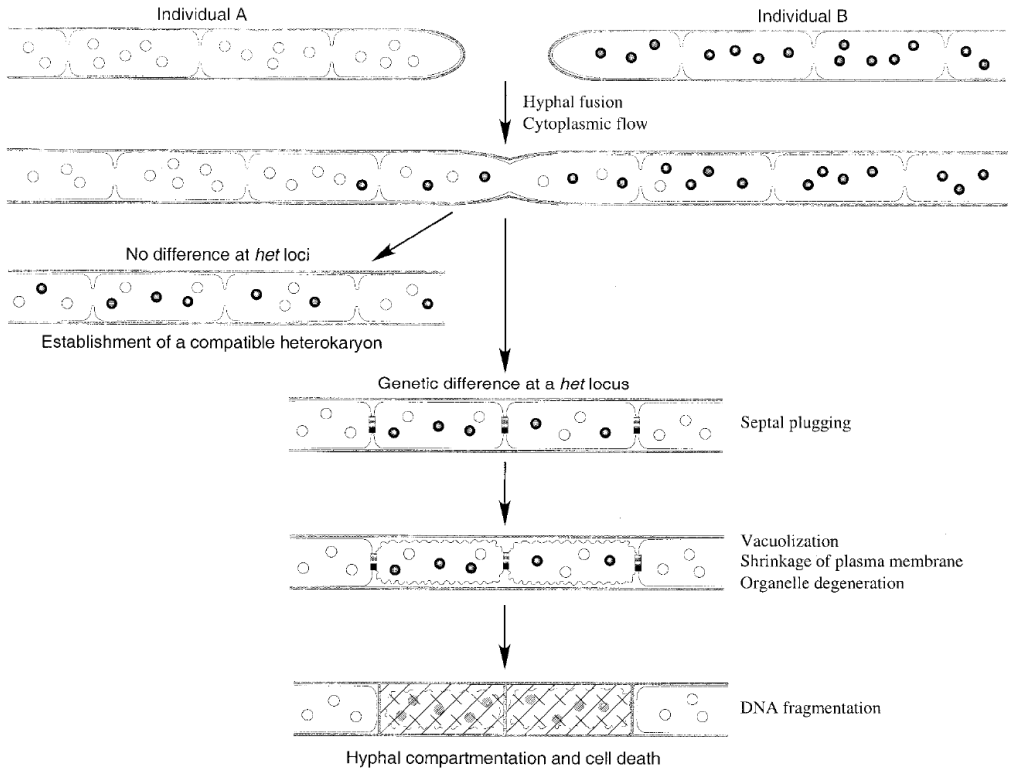

Figure 10 - Schematic diagram of the main biological and morphological consequences of hyphal fusion between two fungal individuals.
If the two fungal individuals are identical in allelic specificity at all *het* loci, an heterokaryon is formed. However, if the two fungal individuals differ in allelic specificity at a *het* locus, the septa in the hyphal fusion cell are occluded and the hyphal fusion cell (and often surrounding cells) undergo cell death. Adapted from reference (69) with permission (American Society for Microbiology).

In *N. crassa*, 11 *het* loci mediate nonself recognition and because they are effectively unlinked, the number of possible *het* genotypes in a segregation population is at least 2^{11} (67, 69, 78). The *het-c* incompatibility, probably the best studied, is mediated by *het-c pin-c* interactions (69, 73). Alternative haplotypes of plasma membrane-localized HET-C (HET-C1, HET-C2) interact with the alternative haplotypes of the cytoplasmic PIN-C (PIN-C1, PIN-C2) (73, 78). This results in intracellular signaling and activation of the transcription factor VIB-1 (80), which is downstream of a negative regulation by the IME-2 kinase (71) and is required for the expression of nonself recognition-related genes that encode proteins with HET domains, namely *pin-c*, *tol*, and *het-6* (66). Other *het* genetic

determinants include *het-6* (incompatibility mediated by interactions between the proteins encoded by *un-24* and *het-6* (74, 75)) and mating type loci (*mat-A*, *mat-a* and *tol* (68, 76, 77, 79)).

Incompatible heterokaryons show a macroscopic phenotype of slow growth and diminished conidiation, together with hyphal compartmentalization and cell death (67, 70, 72). This includes the appearance of apoptotic hallmarks such as DNA condensation and fragmentation, plasma membrane shrinkage, vesicle formation and internalization of vital dyes (67, 70, 102). The production of ROS and the induction of genes involved in phosphatidylinositol and Ca^{2+} signaling pathways are also implicated in the phenomenon (70). Heterokaryon incompatibility in *N. crassa* was also shown to be induced by the ectopic expression of the bacterial HET-C homologue from *Pseudomonas syringae*, phcA (103).

In *P. anserina*, autophagy was associated with the process of heterokaryon incompatibility (90, 104). Intriguingly, treatment with rapamycin, an inhibitor of TOR kinase, mimics the typical alterations of heterokaryon incompatibility, namely the induction of *idi* genes, cytological alterations such as increased septation, vacuolization, coalescence of lipid droplets and induction of autophagy and cell death (105). The overexpression of the isolated HET domain is sufficient to induce cell death in Podospora (106).

Cell death has been also linked with cellular responses during host-pathogen interactions involving plant pathogenic fungi, which are all of the filamentous type. Available data demonstrates that host plant cells are able to induce fungal PCD as a defensive reaction to infection. Arabidopsis cells produce a phytoalexin called camalexin that induces cell death in the necrotrophic fungus *Botrytis cinerea* (85). Upon infection, germination and first contact with the plant, the fungus experiences extensive cell death (30-48 hours post-inoculation) though recovering at later stages (after 72 hours) when lesions in the plant start to appear. However, Shlezinger and collaborators demonstrated that overexpression of the anti-apoptotic gene *BcBIR1* confers enhanced pathogenicity and resistance to cell death, as shown by the drastic reduction in cell death levels of the *BcBIR1*-overexpressing strain after 30-48 hours of inoculation (85). Conversely, a Δ*BcBIR1* knockout strain exhibited the opposite phenotypes, i.e., hypersensitivity to cell death and reduced virulence. The N'-terminal portion of BcBir1 was shown

to mediate its anti-apoptotic activity. Other plant defence compounds like hexanoic acid and lovastatin also induce cell death in *B. cinerea* and *Mucor racemosus* (85, 107, 108). In line with these results, tomato cells produce the saponin α-tomatine, a sesquiterpene glycoside with fungicidal activity that induces ROS- and metacaspase-dependent cell death in *Fusarium oxysporum* (109). In addition, during host-pathogen interactions, fungal cells may manipulate the mechanisms of plant PCD for their benefit. For example, *Alternaria alternata* produces a mycotoxin called AAL, with structural similarities to sphinganine, that induces cell death in tomato cells by interfering with the sphingolipid biosynthesis pathway of the host (110). This leads to the accumulation of dihydrosphingosine that mediates AAL-induced cell death.

It is worth to mention that some of the aforementioned examples of cell death in fungi are exclusive of filamentous species (*e.g.*, heterokaryon incompatibility) underlining the advantage of using filamentous fungi as a model to study cell death.

PCD in filamentous fungi after exposure to stress stimuli

Fungi undergo cell death in response to environmental stress. Indeed, most of the available studies on PCD in fungi involve the exposure of cells to death-inducing agents or growth in culture media lacking certain components important for cell survival. Table 3 is a comprehensive condensed review of available reports on this matter, with a focus on filamentous fungi. It contains a brief description of the involvement of Ca^{2+}, ROS and activity of metacaspases during cell death induction by each of the listed stimuli as these parameters seem to be common mediators of fungal cell death. The broad diversity of fungal cell death-inducing stimuli suggests that, during evolution, fungi kept an appropriate set of molecules to adequately respond to environmental stress with cell death. For extensive and specific details associated with each stimulus, the reader is referred to the original publications. Information on the mechanisms of selected cell death-inducing compounds is subsequently described in more detail.

Table 3 - PCD in filamentous fungi exposed to cell death-inducing stimuli.

Stimulus	Organism	Molecules	Ca^{2+}	ROS	MC	Reference(s)
Sphingolipids						
Dihydrosphingosine	*Aspergillus nidulans*	-	NA	NA	NA	(111, 112)
Phytosphingosine	*Neurospora crassa*, *Aspergillus nidulans*	*Nc*: NUO9.8, NUO14, NUO21, NUO21.3c, NUO30.4, NUO51, NUO78, AIF, AMID, ATP synthase subunit 4, (aldehyde dehydrogenase), TRANSLIN, TRAX	no [c]	yes [d]	yes [e]	(111-116)
Ceramide	*Neurospora crassa*	-	NA	NA	NA	(112)
Cell wall or plasma membrane-disturbing agents						
Amphotericin B	*Aspergillus fumigatus*	-	NA	NA	no	(117, 118)
Caspofungin	*Aspergillus fumigatus*	-	NA	NA	NA	(118)
Itraconazole [a]	*Aspergillus fumigatus*, *Rhizopus oryzae*, *Cunninghamella bertholletiae*, *Mucor circinelloides*	-	NA	yes	yes	(119, 120)
Posaconazole [a]	*Rhizopus oryzae*, *Cunninghamella bertholletiae*, *Mucor circinelloides*	-	NA	yes	yes	(119, 120)
Chitosan	*Neurospora crassa*	-	yes	NA	NA	(121)
Plant-derived compounds						
Camalexin	*Botrytis cinerea*	*Bc*: BcBir1	NA	yes	NA	(85)
Lovastatin	*Mucor racemosus*, *Botrytis cinerea*	*Mr*: MRas1, MRas3, (cAMP signaling pathway), (PI3K)	NA	NA	NA	(85, 108)
Hexanoic (caproic) acid	*Botrytis cinerea*, *Ustilago maydis*	*Bc*: BcNma; *Um*: Mfe2, Mfe2b, Had1, Had2	NA	NA	NA	(107, 122)
α-Tomatine	*Fusarium oxysporum*	-	yes [f]	yes	yes	(109)
SUGARWIN2	*Colletotrichum falcatum*	-	NA	NA	NA	(123)
Dill essential oil	*Aspergillus flavus*	-	NA	yes	NA	(124)
Anethole	*Aspergillus fumigatus*	-	NA	yes	yes	(125)

Fungi- and bacterial-derived compounds						
PAF	*Neurospora crassa*, *Aspergillus nidulans*	*An*: FadA	yes	yes	NA	(126, 127)
Trichokonin VI	*Fusarium oxysporum*, *Ascochyta citrullina*, *Botrytis cinerea*, *Phytophtora parasitica*, *Verticillium dahliae*	-	yes [f]	no	no	(128)
Ophiobolin A	*Mucor circinelloides*, *Rhizopus stolonifer*	-	NA	NA	NA	(129)
L-amino acid oxidase Th-L-AAO	*Botrytis cinerea*	-	NA	yes	NA	(130)
Farnesol	*Aspergillus nidulans*, *Fusarium graminearum*, *Penicillium expansum*	*An*: PrpA, NucA, CycA, FadA, SfaD, AifA, PkcA, AtgH, PkcA, CasA, CasB, HacA, MAPK signaling pathway	NA	yes	yes	(131-138)
Staurosporine	*Neurospora crassa*	*Nc*: NUO9.8, NUO14, NUO30.4, NUO51, ABC-3	yes [c]	yes	no [c]	(114, 139, 140)
WH1 fungin	*Rhizoctonia solani*	-	NA	yes	yes	(141)
De novo designed antimicrobial peptides						
PAF26 (PAF95, PAF96)	*Neurospora crassa*, *Aspergillus fumigatus*	-	yes	NA	NA	(142, 143)
$_{D}$(KLAKLAK)$_{2}$	*Rhizopus oryzae*, *Mucor circinelloides*	-	NA	yes	yes	(144)
Oxidative stress inducers						
Hydrogen peroxide	*Aspergillus fumigatus*, *Botrytis cinerea*, *Colletotrichum trifolii*, *Neurospora crassa*	*Bc*: BcBir1, BcNma	NA	yes	no	(85, 107, 113, 116, 117, 145-147)
Paraquat	*Neurospora crassa*	*Nc*: NDE-1, NDE-2 [b]	NA	yes	NA	(148, 149)
Metals						
Cu^{2+}	*Heliscus submersus*, *Flagellospora curta*,	-	NA	yes	yes	(150)

	Varicosporium elodeae					
Zn^{2+}	*Heliscus submersus*, *Flagellospora curta*, *Varicosporium elodeae*, *Fusarium verticillioides*	-	NA	yes	yes	(150, 151)
Cr (VI)	*Neurospora crassa*	-	NA	yes	NA	(152)
Osmotic stress						
Water (7 days)	*Botrytis cinerea*	*Bc*: BcNma	NA	NA	NA	(107)
Salt (NaCl)	*Fusarium proliferatum*	*Fp*: FpHog1	NA	yes	NA	(153)
Hyperosmotic stress	*Fusarium proliferatum*	*Fp*: FpHog1	NA	yes	NA	(153)
Photo-induction						
Ultraviolet light	*Colletotrichum trifolii*	-	NA	yes	NA	(146)
Photodynamic inhibition (aPI)	*Trichophyton rubrum*	-	NA	yes	NA	(154)
Nutrient limitation						
Carbon starvation	*Aspergillus fumigatus*, *Aspergillus nidulans*, *Aspergillus niger*	*An*: AtmA, XprG, NagA	NA	yes	yes	(155-159)
Auxotrophic strains lacking adequate substrates	*Neurospora crassa*	-	NA	yes	NA	(160, 161)
Genetic induction						
Dominant activated ''oncogenic'' Ras	*Colletotrichum trifolii*	*Ct*: CtRas	NA	yes	NA	(146)
Δ*pig-a*; *pig-a* conditional mutant	*Aspergillus fumigatus*	*Af*: PigA, QutG, PI3K	yes	NA	no	(162, 163)
Δ*choC*	*Aspergillus nidulans*	*An*: ChoC	NA	NA	NA	(164)
Kalilo plasmid-bearing strains	*Neurospora crassa*, *Neurospora intermedia*	-	NA	NA	NA	(165, 166)
Human BAX expression	*Colletotrichum gloeosporioides*	-	NA	NA	NA	(167)
Others						
Moderate heat shock (45ºC) + glucose deprivation (2-deoxyglucose)	*Neurospora crassa*	*Nc*: CEL-1, OS-2, (biotin)	NA	NA	NA	(112, 168)
Confrontation	*Podospora*	*Pa*: PaNOX1, PaASK1	NA	yes	NA	(169)

between different species	*anserina*, *Penicillium chrysogenum*	

[a] In combination with tacrolimus, antimycin A or benzohydroxamate (119, 120); [b] A double mutant strain Δ*nde1*Δ*nde2* is substantially more resistant to paraquat than wild type (145); [c] Gonçalves *et al*, unpublished results; [d] Phytosphingosine induces ROS production although ROS scavenging does not block cell death; [e] Only Δ*casA* was tested and *A. nidulans* also possesses *casB*; [f] Although alterations in the intracellular levels of Ca^{2+} were not measured, inhibition of Ca^{2+} channels or addition of Ca^{2+} chelators blocks cell death (109, 128). Columns "Ca^{2+}", "ROS" and "MC" denote, for the effect of each stimulus, the involvement of Ca^{2+}, ROS or metacaspases, respectively. NA: not assessed.

N. crassa was chosen as the main model for the experiments presented in this dissertation. Therefore, a more detailed review of the available reports on the mechanisms of cell death in this filamentous fungus is presented here. In an early report on cell death in filamentous fungi, Strauss showed, in the 1950s, that unstable attempts of auxotrophic strains of *N. crassa* to grow in the absence of the required nutrient result in cell death (161). In the case of the lack of dietary inositol in inositol-requiring mutants, the death process seems to be involve ROS, since the addition of antioxidants is protective (160). In recent years, it was observed that other stimuli lead to cell death in *N. crassa*, including the sphingolipids phytosphingosine and ceramide (112-114, 116), chitosan polymers (121), PAF (126) and PAF26 (142) (a natural and a *de novo* designed antifungal peptide, respectively), oxidative stress inducers like hydrogen peroxide and paraquat (113, 116, 145, 149), staurosporine (114, 139, 140), chromium (152), a combined stress of temperature and carbohydrate deprivation (112, 168) or senescence due to the presence of kalilo mitochondrial plasmids isolated from Hawaiian strains of *Neurospora intermedia* (165, 166). During the last years, our group has focused on the study of the molecular basis of cell death using a chemical induction approach. To induce cell death we mainly used phytosphingosine, hydrogen peroxide or staurosporine (Fig. 11).

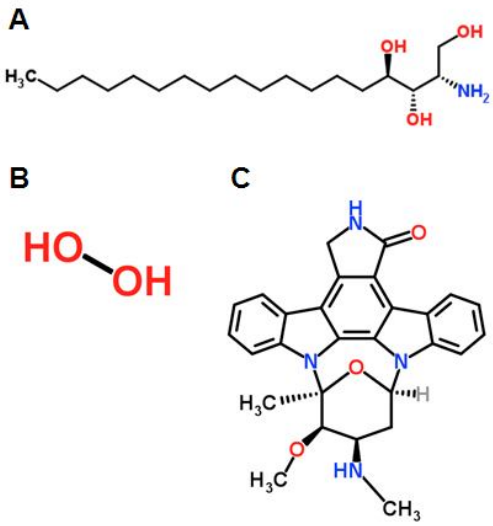

Figure 11 - Chemical structures of cell death-inducing agents: phytosphingosine (A), hydrogen peroxide (B) and staurosporine (C).
Chemical structures were obtained from http://www.chemspider.com/.

Phytosphingosine is a natural long-chain sphingoid base (170). The evidence that this sphingolipid has potent antifungal activity against *A. nidulans* with mitochondrial involvement (111), prompted our group to investigate its effects in *N. crassa*. Treatment of conidia with phytosphingosine results in reduced viability, impairment of asexual spore germination, production of ROS, YO-PRO1 staining and DNA condensation and fragmentation, suggesting the induction of an apoptosis-like cellular death (113, 114). Analysis of gene expression during phytosphingosine-induced cell death by DNA microarrays revealed that most of the alterations at the transcriptional level correspond to upregulation of genes. However, there is a very strong enrichment of genes encoding mitochondrial proteins in the set of genes that are downregulated by the drug that likely explains its effects in the fungus (116). This may be correlated with the fact that deletion of genes encoding subunits of the mitochondrial complex I, like NUO9.8, NUO14, NUO21, NUO21.3c, NUO30.4, NUO51 and NUO78 (but not the deletion of other components of the respiratory chain) confers increased resistance to phytosphingosine. The same resistance profile is paralleled by the treatment of complex I mutants with hydrogen peroxide, indicating shared intracellular mechanisms of response to treatment with phytosphingosine and hydrogen peroxide.

Complex I mutant strains generate less ROS than wild type when exposed to phytosphingosine (113). Transcriptional analyses of hydrogen peroxide-treated wild type versus Δ*nuo14* cells showed that genes encoding mitochondrial proteins are the most enriched category among those with higher expression in the mutant in the presence of the insult (116). Thus, absence of a functional complex I results in lowered production of ROS upon treatment with phytosphingosine and confers increased tolerance to some drug-induced transcriptional alterations and this may explain why these cells cope better with the growth insult elicited by phytosphingosine and hydrogen peroxide. The involvement of mitochondria during phytosphingosine-induced cell death is further stressed from findings that deletion mutants for subunit 4 of mitochondrial ATP synthase, for a mitochondrial aldehyde dehydrogenase and for the homologue of the mammalian AIF are more resistant to the drug than wild type. On the other hand, Δ*amid* cells, lacking a homologue of the mammalian apoptosis-inducing factor-homologous mitochondrion-associated inducer of death (AMID) are more sensitive to phytosphingosine than wild type (113). Deletion of the tRNA processing molecules TRANSLIN and TRAX confers increased resistance to phytosphingosine (115). More recently, our group observed that treatment with phytosphingosine, as well as staurosporine, cause the export of GSH (114), although both drugs induce cell death through very distinct mechanisms (see below). Addition of exogenous GSH does not revert the effects of phytosphingosine, neither in *N. crassa* (114) nor in *A. nidulans* (111).

The combination of a moderate heat shock (45ºC) and analog-induced glucose deprivation (with 2-deoxyglucose) is lethal for *N. crassa*, particularly in HSP30-defective strains, and involve components of the fatty acid biosynthetic pathway, namely fatty acid synthase and the cofactor biotin, and the MAPK OS-2 (112, 168). Under these conditions, there is an accumulation of C_{18}(OH)-phytoceramide and C_{24}(OH)-phytoceramide (112). Spores in a very initial growth phase (2 hours) are refractory to the combined stress and do not accumulate C_{18}(OH)-phytoceramide, indicating that this sphingolipid is probably directly related to cell death. Also, there is evidence in *S. cerevisiae* that the response to distinct cellular stresses such as heat (171) and nitrogen starvation (172) is correlated with the accumulation of phytosphingosine species. Additionally, yeast mutant cells defective in the addition of inositol phosphate to ceramide are particularly sensitive to treatment with phytosphingosine (173). Exposure to ceramide also induces cell

death in *N. crassa* (112). Hence, it appears that accumulation of sphingolipids is a signal for fungal PCD.

Staurosporine is a bacterial alkaloid initially isolated from *Streptomyces staurosporeus* during a screening for protein kinase C (PKC) inhibitors (174) that was later shown to display a broad kinase inhibitory activity (175). The PKC homologue Pkc1 of *S. cerevisiae* was validated as an essential target of staurosporine (176). This drug displays strong anticancer and antimicrobial activities and is widely used by the scientific community as a prototypical cell death-inducing agent. Importantly, some staurosporine analogues displaying better selectivity profiles, such as UCN-01, CGP41251 or PKC412 are currently under evaluation in clinical trials for the treatment of different forms of cancer (177), accentuating the need for the comprehension of the mechanisms of action of this type of drugs. In *N. crassa*, staurosporine induces loss of cell viability, marked impairment of conidial germination, chromatin fragmentation, YO-PRO1 staining and early ROS production (114, 139, 140). In contrast to phytosphingosine, deletion of some subunits of mitochondrial complex I such as NUO9.8, NUO14, NUO30.4 and NUO51 (but not others like NUO78) results in hypersensitivity to staurosporine. The complex I assembly status of these mutant strains alone cannot explain the increased susceptibility to staurosporine because cells with similar assembly phenotypes display different sensitivity to the drug. Thus, it seems that some of the proteins play a specific role during intracellular cell death signaling or execution. Staurosporine and phytosphingosine definitively act by different mechanisms, but mitochondria and respiration are central for the cell death process induced by both drugs.

Because of the involvement of mitochondrial complex I during the fungal response to staurosporine, we decided to combine this drug with the classical complex I inhibitor rotenone. It was observed that the combination of the drugs displays synergistic activity against the growth of *N. crassa* and the clinically relevant fungi *Aspergillus fumigatus* and *Candida albicans* (139). Surprisingly, this synergistic behavior is also observed in complex I mutant strains (in which the enzyme is already nonfunctional), suggesting a complex I-independent for the action of rotenone. Indeed, other complex I inhibitors (piericidin A and diphenyleneiodonium) do not act like rotenone in combination with staurosporine

and the combination staurosporine plus rotenone is synergistic even against *S. cerevisiae* cells which are devoid of complex I.

The exogenous addition of GSH or its precursor N-acetyl-cysteine (NAC) effectively blocks staurosporine-induced cell death, pointing to the importance of ROS generation during the fungal response to this drug (139). Our group reported recently, for the first time in fungi, that the export of GSH is a crucial event during the cell death program driven by staurosporine (114). It seems that GSH efflux following treatment with staurosporine (or phytosphingosine, with even faster kinetics) is an early and specific event of cell death rather than a secondary effect such as a detoxification mechanism. Thus, *N. crassa* exports GSH when exposed to staurosporine causing a change in the intracellular environment to a more oxidative redox state. The consequent decrease of the internal GSH/GSSG ratio modulates intracellular redox signaling and may facilitate the oxidation of proteins or lipids. A combined treatment with staurosporine and rotenone results in increased depletion of GSH (139).

Analysis of transcriptional alterations associated with treatment with staurosporine by DNA microarrays revealed that the drug induces high levels of expression of a gene encoding a member of the ABC (ATP-binding cassette)-transporter family, *abc-3* (140). This result was confirmed at the gene level by qRT-PCR and at the protein level by western blotting with a specific antibody. This antibody, made in our laboratory, allowed the localization of ABC-3 at the cell surface. Interestingly, deletion of *abc-3* results in extreme sensitivity to staurosporine. Because of the significant homology between ABC-3 and the human P-glycoprotein, shown to mediate multidrug resistance in cancer cells (178), the levels of intracellular and extracellular staurosporine after treatment of *N. crassa* cells were measured. To achieve this, a method that took advantage of the fact that staurosporine fluoresces when excited with UV light was devised. ABC3 was found to perform drug efflux to the extracellular space, becoming the first time-reported transporter of the broadly used staurosporine (140). In agreement with this, a combined treatment of staurosporine and the P-glycoprotein inhibitors verapamil or sodium orthovanadate results in synergistic inhibition of growth in *N. crassa* as well as in the pathogenic *A. fumigatus* and *C. albicans*, likely due to blockage of staurosporine efflux.

The available literature on the effects of staurosporine in fungi other than *N. crassa* is scarce. In *S. cerevisiae*, a group of genes termed *STT* (for "staurosporine- and temperature-sensitive"), whose respective deletion strains are particularly susceptible to staurosporine, were isolated. This set of genes includes protein kinases such as Pkc1, Pi4k and Bck1, mediators of Golgi to vacuole protein sorting (Vps18, Vps34, Vps11, Vps45 and Vps33), a protein involved in glycophosphatidylinositol anchor synthesis (Gpi1), the acetoacetyl-CoA thiolase involved in ergosterol biosynthesis Erg10, vacuolar H+-ATPase mutants (Vma1, Vma2, Vma3, Vma4, Vma11, Vma12 and Vma13) and a subunit of oligosaccharyltransferase (176, 179-181).

PAF and farnesol are two of the stimuli that are well established as cell death inducers in filamentous fungi. PAF (for "Penicillium antifungal protein") is a small (55 amino acids), basic, cysteine- and lysine- rich antifungal protein abundantly secreted into the supernatant by *Penicillium chrysogenum* that displays an inhibitory activity against a broad range of filamentous fungi (182). Interestingly, PAF is not toxic against prokaryotes or yeasts (183) nor against human endothelial cells (184), suggesting its usefulness in antifungal therapies. *A. nidulans* cells exposed to PAF exhibit several apoptotic halllmarks including DNA fragmentation, phosphatidylserine externalization and production of ROS (127). In this organism, it was shown that G-protein signaling, as well as the cAMP/PKA and PKC/MAPK pathways are involved in the effects of PAF (127, 185). PAF also induces cell death in *N. crassa* accompanied by a disruption of intracellular Ca^{2+} homeostasis (126).

Farnesol is a non-sterol isoprenoid formed by the dephosphorylation of farnesyl pyrophosphate (186). In *in vitro* and *in vivo* human cancer models, this drug inhibits proliferation, induces apoptosis and is effective in chemoprevention (187). In *C. albicans*, farnesol is secreted as a quorum-sensing molecule that prevents the yeast to mycelium conversion (188). In *A. nidulans*, farnesol triggers apoptotic-like cell death with mitochondrial involvement, since pre-treatment with the mitochondrial complex V (ATP synthase) inhibitor oligomycin as well as the ROS scavenger NAC markedly blocked farnesol-induced apoptosis (134). Several molecules and pathways have been proposed as involved in the *A. nidulans* response to farnesol, including G-protein signaling (FadA, SfaD), MAPK pathway (PkcA), autophagy (AtgH), apoptotic machinery (AifA, CasA, CasB, PrpA) and

mitochondrial alternative NAD(P)H dehydrogenases (NdeA, NdeB, NdiA) (133, 134, 137, 138). Farnesol also kills *Fusarium graminearum* and *Penicillium expansum* (132, 136). Based on these data, it is possible that farnesol is secreted by *C. albicans* cells not only to inhibit the yeast-mycelium conversion but also as a mechanism of defence and competition against other fungi.

The molecular machinery of fungal apoptotic-like death

Most of the common regulators and executioners of mammalian apoptosis do not possess evident sequence homologues in fungal genomes (46, 47). However, it is now clear that fungi undergo apoptotic-like cell death in response to several stimuli, suggesting that proteins with low (or no) sequence similarity behave as functional homologues of the mammalian mediators of cell death. In line with this, heterologous expression in fungi of mammalian BCL-2 family members, which are almost absent in fungal species, induce or prevent cell death (42-45, 167), suggesting that they are recognized and maybe interact with endogenous molecules and trigger a biological response. Additionally, no (sequence) homologues of the mammalian extrinsic apoptotic pathways are found in fungi. Nevertheless, there are fungal sequence homologues of a number of mammalian mediators of cell death. Filamentous fungi were shown to possess additional proteins with homology to cell death-related molecules of mammalian cells when compared with yeasts (189). *In silico* searches also predict dozens of cell death-associated genes in filamentous species that seem to be absent in *S. cerevisiae*, a part of them being fungal-specific and related to heterokaryon incompatibility. Moreover, the similarity between mediators of cell death in humans and filamentous fungi (like BIR1, AMID, CulA and HtrA) is higher than the similarity of the same proteins between yeasts and filamentous species (189). Intriguingly, sequence conservation between mammalian and fungal cell death mediators is normally domain-centered, that is, there is similarity in a determined domain of the protein but the remainder of the sequence is divergent. There is a tendency for fungi to possess similarity in certain elements of cell death-related proteins that are important for their apoptotic role. Additionally, these domains present similarities but are not identical or near-identical, suggesting that fungi may carry more ancient forms of these proteins/domains (46, 47).

Shlezinger *et al* developed an automatic *in silico* domain-based procedure to identify putative fungal mediators of cell death and found that, from a list of classical animal apoptotic-related domains, only the BIR (baculovirus inhibitor of apoptosis protein repeat) domain was found in fungi (190). One BIR-containing protein was identified in *B. cinerea* (BcBir1) and functional characterized as an anti-apoptotic molecule involved in interactions with host plants, as described above (85). Recently, a pro-apoptotic protein called Bxi1/Ybh3, homologue of the human LFG4, was found to contain a BH3-like signature at the C'-terminal portion and to translocate to the mitochondria to trigger apoptosis in *S. cerevisiae* (191). BH3 domains are present in some members of the BCL-2 family (40). Homologues of Bxi1 in other fungi were predicted but functional verification has not yet been done.

In opposition to the extrinsic apoptotic pathway, the mitochondrial component of mammalian apoptosis ("intrinsic pathway) seems to be more conserved in fungi. Cytochrome *c* is an electron carrier of the mitochondrial intermembrane space and becomes a pro-apoptogenic molecule upon induction of cell death, being released from the organelle (39). *S. cerevisiae* cytochrome *c*, Cyc1, is released from mitochondria upon exposure to acetic acid (192, 193). In filamentous species, this phenomenon was shown to occur in response to the peptides $_{D}(KLAKLAK)_2$ (144) and WH1 fungin (141), as well as upon exposure to a combined treatment of azole drugs and tacrolimus (119). *A. nidulans* cytochrome *c* is not released from mitochondria during farnesol-induced cell death (131).

In mammals, AIF and EndoG are DNA nucleases that normally reside in the mitochondria where they play a role during normal physiological processes. Upon induction of apoptosis, normally independently of the activity of caspases, these two molecules translocate to the nucleus and cleave the DNA (39). AIF is an oxidoreductase with NADH dehydrogenase activity involved in the biogenesis and maintenance of the respiratory chain, namely complexes I and III (194). Interestingly, in *N. crassa*, AIF deletion does not affect complex I assembly nor function (148). In yeast, the AIF homologue, Aif1 also migrates to the nucleus during apoptotic cell death where it causes DNA condensation and fragmentation (195). In *N. crassa*, *aif* disruption leads to increased resistance to phytosphingosine and hydrogen peroxide (113). In *A. nidulans*, *aifA* is induced by farnesol and deletion of AifA confers increased sensitivity to this drug and

hydrogen peroxide, likely due to increased ROS production (133, 138). These apparently contrasting results might be linked to compensatory mechanisms since AIF belongs to a small family of proteins that also includes the AIF-homologous mitochondrion-associated inducers of death (AMIDs). Human AMID (or PRG3 for "p53-responsive gene 3") is a NAD(P)H oxidase that induces caspase-independent apoptosis (196). Our group characterized the normal localization of AIF and the two AMID proteins of *N. crassa*: AIF appears to be localized in both the mitochondria and the cytoplasm, while AMID was found exclusively in the cytoplasm. AMID2 was detected in cell extracts from an Δ*amid* strain and barely in the wild type strain, in both mitochondria and cytoplasm, suggesting overlapping functions for the two AMID proteins (148). The disruption of *N. crassa* AMID causes an increase in the sensitivity to phytosphingosine and hydrogen peroxide (113). In *P. anserina*, deletion of *amid*, *amid2* and *aif2* results in an increase in lifespan extension (91, 197). AIF and AMID proteins are related to the alternative NAD(P)H dehydrogenases present in the mitochondria of fungi and plants (148). The putative role of alternative NAD(P)H dehydrogenases during cell death will be discussed further ahead.

Mammalian EndoG seems to be involved in mitochondrial DNA replication (198), but is released from the mitochondria in a caspase-independent manner and cleaves nuclear DNA during apoptosis (39). In yeast, Nuc1 seems to behave similarly to its human EndoG homologue, as it translocates to the nucleus after exposure to hydrogen peroxide (199). However, in *A. nidulans* the EndoG homologue NucA is not involved in farnesol-induced cell death (131). In animals, HtrA2/Omi is a mitochondrial pro-apoptotic protein that binds to inhibitor of apoptosis proteins and alleviate their inhibitory effect on caspases (39). In yeast, its homologue Nma111, although not mitochondria- but nucleus-localized, is also pro-apoptotic (200). In *B. cinerea*, genetic manipulation of the HtrA2/Omi homologue BcNma by overexpression or deletion leads to enhanced or reduced appearance of apoptotic markers, respectively (107). Intriguingly though, the overexpression and mutant strains are not different from wild type cells when exposed to different cell death-inducing stresses.

With regard to the similarities and differences between animal, plant and microbial PCD, the activity of caspases had special relevancy in recent years and will be covered here in detail. Caspases, whose designation derives from

“cysteine-dependent aspartate specific proteases” (201), are cysteine-dependent proteases that cleave their substrates after aspartic acid residues in target proteins (202, 203). Caspases are synthesized as inactive zymogens (procaspases) and are activated upon a cell death stimulus. Procaspases are single chain proteins organized in a similar manner (Fig. 12). They contain a N’-terminal pro-domain followed by the large (p20) and small (p10) domains, that interact with each other after activation, resulting in a dimer of (p20)(p10)(p20)’(p10)’ symmetry with two active sites per molecule. The small subunit possesses several residues that form the substrate-binding groove while the large subunit contains the catalytic dyad residues histidine and cysteine. Based on their structure and function, caspases can be classified in three groups: inflammatory, initiator and effector caspases (202, 203).

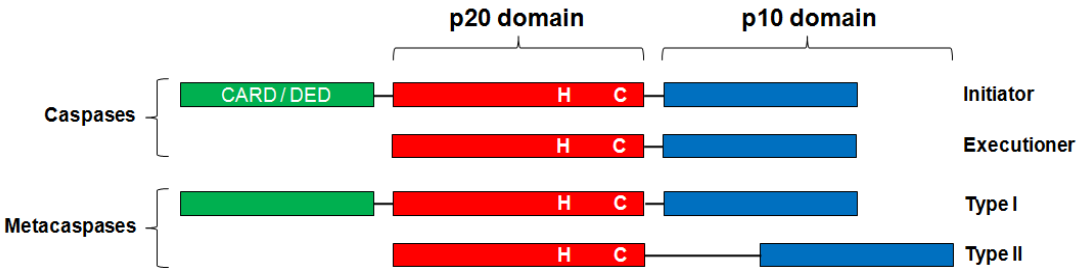

Figure 12 - Main protein sequence features of caspases and metacaspases.
See text for details. The catalytic dyad residues histidine (H) and cystein (C) are represented. CARD: caspase recruitment domain; DED: death effector domain.

At the beginning of this century, two novel caspase-related families were identified, using an *in silico* approach: the metacaspases and the paracaspases (204). Paracaspases are involved in the development of MALT lymphoma but not in cell death execution and contain a N’-terminal death domain and one or two immunoglobulin domains (204). They will not be reviewed here. The nomenclature and involvement of metacaspases in cell death is currently a hot topic and opposite opinions regarding the subject have been expressed (205-207). Namely, although the participation of metacaspases in cell death was solidly demonstrated (208, 209), the definition of this group of molecules as genuine caspases is still arguable (205-207).

Metacaspases can be divided in type I and type II (Fig. 12). Type I metacaspases possess a N’-terminal region evocative of the prodomain of initiator

and inflammatory caspases with a proline-rich repeat motif (204). Type II metacaspases lack such a prodomain but exhibit a linker sequence between the putative large and small subunits (204, 210). Metacaspases (as well as paracaspases) have the catalytic histidine/cysteine dyad and secondary structure predictions indicate the presence of the caspase/hemoglobinase fold (204, 207). Metacapases possess sequence similarity with mammalian caspases in particular in the catalytic p20 and p10 domains. Importantly, it was shown that metacaspases have a major difference with caspases: instead of cleaving after after aspartic acid residues, they cleave after basic arginine or lysine (210-212). Does the aspartic acid specificity of animal caspases represent an evolutionary process of gene duplication leading to the diverging of them from metacaspases? This has been suggested but is still a not proved hypothesis (205, 206). Tudor staphylococcal nuclease (TSN) was described as the first natural substrate of a metacaspase, being processed by the type II metacaspase of *Picea abies* mcII-Pa (208). The same study showed that the activity of mcII-Pa on TSN is associated with cell death. Recently, Coll and colleagues showed that AtMC1 and AtMC2, antagonistically control PCD in *Arabidopsis thaliana* (209).

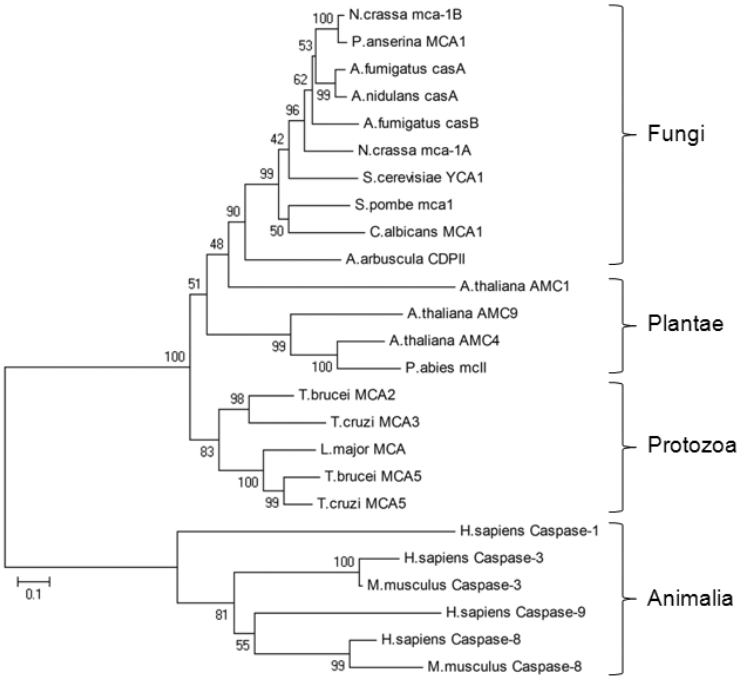

Figure 13 - Bootstrap neighbor-joining tree of selected metacaspases and caspases protein sequences.
The tree was built using MEGA5 (213).

In eukaryotes, metacaspases are present in the kingdoms Protozoa, Fungi, Plantae and Chromista, being absent in animals. Type II metacaspases are found only in plants, while type I metacaspases occur in the four kingdoms. Interestingly, the presence of caspases excludes that of metacaspases, suggesting that they may represent variants of the same enzyme that has diverged in evolution (205). Phylogenetic analysis of protein sequences shows a clear clustering of animal caspases and the metacaspases of Fungi, Plantae and Protista (Fig. 13).

In *S. cerevisiae*, the sole metacaspase Yca1 is cleaved like a typical caspase upon treatment with hydrogen peroxide (214). This response is respectively abrogated and stimulated after disruption and overexpression of Yca1. Though, cell death in yeasts is not always metacaspase-dependent (205). Metacaspases where also identified in filamentous fungi. In *A. fumigatus*, apoptotic-like cell death occurring after exhaustion of the carbon source and entry into the stationary phase of growth is associated with intracellular activity against caspase-1 and -8 substrates and blocked by the pan-caspase inhibitor Z-VAD-fmk (156). However, metacaspases do not seem to participate in the *A. fumigatus* response to hydrogen peroxide and amphotericin B (117). In this organism, two metacaspases were identified, CasA and CasB. A double mutant Δ*casA*Δ*casB* showed a similar sensitivity to pro-apoptotic stimuli when compared with the wild type strain (155). However, the double mutant was hypersensitive to compounds that disrupt homeostasis of the ER, suggesting that metacaspases support growth under conditions of ER pressure. Caspase-like activities were detected in protein extracts from *A. nidulans* during sporulation and blocked by the caspase inhibitors DEVD-fmk and IETD-fmk (95). It was shown that metacaspase CasA does not play a role in phytosphingosine-induced cell death and that the Δ*casA* mutant grows and sporulates as well as the parental strain (111). Nevertheless, overexpression of CasA causes inhibition of growth and morphological changes compatible with apoptosis. In *P. anserina*, the behavior of two metacaspases (PaMCA1 and PaMCA2) was studied in ageing. Disruption of each one of the metacaspases or double disruption leads to increase in lifespan, specially in the Δ*PaMca1* mutant (91). Metacaspase-dependent activity occurred in senescent but not in juvenile cultures and was lower in the mutant strains, but only for the substrate DDR and not for classical caspase substrates. Fifteen days-old mycelia from Δ*PaMca1* was more resistant to hydrogen peroxide than wild type. In *N.*

crassa, none of the two identified metacaspases (MCA-1A and MCA-1B) is required for heterokaryon incompatibility-related cell death (70). Yet, the expression of the transcripts of both metacaspases was increased under those conditions. The metacaspase transcript of *mca-1A* is overexpressed in response to phytosphingosine (116). Metacaspases have been also linked to the response of other filamentous fungi to a number of stimuli (Table 2 and 3).

PARP-1 is physiologically involved in DNA repair and a target of caspases during mammalian apoptosis (39, 215). PARP homologues are absent in yeast but present in filamentous fungi (189). The *A. nidulans* PARP homologue PrpA plays a role in the response to DNA damage and is required for farnesol-induced cell death (135). In the same fungus metacaspases seem to degrade a PARP-like protein during cell death that accompanies the process of sporulation (95). Very recently, PARP was described as a substrate of *P. anserina* metacaspases (216).

Of course, the study of PCD in fungi must not be restricted to the analysis of putative homologues of known mammalian mediators of cell death. On the contrary, one of the advantages of using fungi as model organisms is to make use of their simplicity, genetic tractability and sequenced genomes to identify novel mediators of PCD. These are some of the features of *N. crassa* that prompted us to use it to study PCD.

1.3) Mitochondrial bioenergetics systems

Introduction to mitochondrial biology

Mitochondria (from the Greek *mitos* and *chondros*, meaning “thread” and “granule”, respectively) are the dynamos of the eukaryotic cell due to their major role in energy production under aerobic conditions. They are double membrane organelles: the protein-rich core of the organelle is known as the matrix, whereas the outer and inner mitochondrial membranes delimitate the intermembrane space (Fig. 14). The inner membrane forms a series of invaginations designated as *cristae*. Mitochondria take up pyruvate formed during the first stage of carbon metabolism (glycolysis) and fatty acids and convert them in energy as follows: 1) pyruvate and fatty acid are broken down to acetyl-CoA; 2) acetyl-CoA is oxidized via the tricarboxylic acid cyle (also known as Krebs cycle or citric acid cycle) with

the generation of CO_2 and reduction of NAD^+ to NADH and FAD to $FADH_2$; 3) high-energy electrons carried by NADH and $FADH_2$ are passed along the electron transport chain embedded in the inner membrane to O_2; 4) the formation of a proton gradient across the inner membrane occurs concomitantly with the electron transport and oxidation of NADH and $FADH_2$; 5) this gradient is dissipated by the ATP synthase complex leading to the formation of ATP from ADP and P_i available in the matrix. The last steps of the process involving the mitochondrial respiratory chain are known as oxidative phosphorylation. Mitochondria are very mobile (normally moving associated with microtubules) and plastic (being able to change their shape frequently by fusion and fission). They possess a proper genome, a double-stranded DNA circular molecule (mtDNA) that contains some protein coding genes and machinery needed for their transcription and translation. Apart from the generation of energy, mitochondria are involved in several other cellular processes, as cell death and Ca^{2+} storage (217).

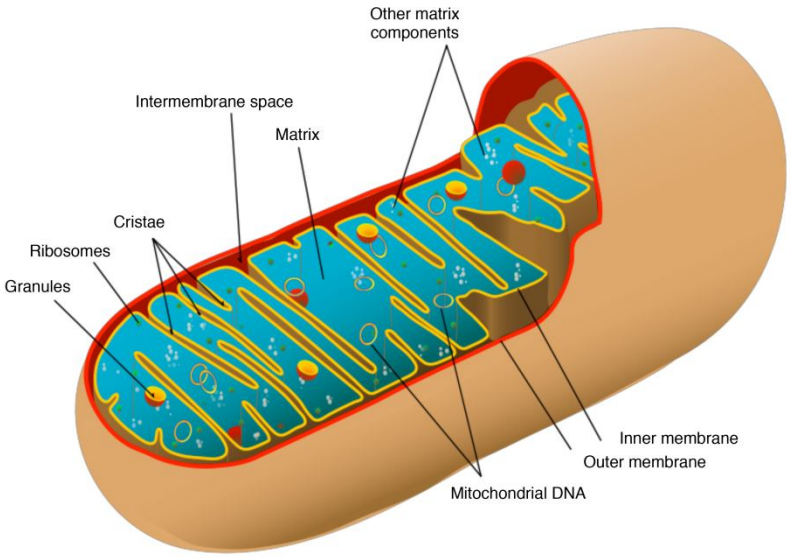

Figure 14 - Structure of a mitochondrion.

The mitochondrial electron transport chain with a focus on complex I

The respiratory chain lies in the mitochondrial inner membrane and is composed by multi-subunit enzymatic complexes (complex I, II, III and IV), together with ubiquinone (coenzyme Q) and cytochrome *c* (Fig. 15). These complexes possess several protein-associated prosthetic groups (flavin mononucleotide (FMN), flavin adenine dinucleiotide (FAD), iron-sulfur clusters

(FeS), copper, heme) that transport electrons. Ubiquinone and cytochrome *c* transfer electrons between complexes. The proton pumping activity of complex I (NADH:ubiquinone oxidoreductase; uses NADH as a source of electrons transferring them to ubiquinone via FMN and a series of iron-sulfur clusters), III (ubiquinol cytochrome *c* reductase; transfers electrons from the reduced ubiquinone or ubiquinol to cytochrome *c*) and IV (cytochrome *c* oxidase; catalyses electron transfer to molecular oxygen, which is reduced to water) generates the electrochemical gradient that triggers the rotation of the ATP synthase (complex V) F_0 and F_1 domains leading to the formation of ATP from the phosphorylation of ADP (218, 219). Complex II (succinate dehydrogenase) transfers electrons from succinate to ubiquinone providing an alternative electron entry point into the respiratory chain, without proton pumping. Three ATP molecules are formed from each NADH molecule (217). The respiratory chain complexes are composed by several proteins (for instance, the mammalian complex I possesses 45 subunits) which are encoded both by nuclear DNA and by mtDNA, with the exception of complex II, which is exclusively encoded by nuclear DNA (218, 219). Respiratory complexes are arranged in supramolecular structures, the respirasomes. For instance, the respiratory chain can be assembled in I_2, I-III_2-IV_{0-4} and III_2-IV_{0-4} supercomplexes, as shown by blue native polyacrilamide gel electrophoresis (BN-PAGE) studies in *N. crassa* (220). More recent data points to the idea that a higher level of organization of the respiratory chain exists, with the respirasomes interconnected with dimers of complex III plus tetramers of complex IV supercomplexes associated into a respiratory string (221).

Complex I is the first and major entry point of electrons into the respiratory chain (14, 15, 222) with exception of some organisms as yeasts, where it is absent (223). Complex I provides most of the proton motive force subsequently used for ATP synthesis (224) and is the largest of the respiratory chain complexes: the bovine (*Bos taurus*) enzymes is composed by 45 subunits (225) whereas the *N. crassa* complex I contains at least 39 subunits (226). It forms a L-shaped structure, with one hydrophobic arm implanted in the mitochondrial inner membrane (membrane arm) and one hydrophilic arm projecting into the mitochondrial matrix (peripheral arm) (222, 224). Complex I is considerably conserved from bacteria to humans, especially at the core subunits (227). Assembly of the complex, which occurs by modules named N, Q and P (226-228).

Complex I can be inhibited by several types of chemicals, being rotenone the prototypical one (229).

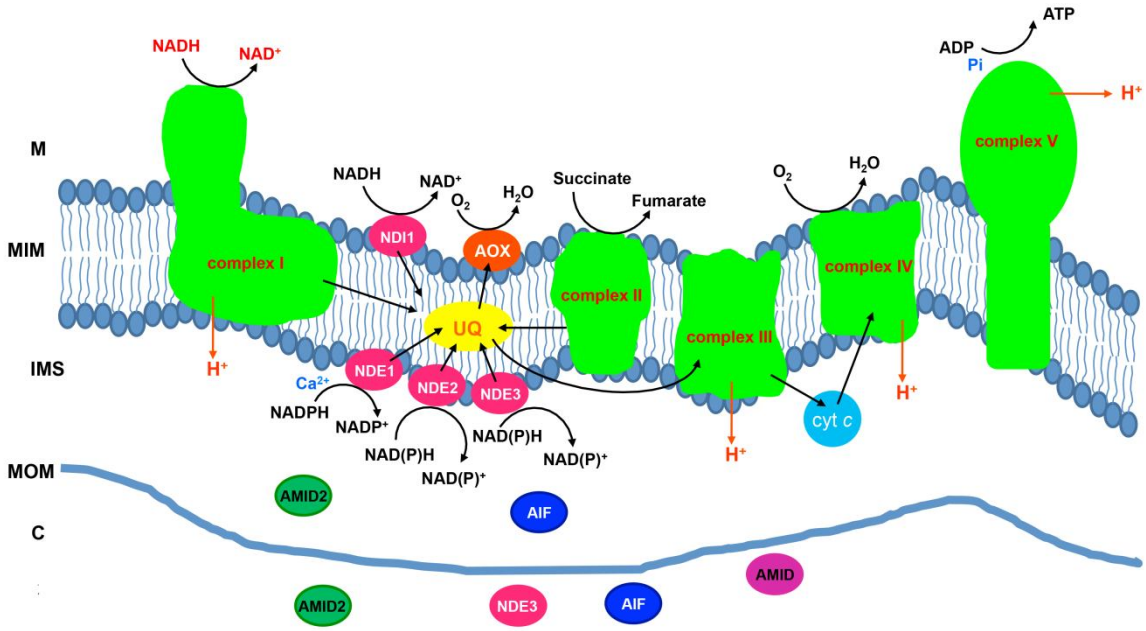

Figure 15 - The mitochondrial respiratory chain, alternative NAD(P)H dehydrogenases, alternative oxidase systems and AIF-family proteins of *N. crassa*.
M: mitochondrial matrix; MIM: mitochondrial inner membrane; IMS: intermembrane space; MOM: mitochondrial outer membrane; C: cytosol.

Defects in the oxidative phosphorylation system has been extensively linked to a plethora of pathological conditions as neurodegenerative disorders like Parkinson's and Alzheimer's diseases or schizophrenia, type 2 diabetes mellitus, Leber hereditary optic neuropathy, myopathies, encephalomyopathies, cardiopathies, Charcot-Marie-Tooth disease and particular types of cancer (230). In most cases, oxidative phosphorylation malfunction is associated with either a combined or isolated deficiency of complex I and normally involves nuclear-encoded subunits, although mutations in mtDNA-encoded subunits have been also identified (230, 231). For example, point mutations in the nuclear genes encoding *NDUFS7*, *NDUFS8* and *NDUFV1* were found in patients suffering from Leigh syndrome, leukodystrophy and myoclonic epilepsy (231). Because the proteins encoded by these genes are highly conserved from bacteria to humans, our group developed *N. crassa* strains harboring these disease-associated mutations, thus providing an easily controllable model for the study of their biological consequences (232).

Branched respiratory systems in fungi

In some fungi, plants, protists and bacteria, the electron transport chain is branched into single peptide alternative systems with no proton translocation activity that bypass the canonical pathway. The cyanide-resistant alternative oxidase (AOX) constitutes a well established detour for complexes III and IV whereas type II NAD(P)H dehydrogenases (or simply alternative NAD(P)H dehydrogenases) bypass complex I (233, 234). Alternative NAD(P)H dehydrogenases are particularly important not only because they oxidize NAD(P)H and reduce quinones but also because they serve as entry points for electrons into the respiratory chain (14, 15). Their importance is firmly demonstrated in *S. cerevisiae*, where complex I is absent (223) and type II NAD(P)H dehydrogenases are the only existing NAD(P)H oxidases (235, 236). These enzymes are flavoproteins resistant to classical complex I inhibitors such as rotenone or piericidin A and there is no selective and reliable drug to block them so far, although inhibition is feasible with diphenyleneiodonium (233, 237, 238). Alternative NAD(P)H dehydrogenases usually, but not strictly, contain FAD as the sole prostethic group (15, 233, 234). Recently, an *in silico* approach identified putative alternative NAD(P)H dehydrogenases in a few metazoan organisms, but a functional verification is still missing (239).

In *N. crassa*, four alternative rotenone-insensitive NAD(P)H dehydrogenases have been characterized in addition to complex I (Fig. 15 and Table 4) (14, 15). They are associated with the inner mitochondrial membrane, but while one of them, NDI-1 (240), is localized at the matrix side of the membrane, the other three, NDE-1 (241, 242), NDE-2 (243) and NDE-3 (244), are facing the intermembrane space. Interestingly, NDE-3 was found to be present not only within mitochondria but also in the cytosol (244).

Plants contain even more type II NAD(P)H dehydrogenases than fungi. Seven of these enzymes have been identified in *A. thaliana*: three external (NDB1, NDB2 and NDB4), three internal (NDA1, NDA2 and NDC1) (245) and one uncharacterized (NDB3). The mitochondrial import and localization to either side of the inner membrane seems to be dependent on motifs in the N'-terminal portion of the proteins (246). Interestingly, it was shown that dual targeting to mitochondria

and chloroplasts or peroxisomes is possible in some cases, although its functional relevance is unknown (247).

Alternative NAD(P)H dehydrogenases may be organized in supramolecular structures, similarly to the respiratory chain, as there is evidence showing that these enzymes form a complex with a glycerol-3-phosphate dehydrogenase, two L-lactate-dehydrogenases, a few enzymes from the tricarboxylic acid cycle, two probable flavoproteins and an acetaldehyde dehydrogenase in yeast (248). In *Yarrowia lipolytica* there is evidence of the association between the alternative external NADH dehydrogenase and complex IV, particularly in high energy-requiring, logarithmic-growth phase cells (249, 250). In *N. crassa*, there is no evidence of the formation of supercomplexes including any of the alternative NAD(P)H dehydrogenases (220), but evidence points to some kind of interaction between NDE-2 and complex I (243). *N. crassa* NDE-1 stands out because of its unique NADPH selectivity and regulation by pH and Ca^{2+} (242), the latter feature likely related to the presence of a conserved Ca^{2+}-binding domain (241). In plants, the external NDB1 oxidizes NADPH in a Ca^{2+}-dependent manner while NDB2 is a NADH dehydrogenase stimulated by Ca^{2+} (251, 252).

Table 4 - Main features of *N. crassa* alternative NAD(P)H dehydrogenases.

Protein	Topology	Substrate specificity	Ca^{2+}	pH	Reference(s)
NDE-1	External	Cytosolic NADPH	Ca^{2+}-dependent	Physiological pH	(241, 242)
NDE-2	External	Cytosolic NADH and NADPH	-	NADH throughout the pH range and NADPH at acidic pH	(243)
NDE-3	External	Cytosolic NADH and NADPH	-	NA	(244)
NDI-1	Internal	Matrix NADH	Ca^{2+}-stimulated? [a]	NA	(240, 243)

[a] Ca^{2+} stimulates the oxidation of cytosolic NADH in a Δ*nde1*Δ*nde2* double mutant, but not in the triple mutant Δ*nde1*Δ*nde2*Δ*ndi1*, indicating that NDI1 may be stimulated by Ca^{2+} (243). NDE3 was only described later (244). NA: not assessed.

The physiological role of alternative NAD(P)H dehydrogenases is still somehow controverse, although it is fairly well established that they confer metabolic plasticity allowing cells to adapt to different environmental conditions and stresses. They may act as overflow systems regulating cytosolic and mitochondrial reducing equivalents (NADH, NADPH) at physiological levels, thus

avoiding potential tricarboxylic cycle repression by elevated NADH levels and excessive levels of ROS (15, 233, 234, 253). Yeast Ndi1 was shown to reduce mammalian complex I-mediated ROS generation (254). In opposition, *S. cerevisiae* alternative NADH dehydrogenases were proposed as potential sources of superoxide radicals by some works (255-257).

In *N. crassa*, expression of alternative NAD(P)H dehydrogenases genes greatly depends on the growth phase (148, 240, 243, 244). It is not possible to obtain viable double mutants between NDE-2 and complex I mutants that lack a functional enzyme, suggesting that NDE-2 and complex I interact in a yet unidentified pathway (243).

Humans do not posses alternative NAD(P)H dehydrogenases, but some investigations were conducted to evaluate the possibility of using these enzymes in gene-based therapies. Heterologous expression of the yeast Ndi1 restores respiration in complex I-deficient human cells (258) and was also shown to be protective in *in vivo* models of Parkinson's disease (259, 260), Leber's hereditary optic neuropathy (261) and breast cancer (262). These results further highlight the importance of understanding the molecular pathways involving type II NAD(P)H dehydrogenases.

Mitochondrial respiratory chain, alternative NAD(P)H dehydrogenases and PCD

The permeabilization of the mitochondrial outer membrane and release of intermembrane pro-apoptotic molecules clearly places mitochondria in the centre of the execution of PCD (39). In recent years it has also become clear that components of the respiratory chain are also important regulators of cell death.

GRIM-19 (for genes associated with retinoid-IFN-induced mortality-19; also known as NDUFA13) possesses a dual function as a structural component of mitochondrial complex I and as a pro-apoptotic initiator in response to interferon-β and retinoic acid (263-265). It was later shown that apparently, not only GRIM-19 but also NDUFS3 from complex I and other components of the respiratory chain regulate interferon-β and retinoic acid-induced cell death by modulating ROS production and gene expression (266). Additionally, a 2.7-kilobase virally encoded RNA was demonstrated to protect cytomegalovirus-infected human cells from

rotenone-induced cell death by modulating the perinuclear relocalization of GRIM-19 (267). Importantly, GRIM-19 is involved in tumorigenesis (268). NDUFS3 was shown to be cleaved after lysine 56 specifically by granzyme A (and not by granzyme B), a cell death-inducing protease that is delivered by killer lymphocytes (cytotoxic T lymphocytes and natural killer cells) in order to eliminate cells that are targeted for destruction (269). Granzyme A is able to access the mitochondrial matrix and to interfere with the oxidation of NADH and generation of superoxide through the cleavage of NDUFS3. NDUFS1 is a critical mitochondrial substrate of caspases during apoptosis (270). Site-directed mutagenesis of the NDUFS1 cleavage site slows down the loss of the mitochondrial membrane potential ($\Delta\Psi m$), ATP levels, ROS accumulation and phosphatidylserine externalization. It was also shown that during apoptosis, the activity of caspase-3 specifically disrupts complexes I and II-mediated oxygen consumption and electron transport, leading to ROS generation and loss of $\Delta\Psi m$ (271). Silencing of *NDUFA6* induces apoptosis in HIV-1-infected cells (272).

Interestingly, it appears that, under caspase inhibition, the development of the cell death process is more associated with loss of respiration, particularly at the level of complexes I and IV, rather than with the release of apoptogenic molecules from the mitochondrion (273). Additionally, osteosarcoma cell lines devoid of mtDNA, and, consequently, of functional oxidative phosphorylation and $\Delta\Psi m$, are more resistant to staurosporine-induced cell death than their parental cells (274). The process seems to be controlled by the BCL-2 family anti-apoptotic member BCL-XL. The anti-apoptotic protein BCL-2 regulates cytochrome *c* oxidase activity, oxygen consumption and mitochondrial respiration in cancer cells (275). Complex II has been also studied as a mediator of cell death: the specific succinate:ubiquinone oxidoreductase activity of complex II (but not its activity as a succinate dehydrogenase) is hindered during apoptosis, resulting in the production of superoxide (276).

In *Caenorhabditis elegans*, a mitochondrial mutant of the Rieske iron-sulfur protein of complex III, defective in oxidative phosphorylation, displays increased resistance to hemiasterlin (277). In *N. crassa*, disruption of *nuo9.8*, *nuo14*, *nuo30.4* and *nuo51* (homologues of human *NDUFA1*, *GRIM-19*, *NDUFS3* and *NDUFV1*, respectively) leads to a high susceptibility to staurosporine (139). In contrast, loss of these genes as well as *nuo21*, *nuo21.3c* and *nuo78* (homologues

of human *NDUFS4*, *NDUFS8* and *NDUFS1*, respectively) confers increased resistance to phytosphingosine (113). In *C. albicans*, 10 out of 12 complex I mutants as well as a Δ*goa1* mutant with complex I dysfunction display hypersensitivity to fluconazole (278, 279). In *S. cerevisiae*, respiratory-deficient cells lacking mtDNA show increased resistance to acetic acid-induced apoptotic-like cell death (192). Also in yeast, a functional complex V is required for BAX-induced cell death (280). Interestingly, the BH3-like protein Bxi1 induces apoptotic death through the interaction with the mitochondrial carrier protein Mir1 and the core subunit of complex III Cor1 (191). Recently, it was shown that yeast complex III and cytochrome *c* are protective against hydrogen peroxide-induced cell death (281). In *N. crassa*, strains devoid of functional complex III are less sensitive than the wild type to the herbicide paraquat (149). Also, a strain with a point mutation in a valyl tRNA synthetase that leads to severe respiratory deficiency presents increased tolerance to hydrogen peroxide (147).

Remarkably, some works also point to a role of fungal alternative NAD(P)H dehydrogenases in cell death. In *S. cerevisiae*, overexpression of the internal Ndi1 (considered the yeast AMID homologue), but not of the external Nde1, leads to ROS-mediated apoptosis-like cell death, particularly in glucose-rich media (257). The authors showed that the disruption of both of these NADH dehydrogenases results in lower ROS production and increased chronological life span accompanied with reduced fitness. More recently, yeast Ndi1 was also shown to be involved in cell death induced by different stimuli like hydrogen peroxide, acetic acid and manganese, independently of its oxidoreductase activity (282). During the execution of manganese-induced cell death, a N'-terminal portion of Ndi1 is cleaved and the protein translocates to the cytoplasm. However, in sharp contrast, some reports show that the overexpression of yeast Ndi1 in human cell lines prevents rotenone- and paraquat-induced cell death (283, 284). The role of alternative NAD(P)H dehydrogenases in the protection or enhancement of ROS production is still uncertain, as different works report opposite observations (145, 250, 254, 255, 284-286).

In *N. crassa*, a double mutant devoid of NDE-1 and NDE-2 shows lower ROS production and increased catalase activity and resistance to paraquat (145). Particularly, NDE-2 appears to play a role in mitochondrial ROS generation. In *A. nidulans*, the expression of genes encoding NAD(P)H dehydrogenases are

induced upon exposure to different cell death stimuli, especially farnesol (138). Moreover, while the overexpression of NdiA augments the resistance to farnesol, the deletion of NdeA results in hypersensitivity to the drug. The latter is likely due to the observed increased accumulation of ROS in the presence of farnesol. As a complement to this information, reports in yeast show that a Δ*NDE1* knockout strain is more resistant to artemisinin and dimeric naphthoquinones (287, 288).

Despite the aforementioned controversy on the role of NAD(P)H dehydrogenases during oxidative stress, the current view, based on several works in different model organisms, is that these enzymes seem to be activated in conditions of excessive oxidative cellular environment, diverging electron transfer from the canonical respiratory chain pathway, thus avoiding an overflow of the system and deleterious ROS production (250, 285). Importantly, alternative NAD(P)H dehydrogenases are homologues of AIF-family proteins, such as AIF and AMID, well established as cell death executioners. Indeed, in *N. crassa*, analysis of gene expression profiles of alternative NAD(P)H dehydrogenases and AIF-like genes in simple, double and triple deletion strains for members of these families of genes showed that compensatory mechanisms occur (145, 148, 244). For instance, *ndi-1* is upregulated in a Δ*nde-1*Δ*nde-2* and in a Δ*nde2* strain, *amid* and *amid2* are upregulated in a triple Δ*ndi-1*Δ*nde-1*Δ*nde-2* mutant, *nde-1* is upregulated in Δ*nde-3* cells and *nde-2* is upregulated in Δ*ndi-1*, Δ*nde-1* and Δ*nde-3* single mutants. Thus, we sought to better understand the role of these enzymes during PCD in *N. crassa*.

1.4) Calcium in cell life and death

Introduction

Calcium (Ca^{2+}) is an ubiquitous and essential intracellular messenger in all organisms, from prokaryotes to humans. The ion binds to specific sequence regions of a diverse range of proteins, known as EF-hand or EF-hand-like domains, and promotes conformational and electrostatic alterations. These interactions modulate protein activity and contribute to a cascade of signaling events that ultimately defines a Ca^{2+}-mediated cellular response to a stimulus (289-292).

Excessive of defective levels of intracellular Ca^{2+} can be fatal and, therefore, the regulation of Ca^{2+} homeostasis is a complex and tightly controlled process, accomplished through a fine cooperation between different cellular compartments. In order to keep the adequate concentration of intracellular Ca^{2+}, cells chelate, compartmentalize or remove the ion using active (pumps and transporters) and passive (Ca^{2+}-binding proteins) systems (289-292). In fungi, the established resting concentration of cytosolic Ca^{2+} is 100-350 nM (293-295) whereas in animals it is 100-200 nM (296).

Cells mobilize Ca^{2+} to the cytosol via the opening of channels in the plasma membrane (for Ca^{2+} influx from the external medium) or in the membranes of organelles that act as intracellular stores. Upon a stimulus, intracellular Ca^{2+} signaling is mediated by a transient increase in the concentration of cytosolic Ca^{2+}. The progress of a Ca^{2+} transient through the cytoplasm is defined as a wave (297). The amplitude, propagation and duration of Ca^{2+} waves is stimulus-dependent (298). Because diffusion is not enough to propagate Ca^{2+} waves through the cytoplasm, after the initial stimulus-induced transient of Ca^{2+}, a phenomenon of Ca^{2+}-induced Ca^{2+} release from intracellular stores occurs (299): intracellular Ca^{2+} stores that are “caught” by the initial part of the Ca^{2+} wave respond by releasing their own Ca^{2+} that is also diffused, leading to the propagation of the signal. After the initiation and propagation of the Ca^{2+} waves, the cytosolic levels of the ion return to their resting state. This occurs thanks to the action of Ca^{2+} pumps and channels in the plasma membrane or in the membrane of intracellular organelles. Unique Ca^{2+}-signatures are associated with particular Ca^{2+} transients and encode information to the signaling machinery of the cell, leading to specific cellular responses (289-291, 297).

An outstanding variety of intracellular organelles are able to accumulate Ca^{2+} including the Golgi apparatus, endosomes, secretory granules, lysosomes and nuclei, though the classical Ca^{2+} storehouses are the ER, vacuoles and mitochondria (289-291). Remarkably, recent investigations have shed light on the molecular identity of the machinery responsible for the transport of Ca^{2+} into and from the mitochondria (reviewed in (300)). In mammalian cells, accumulation of Ca^{2+} by the mitochondrial matrix occurs mainly through the mitochondrial calcium uniporter (MCU) at the inner mitochondrial membrane, although there is some evidence indicating the presence of supplementary molecules with the ability to

move Ca^{2+} into the mitochondria, namely mRyR type 1, LETM1, and coenzyme Q10. The voltage-dependent anion-selective channels (VDACs) are also involved in Ca^{2+} transport across the outer mitochondrial membrane. Indeed, VDAC1 seems to be accountable for the mitochondrial import of cell death-related Ca^{2+} signals from the ER (301). In mammalian mitochondria, Ca^{2+} efflux may occur through the Na^{+}/Ca^{2+} exchanger (mNCX). Additionally, the unspecific aperture known as the permeability transition pore (mPTP) constitutes a rather non-physiological but possible alternative route of Ca^{2+} efflux by mitochondria (300). Within this organelle, Ca^{2+} is able to influence the metabolic state of the cells, primarily through the activation of enzymes involved in the Krebs cycle like pyruvate dehydrogenase, isocitrate dehydrogenase and oxoglutarate dehydrogenase (302, 303). This provokes a rise in NAD(P)H and consequently in oxidative phosphorylation. Another link between mitochondrial Ca^{2+} and metabolism was demonstrated in fungi and plants, in which external alternative NAD(P)H dehydrogenases are stimulated by Ca^{2+} (242, 304).

The best-studied Ca^{2+}-binding moiety of proteins is the classical EF-hand, a Ca^{2+}-interacting loop flanked by two helices. The loop contains active Ca^{2+}-binding glutamate and aspartate residues (305). However, there are variations to this motif, especially at the structural level, and it is now accepted that more than a dozen of different types of Ca^{2+}-binding domains exist (306). Particularly, several proteins were shown to hold a Dx[DN]xDG pattern, clearly distinct from the classical EF-hand because of the variability of structural contexts flanking the Ca^{2+}-binding region (307, 308). Though initially identified in bacteria (309), it was later perceived that this domain is widespread across all kingdoms (307, 308), including a fungal caleosin (308, 310) and a lectin from *Psathyrella velutina* (307, 311).

Genetically-encoded Ca^{2+} reporters are among the most reliable options for the study of intracellular Ca^{2+} dynamics and such a method was recently developed for filamentous fungi using a codon optimization strategy on the photoprotein aequorin from the jellyfish *Aequorea victoria* (312). More specifically, aequorin binds Ca^{2+} and, in the presence of the cofactor coelenterazine, the reaction leads to the formation of apoaequorin, carbon dioxide and coelenteramide. The energy from this reaction is released as blue light (313). The

rate of photon emission is proportional to the levels of Ca^{2+}, allowing the determination of Ca^{2+} concentrations.

Ca^{2+} in fungal life: its role in the biology of N. crassa and other fungi

N. crassa is a good model for the study of Ca^{2+} dynamics as its genome sequencing revealed a rich and versatile assortment of molecules involved in Ca^{2+} handling, including channels, pumps and signaling transducers (2, 28, 314, 315). So far, about 50 Ca^{2+}-binding proteins have been reported and a substantial fraction of them has been functionally studied (Table 5). The *N. crassa* signaling machinery apparently lacks recognizable receptors for ryanodine, cyclic ADP ribose and inositol-1,4,5-triphosphate (IP_3) (314, 315). Intriguingly, however, is the evidence that IP_3 is able to activate Ca^{2+} channels in *N. crassa* (10, 316) and that it is present in the lipid extract of *N. crassa* mycelia (317). The genome of *N. crassa* also seems to lack an extracellular Ca^{2+}-sensing receptor, as reported for animals (318) and plants (319). On the other hand, *N. crassa* possesses Ca^{2+}/Na^{+} and Ca^{2+}/H^{+} exchangers whereas these groups of proteins are mutually exclusive in animals and plants (314, 315). Importantly, since a substantial fraction of the genome remains to be characterized, additional members of Ca^{2+} machinery may exist.

Table 5 - Ca^{2+} handling machinery of *N. crassa*.

Type of protein	Brief description	Gene	Protein
Ca^{2+}-permeable channel	Ca^{2+} channel proteins are responsible for the transport of Ca^{2+} across cell membranes, both in the plasma membrane or in intracellular organelles.	NCU02762	CCH-1
		NCU06703	MID-1
		NCU02219	FIG-1
		NCU11680	YVC-1
Ca^{2+}- and cation-ATPase	Ca^{2+}- and cation-ATPases hydrolyze ATP to catalyse the active pumping of Ca^{2+} across biological membranes, reducing $[Ca^{2+}]_c$.	NCU03305	NCA-1
		NCU04736	NCA-2
		NCU05154	NCA-3; TRM-9
		NCU03292	PMR-1
		NCU08147	PH-7; ENA-2
		NCU04898	
		NCU03818	
		NCU05046	ENA-1
		NCU07966	TRM-1
		NCU10143	

Ca^{2+}/H+ exchanger	Ca^{2+}-exchangers exchange positive ions across membranes to reduce $[Ca^{2+}]_c$ to resting levels, transporting Ca^{2+} into intracellular Ca^{2+}-stores or out of the cell. In *N. crassa* data suggests that the ATP-driven Ca^{2+}/H^+ exchange system has a stoichiometric ratio of at least $Ca^{2+}/2H^+$ (294), while the stoichiometry for Ca^{2+}/Na^+ exchangers is not known.	NCU07075	CAX
		NCU00916	TRM-15
		NCU00795	TRM-14
		NCU06366	TRM-18
		NCU07711	
		NCU05360	
Ca^{2+}/Na+ exchanger		NCU02826	TRM-16
		NCU08490	TRM-20
Phospholipase C (δ-type)	Phospolipase C converts the plasma membrane phospholipid phosphatidylinositol-4,5-bisphosphate (PIP_2) into the second messengers inositol-1,4,5-trisphosphate (IP_3) and 1,2-diacylglycerol (DAG).	NCU06245	PLC-1
		NCU01266	PLC-2
		NCU11415	PLC-3
		NCU02175	PLC-4
Calmodulin	Several Ca^{2+}- and/or calmodulin-binding proteins have been reported in *N. crassa*, with several distinct functions during Ca^{2+}-mediated signaling.	NCU04120	CMD-1
Calcineurin catalytic subunit		NCU03804	CNA-1
Calcineurin catalytic subunit/variant		NCU03833	CNB-1
Calnexin/calreticulin		NCU09265	
Calpactin I heavy chain		NCU04421	ANX-14
Other Ca^{2+}- and/or calmodulin-binding proteins		NCU05225	NDE-1
		NCU02115	
		NCU01564	MIC-4
		NCU06948	
		NCU04379	CSE-1; NCS-1
		NCU02738	PEF-1
		NCU09871	
		NCU01241	
		NCU06347	
		NCU06617	
		NCU03750	
		NCU02283	CAMK-2
		NCU09123	CAMK-1
		NCU02814	PRD-4
		NCU09212	CAMK-4
		NCU06650	
		NCU02411	
		NCU06177	CAMK-3
		NCU04265	INV
		NCU00914	STK-16

Compiled from references (314, 315). Some of these proteins have not been functional confirmed for their Ca^{2+}-binding role.

In tip-growing organisms like *N. crassa*, Ca^{2+} is important for polarized growth. Hyphal growth has been reported to rely on a tip-high Ca^{2+}

gradient not maintained by extracellular Ca^{2+} influx (320), but internally derived by means of IP_3-activated Ca^{2+} channels (9-11). Evidence has been obtained that IP_3 is generated by a stretch-activated tip-localized phospholipase C which senses tension due to hyphal expansion and converts phosphatidylinositol-4,5-bisphosphate (PIP_2) to IP_3 and diacylglycerol (DAG) (10, 11). IP_3 promotes the release of Ca^{2+} through a large conductance channel associated with the vacuolar membrane (10, 316) and a small conductance channel associated with the ER/Golgi body system-derived vesicles that accumulate near the hyphal tip (10). Only the latter is believed to be involved in the generation of the tip-high Ca^{2+} gradient (10, 321). The accumulation of Ca^{2+}-containing mitochondria at the tip of hyphae is significant for the maintenance of a Ca^{2+}-gradient required for the cells to grow (322). The existence of a continuous tip-high Ca^{2+} gradient in growing hyphae has recently been challenged (323). In this study, imaging of calcium using a genetically encoded calcium reporter expressed in Fusarium and Magnaporthe demonstrated that calcium spikes with an irregular frequency occur in growing hyphal tips, with the result that the tip-focused gradient appears and disappears in hyphae extending at constant rates.

N. crassa possesses four δ-type phospholipase C molecules (314, 315) with conserved domains (Fig. 16). The disruption of *plc-1* leads to slow growth and aberrant branching (“spreading colonial” growth), although the gene is not required for polar growth at the tip (324). Silverman-Gavrila and Lew showed that the incubation with phospholipase C inhibitors results in reduced or stopped hyphal extension (10). Additionally, sequencing of *plc-1* and polymorphism analysis in wild isolates of *N. crassa* revealed a high natural variability (324). Regarding phospholipase C signaling, it is important to mention that this pathway, in mammalian cells, is the main modulator of transient receptor potential (TRP) channels, which are permeable to Ca^{2+}. The TRP channel family comprises several subfamilies: classical (TRPC), vanilloid (TRPV), melastatin (TRPM), polycystin (TRPP), mucolipin (TRPML) and ankyrin (TRPA) (325). In *N. crassa*, the only known TRP-type channel is YVC-1 (315). In Saccharomyces, the homologue of YVC-1 is localized in the vacuolar membrane and is involved in the release of Ca^{2+} to the cytosol (326) after activation by stretch (327) and PIP_2 (328). Recently, an *in silico* genomic analysis identified additional TRP channel

homologues in some fungal pathogens such as Aspergillus, Saccharomyces, Candida and Cryptococcus (329).

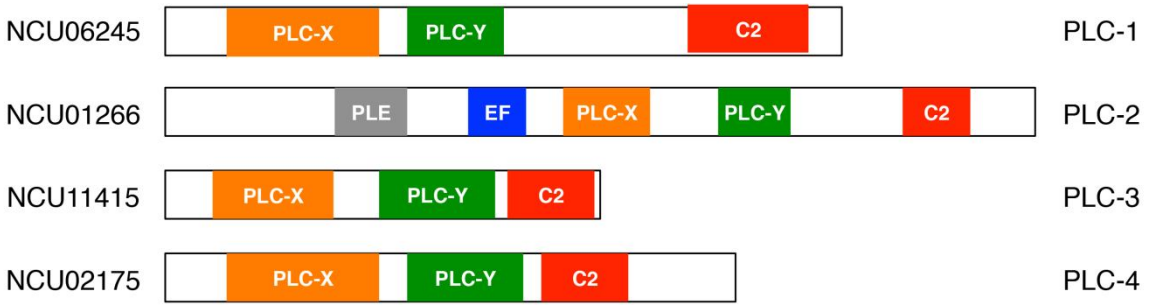

Figure 16 - Domain organization of the four phospolipase C proteins encoded by the *N. crassa* genome.
PLC-X: Phospholipase C, phosphatidylinositol-specific, X domain; PLC-Y: Phospholipase C, phosphatidylinositol-specific, Y domain; C2: C2 Ca^{2+}-dependent membrane targeting domain or C2 Ca^{2+}-/lipid- binding domain; PLE: Pleckstrin homology domain; EF: EF-hand domain.

Besides its role in tip growth, the fungal Ca^{2+}-signaling machinery has been shown to be important for diverse processes, including virulence, circadian rhythms, nutrient sensing, cell wall regeneration, chemotropic interaction and cell death (330). Some examples are presented here in order to illustrate this diversity of roles. The Ca^{2+}-ATPase Pmr1 is required for proper protein glycosylation and polarized actin distribution, affecting polarized cell growth and cytokinesis in *S. pombe* (331). The Ca^{2+} transporter PmcA of *A. fumigatus* is essential for fungal infection through an interaction with the calcineurin signaling pathway (332). Similarly, the *C. neoformans* Ca^{2+}/H^{+} exchanger Vcx1 is involved in virulence (333). The phospholipase C MoPLC1 of *Magnaporthe oryzae* is required for appressorium formation and pathogenicity (334). *N. crassa* CSE1 is important for germling communication and fusion (335). In *Beauveria bassiana*, an entomopathogenic fungus, the CSE1 homologue Bbcsa1 is necessary for early penetration steps during host infection (336). Disruption of FIG1 from *F. graminearum* leads to a complete arrest of pertithecia formation, indicating a role in sexual development (337). Cch1 and Mid1 are involved in ascospore discharge in *Giberella zeae* (338) and deletion of *mid1* causes loss of virulence in *Claviceps purpurea* (339). In *S. cerevisiae*, Mid1 is required for Ca^{2+} influx during mating (340).

The *cch-1* and *mid-1* genes are present in several different fungi and represent two of the best-studied components of the Ca^{2+}-handling machinery. Ca^{2+} uptake from the extracellular milieu may occur through different mechanisms, depending on the stimulus. The high-affinity Ca^{2+} uptake system (HACS) is the best described. It comprises the channel Cch1 and the regulatory proteins Mid1 and Ecm7 (341, 342). The exact role of MID-1 is unclear, as the protein has also been reported to behave as a non-selective stretch-activated cation channel in some systems (343, 344). The HACS seems to be particularly active in minimal media, whereas the low-affinity Ca^{2+} system (LACS) is more active in nutrient-rich media (342). So far, the only known member of the LACS system is the Fig1 channel, which is involved in mating (337, 345). A glucose-induced Ca^{2+} influx system was recently proposed (346) but its molecular components are unknown.

In fungi, particularly in *N. crassa*, the vacuole seems to be the major intracellular Ca^{2+} storage organelle (347). Indeed, using a cell fractionation strategy, Bowman and colleagues estimated that 10% of the cell Ca^{2+} was present in a pellet containing cell walls and unbroken cells, while the remainder 90% was distributed in three separate cell fractions: a dense organelle fraction containing mainly mitochondria and vacuoles and representing approximately 10% of the cell Ca^{2+}; a heterogeneous microsomal fraction including ER, Golgi apparatus, nuclei, plasma membranes and transport vesicles with approximately 40% of the cell Ca^{2+}; and a high-speed supernatant fraction, likely comprising broken vacuoles, also with approximately 40% of the cell Ca^{2+}. Mitochondria were estimated to contain about 4% of the cellular Ca^{2+}, whereas the ER appears to contain little Ca^{2+}, supporting the idea that the vacuoles are indeed the main intracellular Ca^{2+} reservoir (347). Indeed, an early work on *N. crassa* Ca^{2+} biology reported that the vacuoles are the organelles responsible for sequestering excess amounts of cytosolic free Ca^{2+}, likely coupled to the activity of a H^+/ATPase (348). A recent work proposed that cell wall-bound Ca^{2+} constitutes 25% of total mycelia Ca^{2+} in *N. crassa* (349).

Ca^{2+} in fungal death: its role during fungal PCD

Ca^{2+} and cell death are intimately connected, especially because of the vital role of Ca^{2+} as an intracellular messenger affecting numerous signaling pathways that determine cell fate. Therefore, it is not surprising that cells commonly respond to cell death stimuli with flutuations in the intracellular levels of this divalent ion. Despite intensive research on the "double-edged sword" nature of Ca^{2+}, the protective *versus* toxic role of the ion regarding cell death stimulation is still under debate. On the one hand, transient or stable modifications in the cytosolic levels of Ca^{2+} can operate as survival signals, leading to the activity of anti-death proteins or stimulating transcriptional defence responses. Indeed, a mechanism known as store-operated Ca^{2+} entry (SOCE, also designated capacitative Ca^{2+} entry) occurs in the cells (350). In response to Ca^{2+} depletion in intracellular stores, namely in the ER, cells activate plasma membrane channels that promote Ca^{2+} influx from the external medium, which is then used to refill the intracellular organelles and restore the homeostatic levels of the ion. This represents one of the Ca^{2+}-mediated cell survival systems.

On the other hand, the loss of Ca^{2+} homeostasis can behave as a pro-death signal, since overload or a simple perturbation of the distribution of the ion within storage organelles is sufficient to trigger cell death in some systems (292, 350). A paradigmatic example of cell damage due to Ca^{2+} overload is well patent in the mitochondrial response when its Ca^{2+} levels exceed the physiological threshold (351). Mitochondria possess low affinity Ca^{2+} uniporters that allow the accumulation of large amount of Ca^{2+} within their matrix, representing a high capacity of Ca^{2+} storage. Mitochondrial Ca^{2+} uptake regulates several functions, including oxidative metabolism. However, if the amount of sequestered Ca^{2+} exceeds the mitochondrial capacity, the organelle collapses through the opening of the megachannel known as the mitochondrial permeability transition pore (mPTP). The mPTP releases the excess Ca^{2+} but also apoptogenic molecules such as cytochrome *c*, triggering the apoptotic cascade. Recently, the mPTP was shown to be composed by dimers of the mitochondrial ATP synthase (352). Another good example of a pro-death role of Ca^{2+} is imaged in the activation of the calpain-mediated proteolysis of the apoptosis effector AIF (353).

In yeast species like *S. cerevisiae*, *C. albicans* and *C. neoformans*, cytosolic Ca^{2+} increases are a common feature of the cellular response to a number of antifungal stresses (354), including pheromone (355), the plant essential oils carvacrol (356) and eugenol (357), amiodarone (355, 358) and ER stress-inducing agents like tunicamycin and azole drugs (341, 359), just to enumerate a few examples. In *N. crassa*, a rise in the cytosolic levels of Ca^{2+} was associated with cell death induced by chitosan (121), PAF (126) and PAF26 (142).

2. Materials and methods

Strains, culture media and chemicals

Standard procedures for the handling of *N. crassa* cells were employed (360). Cells were grown in Vogel's MM plus 1.5% (w/v) sucrose (13). Agar at 1.5% (w/v) concentration was added to obtain solid medium. Conidia were harvested by the addition of sterile $_{d}$H2O, agitation and filtration through cheesecloth in 7-day cultures on Vogel's MM with agar at 26ºC. Wild type (FGSC 2489), wild isolates and other strains are available from the Fungal Genetics Stock Center (31) or were previously generated in the laboratory and described: deletion strains for alternative NAD(P)H dehydrogenases (240, 242-244), *nuo51* (361) *nuo14* (226), *nuo78* (362) and the *nuo51*-expressing strains nuo51 rescue, nuo51 A353V and nuo51 T435M (232). The strains used for the genome-wide association study were collected in Louisiana, USA and described in (335). *A. fumigatus* ATCC 46645 and *C. albicans* SC5314 strains were used in some experiments. For *A. fumigatus*, after 5 days of growth in Saboraud's glucose agar at 37ºC, spore suspensions were obtained by gentle agitation with 0.01% (v/v) Tween 80 in sterile $_{d}$H2O and filtration through cheesecloth. For *C. albicans*, the cells were incubated in yeast Winge liquid medium at 30°C, agitated at 200 rpm overnight, harvested by centrifugation, and resuspended in phosphate-buffered saline (PBS).

For experiments employing culture medium without or with excess levels of Ca^{2+}, calcium chloride ($CaCl_2$) was omitted from the Vogel's stock solution and, when adequate, added before the experiment. For these experiments the concentration of KH_2PO_4 in the 50x Vogel's stock solution was limited to 10 mM to avoid precipitation with supplemental calcium (126).

The following chemicals were used: staurosporine (LC Laboratories), dimethyl sulfoxide (DMSO), hydrogen peroxide, cinnamic acid, amphotericin B, A23187 (calcimycin), ML204, flufenamic acid, xestospongin C, calcium chloride, sodium chloride, rotenone, oxaloacetic acid, antimycin A, potassium cyanide, oligomycin, carbonyl cyanide m-chlorophenylhydrazone (CCCP), diphenyleneiodonium (DPI), GSH and NAC (Sigma-Aldrich), 1,2-bis(ortho-aminophenoxy)ethane-N,N,N',N'-tetrasodium (BAPTA), thapsigargin, Ru360, lithium chloride ($LiCl_2$) and UCN-01 (Merck Biochemicals), phytosphingosine

(Avanti Polar Lipids), 4-methyl-4'-[3,5-bis(trifluoromethyl)-1H-pyrazol-1-yl]-1,2,3-thiadiazole-5-carboxanilide (YM-58483 / BTP2) and 2-aminoethoxydiphenyl borate (2-APB) (Tocris Bioscience), 1-[6-((17β-3-methoxyestra-1,3,5(10)-trien-17-yl)amino)hexyl]-1H-pyrrole-2,5-dione (U-73122) (Alexis Biochemicals) and bafilomycin A1 (Wako). At least three independent experiments were performed for each assay.

Growth assays

Hyphal growth at 26ºC was obtained by measuring colony elongation over time after the inoculation of 20 µl with $5x10^4$ conidia on the center of a large Petri dish (14.2 cm diameter) containing solid Vogel's MM. In some experiments, hyphal growth throughout time was measured after inoculation of the same concentration of conidia in glass race tubes.

For growth assessment in liquid Vogel's MM, $1x10^4$ conidia/ml were incubated at 26ºC, 100 rpm, under constant light in 96-well plates (200 µl/well). Absorbance at 620 nm (126) or 450 nm (363) was followed during 24 hours and the percentage of growth for each condition *versus* the control was calculated. Micrographs were taken on an Olympus CKX41 inverted microscope with Hoffman optics and the percentage of germinated cells was calculated using ImageJ (NIH).

Cell death assays

For the spot assay, nine serial three-fold dilutions were prepared for each strain starting with 6.6×10^7 cells/ml, so that the last spot contained approximately 50 conidia. Five µl from each dilution were spotted separately on plates containing glucose-fructose-sorbose medium with agar (GFS) (360) supplemented with the appropriate chemicals. Cells were incubated at 26ºC (37ºC for *A. fumigatus*) and pictures taken ~72 hours after inoculation. Sabouraud medium was used for *A. fumigatus* and *C. albicans*.

The levels of cell death were determined by flow cytometry after staining cells with YOPRO-1 (Life Technologies) or propidium iodide (PI, Sigma-Aldrich). An inoculum of $1x10^6$ conidia/ml was incubated for 4 hours in the indicated medium at 26ºC (140 rpm, constant light). Staurosporine was added and growth resumed for further 2 hours. The cells were harvested by centrifugation, washed

twice with PBS and incubated with 0.1 µM YOPRO-1 (samples were kept 20 minutes on ice before reading) or 2 µg/ml PI (samples were read immediately). For each experiment and strain a control without staining was prepared to define autofluorescence. When indicated, a pre-treatment of 15 minutes was applied to the cells before the addition of staurosporine. Samples were read in a BD FACS Calibur or a Beckman-Coulter EPICS XL-MCL and data analyzed with FlowJo (Tree Star).

For the microscopic evaluation of PI uptake, conidia at $2x10^6$ cells/ml were grown on 8-well microscope chambers (26ºC, dark, no agitation) and stained with 5 µg/ml PI to examine cell membrane rupture. After 6 hours of growth, 50 µM staurosporine or DMSO was applied and differential interference contrast and fluorescence micrographs taken at determined time points using a Nikon TE2000 microscope (Chroma filter set: excitation 535/50 nm, 565 nm LP dichroic mirror, emission 590 nm LP). The percentage of PI-positive cells was quantified using ImageJ (NIH).

ROS, mitochondrial mass and membrane potential and cell viability assays

The production of ROS was measured using the fluorescent probe dihydrorhodamine 123 (Sigma-Aldrich). After growing $1x10^6$ conidia/ml for 4 hours in the indicated medium at 26ºC, 20 µg/ml dihydrorhodamine 123 and staurosporine were added for further 30 minutes. Samples were harvested by centrifugation and washed twice with PBS before being resuspended in PBS.

Mitochondrial mass was measured with nonyl acridine orange (Promokine). Conidia at $1x10^6$ cells/ml were grown for 30 minutes in Vogel's MM, treated with staurosporine and cultured for 2 further hours. Cells were washed twice with PBS and incubated with 5 µM nonyl acridine orange for 15 minutes at room temperature.

The mitochondrial membrane potential was determined using MitoTracker Red (CMXRos, Life Technologies). Conidia at $1x10^6$ cells/ml were grown for 2 hours in Vogel's MM at 26ºC and treated for 2 further hours with staurosporine. MitoTracker Red at 250 nM was added in the last 30 minutes of culture. Samples were harvested by centrifugation and washed twice with PBS before being resuspended in PBS.

Cell viability was assessed using the fluorescent probe fluorescein diacetate (FDA, Sigma-Aldrich). Conidia at $1x10^6$ cells/ml were grown for 1 hour in Vogel's MM, treated with staurosporine and cultured for 4 further hours. Cells were washed twice with PBS and incubated with 2 µg/ml FDA for 15 minutes at room temperature.

For each experiment and strain a control without staining was prepared to define autofluorescence. When indicated, a pre-treatment of 15 minutes was applied to the cells before the addition of staurosporine. Samples were read in a BD FACS Calibur or a Beckman-Coulter EPICS XL-MCL and data analyzed with FlowJo (Tree Star).

Intracellular Ca^{2+} measurement with aequorin

Genetically-encoded Ca^{2+} reporters are the most reliable option for the study of intracellular Ca^{2+} dynamics and such a method was recently developed for filamentous fungi using a codon optimization strategy on the photoprotein aequorin (312). The pAB19 vector containing the gene encoding aequorin was used to transform *N. crassa* cells by electroporation with an Eppendorf Multiporator (1800 V, 5 ms). Aequorin-expressing conidia were obtained and incubated at a concentration of $2x10^6$ cells/ml with 5 µM coelenterazine (Santa Cruz Biotechnology) in Vogel's MM. Aliquots of 100 µl were added to each well of white opaque 96-well plates and incubated for 6 hours at 26ºC, in the dark without agitation. Then, emitted luminescence (RLU, relative light units) was captured throughout time on a Bio-Tek Synergy HT microplate reader. Triplicate to hexaplicate experiments were performed. Due to equipment constraints, we were unable to convert luminescence data to Ca^{2+} concentrations. Therefore, a normalization of the results was performed to allow comparisons between different experiments. The maximum levels of aequorin expression for each strain in each experiment were determined in extra wells of the 96-well plates. One-hundred µl of 3M $CaCl_2$ in 20% ethanol were pipetted to each well and luminescence was acquired for 3 minutes. This total emitted luminescence was used to normalize the experimental RLU for each strain in each experiment and the obtained values were summed to calculate the area under the curve ("area"). The values from staurosporine-treated samples were subtracted by the values of control samples to

obtain the “staurosporine-induced amplitude of response”. When specified, a pre-incubation step of 15 minutes with a chemical stimulus was applied before staurosporine (or DMSO). In all instances, the volume of chemical added to the wells was 10 µl (from an appropriate stock solution), to ensure good homogenization. The curves presented here correspond to the average of at least three independent experiments. The typical staurosporine-induced Ca^{2+} signature of wild type cells was obtained from 30 independent experiments.

Transmission electron microscopy of pyroantimonate staining of Ca^{2+}

Conidial cultures of $2x10^6$ cells/ml were incubated without agitation for 6 hours, in the dark, at 26ºC, followed by the indicated treatments and time. Cells were collected by centrifugation (5000 rpm, 10 minutes), washed twice with 0.2M phosphate buffer, resuspended in fixative solution (2.5% glutaraldehyde, 0.1M phosphate buffer) and incubated overnight at room temperature. After pelleting by centrifugation and resuspending in 0.2 M phosphate buffer, samples were washed during 2 hours with the same buffer changing it twice. The samples were further washed 3 times for 10 minutes with $_dH2O$ and mixed with a 2% (w/v) osmium tetroxide, 2% (w/v) potassium pyroantimonate solution for 2 hours. After centrifugation, 50% ethanol was mixed for 15 minutes and then 75% ethanol for 30 minutes. This procedure was repeated for 90%, 95% and twice for 100% ethanol. After washing twice for 15 minutes with propylene oxide, the samples were infiltrated with propylene oxide:epon resin with increasing concentrations of epon (3:1, 1:1 and 1:3) for 1 hour each and finally embedded in epon for 15 minutes at 60ºC. The inclusion was performed placing the sample in embedding molds with epon and incubating for 2 to 3 days at 60ºC for polymerization. Ultrathin section with 70 nm were made using a diamond knife, collected in 300 mesh copper grids and stained with 3% aqueous solution of uranyl acetate and lead citrate (or uranyl acetate alone) for 10 minutes. The grids were observed in a JEOL100 CX II electron microscope, operated at 60 kV.

Semi-quantitative real time PCR (qRT-PCR)

Conidia at a concentration of $1x10^6$ cells/ml were grown in Vogel’s MM for 5 hours at 30ºC followed by the addition of staurosporine or DMSO and grown for

one more hour. Cells were harvested by centrifugation (5000 rpm, 5 minutes) and RNA isolation was performed using a PureLink RNA Mini kit (Life Technologies) or a ZR Fungal/Bacterial RNA MicroPrep kit (Zymo Research), according to the manufacturer's protocol. One µg of RNA was used for cDNA preparation using the SuperScript First-Strand Synthesis System kit (Life Technologies) following the provided protocol. A mix containing SYBR Green (Bio-Rad) and specific primers (*czt-1* FW: GGTGACAACGACGACGAGATGG; *czt-1* RV: GAGTCCTGGTTAGTTCGCTTACGG; *actin* FW: GGCATCACACCTTCTACAACGAG; *actin* RV: ATGTCAACACGGGCAATGGC) was prepared and amplification done with a Bio-Rad iCycler iQ5. Triplicates were obtained in each experiment and threshold cycle values within an interval of ± 0.5 cycle in the same experiment were accepted. Relative gene expression was determined by the $2^{-\Delta\Delta Ct}$ method (364). For the quantifications, *actin* (NCU04173) was used as control and cDNA from the wild type strain not exposed to staurosporine as calibrator. For the time-course analysis of the basal expression of *czt-1* during germination, no calibrator was used and gene expression calculated using $2^{-\Delta Ct}$.

Protein sequence analysis

The following bioinformatics tools were employed for alignments, domain prediction, subcellular localization prediction, phylogenetic tree building and Ca^{2+}-binding motifs prediction: NCBI BLAST (365), NCBI PSI-BLAST (366), ClustalW2 (367), InterProScan (368), MEMSAT3 (369), TMHMM (370), WoLF PSORT (371), Mega5 (213) and CaPS (305). Protein sequences were obtained through available databases: Broad Institute *Neurospora crassa* Database (http://www.broadinstitute.org/annotation/genome/neurospora/MultiHome.html), *MIPS Neurospora* crassa Genome Database (mips.helmholtz-muenchen.de/genre/proj/ncrassa/) and UniProt (http://www.uniprot.org/).

Statistical analysis

Statistical analysis of the data was performed using SPSS 20 (SPSS Inc.). The non-parametric Mann-Whitney test was used for comparisons between two groups. P-values ≤ 0.05 were considered statistically significant.

High-throughput RNA sequencing (RNA-seq)

Conidial suspensions at $1x10^6$ cells/ml were incubated in Vogel's MM for 6 hours (26ºC, 140 rpm, constant light) followed by the addition of staurosporine (or DMSO) for 1 more hour. Cells were harvested using 0.45 µm filters and immediately frozen in liquid nitrogen. Total RNA was isolated by the Trizol-Phenol-Chloroform method. After digestion of 25 µg RNA with TURBO DNAse (Life Technologies), mRNA was purified using Dynabeads oligo(dT) magnetic beads (Life Technologies). The mRNA was chemically fragmented using the Ambion RNA fragmentation kit (Life Technologies). First and second strand cDNA synthesis was achieved using appropriate kits (Life Technologies). The illumina TruSeq kit was employed to generate the cDNA libraries with indexing adapters essentially following the manufacturer's protocol. After purification of the libraries with AMPure XP beads (Roche), the quality of the libraries was analyzed in a Agilent 2100 Bioanalyzer. The cDNA libraries were sequenced in a illumina HiSeq2000 and single reads of 50 bp were obtained. Sequencing data was handled essentially with Tophat, Cufflinks and Cuffdiff (372). Expression levels are presented as Fragments/Reads Per Kilobase of transcript per Million mapped reads (FPKM/RPKM). The resulting datasets are available at the NCBI GEO database (http://www.ncbi.nlm.nih.gov/geo/; series record: GSE52153 and GSE53013). CummeRbund (372) was used to generate scatter and volcano plots. Functional enrichment of sets of genes was assessed with FunCat (373).

Single nucleotide polymorphism (SNP) identification

Maq (374) was used to map RNA-seq reads to the genome sequence of N. crassa strain FGSC 2489 (28) and for the identification of SNPs. RNA-seq reads that mapped to multiple locations or SNPs located in regions of low consensus read quality were eliminated from analysis. Only those that were bi-allelic were retained, yielding a complete data set of $1.09x10^6$ SNPs. The complete SNP set used in this analysis was previously published (335). For markers used as input into calculations of genetic association with the staurosporine resistance phenotype, we filtered the complete SNP set to retain only sites at which the minor allele was present at >10% frequency.

Genome-wide association study

The expression level of *czt-1* from the Louisiana population of N. crassa wild strains (335, 375) was used as a quantitative proxy for staurosporine resistance (please see Results for details). For each strain, the normalized expression level of *czt-1* (as RPKMs) was compared to the mean for all strains. A strain showing higher than average expression of *czt-1* (46 strains) was considered to have “high” expression of *czt-1* and was binned as more resistant to staurosporine. Conversely, a strain showing lower than average expression of *czt-1* (67 strains) was considered to have “low” expression of *czt-1* and was binned as less resistant to staurosporine. Each SNP marker was then tested in turn, from our set of SNPs with >10% minor allele frequency, for co-inheritance with qualitative determination of “highscore” using Fisher's exact test. Significance values were determined using an empirical null distribution of p-values from the observed data. For this, we performed 1000 permutations. For each permutation, the phenotype category was shuffled relative to the genotypes and the minimum p-value was retained. Any nominal p-value larger than a minimum observed permuted p-value was considered as a possible false positive and removed from consideration.

3. Results

3.1) Staurosporine-induced cell death is accompanied by a dynamic transcriptional response in *N. crassa*

Staurosporine induces metacaspase-independent cell death in N. crassa

Staurosporine induced cell death in *N. crassa* accompanied by typical cellular features such as increased staining with propidium iodide (PI) and YOPRO-1 (Fig. 17A-B and (114)), decreased staining with fluorescein diacetate staining (Fig. 18A) and colony forming ability (139), increased ROS production (Fig. 18B and (139)), loss of ΔΨm (Fig. 18C), mitochondrial mass reduction (Fig. 18D), impaired germination, DNA fragmentation as assessed by TUNEL staining (140), and GSH export (114).

We tested whether staurosporine-induced cell death in *N. crassa* is dependent on the presence of metacaspases. The genome of *N. crassa* encodes two metacaspases, MCA-1A (NCU09882) and MCA-1B (NCU02400). Both the evaluation by YOPRO-1 staining (Fig. 17C) and by the spot assay (Fig. 17D) revealed that the levels of staurosporine-induced cell death in wild type cells and in cells lacking one or both metacaspases were similar. The metacaspases mutants were also tested for sensitivity to other cell death stimuli, more specifically phytosphingosine, hydrogen peroxide and actinomycin D. Despite a slight increased resistance of the Δ*mca-1B* and Δ*mca-1A*Δ*mca-1B* strains to hydrogen peroxide, the overall conclusion is that all these stimuli appear to inhibit the growth of *N. crassa* independently of the action of metacaspases (Fig. 17D).

In order to investigate the relevance of the increased ROS production upon exposure to staurosporine, we measured cell death in cells pre-incubated with the ROS scavenger NAC. NAC protected cells from staurosporine-induced cell death, as evaluated by YOPRO-1 staining (Fig. 19A) and spot assay (Fig. 19B). This

indicates that the production of ROS is necessary for staurosporine-induced cell death.

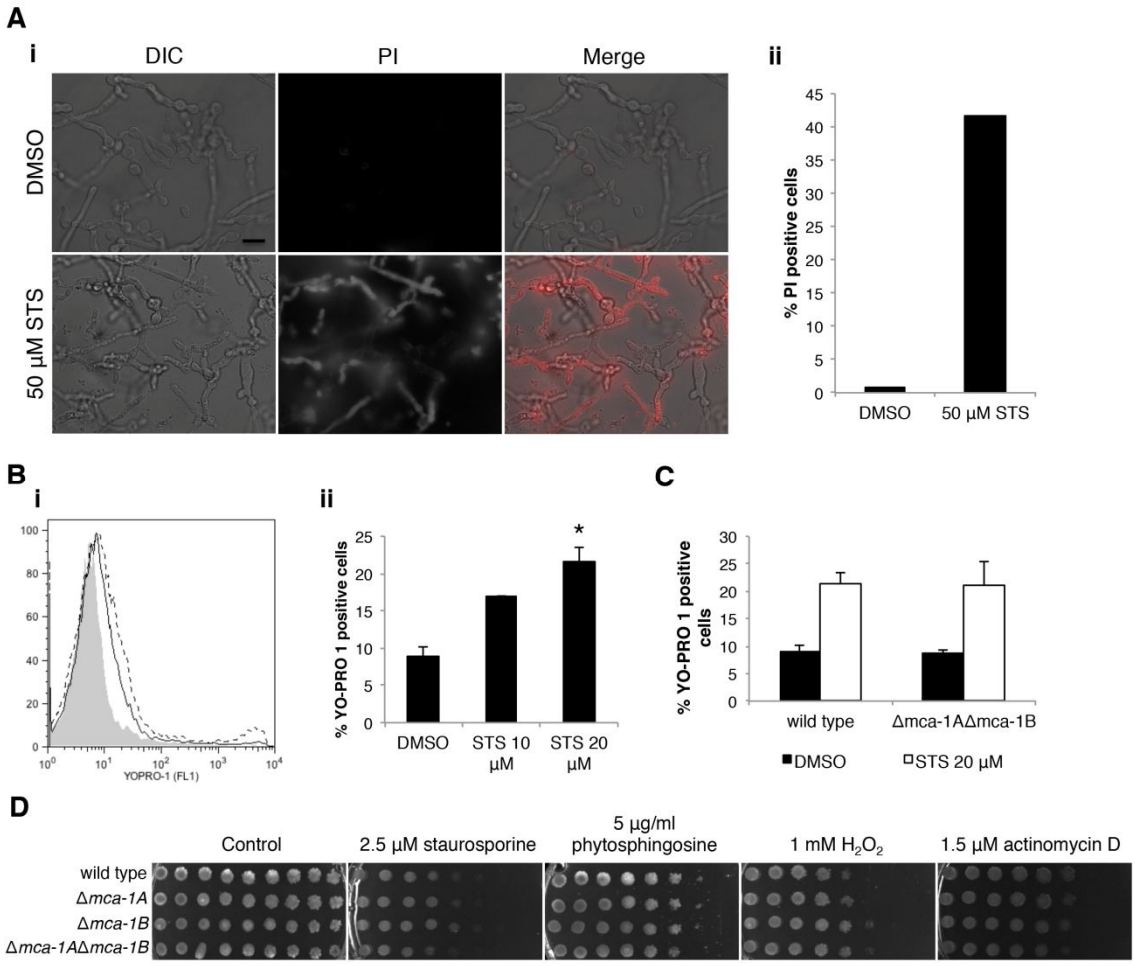

Figure 17 - Staurosporine induces metacaspase-independent cell death in *N. crassa*.
A- Permeability to PI was analyzed microscopically after treatment with 50 µM staurosporine (STS). The left panel (i) shows representative micrographs whereas the right panel (ii) displays the percentage of PI-positive cells after 16 hours of treatment. Scale bar: 50 µm. B- YOPRO-1 uptake was evaluated by flow cytometry. The left panel (i) shows a representative histogram: DMSO (shadowed), 10 µM (solid line) and 20 µM STS (dashed line). Quantifications of YOPRO-1-positive cells are shown in the right panel (ii). C- YOPRO-1 staining was assessed in 20 µM STS-treated wild type cells and in cells lacking both *N. crassa* metacaspases (Δ*mca-1A*Δ*mca-1B*). D- The sensitivity to staurosporine, phytosphingosine, hydrogen peroxide (H_2O_2) and actinomycin D of wild type, Δ*mca-1A*, Δ*mca-1B* and Δ*mca-1A*Δ*mca-1B* strains was evaluated by spotting conidia in GFS supplemented with the indicated concentrations of drugs.

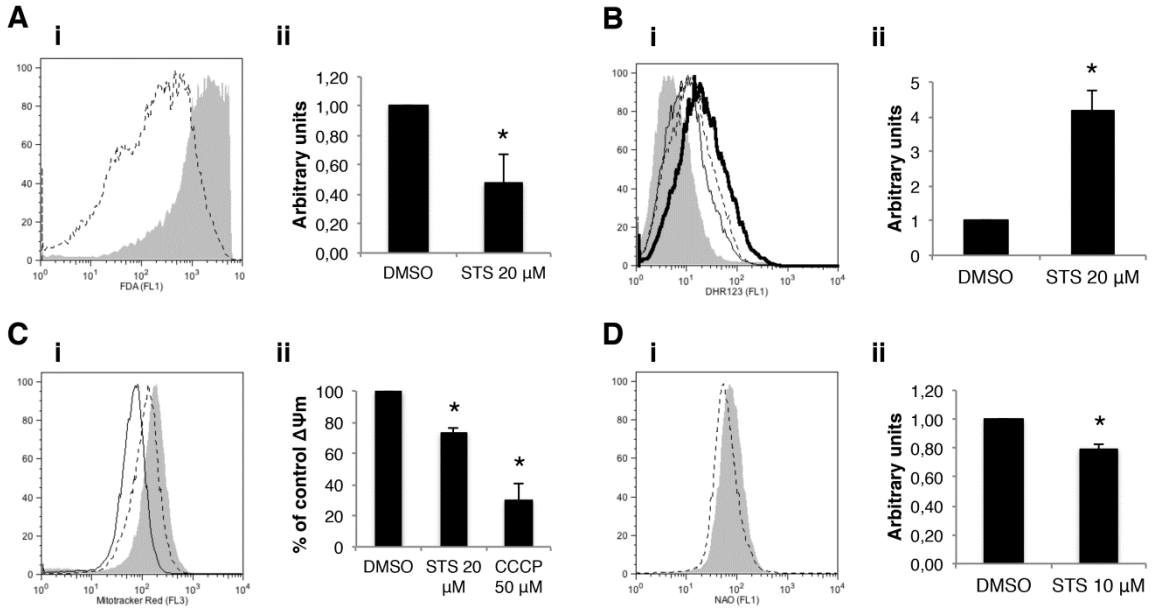

Figure 18 - Staurosporine leads to loss of viability, increased ROS production, loss of mitochondrial membrane potential and reduced mitochondrial mass.

In A-D, left panels (i) shows a representative flow cytometry histogram and right panels (ii) the respective quantification. A- Cell viability was evaluated by measuring loss of staining with fluorescein diacetate in 20 µM staurosporine (STS)-treated wild type cells. (i) DMSO (shadowed); 20 µM STS (dashed line). B- ROS production was assessed by dihydrorhodamine 123 staining. (i) DMSO (shadowed); 20 µM STS for 5 minutes (thin solid line); 20 µM STS for 15 minutes (dashed line); 20 µM STS for 30 minutes (bold solid line); (ii) quantification for the 30 minutes-time point. C- The loss of ΔΨm was measured with Mitotracker Red. (i) DMSO (shadowed); 20 µM STS (dashed line); CCCP at 50 µM (solid line) was used as a control. D- Mitochondrial mass was estimated by staining with nonyl acridine orange. (i) DMSO (shadowed); 10 µM STS (dashed line).

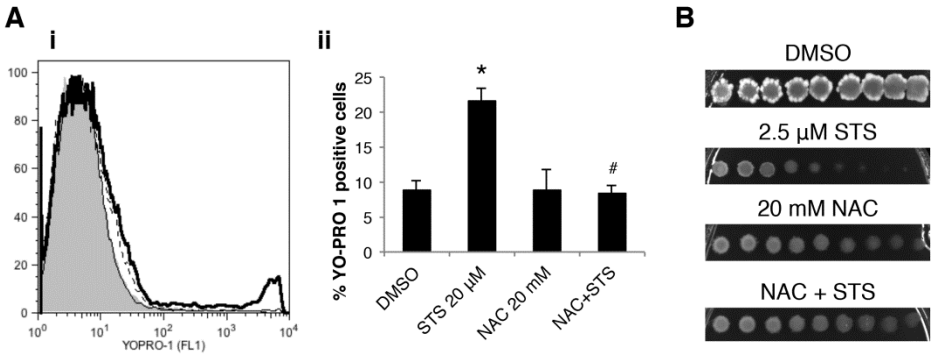

Figure 19 - Staurosporine-induced cell death is ROS-dependent.

A- Cell death was assessed by staining cells with YOPRO-1. The left panel (i) shows a representative histogram (DMSO (shadowed); 20 mM NAC (thin solid line); 20 µM staurosporine (STS) (bold solid line); 20 mM NAC plus 20 µM STS (dashed line)) whereas the respective quantification is presented in the right panel (ii). B- Modulation of staurosporine-induced cell death by NAC was also evaluated by spotting conidia in GFS supplemented with the indicated chemicals.

DNA microarray data allows the identification of putative mediators of staurosporine-induced cell death

DNA microarray studies in our group previously identified NCU09141 as the gene whose expression is mostly induced by staurosporine (140). Despite being annotated in *N. crassa* genome databases as “probable pyridoxine 4-dehydrogenase”, we found that the protein encoded by NCU09141 presents sequence similarity with β-subunits of human voltage-gated potassium (K^+) channels (Fig. 20A). Interestingly, NCU02887, annotated as a ”probable K^+ channel β subunit protein”, is similar to NCU09141 (Fig. 20A) and also highly induced by staurosporine (140). Given that NCU09141 and NCU02887 are induced by staurosporine and that they present homology to subunits of of voltage-gated K^+ channels, we tested the effect of combining staurosporine with 4-aminopyridine, an inhibitor of that type of channels (376). The combination of 4-aminopyridine and staurosporine resulted in a strong synergistic effect against the growth of *N. crassa* cells, as well as against the growth of the clinically relevant pathogens *A. fumigatus* and *C. albicans* (Fig. 20B). These results emphasize the role of K^+ channels during staurosporine-induced cell death and highlight the potential of transcriptional profiling for the identification of novel proteins involved in cell death. NCU09141 was also shown to be upregulated by phytosphingosine (116) and menadione (377). The efflux of K^+ is a common characteristic of apoptosis (378). Interestingly, an increasingly number of reports has been showing that voltage-gated K^+ channels-mediated K^+ efflux play an important role as a counterbalance to Ca^{2+} influx under certain conditions (379) and Ca^{2+} influx is an important event during staurosporine-induced cell death in *N. crassa* (see below).

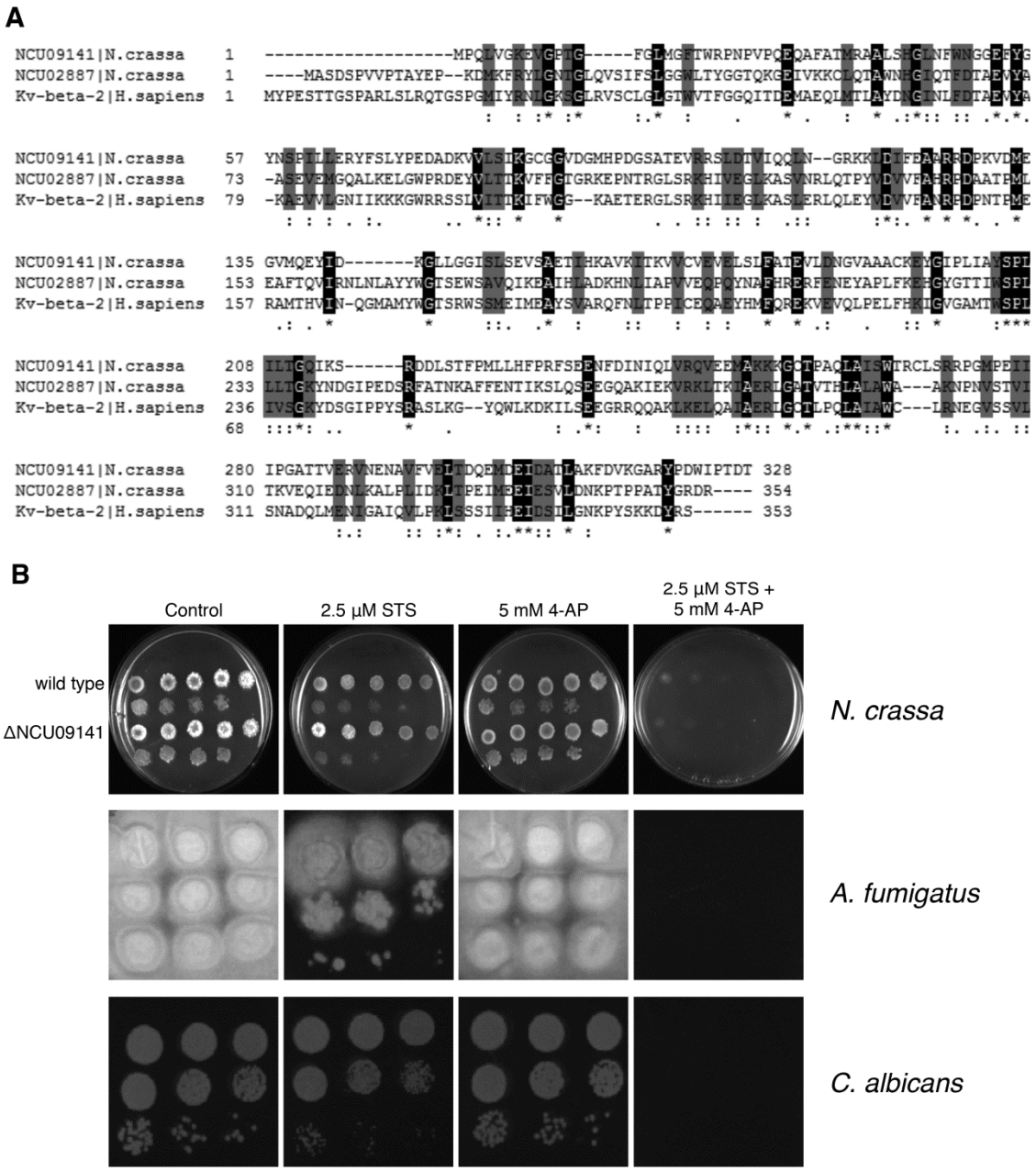

Figure 20 - NCU09141 displays sequence similarity to a β-subunit of shaker-related subfamily voltage-gated K^+ channels and 4-aminopyridine, an inhibitor of such channels, acts synergistically with staurosporine.

A- The protein sequences of *N. crassa* NCU09141 (Uniprot accession number: Q7S2K8), *N. crassa* NCU02887 (Q7SHL7) and *Homo sapiens* Kv beta 2 (Q13303-2) were aligned using ClustalW. Identical residues are black shaded while conserved substitutions are gray shaded. Symbols: * identical residues in all sequences; : conserved substitutions; . semiconserved substitutions. B- The spot assay was used to evaluate the sensitivity of *N. crassa* (wild type and ΔNCU09141 strains), *A. fumigatus* and *C. albicans* to the combination of the indicated concentrations of staurosporine (STS) and 4-aminopyridine (4-AP).

The spot assay was also employed to evaluate the sensitivity profile of about 40 other deletion strains whose respective genes were induced by staurosporine (or phytosphingosine). A few of them revealed altered sensitivity to staurosporine in comparison with the wild type strain, more specifically ΔNCU03229, ΔNCU06419 and ΔNCU04512 (more resistant), ΔNCU00355, ΔNCU05338, ΔNCU06911, ΔNCU09648, ΔNCU04699, ΔNCU04490, ΔNCU06230 and ΔNCU00605 (slightly more resistant), and ΔNCU08948 (slightly more sensitive) (Fig. 21). Table 6 presents the main features of the correspondent deleted proteins. These results provide a good hint about genes that seem play a role during cell death induction by staurosporine.

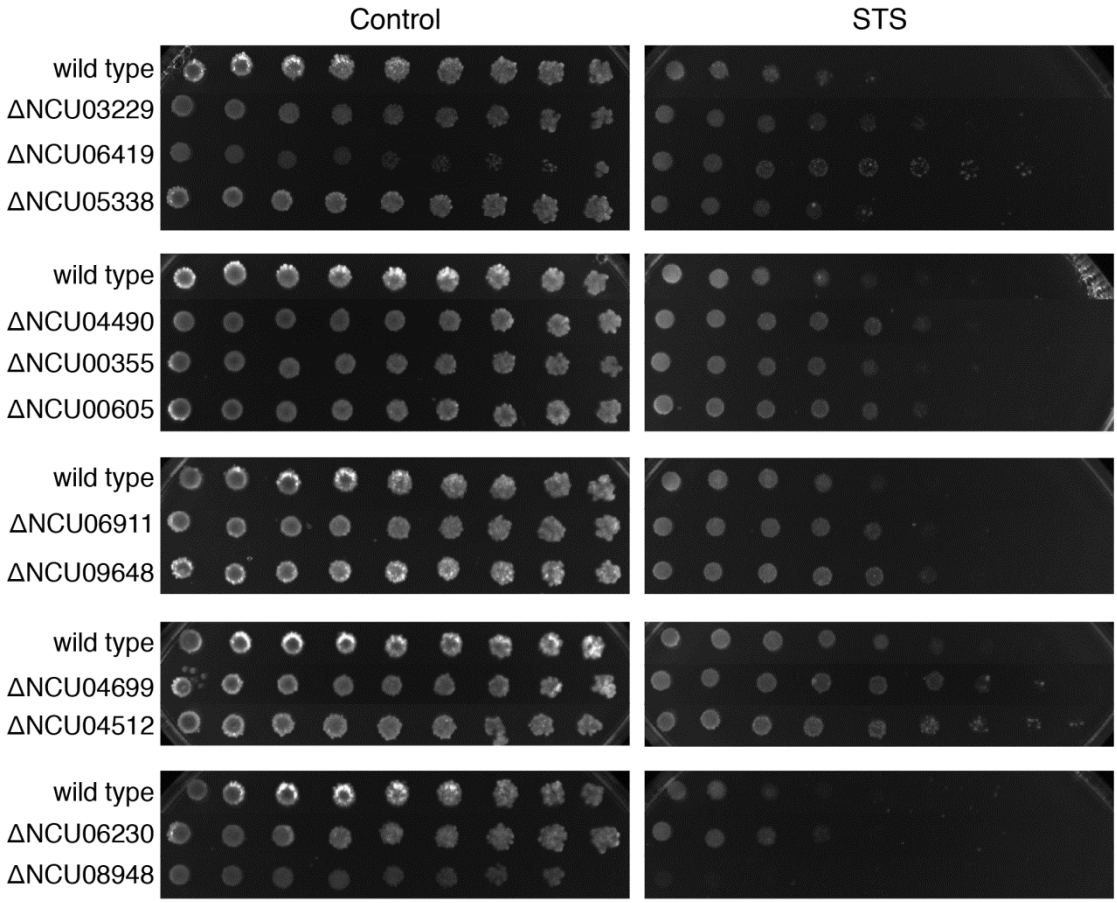

Figure 21 - Several deletion strains for staurosporine-induced genes present altered susceptibility to the drug.
Conidia from the indicated strains were spotted on GFS medium supplemented with 5 µM staurosporine (STS).

Table 6 - Summary of the main features of proteins identified by microarray analysis (correspondent genes induced by staurosporine) and whose absence confers altered sensitivity to staurosporine.

Gene	Protein	Description	Observations
NCU03229	TIM-44	Translocase of inner mitochondrial membrane 44	Slightly more sensitive to hydrogen peroxide than wild type
NCU06419	MEK-1	Mitogen-activated protein kinase	Also induced by phytosphingosine (116) and during HI (70); More sensitive to hydrogen peroxide and phytosphingosine than wild type
NCU04512	-	Related to transcriptional corepressor HIR3	-
NCU00355	CAT-3	Catalase-3	Repressed during HI (70)
NCU05338	-	-	Also induced by phytosphingosine (116)
NCU06911	-	-	Repressed during HI (70)
NCU09648	-	Aldehyde dehydrogenase	Repressed during HI (70)
NCU04699	CHOL-2	Methylene-fatty-acyl-phospholipid synthase	Repressed during HI (70)
NCU04490	-	-	Also induced by phytosphingosine (116)
NCU06230	STK-39	Serine/threonine protein kinase-39	Also induced by phytosphingosine (116)
NCU00605	-	ThiF domain-containing protein	-
NCU08948	-	Related to nuclear envelope protein NEM1	Also induced by phytosphingosine (116); Slightly more sensitive to actinomycin D than wild type

Transcriptional profiling of staurosporine-induced cell death by RNA sequencing reveals that the drug influences different cellular pathways

More recently, we studied the transcriptional response to staurosporine using high-throughput RNA sequencing (RNA-seq), which offers a far more accurate measurement of gene expression than DNA microarrays (380). One hour of treatment with 20 μM staurosporine was sufficient to elicit a dynamic transcriptional response, with 28.1% of the genes having their expression significantly altered (Fig. 22A). From these, about half were induced (989 genes) and half were repressed (1038 genes, Fig. 22B). The results validate our previous microarray approach (140), although much more altered genes were now found

and the concentration used for the RNA-seq experiments (20 µM) was slightly higher than the one used in the microarrays (12.5 µM).

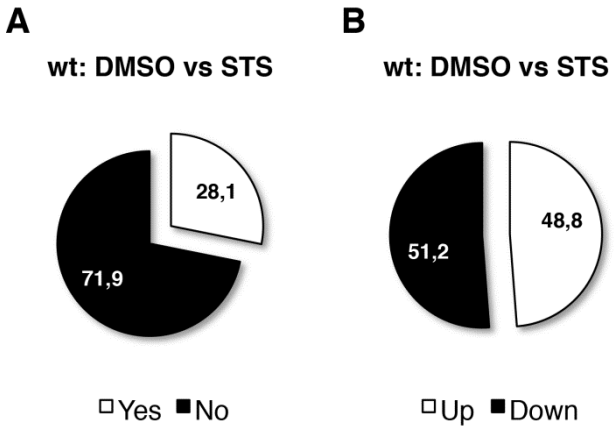

Figure 22 - Summary of the transcriptional response to staurosporine in wild type cells.
A- The percentage of genes with altered expression upon treatment with staurosporine is represented by the white portion of the pie chart. B- Percentage of upregulated (white) and downregulated (black) genes.

To understand the biological processes represented by these genes, we looked for functional enrichment among induced and repressed genes using FunCat. Although several genes are not catalogued by this database, it was possible to find a few enriched categories (Table 7). On the upregulation side, there was a particular enrichment of ‘vesicular transport’, ‘modification with sugar residues’ and ‘fatty acid metabolism’. On the downregulation side, there was a very strong enrichment of some categories, namely those related to ‘ribosome biogenesis’, ‘rRNA processing’, ‘translation’ and ‘RNA binding’. It seems that the protein synthesis machinery is critically impaired by staurosporine. Genes encoding mitochondrion-related functions were also enriched in the staurosporine-repressed set of genes: ‘anaerobic respiration’, ‘aerobic respiration’, ‘electron transport’, ‘energy generation’ and ‘mitochondrial transport’. The downregulation of genes comprising the ‘respiration’ category indicates that the treatment with staurosporine may cause a metabolic shift in the cells. In line with this and the fact that staurosporine is a potent ROS inducer, it has been observed in yeast that a shift in primary carbon metabolism is the fastest response to oxidative stress and that this is associated with defined transcriptional alterations (381). Thus, staurosporine elicits a dynamic transcriptional response in *N. crassa*.

Table 7 - Functional category enrichment analysis (FunCat) of genes induced and repressed by staurosporine in the wild type strain.

ID	Category	P-value
Induced genes		
01.05.02.07	sugar, glucoside, polyol and carboxylate catabolism	3.25E-05
01.06.05	fatty acid metabolism	1.63E-05
14.07.02	modification with sugar residues (eg, glycosylation, deglycosylation)	9.28E-06
16.17.07	magnesium binding	8.28E-05
20.09.07	vesicular transport (Golgi network, etc)	1.07E-06
Repressed genes		
01.03	nucleotide/nucleoside/nucleobase metabolism	1.89E-05
01.05.13	transfer of activated C- groups	7.38E-08
02.11	electron transport and membrane-associated energy conservation	1.60E-05
02.13.01	anaerobic respiration	7.10E-05
02.13.03	aerobic respiration	1.91E-09
02.45.15	energy generation (eg, ATP synthase)	4.03E-06
11.02.01	rRNA synthesis	8.37E-14
11.02.02	tRNA synthesis	9.50E-06
11.04.01	rRNA processing	9.03E-46
11.06.01	rRNA modification	1.22E-07
12.01	ribosome biogenesis	1.51E-137
12.01.01	ribosomal proteins	8.44E-105
12.04	translation	1.50E-65
12.07	translational control	1.31E-08
16.01	protein binding	1.38E-23
16.03.03	RNA binding	1.70E-32
20.01.15	electron transport	1.56E-05
20.09.04	mitochondrial transport	1.97E-12
42.16	mitochondrion	8.43E-08

3.2) Calcium is a crucial player during staurosporine-induced cell death

Staurosporine induces a well defined Ca^{2+}-signature derived from extracellular and internal Ca^{2+} stores

After six hours of culture, wild type *N. crassa* cells expressing the codon-optimized bioluminescent cytosolic free Ca^{2+} ($[Ca^{2+}]_c$) reporter aequorin (312) were incubated with 20 µM staurosporine and luminescence was monitored over time. Staurosporine induced a well defined cytosolic Ca^{2+}-signature of $[Ca^{2+}]_c$ changes (Fig. 23A). The signature includes two major Ca^{2+} peaks which we identified as "A" and "B" and a third broad increase in cytosolic Ca^{2+} ("C"). "A" occurs immediately upon addition of staurosporine and lasts for approximately 20 minutes and "B", having the highest amplitude, occurs after 35-40 minutes and lasts for approximately 80 minutes. UCN-01, a natural stereoisomer of 7-hydroxystaurosporine currently in clinical trials for cancer treatment (177), also provokes an immediate peak of $[Ca^{2+}]_c$ although the overall Ca^{2+} signature is different from that caused by staurosporine (Fig. 23B). Other cell death-inducing drugs, namely phytosphingosine (113, 114, 116) and amphotericin B (117) did not cause noticeable modifications in Ca^{2+} levels, at least at the concentrations tested (Fig. 23C).

In *N. crassa*, free Ca^{2+} is stored in different intracellular organelles and in the cell wall and its distribution depends on the growth phase (321, 347, 349). We aimed to identify the source(s) of Ca^{2+} that give rise to the staurosporine-induced $[Ca^{2+}]_c$ signature in the cytosol and started by looking at the contribution of extracellular Ca^{2+}. Pre-incubation with the membrane-impermeant Ca^{2+} chelator BAPTA resulted in complete abolition of the staurosporine Ca^{2+}-signature (Fig. 24A, i-ii and 24F-G). BAPTA added at different time points after incubation with staurosporine (15, 40 or 180 minutes) abolished the subsequent elevations in $[Ca^{2+}]_c$ (Fig. 24A, iii-v). This indicates that Ca^{2+} influx occurs continuously throughout the staurosporine-induced Ca^{2+}-signature.

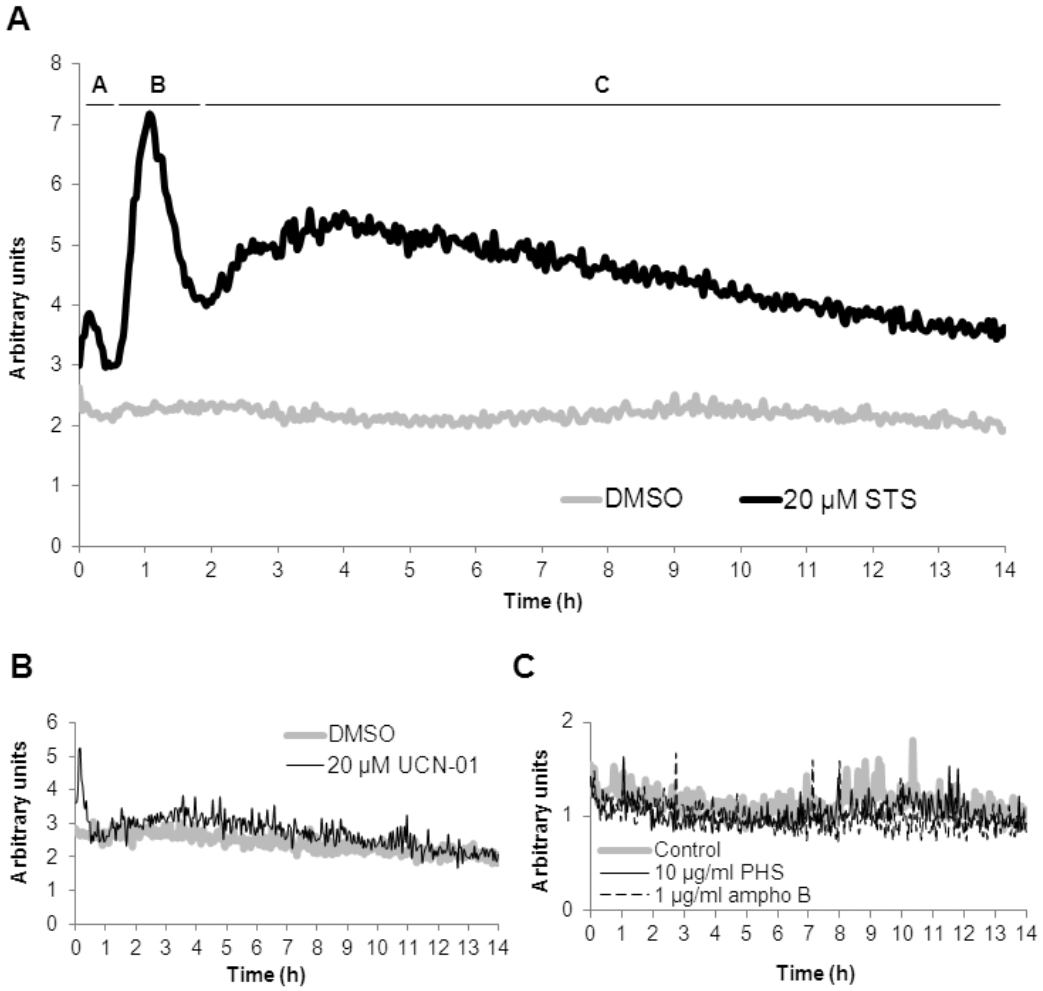

Figure 23 - Staurosporine induces a well-defined intracellular Ca^{2+} response.
A- Aequorin-expressing wild type cells grown for 6 hours were incubated with 20 µM staurosporine (STS) and the time-course emission of luminescence was monitored over time. The cytosolic STS Ca^{2+}-signature contained two major Ca^{2+} transients (phases "A" and "B") and a third broad $[Ca^{2+}]_c$ increase ("C") and represents an average of 30 independent experiments, each with 3 to 6 replicates. The "staurosporine-induced amplitude of response" was calculated after subtracting the DMSO curve from these data and is shown in subsequent figures for reference. B,C- The Ca^{2+} response was also obtained after treatment of cells with 20 µM UCN-01 (B), 10 µg/ml phytosphingosine (PHS) or 1 µg/ml amphotericin B (ampho B) (C).

Since staurosporine induces cell death in *N. crassa* (114, 139, 140), Ca^{2+} influx could arise from non-specific entry due to plasma membrane permeabilization. However, the percentage of PI-positive cells, indicative of permeabilized cells, was lower than 10% during the initial three hours following staurosporine treatment (Fig. 24B, i-ii). Moreover, the transient $[Ca^{2+}]_c$ peaks ("A" and "B") suggests that uncontrolled, non-specific Ca^{2+} influx into the cell, which would result in a steady increase in $[Ca^{2+}]_c$, does not occur. The third phase ("C") of the Ca^{2+}-signature is more compatible with such a situation. We conclude from

these experiments that Ca^{2+}-permeable channels in the plasma membrane are involved in generating the $[Ca^{2+}]_c$ transients during phases “A” and “B” and suggest that they may represent important signaling events in staurosporine-induced cell death.

The contribution of the ER to the staurosporine-induced Ca^{2+} signature was evaluated by treating cells with the ER-selective Ca^{2+}-ATPase inhibitor thapsigargin. Thapsigargin causes the depletion of ER Ca^{2+} and prevents Ca^{2+} sequestration by this organelle (382). Pre-treatment with thapsigargin changed the signature of the Ca^{2+} response to staurosporine and peak “A” was absent (Fig. 24C and 24F-G). Since Ca^{2+} in the ER is likely depleted by thapsigargin before the addition of staurosporine, this result is consistent with Ca^{2+} release from the ER contributing to peak “A”. However, inhibition of the ER Ca^{2+}-ATPase resulted in an increase in the amplitude of “B” compared with the untreated control suggesting that ER Ca^{2+}-ATPase activity plays a significant role in sequestering Ca^{2+} during this second phase of $[Ca^{2+}]_c$ increase. The amplitude of the prolonged $[Ca^{2+}]_c$ elevation during phase “C” was also increased in thapsigargin pre-treated cells indicating that continued Ca^{2+}-ATPase activity may also be required during this period.

In *N. crassa*, the vacuoles are responsible for the sequestration of Ca^{2+} under stress conditions to avoid the toxic accumulation of Ca^{2+} in the cytosol (348). We used bafilomycin A1 to assess whether the complex and heterogeneous vacuolar system in *N. crassa* (347) plays a role as a Ca^{2+}-store during the staurosporine-induced Ca^{2+}-signature. Bafilomycin A1 has previously been used to inhibit Ca^{2+} uptake by vacuoles and smaller acidic vesicles by blocking H^+-ATPase activity, which results in disruption of the proton gradient required for Ca^{2+} uptake by the vacuolar Ca^{2+}/H^+ exchanger (383). The presence of bafilomycin A1 resulted in a $[Ca^{2+}]_c$ increase in peaks “A” and “B” but not during peak C following staurosporine treatment (Fig. 24D and 24F-G). These results are consistent with the vacuolar system playing a role in sequestering Ca^{2+} during phases ‘”A” and “B” of the staurosporine-induced Ca^{2+} response but, in contrast to the ER, extinguishes its Ca^{2+} sequestering capacity after peak “B”.

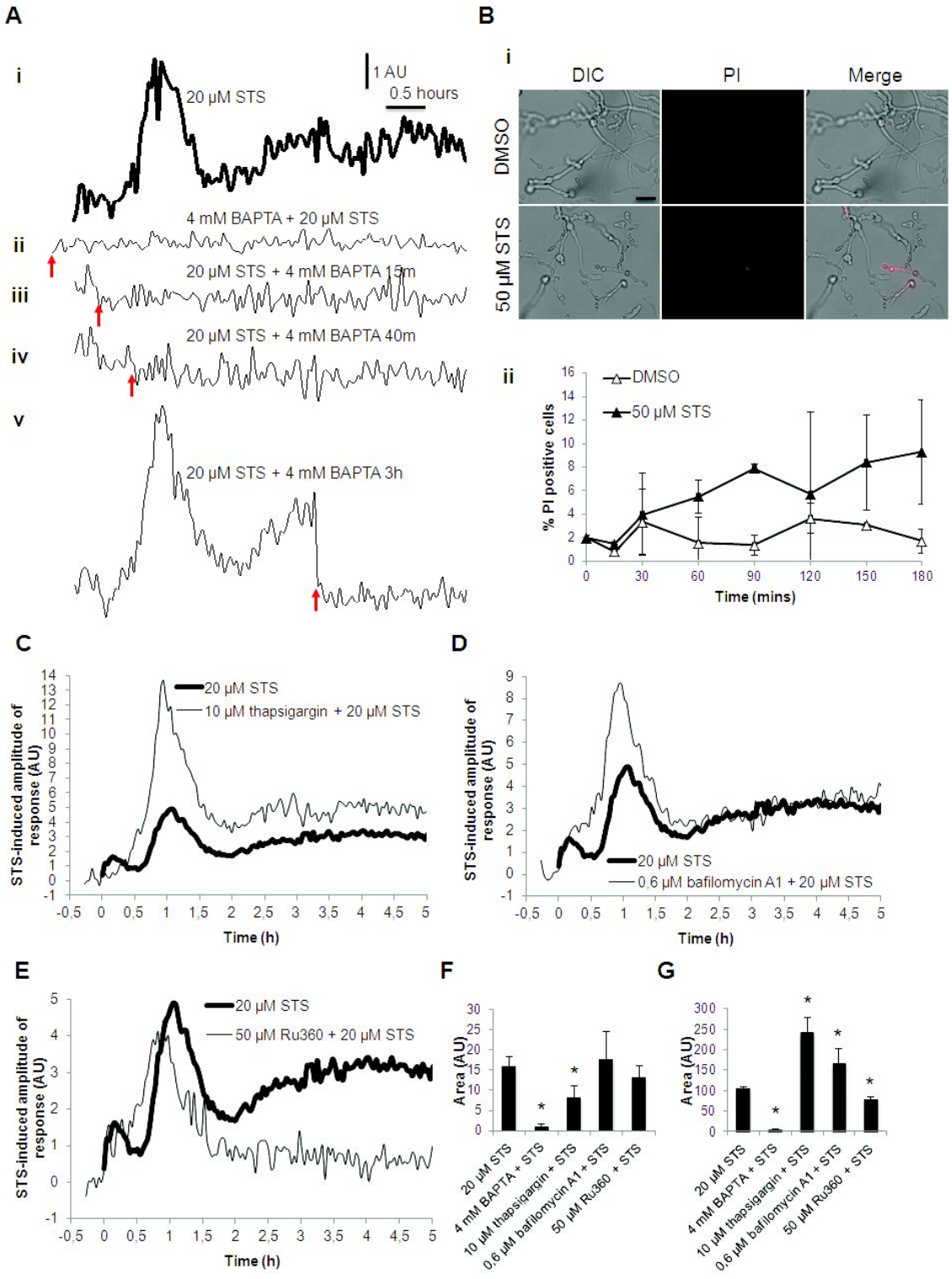

Figure 24 - The staurosporine-induced Ca^{2+}-signature results from Ca^{2+} influx into the cytosol from the extracellular medium and from internal Ca^{2+} stores.

A- Influence of BAPTA on the Ca^{2+}-signature after aequorin-expressing wild type cells were treated with 20 µM staurosporine (STS): (i) no BAPTA control, (ii-v) 4 mM BAPTA was applied at the indicated time points (arrows). The figure represents the staurosporine-induced amplitude of response. B- Membrane permeabilization as a readout of cell death was examined by staining with PI: (i) representative micrographs of cells stained with PI after incubation for 180-minutes with DMSO (control) and 20 µM STS, scale bar: 50 µm, (ii) time course quantification of the percentage

of PI-positive (dead) cells. C-E- Influence of 10 µM thapsigargin (C), 0.6 µM bafilomycin A1 (D) and 50 µM Ru360 (E) on the STS-induced Ca^{2+}-signature response in aequorin-expressing wild type cells. F-G- Quantification (in arbitrary units) of the $[Ca^{2+}]_c$ transients "A" and "B", respectively, in (A), (C)-(E). *, p-value < 0.05.

Mitochondria are also involved in Ca^{2+} sequestration. In mammalian cells, Ca^{2+} uptake by mitochondria occurs mainly through the MCU system. Pre-incubation with the MCU-specific inhibitor Ru360 (385) converted the staurosporine-induced $[Ca^{2+}]_c$ peaks "A" and "B" into a single peak and abolished the extended increase in $[Ca^{2+}]_c$ of phase "C" (Fig. 24E-G). These results suggest that mitochondria play a role in the sequestration of Ca^{2+} during phases "A" and "B". Altogether, our results point to a complex and dynamic response to staurosporine wherein cells mobilize Ca^{2+} from and to the extracellular medium, ER, vacuoles/acidic organelles and mitochondria.

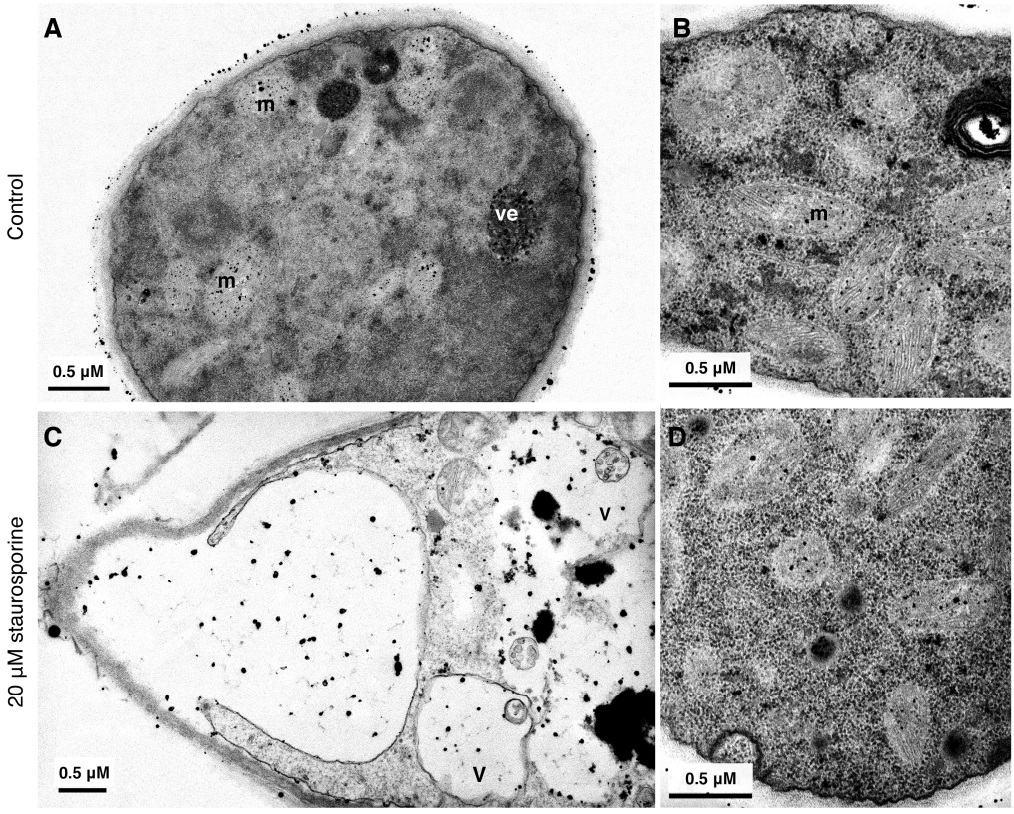

Figure 25 - Microscopic analysis of intracellular Ca^{2+} distribution in *N. crassa*.
A-D- Wild type cells treated with DMSO (A-B) or 20 µM staurosporine (C-D) for 150 minutes were processed for pyroantimonate staining of Ca^{2+} and samples observed by transmission electron microscopy. In A and C, samples were stained with uranyl acetate alone whereas in B and D lead citrate was also used for staining in order to improve the visualization of mitochondrial details. m: mitochondria; ve: electron-dense vesicles; V: vacuoles.

To further characterize the Ca^{2+} response during cell death in *N. crassa*, we analysed Ca^{2+} distribution by pyroantimonate precipitation and transmission electron microscopy. After six hours of culture, Ca^{2+} was predominantly localized in the mitochondria (Fig. 25), consistent with previous findings (322). There was also Ca^{2+} staining within electron-dense vesicles. Treatment with staurosporine resulted in the appearance of vacuoles with pyroantimonate-Ca^{2+} precipitation (Fig. 25), which is consistent with the intracellular Ca^{2+} response to staurosporine in the presence of bafilomycin A1 (Fig. 24D). We were not able to observe cytosolic or ER staining, which one would expect based on the staurosporine-induced Ca^{2+} profiles (Fig. 23A and 24C). This can be explained by the fact that soluble cytosolic Ca^{2+} may be lost during the precipitation or prefixation procedure or because the cytosolic concentration of Ca^{2+} may be below the sensitivity threshold of this technique (386).

Staurosporine activates phospholipase C- and IP_3-mediated recruitment of Ca^{2+}

Phospholipase C converts PIP_2 into IP_3 and DAG. IP_3 acts as a second messenger and by binding to its receptor results in Ca^{2+} mobilization from intracellular stores whereas DAG activates PKC (387). In *N. crassa*, IP_3 has been reported to promote the release of Ca^{2+} from the ER (10) and vacuole (10, 316). We measured $[Ca^{2+}]_c$ dynamics in response to staurosporine treatment in cells pre-treated with the phospholipase C-selective inhibitor U-73122 (388). The $[Ca^{2+}]_c$ response over the entire 5 hour time-course was greatly suppressed (Fig. 26A and 26F-G), consistent with a significant requirement for phospholipase C during this response. Lithium ($LiCl_2$) inhibits inositol monophosphatase, preventing the synthesis of phosphoinositides and reducing phospholipase C activity due to the absence of adequate levels of PIP_2 to be hydrolysed into IP_3 and DAG (389). $LiCl_2$ in the presence of staurosporine significantly reduced the $[Ca^{2+}]_c$ peaks during phases “A” and “B” and almost completely abolished the $[Ca^{2+}]_c$ increase of phase “C” (Fig. 26B and 26F-G). These effects on $[Ca^{2+}]_c$ were very similar to those resulting from the effects of the IP_3 receptor selective inhibitor xestospongin C (390) (Fig. 26C and 26F-G). This suggests that $LiCl_2$ and xestospongin C act by

preventing IP_3 formation and consequent release of $[Ca^{2+}]_c$ from internal stores which seem to participate early on but lasting throughout the entire $[Ca^{2+}]_c$ response to staurosporine.

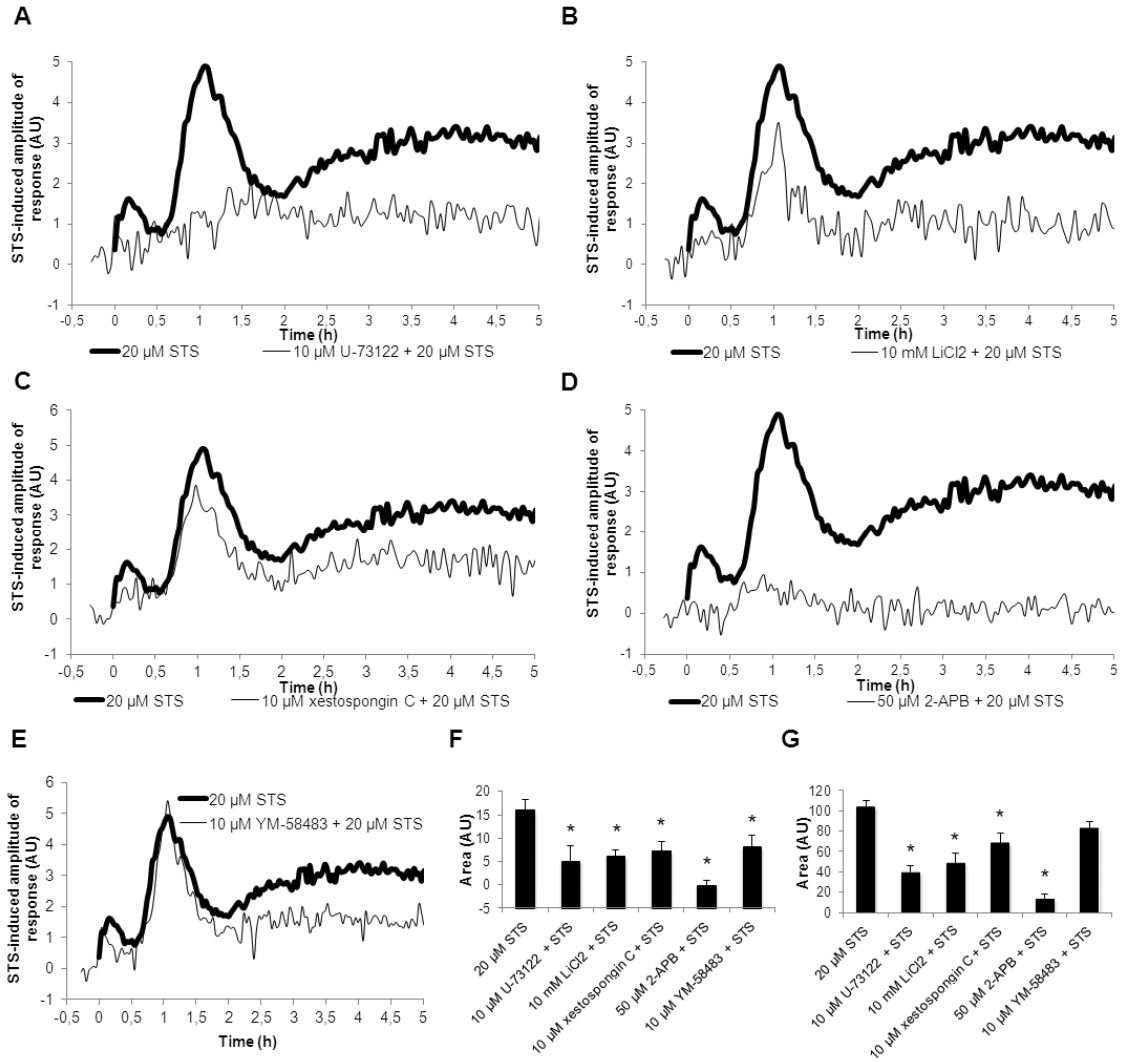

Figure 26 - Staurosporine activates phospholipase C- and IP_3-mediated recruitment of Ca^{2+}.

A-E- Influence of pre-treatment with different inhibitors on the Ca^{2+}-signature after aequorin-expressing wild type cells were treated with 20 µM staurosporine (STS): 10 µM U-73122 (A), 10 mM $LiCl_2$ (B), 10 µM xestospongin (C), 50 µM 2-APB (D) and 10 µM YM-58483 (E). F-G- Quantification (in arbitrary units) of the $[Ca^{2+}]_c$ transients "A" and "B", respectively, in (A)-(E). *, p-value < 0.05.

We also tested the effect of 2-APB which has been previously shown to block an IP_3 receptor-like channel and hyphal growth in *N. crassa* (10). 2-APB blocked most of the $[Ca^{2+}]_c$ response to staurosporine, exhibiting a stronger inhibitory effect than xestospongin C (Fig. 26D and 26F-G). Although 2-APB may be blocking IP_3 receptor-activated Ca^{2+} release, it is likely that its effect results

from the inhibition of TRP channels, as previously claimed (391), which explains the different effects when compared with the selective IP_3 receptor blocker xestospongin C. Altogether, these results strongly indicate that staurosporine promotes the activity of phospholipase C and that the recruitment of Ca^{2+} from intracellular stores requires the generation of IP_3.

Since Ca^{2+} influx from the extracellular space can be triggered by the depletion of IP_3-sensitive Ca^{2+} stores, we evaluated if SOCE (350) was triggering the Ca^{2+}-release-activated Ca^{2+} channel (CRAC). We added the CRAC selective inhibitor YM-58483 (392) before incubation with staurosporine and observed that the beggining of the $[Ca^{2+}]_c$ peak "A" is present, probably corresponding to the IP_3-activated intracellular store depletion phase, while the second part of the same peak is significantly reduced (Fig. 26E-G). Phase "C" was also decreased in YM-58483-pre-treated cells. Thus, it seems that the staurosporine-induced Ca^{2+} response in *N. crassa* includes the process of SOCE which has not been reported in filamentous fungi.

PLC-2 regulates staurosporine-induced cell death and polarized hyphal growth

We examined the sensitivity to staurosporine of the deletion strains for the four predicted phospholipase C genes of *N. crassa* (314, 315, 393). Interestingly, whereas Δ*plc-1* (ΔNCU06245) and Δ*plc-3* (ΔNCU09655) strains were slightly more resistant than wild type, Δ*plc-2* (ΔNCU01266) was substantially more resistant (Fig. 27A). We confirmed the increased resistance to staurosporine of Δ*plc-2* cells by measuring the levels of apoptosis with the YOPRO-1 marker (50). Treatment with staurosporine led to a significant increase in the percentage of apoptotic cells in the wild type but not in the Δ*plc-2* deletion strain (Fig. 27B). A 2-hour treatment with staurosporine caused ~23.4% apoptosis in wild type and ~9.9% in Δ*plc-2* cells. In the absence of PLC-2, the $[Ca^{2+}]_c$ -response to staurosporine was nearly abolished altogether (Fig. 27C-E), paralleling the response of wild type cells pre-treated with the phospholipase C inhibitor U-73122 (Fig. 26A). These results indicate that phospholipase C is required for

staurosporine-induced cell death and support the conclusion that Ca^{2+} signaling is important during the process.

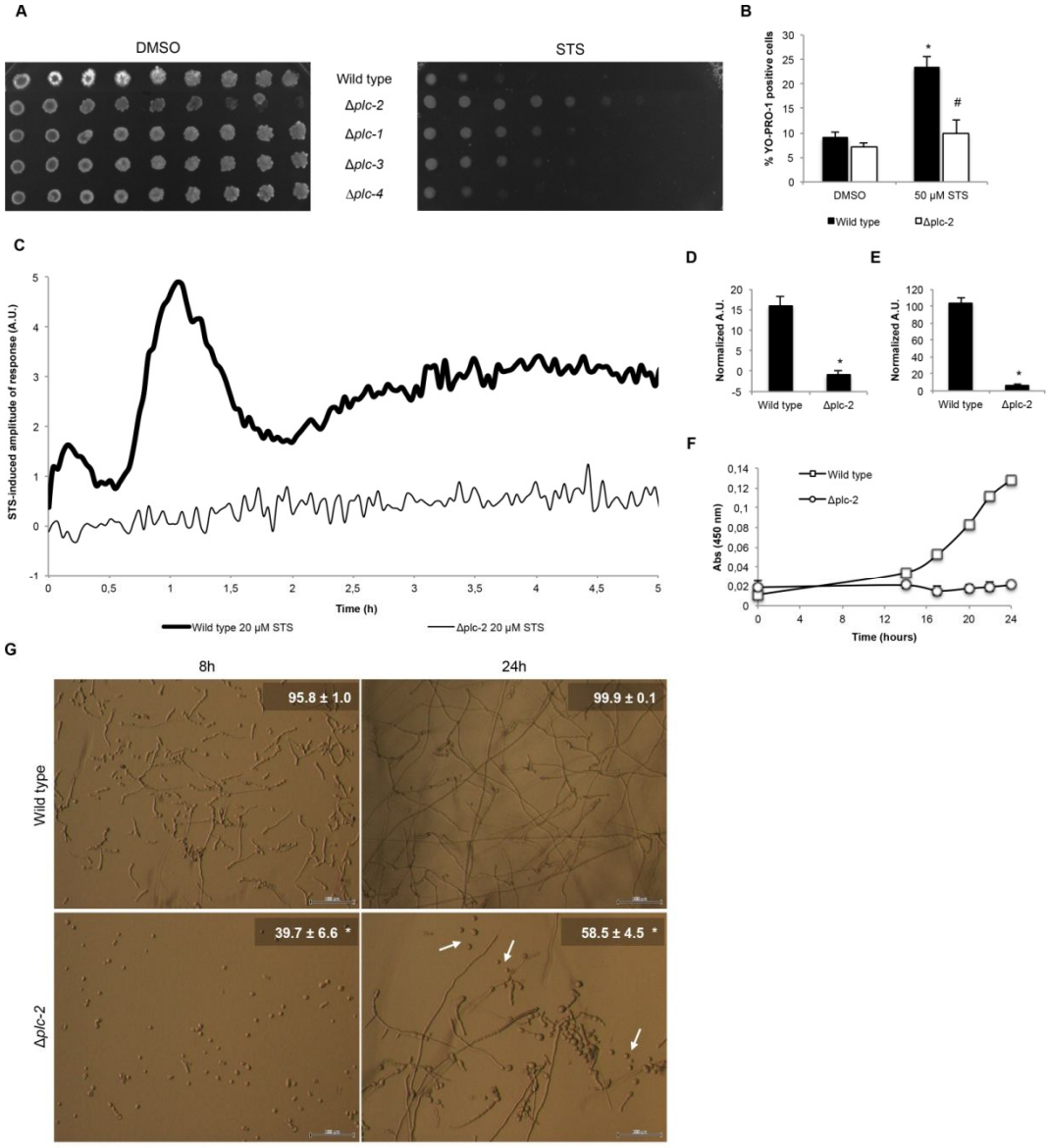

Figure 27 - PLC-2 is required for the Ca^{2+}-signature and cell death induced by staurosporine and is implicated in *N. crassa* hyphal development.

A- The sensitivity profiles of deletion strains for the four *N. crassa* phospholipase C genes evaluated by spotting conidia on GFS medium containing 2.5 µM staurosporine (STS). B- The levels of apoptosis in wild type and Δ*plc-2* cells detected by staining with YO-PRO1 and the positive cells measured by flow cytometry. *, p-value < 0.05 for the comparison 50 µM STS *versus* DMSO on each strain; #, p-value < 0.05 for the comparison of STS-treated wild type *versus* Δ*plc-2* cells. C- Cytosolic levels of Ca^{2+} were measured in aequorin-expressing Δ*plc-2* cells after treatment with 20 µM STS. D-E- Quantification (in arbitrary units) of the $[Ca^{2+}]_c$ transients "A" and "B", respectively, in (C). * , p-value < 0.05. F- Growth of wild type and Δ*plc-2* strains was followed during 24 hours by measuring absorbance at 450 nm. G- Representative micrographs of wild type and Δ*plc-2* strains at 8 hours and 24 hours after inoculation in liquid Vogel's MM. The percentage of germinated cells is indicated on the upper right corner (mean ± SEM). Note the presence of several ungerminated conidia in 24 hour-cultures of Δ*plc-2* (arrows). Scale bar: 100 µm. *, p-value < 0.05.

Deletion of *plc-2* resulted in very poor growth in liquid medium (Fig. 27F). After 8 hours of culture, almost all wild type cells had germinated (95.8%) and normal hyphal elongation was observed (Fig. 27G). In contrast, Δ*plc-2* cells underwent greatly reduced germination (39.7%). The difference was also evident after 24 hours of growth: whereas the wild type strain was fully developed with 99.9% germination and long, branched and fused hyphae, the Δ*plc-2* knockout mutant only underwent 58.5% germination and possessed a few elongated, branched hyphae with little fusion evident. The presence of some germinated hyphae in Δ*plc-2* knockout cultures may be explained by the redundant activity of the other phospholipase C genes, as previously suggested (324).

Staurosporine activates a putative TRP channel involved in Ca^{2+} influx from the external medium

Since the staurosporine Ca^{2+} signature seems to only partially involve SOCE (Fig. 26E), we further investigated the mechanism of Ca^{2+} influx responsible for the $[Ca^{2+}]_c$ phases “A” and “B”. So far, two Ca^{2+} uptake systems have been established in fungi: the high- and the low-affinity Ca^{2+} uptake system (HACS and LACS, respectively). At the molecular level, HACS comprises the CCH-1 and MID-1 channel (342) whereas the channel counterpart in LACS is FIG-1 (345).

A drastic increase in the $[Ca^{2+}]_c$ peaks “A” and “B” was observed in Δ*cch-1* cells (ΔNCU02762) exposed to staurosporine (Fig. 28A and 28C-D). This was also mainly due to extracellular Ca^{2+} uptake because it was prevented by pre-treatment with the Ca^{2+} chelator BAPTA (Fig. 28A and 28C-D). The $[Ca^{2+}]_c$ response in the Δ*fig-1* mutant (ΔNCU02219) was more similar to the wild type, despite a slight $[Ca^{2+}]_c$ amplitude increase in phase “B” and a decrease in phase “C” (Fig. 28B-D). These data strongly suggest that Ca^{2+} uptake during staurosporine-induced cell death involves channel activity distinct from that of the CCH-1/MID-1 high-affinity system or the FIG-1 low-affinity system. This unknown influx system was stimulated by staurosporine especially in the absence of CCH-1. Remarkably, complete abolition of the staurosporine $[Ca^{2+}]_c$ signature was observed when Δ*cch-1* cells were pre-treated with 2-APB (Fig. 28A and 28C-D), which is known to

inhibit the IP_3 receptor but also TRP channels (391). As previously reported (394), we were unable to generate a Δ*mid-1* strain expressing aequorin at sufficient levels for $[Ca^{2+}]_c$ measurement. MID-1 (NCU06703) is considered to be a regulatory partner of CCH-1 (342, 395, 396) although there are reports of MID-1 behaving as a non-selective stretch-activated cation channel (343, 344). Nonetheless, the knockout of *mid-1* phenocopied the *cch-1* deletion, as both strains showed defects such as reduced aerial hyphae, conidiation (Fig. 29A) and mycelial extension rate (Fig. 29B), consistent with both proteins acting together.

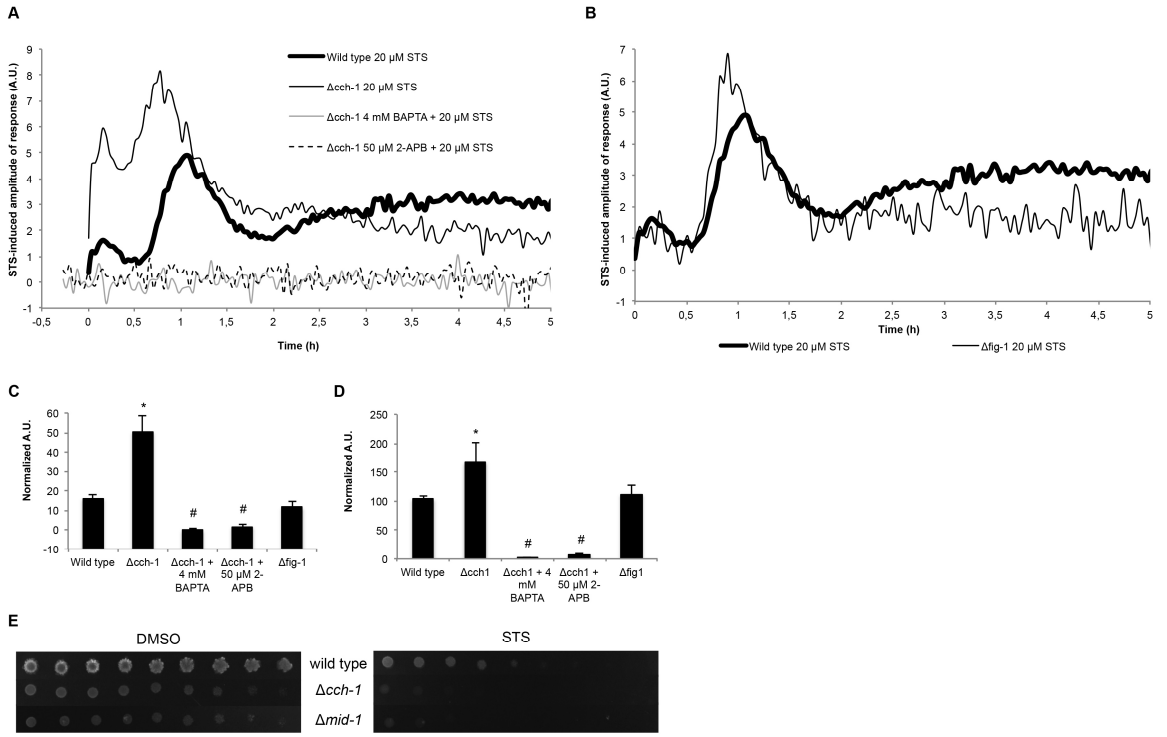

Figure 28 - Staurosporine-induced Ca^{2+} influx occurs via an uptake system distinct from the high- and low-affinity Ca^{2+} systems.

A-B- The Ca^{2+}-signature in response to 20 µM staurosporine (STS) was compared in aequorin-expressing wild type and Δ*cch-1* (A) or Δ*fig-1* (B) cells. Influence of pre-treatment with 4 mM BAPTA and 50 µM 2-APB on Δ*cch-1* STS-induced Ca2+-signature is shown in (A). C-D- Quantification (in arbitrary units) of the $[Ca^{2+}]_c$ transients "A" and "B", respectively, in (A)-(B). *, p-value < 0.05 for the comparison of Δ*cch-1 versus* wild type; #, p-value < 0.05 for the comparison of BAPTA and 2-APB pre-treated Δ*cch-1* cells *versus* Δ*cch-1* with STS alone. E- The sensitivity of Δ*cch-1* and Δ*mid-1* strains evaluated by spotting conidia on GFS medium containing 2.5 µM STS (E).

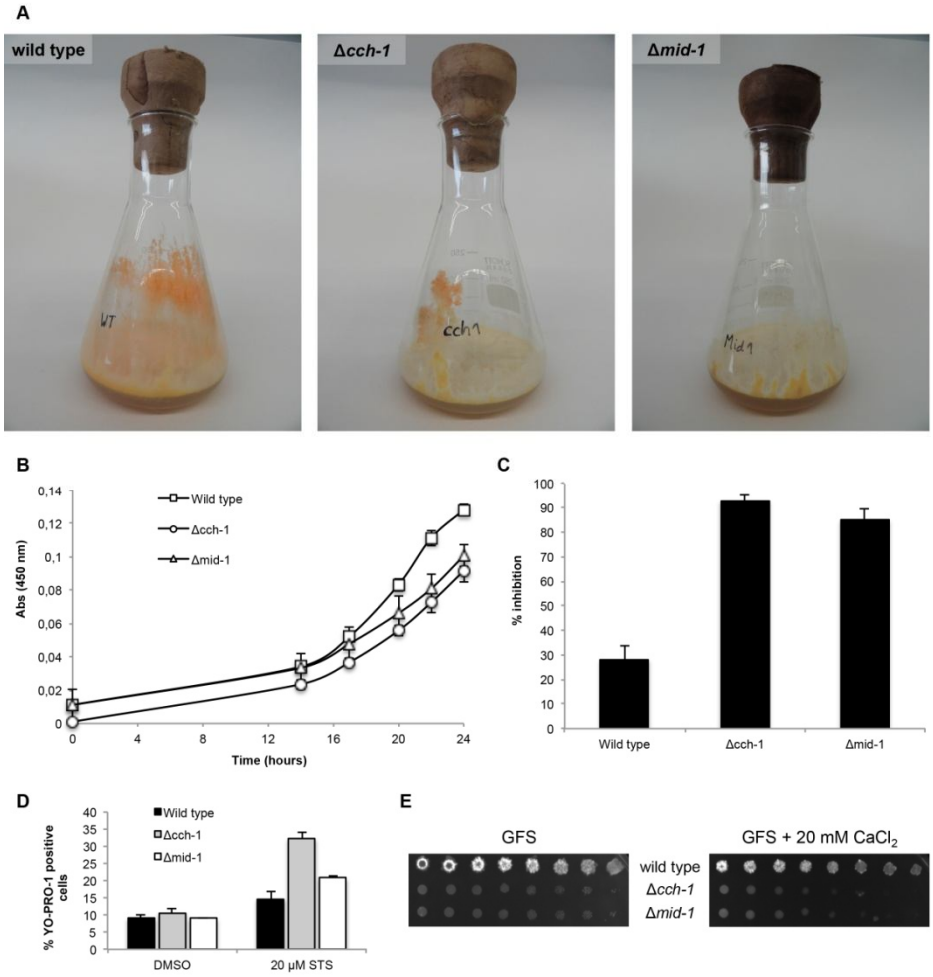

Figure 29 - Deletion of *cch-1* and *mid-1* results in abnormal development of aerial hyphae, conidiation, growth rate and an increased susceptibility to staurosporine and $CaCl_2$.

A- Wild type, Δ*cch-1* and Δ*mid-1* cells grown in solid Vogel's MM for 7 days. B- Growth of wild type, Δ*cch-1* and Δ*mid-1* cells over 24 hours by measuring absorbance at 450 nm. C- Percentage of growth inhibition caused by a 24-hour treatment with 2.5 µM staurosporine, as determined by measuring absorbance at 450 nm. D- The levels of staurosporine-induced apoptosis in wild type, Δ*cch-1* and Δ*mid-1* detected by staining with YO-PRO1 and determining the percentage of positive cells by flow cytometry. E- The growth of wild type, Δ*cch-1* and Δ*mid-1* in the presence of 20 mM $CaCl_2$ evaluated by the spot assay.

Given the accentuated Δ*cch-1* $[Ca^{2+}]_c$ signature during phases "A" and "B" in response to staurosporine (Fig. 28A), we assessed the susceptibility of Δ*cch-1* and Δ*mid-1* cells to staurosporine and observed that both are hypersensitive to the drug (Fig. 28E). This is corroborated by the analysis of the inhibitory effect of staurosporine on growth in liquid culture (Fig. 29C) and YOPRO-1 staining to measure apoptosis (Fig. 29D). The absence of CCH-1 and MID-1 also causes decreased tolerance to excess levels of Ca^{2+} (Fig. 29E). Deletion of *fig-1* resulted in a slight increase in susceptibility to staurosporine (Fig. 30A). Thus, the

upregulation of a Ca^{2+} influx system in the absence of CCH-1 (and possibly MID-1) is correlated with increased cell death.

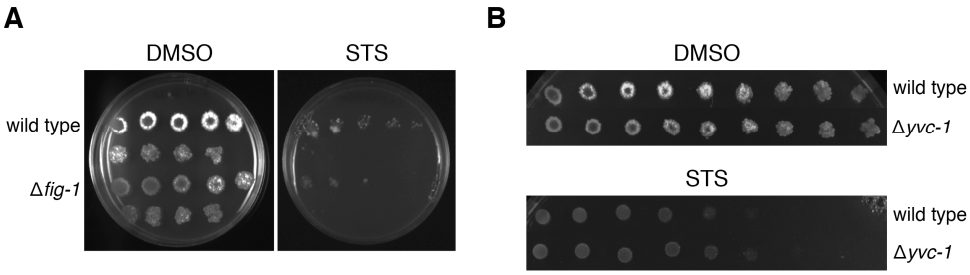

Figure 30 - Staurosporine sensitivity profile of Δ*fig-1* and Δ*yvc-1* mutant strains.
Sensitivity of Δ*fig-1* (A) and Δ*yvc-1* (B) strains was evaluated by spotting conidia on GFS medium containing 2.5 µM staurosporine (STS).

In animals, Ca^{2+} influx can be mediated by TRP channels, known to be regulated by the phospholipase C pathway (325). Because of the importance of phospholipase C during the response to staurosporine, we hypothesized a TRP channel involvement in Ca^{2+} influx from the extracellular medium. The presence of flufenamic acid, a non-selective blocker of some TRP channels (397), nearly abolished the staurosporine-induced $[Ca^{2+}]_c$ signature (Fig. 31A and 31E-F). $[Ca^{2+}]_c$ measurements in the presence of ruthenium red, a classical inhibitor of the MCU and a pan-inhibitor of TRP channels (391), also resulted in strong suppression of the $[Ca^{2+}]_c$ response to staurosporine (Fig. 31B and 31E-F). This is in agreement with the fact that pre-incubation with 2-APB, an IP_3 receptor inhibitor but also a blocker of TRP channels (391), potently reduced the $[Ca^{2+}]_c$ response to staurosporine (Fig. 26D).

Because our data provides evidence that phospholipase C is activated by staurosporine and that the consequent depletion of PIP_2 is an activation factor for a specific TRP channel, TRPC4 (398), we analysed the $[Ca^{2+}]_c$ response to staurosporine in the presence of ML204, a specific antagonist of TRPC4 and TRPC5 (399). With this inhibitor, the $[Ca^{2+}]_c$ peaks associated with phases “B” and “C” were significantly reduced (Fig. 31C and 31E-F). The effect of ML204 was not as drastic as the other TRP inhibitors and this might be explained by the fact that it is very selective against mammalian TRPC4 and TRPC5 (399) and no obvious sequence homologues are present in *N. crassa*. Altogether, the differences in the $[Ca^{2+}]_c$ response to staurosporine-induced cell death in the presence of flufenamic acid, ruthenium red, 2-APB, ML204, BAPTA and U-73122, together with the

deficient Ca^{2+} response of the Δ*plc-2* mutant strain, suggests that staurosporine induces the opening of a TRP-like channel regulated by phospholipase C.

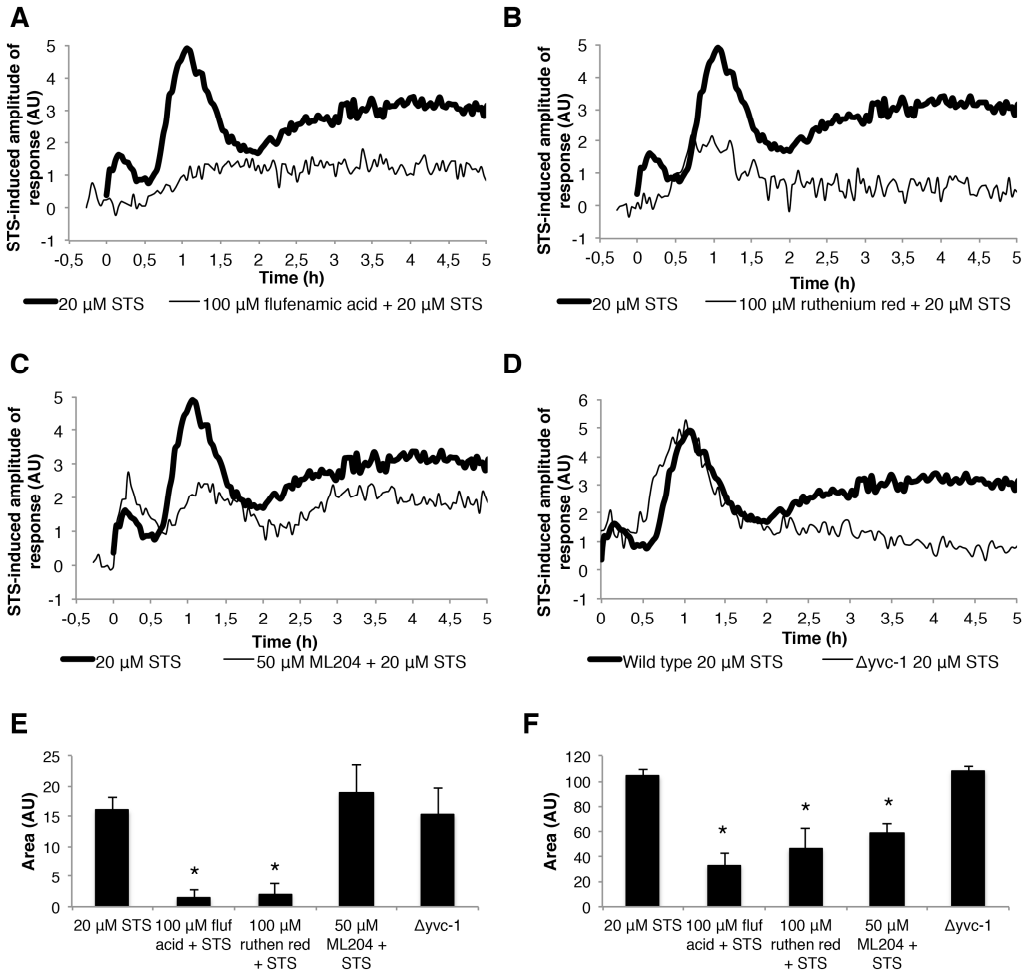

Figure 31 - Staurosporine activates a TRP-like channel responsible for extracellular Ca^{2+} influx.

A-C- The Ca^{2+}-signatures in response to 20 µM staurosporine (STS) in aequorin-expressing wild type cells after pre-treatment with different Ca^{2+} modulating drugs: 100 µM flufenamic acid (A), 100 µM ruthenium red (B) and 50 µM ML204 (C). D- The Ca^{2+}-signatures in response to 20 µM STS in aequorin-expressing Δ*yvc-1* cells. E-F- Quantification (in arbitrary units) of the $[Ca^{2+}]_c$ transients "A" and "B", respectively, in (A)-(D). *, p-value < 0.05.

So far, the only TRP channel reported in *N. crassa* is YVC-1 (NCU07605 or NCU16725 in a recent annotation) (314, 315). The initial part of the staurosporine-induced $[Ca^{2+}]_c$ signature was similar in wild type and Δ*yvc-1* cells (phases "A" and "B"), despite of a decrease in $[Ca^{2+}]_c$ during phase "C" (Fig. 31D-F). The growth of Δ*yvc-1* was inhibited by staurosporine similar to that of the wild type strain (Fig. 30B). A role for this protein in extracellular Ca^{2+} uptake would not be anyway expected, since the YVC-1 yeast homologue is localized in the vacuolar

membrane (326). Altogether, our pharmacological and genetic approach points to a Ca^{2+}-permeable channel with properties of a TRP-like channel that is distinct from YVC-1, and which is the mediator of Ca^{2+} influx from the extracellular medium during staurosporine-induced cell death.

Extracellular Ca^{2+} availability impacts staurosporine-induced cell death and intracellular Ca^{2+} signaling

We wanted to further understand the relevance of extracellular Ca^{2+} for the *N. crassa* response to staurosporine. We hypothesized that the response to staurosporine of cells growing with different Ca^{2+} concentrations would vary, since Ca^{2+} influx from the extracellular medium occurs in response to the drug. We prepared a culture medium, designated '0 Ca^{2+}', by removing $CaCl_2$ from Vogel's MM. Little amounts of Ca^{2+}, as impurities from the other reagents in the solution allowed *N. crassa* to grow well in such conditions (Fig. 32A, middle panel). In contrasting experiments, we supplemented Ca^{2+}-free medium with an excess of 20 mM $CaCl_2$ (we designated this medium '20 mM $CaCl_2$'), which represents an approximately 30 fold (but not toxic) increase when compared with the 0.68 mM concentration of $CaCl_2$ in standard Vogel's MM (13) (Fig. 32A, lower panel). We inoculated wild type cells on the centre of Petri dishes containing standard, 0 Ca^{2+} or 20 mM $CaCl_2$ solid Vogel's MM supplemented with staurosporine and measured radial growth during a 104 hours time course. The drug inhibited growth in all media (Fig. 32A-C). However, the inhibitory effect was amplified in the absence of Ca^{2+} (*e.g.*, ~39% of inhibition after 32 hours of treatment with 1 µM staurosporine in 0 Ca^{2+} *versus* ~14% in standard MM). On the other hand, growth inhibition was partially blocked in 20 mM $CaCl_2$ medium (*e.g.*, ~37% of inhibition after 32 hours of treatment with 2.5 µM staurosporine in 20 mM $CaCl_2$ *versus* ~65% in standard MM). In GFS medium the outcome of modifying the extracellular concentration of Ca^{2+} is similar: in 0 Ca^{2+} medium the effects of staurosporine were exacerbated whereas in the presence of 20 mM $CaCl_2$, growth inhibition was partially blocked (Fig. 32D). Enhancement and suppression of inhibition of growth by 0 Ca^{2+} and 20 mM $CaCl_2$, respectively, was not reproduced in cells treated with phytosphingosine

(Fig. 33), in agreement with the fact that this compound does not cause alterations in the levels of cytosolic Ca^{2+} (Fig. 23C).

In order to check cell death, we analysed YOPRO-1 and PI staining by flow cytometry. A 2-hour treatment with staurosporine in standard MM resulted in ~22% and ~17% of YOPRO-1 and PI positive cells, respectively (Fig. 32E-F). In 0 Ca^{2+} medium, these levels were augmented to ~40% and ~34%, respectively. In contrast, the percentage of YOPRO-1- and PI-positive cells was reduced to ~15% and ~6%, respectively, in 20 mM $CaCl_2$ medium.

The production of ROS (Fig. 18B) is an essential event during the response of *N. crassa* to staurosporine, as the addition of antioxidants blocks cell death (Fig. 19A-B). We asked if the availability of Ca^{2+} in the culture medium influenced cellular ROS production induced by staurosporine. While in standard MM cells stressed for 30 minutes with staurosporine displayed a ~4.2 fold-increase in ROS accumulation, the equivalent accumulation was ~10.4 and ~1.3 in 0 Ca^{2+} and 20 mM $CaCl_2$ media, respectively (Fig. 32G). Given the importance of ROS formation for cell death provoked by staurosporine, this Ca^{2+}-ROS dependence is likely related to the distinct cell death phenotypes in the different culture media.

To further stress the modulatory effect of altering the levels of Ca^{2+} in staurosporine-induced cell death, we combined the drug with the Ca^{2+} chelator BAPTA and the Ca^{2+} ionophore A23187 (calcimycin) in GFS plates with standard MM. As expected, extracellular Ca^{2+} blockage with BAPTA synergized whereas elevation of intracellular Ca^{2+} with A23187 antagonized the effects of staurosporine (Fig. 32H). Pre-incubation with BAPTA significantly enhanced apoptotic levels induced by staurosporine, whereas they were partially inhibited by A23187, as measured by YOPRO-1 staining (Fig. 32I). Altogether, these data consistently indicates that the absence of Ca^{2+} enhances staurosporine-induced cell death, whereas excess (but not toxic) concentrations of Ca^{2+} partially prevent it.

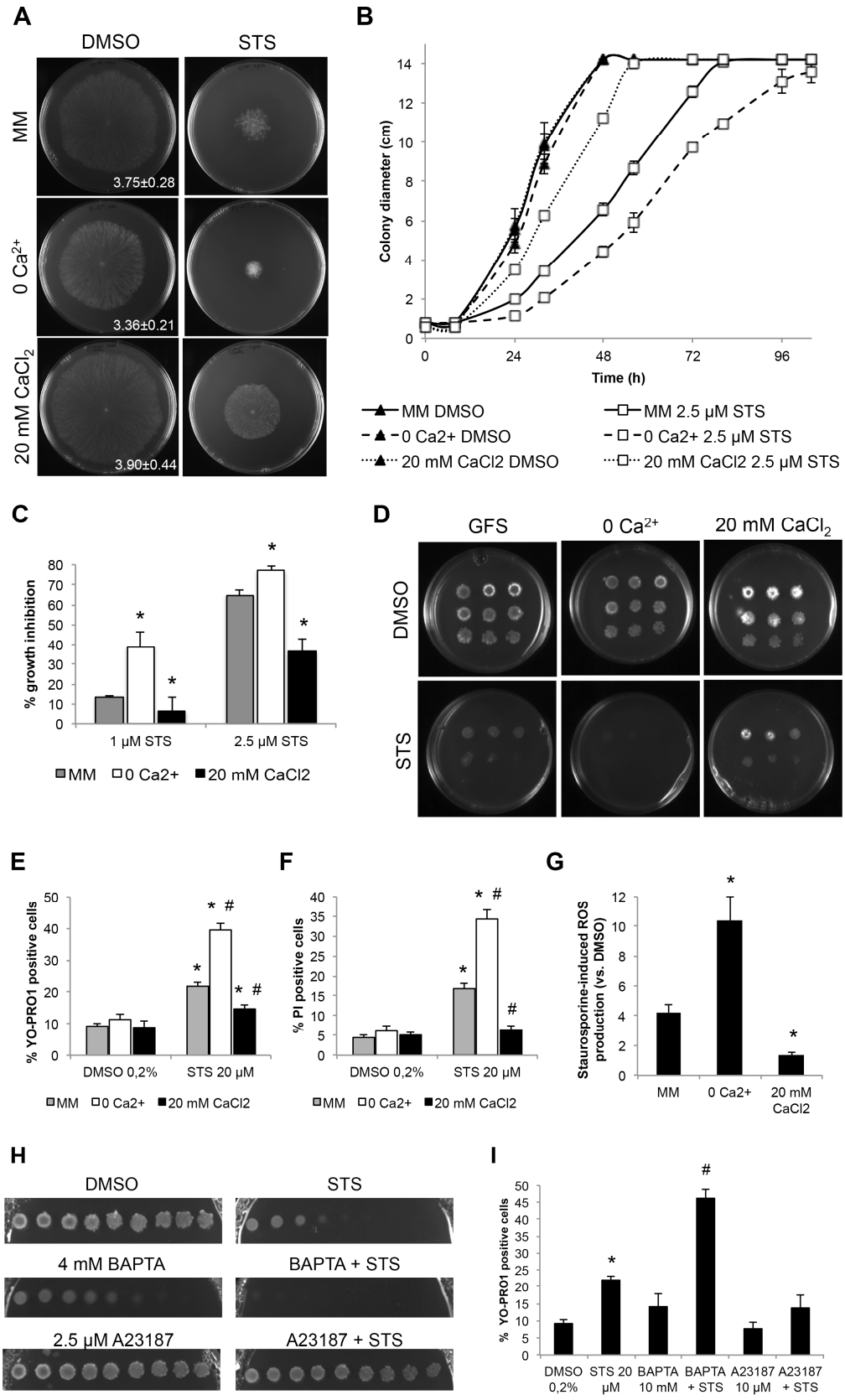

Figure 32 - Extracellular Ca^{2+} protects cells from staurosporine-induced growth inhibition, cell death and ROS production whereas Ca^{2+} limitation renders cells hypersensitive to the drug.

A-C- Wild type conidia were inoculated on the centre of a Petri dish containing Vogel's MM with different concentrations of Ca^{2+} and 2.5 µM staurosporine (STS). Growth at 32h (A), throughout time (B) and the percentage of growth in STS-treated cells *versus* control (C) are shown. In (A), the growth rate (mm/h) is indicated in the lower right corner of the panels. *, p-value ≤ 0.05. D- Wild type conidia were spotted in GFS medium supplemented with different concentrations of Ca^{2+} and 5 µM STS and incubated for 3 days. E-F- Cell death following treatment of the cells with 20 µM staurosporine in the indicated liquid culture media was assessed by flow cytometry measurements of YOPRO-1- (E) or PI- (F) positive cells by flow cytometry. *, p-value ≤ 0.05 for the comparison STS *versus* DMSO on each media; #, p-value ≤ 0.05 for the comparison between media after the treatment with STS. G- Accumulation of ROS in cells treated with 20 µM staurosporine in the indicated liquid culture media was examined by staining with DHR123 and calculating the fold increase in ROS production *versus* DMSO. *, p-value ≤ 0.05. H-I- Growth inhibition and cell death in 2.5 µM STS-treated cells in the presence of BAPTA or A23187 was assessed by spotting wild type cells in GFS medium (H) or growing them in standard liquid medium followed by staining with YO-PRO1 (I) *, p-value ≤ 0.05 for the comparison STS *versus* DMSO; #, p-value ≤ 0.05 for the comparison between STS alone and BAPTA+STS.

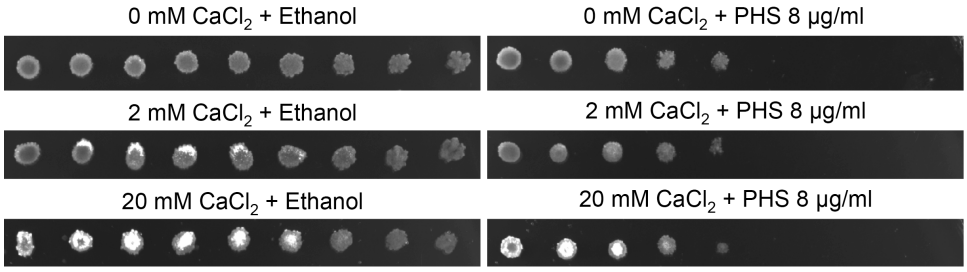

Figure 33 - Extracellular Ca^{2+} does not affect *N. crassa* sensitivity to phytosphingosine.
Serial dilutions of wild type cells were spotted in GFS medium containing 8 µg/ml phytosphingosine (or ethanol as control) and different concentrations of $CaCl_2$, as indicated.

As shown, staurosporine induces a three-step cytosolic Ca^{2+} response comprising signals "A", "B" and "C" in *N. crassa* cells (Fig. 23A). In the absence of Ca^{2+} (0 Ca^{2+} medium), the Ca^{2+} response to staurosporine was compromised, with an almost disappearance of peaks "A" and "B" (Fig. 34A-B). In medium with 20 mM $CaCl_2$ there was a strong boost on peak "A", while peak "B" remained similar to standard MM. This is in agreement with our observations that extracellular Ca^{2+} uptake is important during the whole extent of the Ca^{2+} response (Fig. 24A). The differences observed in the staurosporine-induced cytosolic Ca^{2+} profile in 0 Ca^{2+} medium (Fig. 34A; the initial part of the response is supressed but cytosolic Ca^{2+} increases after 2 hours of treatment) *versus* standard medium treated with BAPTA (Fig. 24A; complete abolition of the Ca^{2+} signals), indicate that the Ca^{2+} present in the impurities of the other reagents composing the 0 Ca^{2+} culture medium is taken

by the cells. Nevertheless, this only occurs in a later stage of the response (signal "C").

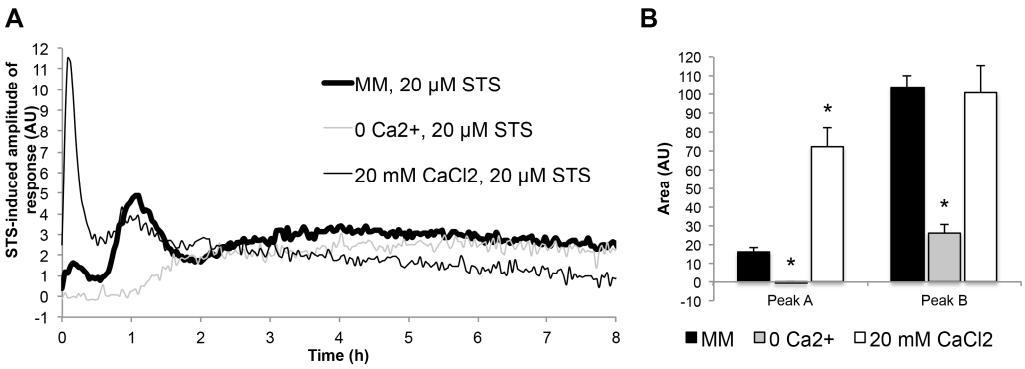

Figure 34 - Extracellular Ca^{2+} availability affects intracellular Ca^{2+} dynamics in response to staurosporine.

A- Aequorin-expressing wild type cells were cultured for 6 hours in the indicated media and after the addition of 20 µM staurosporine (STS), luminescence was followed throughout time and STS-induced amplitude of response calculated. B- Quantification (in arbitrary units) of the $[Ca^{2+}]_c$ transients "A" and "B", respectively, in (A). *, p-value < 0.05.

Distinct transcriptional programs are associated with extracellular Ca^{2+} availability in staurosporine-treated cells

Treatment with 20 µM staurosporine lead to significant alterations in the expression of ~28% of the *N. crassa* genes (1921 genes), as observed by RNA-seq studies (Fig. 22A). The extent of this transcriptional response was amplified in the absence of Ca^{2+} (~36% of genes are altered by the drug (2749 genes)), and markedly suppressed by the excessive concentration of 20 mM $CaCl_2$ (~6% of altered genes (454 genes)) (Fig. 35A-B). In standard medium, the fraction of induced and repressed genes was almost the same (Fig. 22B). In 0 Ca^{2+} medium, 43.1% of the altered genes were upregulated whereas 56.9% where downregulated. Remarkably, in the presence of excessive Ca^{2+} most of the altered genes were repressed (~68%).

We analysed the distribution of the individual genes induced and repressed by staurosporine in the different culture media using Venn diagrams. In 0 Ca^{2+}, 792 (66.8%) of the induced genes were specific to this condition while in 20 mM $CaCl_2$ they were 67 (46.2%) (Fig. 35C). Among repressed genes, 875 (56.0%) and 157 (50.8%) genes were specific to 0 Ca^{2+} and 20 mM $CaCl_2$ media, respectively

(Fig. 35D). Only minor fractions of the altered genes (30 induced and 74 repressed) were common to all conditions.

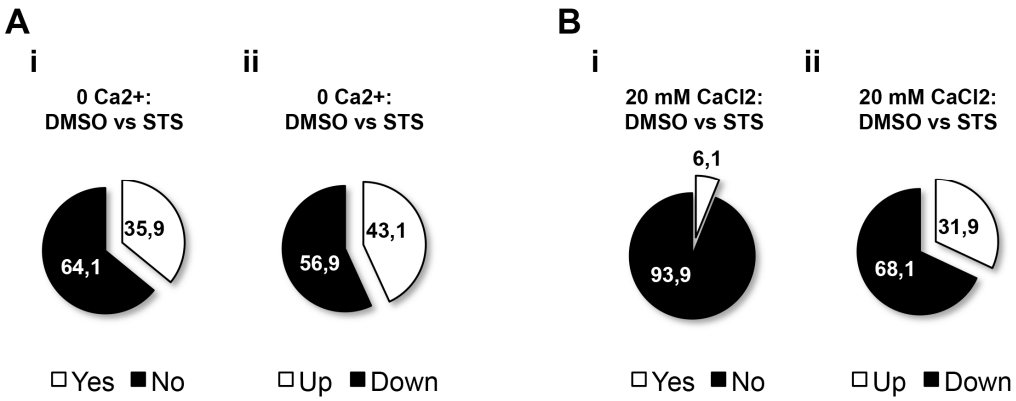

C

MM DMSO vs MM STS (induced genes)	
Total	989
Specific	56.1%
Shared with 0 Ca2+	36.4%
Shared with 20 mM	4.4%
Shared with all	3.0%

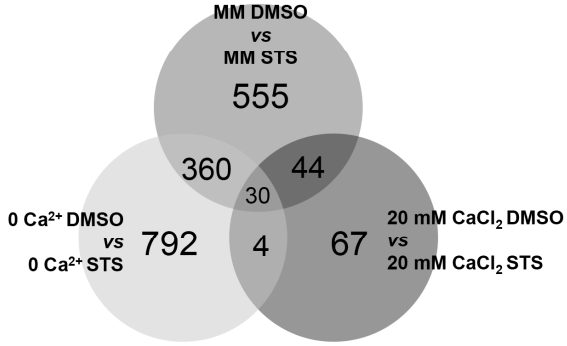

0 Ca^{2+} DMSO vs 0 Ca^{2+} STS (induced genes)	
Total	1186
Specific	66.8%
Shared with MM	30.4%
Shared with 20 mM	0.3%
Shared with all	2.6%

20 mM $CaCl_2$ DMSO vs 20 mM $CaCl_2$ STS (induced genes)	
Total	145
Specific	46.2%
Shared with MM	30.3%
Shared with 0 Ca2+	2.8%
Shared with all	20.7%

D

MM DMSO vs MM STS (repressed genes)	
Total	1038
Specific	28.7%
Shared with 0 Ca2+	57.9%
Shared with 20 mM	6.3%
Shared with all	7.1%

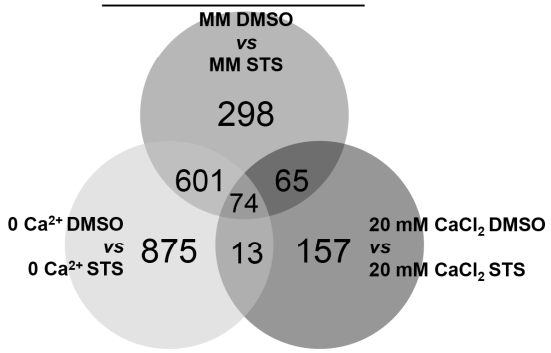

0 Ca^{2+} DMSO vs 0 Ca^{2+} STS (repressed genes)	
Total	1563
Specific	56.0%
Shared with MM	38.5%
Shared with 20 mM	0.8%
Shared with all	4.7%

20 mM $CaCl_2$ DMSO vs 20 mM $CaCl_2$ STS (repressed genes)	
Total	309
Specific	50.8%
Shared with MM	21.0%
Shared with 0 Ca2+	4.2%
Shared with all	23.9%

Figure 35 - Overview of the transcriptional response to staurosporine in minimal media containing different concentrations of Ca^{2+}.

A-B- The percentage of genes with altered expression (i) and the fraction of induced and repressed genes (ii) were calculated for the specific culture medium: 0 Ca^{2+} medium (A) and 20 mM $CaCl_2$ medium (B). C-D- Venn diagrams were used to assess the amount of Ca^{2+}-specific staurosporine-induced (C) and -repressed genes (D). General statistics for Ca^{2+}-specific transcriptional responses are presented.

FunCat was used to examine the enrichment of functional categories in the different gene sets. Specifically in standard MM, staurosporine induced the

expression of genes included in several functional categories like ‘lipid, fatty acid and isoprenoid metabolism’, ‘protein modification’, ‘vesicular transport’ or ‘cell export and secretion’ (Table 8). In 0 Ca^{2+}-specific induced genes, there was no outstandingly strong functional enrichment, though some categories within the ‘Metabolism’ super-category showed statistical significance. Among the 20 mM $CaCl_2$-specific induced genes, there was an enrichment of ‘rRNA processing’ genes.

Table 8 - Functional enrichment analysis (FunCat) of genes induced by staurosporine in specific culture media.

ID	Category	P-value
Standard MM		
01.06	lipid, fatty acid and isoprenoid metabolism	5.03E-06
14.01	protein folding and stabilization	1.05E-04
14.07	protein modification	7.33E-06
14.07.02	modification with sugar residues (eg, glycosylation,	8.58E-07
20.01.03	C-compound and carbohydrate transport	8.20E-04
20.01.13	lipid/fatty acid transport	1.58E-04
20.09	transport routes	2.15E-05
20.09.07	vesicular transport (Golgi network, etc)	2.81E-07
20.09.16	cellular export and secretion	9.91E-05
0 Ca^{2+}		
01.20.01.09	metabolism of aminoglycoside antibiotics	0.0065
01.25	extracellular metabolism	0.0080
01.25.11	extracellular aminosaccharide degradation	0.0065
20 mM $CaCl_2$		
11.04	RNA processing	3.94E-05
11.04.01	rRNA processing	1.84E-04

The most interesting Ca^{2+} concentration-specific differences were found among the downregulated genes. In staurosporine-treated standard medium, cells strongly repressed genes involved in ‘Protein synthesis’, particularly those related with ‘ribosomal biogenesis’ and ‘translation’, as well as genes involved in ‘electron transport’, ‘aerobic respiration’ or ‘energy generation’ (Table 9). In the absence of Ca^{2+}, staurosporine lead to the downregulation of genes included in numerous enriched categories. These encompass various groups within the ‘Metabolism’ super-category such as ‘metabolism of the aspartate family’, ‘purine nucleotide/nucleoside/nucleobase metabolism’, ‘phosphate metabolism’ and

'tetracyclic and pentacyclic triterpenes metabolism'. Also, there was a specific repression of genes involved in 'Cell cycle and DNA processing' and 'Transcription', namely 'mRNA synthesis' and 'mRNA processing'. Categories related to stress responses like 'Protein fate', 'unfolded protein response', 'cellular sensing and response to external stimulus', 'cell growth', 'anti-apoptosis' were also repressed. Finally, while in standard MM there was a downregulation of 'aerobic respiration' genes, in 0 Ca^{2+} other bioenergetic pathways were repressed: 'glycolysis and gluconeogenesis' and 'pentose-phosphate pathway'. These data indicate that a highly complex transcriptional program is established by staurosporine-treated cells growing in the absence of Ca^{2+} that results in the repression of several genes related with an anti-stress response. It seems that, when Ca^{2+} is limited, staurosporine causes the downregulation of cellular defences and this is probably related to the high cellular susceptibility to the drug. The set of genes specifically repressed in 20 mM $CaCl_2$ is also enriched in some functional categories such as 'amino acid metabolism' and 'electron transport'. There was no extraordinarily strong enrichment of FunCat categories in Ca^{2+}-unspecific (that is, similarly altered in the different media) staurosporine-induced and -repressed genes, though some categories present statistical significance, like 'metabolism of alkanes, alkenes, alkanals, alkanols' and 'siderophore-iron transport', respectively. The former is consistent with the alkanoid nature of staurosporine.

Table 9 - Functional enrichment analysis (FunCat) of genes repressed by staurosporine in specific culture media.

ID	Category	P-value
Standard MM		
02.11	electron transport and membrane-associated energy	1.05E-08
02.13	respiration	2.46E-10
02.13.03	aerobic respiration	3.27E-09
02.45	energy conversion and regeneration	1.54E-05
02.45.15	energy generation (eg, ATP synthase)	6.43E-09
12.01	ribosome biogenesis	1.75E-34
12.01.01	ribosomal proteins	3.74E-40
12.04	translation	4.61E-28
16.01	protein binding	3.14E-11
16.03.03	RNA binding	6.12E-05
20.01.15	electron transport	5.26E-05

20.09.04	mitochondrial transport	0.0002
34.01.01.03	homeostasis of protons	9.98E-05
0 Ca^{2+}		
01.01	amino acid metabolism	1.19E-06
01.01.06	metabolism of the aspartate family	2.75E-05
01.03	nucleotide/nucleoside/nucleobase metabolism	1.63E-06
01.03.01	purine nucleotide/nucleoside/nucleobase metabolism	6.05E-05
01.03.16.01	RNA degradation	0.0002
01.04	phosphate metabolism	4.61E-07
01.05.02.04	sugar, glucoside, polyol and carboxylate anabolism	0.0032
01.05.05.04	C- compound anabolism	0.0061
01.05.09.04	aminosaccharide anabolism	0.0056
01.06	lipid, fatty acid and isoprenoid metabolism	2.16E-05
01.06.06.11	tetracyclic and pentacyclic triterpenes (cholesterin, steroids and	7.56E-06
02.01	glycolysis and gluconeogenesis	0.0007
02.07	pentose-phosphate pathway	0.0011
10	cell cycle and DNA processing	2.35E-07
11.02	RNA synthesis	1.74E-08
11.02.03	mRNA synthesis	7.29E-07
11.04	RNA processing	3.07E-07
11.04.03	mRNA processing (splicing, '-, '-end processing)	3.84E-05
14	protein fate (folding, modification, destination)	8.30E-06
18	regulation of metabolism and protein function	4.69E-05
20.01.10	protein transport	9.40E-05
20.03	transport facilities	5.89E-05
20.09	transport routes	2.83E-11
30	cellular communication/signal transduction mechanism	6.17E-05
32.01.07	unfolded protein response (eg, ER quality control)	1.34E-05
34.11	cellular sensing and response to external stimulus	1.39E-06
40.01	cell growth / morphogenesis	8.94E-06
40.10.02.01	anti-apoptosis	0.0026
42.01	cell wall	8.82E-06
42.04	cytoskeleton/structural proteins	3.62E-05
43.01.03.05	budding, cell polarity and filament formation	5.28E-05
20 mM $CaCl_2$		
01.01	amino acid metabolism	1.20E-05
01.01.03	assimilation of ammonia, metabolism of the glutamate group	0.0003
01.06	lipid, fatty acid and isoprenoid metabolism	0.0006
01.07	metabolism of vitamins, cofactors, and prosthetic groups	0.0043
01.20.37.01	metabolism of thioredoxin, glutaredoxin, glutathione	0.0010
02.11	electron transport and membrane-associated energy	9.03E-05
20.01.15	electron transport	0.0001

Altogether, RNA-seq analysis of the fungal reaction to staurosporine in media containing different concentrations of Ca^{2+} revealed that the drug triggers very distinct transcriptional responses. This is probably related to differences in staurosporine-induced cell death levels in the different media.

Lack and excess of Ca^{2+} results in basal alterations in gene expression

The transcriptional response to the lack or excess of Ca^{2+} alone was analysed by comparing gene expression in 0 Ca^{2+}, 20 mM $CaCl_2$ and standard MM. The fraction of genes with altered expression in 0 Ca^{2+} and 20 mM $CaCl_2$ compared with standard MM was 3.9% and 1.8%, respectively (Fig. 36A-B), corresponding to 281 and 129 genes, respectively. While half of the genes altered in 0 Ca^{2+} were induced and half were repressed, in 20 mM $CaCl_2$ most of the altered genes were upregulated (71.3%). Most of the genes were specifically induced or repressed depending on the particular culture medium: 97.2% and 97.1% for 0 Ca^{2+}, respectively, and 95.7% and 89.2% for 20 mM $CaCl_2$, respectively (Fig. 37A-B). Not surprisingly, categories related to 'ion transport', 'homeostasis of cations' and 'homeostasis of anions' were enriched in the set of induced genes in the absence of Ca^{2+} (Fig. 37A), which is possibly linked to a cellular attempt to recover proper conditions of osmolarity. Consistently, these categories were also significantly enriched among the repressed genes in the presence of 20 mM $CaCl_2$ (Fig. 37B). Lack of Ca^{2+} also seems to be associated to a metabolic adaptation of the cells, since there was enrichment in induction of genes of the 'Metabolism' super-category, like 'amino acid metabolism', 'nitrogen, sulfur and selenium metabolism' and 'anaerobic respiration'. The presence of 20 mM $CaCl_2$ caused the induction of genes related to 'electron transport' and 'vesicular transport'. The category 'pH stress response' was enriched in the sets of 0 Ca^{2+}-induced genes and 20 mM $CaCl_2$-repressed genes.

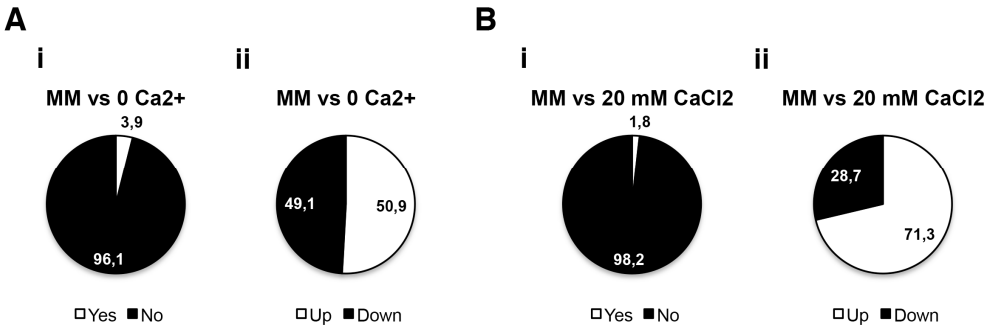

Figure 36 - Overview of the *N. crassa* transcriptional response to limited or excess of Ca^{2+}.

The percentage of genes with altered expression (i) and the fraction of induced and repressed genes (ii) was calculated for 0 Ca^{2+} (A) and 20 mM $CaCl_2$ medium (B), when compared with standard MM.

A

0 Ca^{2+} upregulated genes (139)

ID	Category	P-value
01.01	amino acid metabolism	3.52E-06
01.02	nitrogen, sulfur and selenium metabolism	3.95E-08
02.13.01	anaerobic respiration	0.002958
20.01.01.01	cation transport	2.19E-05
20.01.01.07	anion transport	4.29E-05
20.03	transport facilities	1.59E-06
20.09.18.07	non-vesicular cellular import	3.39E-07
32.01.04	pH stress response	0.001205
34.01.01	homeostasis of cations	0.000272
34.01.03	homeostasis of anions	4.92E-05

20 mM $CaCl_2$ upregulated genes (88)

ID	Category	P-value
02.11	electron transport and membrane-associated energy conservation	0.000179
02.11.05	accessory proteins of electron transport and membrane-associated energy conservation	0.002529
02.13	respiration	0.000695
20.09.18.07	non-vesicular cellular import	9.84E-07

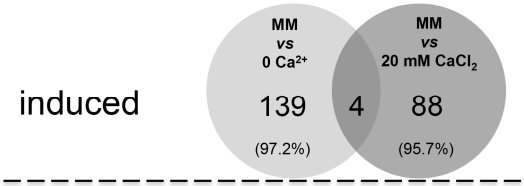

B

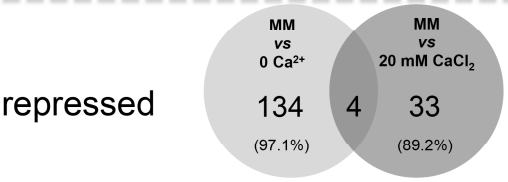

0 Ca^{2+} downregulated genes (134)

ID	Category	P-value
20.03.02.03.01	proton driven antiporter	0.001853

20 mM $CaCl_2$ downregulated genes (33)

ID	Category	P-value
20.01.01.01	cation transport	3.50E-05
20.01.01.07	anion transport	2.61E-06
32.01.04	pH stress response	1.66E-07
34.01.01	homeostasis of cations	7.25E-07
34.01.03	homeostasis of anions	1.80E-07

Figure 37 - Functional enrichment analysis of the transcriptional response to the lack or excess of Ca^{2+}.

The transcriptional response to the absence or excess of Ca^{2+} was investigated by building Venn diagrams showing the distribution of genes with induced (A) or repressed (B) expression in 0 Ca^{2+} and 20 mM $CaCl_2$ medium. Functional enrichment analysis for the specific sets of genes with altered expression is presented.

We looked for alterations in the expression of known Ca^{2+} channels, Ca^{2+}-ATPases, Ca^{2+}-exchangers, Ca^{2+}-dependent signaling molecules and other Ca^{2+} binding proteins (314, 315) (Fig. 38A-G). NCU11680, NCU04736 and NCU07075, encoding the TRP channel YVC-1, the Ca^{2+}-ATPase NCA-2 and the Ca^{2+}/H^{+} antiporter CAX, respectively, were repressed in the absence of Ca^{2+}. NCU04265, encoding the invertase enzyme was induced in the absence of Ca^{2+}. Remarkably, the induction of invertase, encoding an enzyme that hydrolyses extracellular sucrose into glucose and fructose, is a marker of the process of carbon catabolite repression. Invertase gene and activity are induced when the levels of glucose and fructose drop below a threshold (400, 401) or when cells are transferred to a carbon-free medium (402). This further points to an intracellular metabolic remodeling when cells are deprived of Ca^{2+}. NCU08147, encoding the Ca^{2+}-ATPase stress-related ENA-2 was repressed in the presence of 20 mM $CaCl_2$. Finally, NCU05046 and NCU07966, encoding ENA-1 and TRM-1, respectively, were induced by 0 Ca^{2+} and repressed in 20 mM $CaCl_2$ medium.

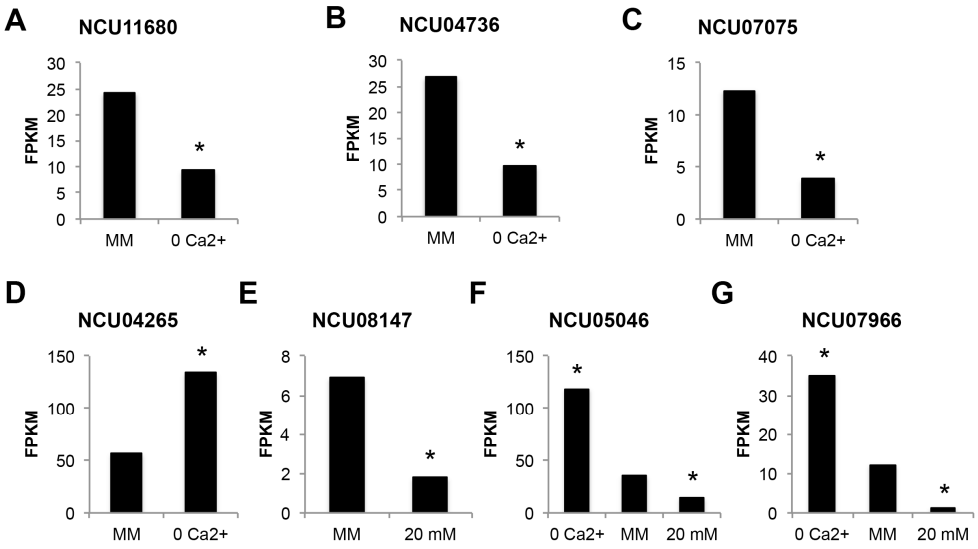

Figure 38 - Expression levels of selected genes encoding components of the Ca^{2+}-machinery in the different culture media.
The genes NCU11680 (A), NCU04736 (B), NCU07075 (C), NCU04265 (D), NCU08147 (E), NCU05046 (F) and NCU07966 (G) are represented.

Identification of putative novel components of the N. crassa Ca^{2+}-handling machinery

We found that 188 genes with unknown function ('hypothetical proteins') had altered expression in 0 Ca^{2+} or 20 mM $CaCl_2$ medium. We screened the respective protein sequences for the presence of Ca^{2+}-binding motifs using CaPS (305) and identified 6 candidates (NCU01697, NCU08524, NCU06116, NCU07582, NCU06607 and NCU03647). The former 4 showed altered expression in 0 Ca^{2+} and the other 2 in the presence of 20 mM $CaCl_2$.

We could not find any strong homology link between NCU06116 and other known proteins, even around the predicted Ca^{2+}-binding motif. Likewise, although the sequence of NCU03647 presents some conserved regions, we could not find any obvious homology to Ca^{2+}-binding proteins. Also, the CaPS tool only predicted, for NCU03647, the loop region of the EF-hand domain but not any of the two helices that typically flank it. The EF-hand loop region alone was predicted for NCU01697 but no strong homology to other known proteins was found. For NCU07582, the EF-hand loop and the entering helix were predicted. Iterative PSI-BLAST searches for distant protein relationships found some similarity between NCU07582 and the stress sensor and component of the cell wall integrity pathway WSC2 from species of the Saccharomyces genus (403). However, WSC2 does not seem to bind Ca^{2+} and the fact that the predicted Ca^{2+}-binding pattern in NCU07582 lacks the exiting helix after the EF-hand loop does not argue in favour of a Ca^{2+}-binding role for this protein. Thus, although preliminary experiments showed that deletion strains for NCU06116, NCU03647 and NCU07582 display increased susceptibility to Ca^{2+} stress (data not shown), we discarded these and NCU01607 (because the respective deletion strain did not show alterations in susceptibility to Ca^{2+} stress) from additional studies.

Of the remaining candidates with a predicted "EF-hand-like" motif, NCU08524 was repressed in Ca^{2+}-free medium whereas NCU06607 was induced by 20 mM $CaCl_2$ (Fig. 39A). It is now recognized that multiple variations to the canonical EF-hand domain exist and it was proposed that a EF-hand-like motif represented by the expression Dx[DN]xDG occurs in all kingdoms, including fungi (307, 308). We aligned the predicted Ca^{2+}-binding motif of NCU08524 and NCU06607 with proteins containing the Dx[DN]xDG motif (307). A good match

was found between NCU08524 and the rhamnogalacturonan lyase YesW from *Bacillus subtilis* (Fig. 39B). A specific group of Dx[DN]xDG-containing proteins known as the 'calcium blades' is characterized by the presence of β-strands flanking the Ca^{2+}-binding motif (307). Consistently, analysis of the secondary structure of NCU08524 shows the presence of strands flanking the DxDxDG domain. PSI-BLAST searches revealed homology relationships between NCU08524 and a fucose-specific lectin from *Macrophomina phaseolina* (Table 10), and a fungal lectin from *Psathyrella velutina* was recently described as a calcium blade containing the Dx[DN]xDG motif (307).

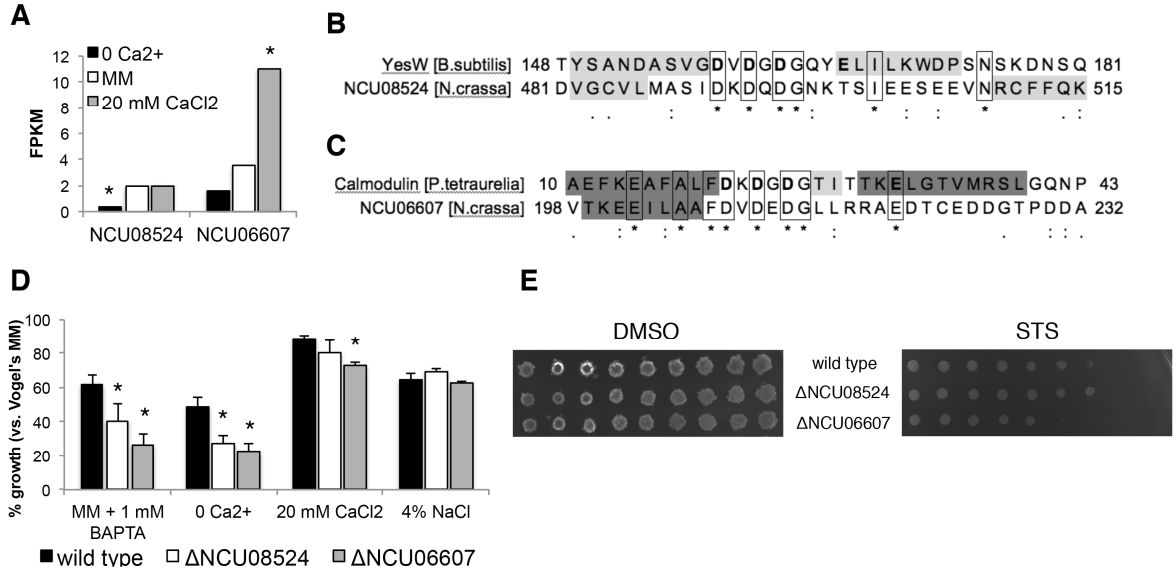

Figure 39 - Identification of putative novel Ca^{2+}-binding proteins.
A- Expression levels of NCU08524 and NCU06607 in 0 Ca^{2+}, standard MM and 20 mM $CaCl_2$ media. *, p-value ≤ 0.05. B-C- Sequence alignments of the EF-hand-like domain of NCU08524 and YesW from *B. subtilis* (accession number: O31526; PDB code: 2z8r) (B) and NCU06607 and calmodulin from *P. tetraurelia* (accession number: P07463; PDB code: 1exr) (C). Experimentally confirmed residues binding Ca^{2+} in YesW and calmodulin are in bold; β-strands and α-helices are shaded in light and dark grey, respectively (crystallographically confirmed for YesW (404) and calmodulin (405) and predicted with MEMSAT3 (369) for NCU08524 and NCU06607). D- The percentage of growth *versus* the control of wild type, ΔNCU08524 and ΔNCU06607 strains stressed with BAPTA, growing in 0 Ca^{2+} or 20 mM $CaCl_2$ medium or treated with 4% (w/v) NaCl was determined by following absorbance at 450 nm. *, p-value ≤ 0.05. E- The spot assay was used to examine the sensitivity of ΔNCU08524 and ΔNCU06607 to 5 μM staurosporine (STS).

A good alignment match was found for the predicted Ca^{2+}-binding motif of NCU06607 and a calmodulin from *Paramecium tetraurelia* (Fig. 39C), which possesses the Dx[DN]xDG motif and binds Ca^{2+} (308). PSI-BLAST searches using

NCU06607 revealed distant similarity to bacterial hemolysin-type calcium-binding protein from *Thalassospira xiamenensis* and von Willebrand factor A from *Halococcus salifodinae* (Table 10). In humans, the A2 domain of von Willebrand factor is known to bind Ca^{2+} and this favours stabilization of the protein (406). There is a strong bias in the localization of proteins possessing the Dx[DN]xDG motif towards the cell surface or secretion (307) and, in agreement with this, a plasma membrane localization together with a transmembrane domain was predicted for NCU08524 whereas NCU06607 has a predicted extracellular localization (Table 10).

Table 10 - Protein sequence features of the two putative novel Ca^{2+}-binding proteins NCU08524 and NCU06607.

Protein	**Ca^{2+}-binding motif** [a]	**CD** [b]	**TMD** [c]	**SL** [d]	**Homology** [e]
NCU08524	491-DKDQDGNKTSIEE-503	Fucose-specific lectin	1	PM: 18; Nu: 4; Mi: 2; Cy: 1	Fungal fucose-specific lectin (*M. phaseolina*) [7E-07; 2] Serine/threonine kinase PKN13 (*C. apiculatus*) [1E-03; 2]
NCU06607	208-DVDEDGLLRRAED-220	No hits	0	Ex: 25	Hemolysin-type calcium-binding protein (*T. xiamenensis*) [3E-08; 2]; FecR (*C. stagnale*) [2E-07; 2]; von Willebrand factor A (*H. salifodinae*) [3E-07; 2]; Cell surface antigen Sca13 (*R. bellii*) [6E-07; 2] Halomucin (*H. walsbyi*) [1E-06; 2] Antigen Cs44 (*C. sinensis*) [1E-04; 2]

[a] Ca^{2+}-binding motifs were predicted with CaPS (305). [b] Conserved domains were predicted with InterProScan (368). [c] The number of transmembrane domains was predicted with TMHMM 2.0 (370). [d] Subcellular localization was predicted with WoLF PSORT (371); PM: plasma membrane; ER: endoplasmic reticulum; Nu: nuclear; Mi: mitochondria; Cy: cytosol; Ex: extracellular; Go: Golgi apparatus; the value in front of each prediction corresponds to the score (the higher the score, the more reliable is the prediction). [e] Homology was predicted with PSI-BLAST (366); the value in front of each prediction (between square brackets) corresponds to the E-value and the PSI-BLAST iteration number.

The growth of ΔNCU08524 and ΔNCU06607 was compared with the wild type strain under different conditions of Ca^{2+} availability. Both mutants showed increased susceptibility to the addition of the Ca^{2+} chelator BAPTA in standard MM and to growth in 0 Ca^{2+} medium (Fig. 39D). ΔNCU06607 also showed significantly reduced growth in the presence of 20 mM $CaCl_2$ when compared with the wild type. The observed differences were not merely due to an unspecific osmotic stress, since the wild type and knockout strains were similarly affected by the addition of 4% (w/v) NaCl. ΔNCU06607 was slightly more sensitive to staurosporine, suggesting that the respective protein is involved in the fungal response to the drug (Fig. 39E).

In summary, the RNA-seq dataset led us to two putative novel components of the *N. crassa* Ca^{2+}-handling machinery. Because they show only distant similarity to characterized proteins, as found using PSI-BLAST, this is likely the reason why they were not spotted before as Ca^{2+}-binding molecules. Some of these similar proteins were experimentally confirmed as Ca^{2+}-binding proteins.

Functional respiratory chain and ROS generation are required for the staurosporine-induced Ca^{2+} response

Previous data from our group suggested that the mitochondrial respiratory chain seems to play an important role during cell death in *N. crassa* (113, 139, 149) and Ca^{2+} is a crucial mediator of staurosporine-induced cell death (as shown above). Thus, we assessed whether the modulation of the activity of the respiratory chain affects the staurosporine Ca^{2+}-signature. We measured the $[Ca^{2+}]_c$ alterations caused by staurosporine in cells pre-incubated with specific inhibitors of the different enzymatic complexes of the mitochondrial respiratory chain. In the presence of the complex I inhibitor rotenone, staurosporine induced a different Ca^{2+} profile: peak “A” was severely reduced, peak “B” disappeared and the prolonged signal “C” began earlier (Fig. 40A and 40E-F). A similar profile was observed with cells pre-incubated with the complex IV inhibitor KCN (220) (Fig. 40C and 40E-F). DPI is a modulator of flavoenzymes, targeting complex I, NAD(P)H oxidases and alternative NAD(P)H dehydrogenases, and inhibits mainly NADPH rather than NADH oxidation (407-409). In the presence of

diphenyleneiodonium, the Ca^{2+} response to staurosporine was also significantly altered, with reduced peaks “A” and “B” (Fig. 40A and 40E-F).

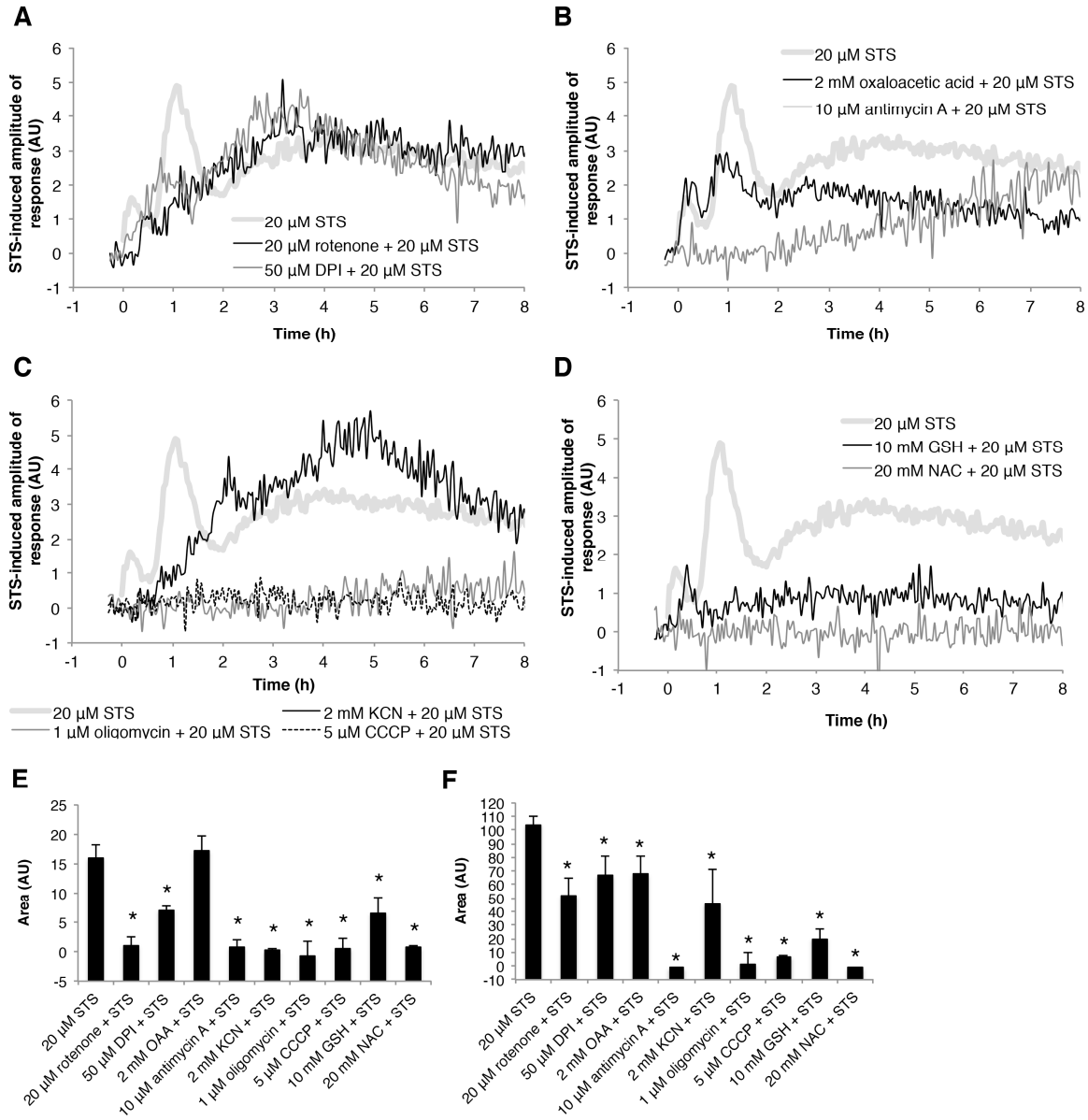

Figure 40 - Normal activity of the mitochondrial respiratory chain and ROS generation are required for the staurosporine-induced Ca^{2+}-signature.

A-D- Influence of pre-treatment with different compounds on the Ca^{2+}-signature after aequorin-expressing wild type cells were treated with 20 µM staurosporine (STS): 20 µM rotenone, 50 µM DPI (A), 2 mM oxaloacetic acid, 10 µM antimycin A (B), 2 mM potassium cyanide (KCN), 1 µM oligomycin, 5 µM CCCP (C), 10 mM GSH and 20 mM NAC (D). E-F- Quantification (in arbitrary units) of the $[Ca^{2+}]_c$ transients “A” and “B”, respectively, in (A)-(D). *, p-value < 0.05.

When complex II was inhibited with oxaloacetic acid there was a reduction on the amplitude of peak “B” while peak “A” was not affected (Fig. 40B and Fig. 40E-F). Inhibition of complex III with antimycin A completely altered the profile of the Ca^{2+} response to staurosporine, as most of the signal was lost and there was a

late increase in cytosolic Ca^{2+} (Fig. 40B and 40E-F). Inhibition of F1-F0 ATP synthase (complex V) with oligomycin drastically impaired the staurosporine Ca^{2+}-signature (Fig. 40C and 40E-F). When mitochondria were depolarized with CCCP, Ca^{2+} signals were totally abolished (Fig. 40C and 40E-F).

Given the involvement of the respiratory chain (a major ROS generator) and that staurosporine strongly provokes oxidative stress (Fig. 18B) required for cell death to occur (Fig. 19A-B), we asked whether this was associated with the Ca^{2+} response. In the presence of the antioxidants GSH or its precursor NAC in concentrations that effectively block ROS accumulation (139), the Ca^{2+} response to staurosporine was robustly suppressed (Fig. 40D-F), suggesting its dependence on ROS accumulation and that ROS production precedes Ca^{2+} influx. To rule out the possibility that this was a GSH- and NAC-specific effect, we also evaluated the staurosporine Ca^{2+}-signature in cells pre-incubated with a different type of antioxidant, trolox (a vitamin E derivative), which also resulted in a substantial blockage of the signal (Fig. 41). All inhibitors of the respiratory chain as well as the ROS scavengers alone did not cause substantial alterations in Ca^{2+} (data not shown). These data indicate that normal activity of the mitochondrial respiratory chain and ROS generation are required for the staurosporine-induced Ca^{2+} response.

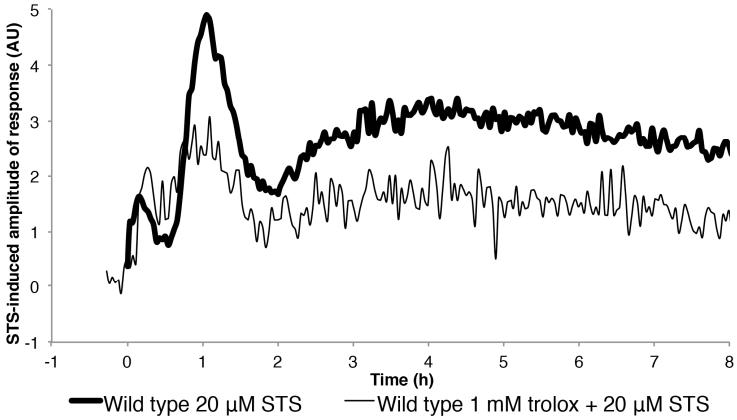

Figure 41 - ROS generation is important for the staurosporine-induced Ca^{2+} response.
Influence of pre-treatment with 1 mM trolox on the Ca^{2+}-signature after aequorin-expressing wild type cells were treated with 20 µM staurosporine (STS).

Alternative NAD(P)H dehydrogenases and subunits of complex I are important mediators of staurosporine-induced cell death

The external alternative NAD(P)H dehydrogenases of *N. crassa* NDE-1 oxidizes NADPH on a Ca^{2+}-dependent basis (242). We hypothesized that NDE-1 could mediate the effects of staurosporine and evaluated the Ca^{2+} response in the deletion strain. Although peak "A" was present, peak "B" was almost absent on Δ*nde-1* cells (Fig. 42A and 42G-H), suggesting the involvement of NDE-1 in the regulation of Ca^{2+} dynamics.

Since the 51 kDa and 14 kDa subunits of the mitochondrial complex I (NUO51 and NUO14, respectively) seem to be involved in the response to staurosporine (139, 226), Ca^{2+} dynamics was also analysed on the respective knockout cells. Peak "A" was significantly reduced on Δ*nuo51* cells, whereas peak "B" was almost absent, similarly to Δ*nde-1* cells (Fig. 42B and 42G-H). In a strain lacking NUO14, the fungal homologue of human GRIM-19, involved in cell death and cancer development (268), the Ca^{2+} response was nearly abolished (Fig. 42C and 42G-H). The Δ*nuo51* and Δ*nuo14* knockout cells do not hold complex I activity although deletion of *nuo51* does not prevent assembly of the complex (226, 361). Spot assays revealed that *nde1*-, *nuo51*- and *nuo14*-deleted cells were hypersensitive to staurosporine (Fig. 42I, i).

The staurosporine-induced Ca^{2+}-signature of a strain lacking NUO78, the 78 kDa subunit of complex I (226), which is not hypersensitive to staurosporine (139) also lacked peak "B" and reduced signal "C" (Fig. 42D and 42G-H). Remarkably, a double knockout strain lacking both NUO51 and NDE-1 (Δ*nuo51*Δ*nde-1*) is only slightly more sensitive to staurosporine than wild type, although the Ca^{2+}-signature induced by the drug is different from wild type, since it presents a reduction in signals "B" and "C" (Fig. 42E and 42G-H). Overall, our results point to a novel regulatory role of intracellular Ca^{2+} dynamics for mitochondrial enzymes involved in cellular respiration, namely complex I and the Ca^{2+}-dependent external non-proton pumping NAD(P)H dehydrogenase NDE-1.

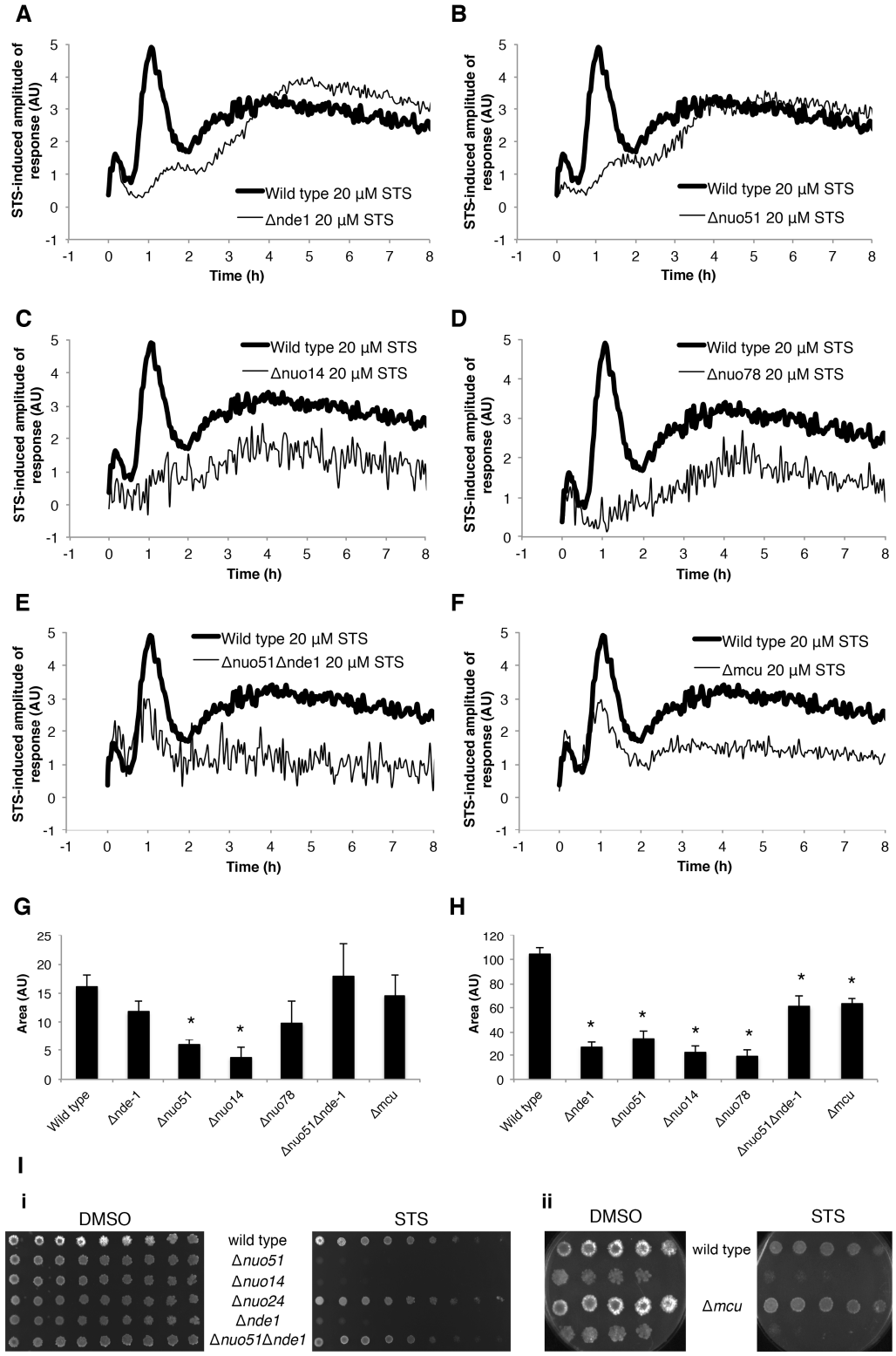

Figure 42 - NDE-1, mitochondrial complex I and MCU are involved in the *N. crassa* response to staurosporine.

A-F- The Ca^{2+}-signature in response to 20 µM staurosporine (STS) was compared in aequorin-expressing wild type and Δ*nde-1* (A), Δ*nuo51* (B), Δ*nuo14* (C), Δ*nuo78* (D), Δ*nuo51*Δ*nde-1* (E) and Δ*mcu* (F) cells. G-H- Quantification (in arbitrary units) of the $[Ca^{2+}]_c$ transients "A" and "B", respectively, in (A)-(F). *, p-value < 0.05. I- The sensitivity of the indicated strains evaluated by spotting conidia on GFS medium containing 2.5 µM STS.

NUO51 is highly conserved from bacteria to mammals, including similarity with the human NDUFV1 (232). Point mutations in *NDUFV1* are causative of mitochondrial disease, namely progressive leukodystrophy and encephalomyopathy (410) and *N. crassa* strains mimicking mutations in *NDUFV1* found in a clinical context were generated (232). We evaluated intracellular Ca^{2+} alterations induced by staurosporine in two strains harboring the A353V and T435M mutations on NUO51 (equivalent to the A341V and T423M human mutations, respectively (410)). Both point mutations resulted in a decrease in the amplitude of all staurosporine-induced Ca^{2+} signals (Fig. 43A-C). Compared to wild type, both the A353V and T435M strains were more resistant to staurosporine (Fig. 43D) and slighty more resistant to hydrogen peroxide and actinomycin D (Fig. 44).

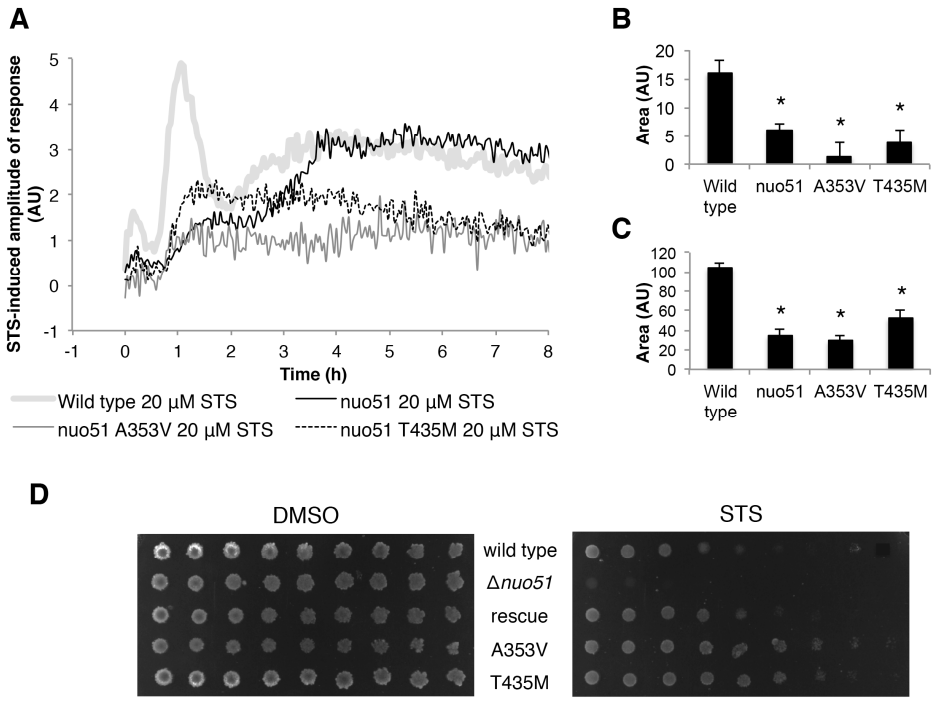

Figure 43 - *N. crassa* models of human disease present abnormal Ca^{2+} dynamics and increased survival in the presence of staurosporine.

A- The Ca^{2+}-signature in response to 20 µM staurosporine (STS) was compared in aequorin-expressing wild type, Δ*nuo51*, nuo51 A353V and nuo51 T435M cells. B-C- Quantification (in arbitrary units) of the $[Ca^{2+}]_c$ transients "A" and "B", respectively, in (A). *, p-value < 0.05. D- The sensitivity of the indicated strains evaluated by spotting conidia on GFS medium containing 2.5 µM STS.

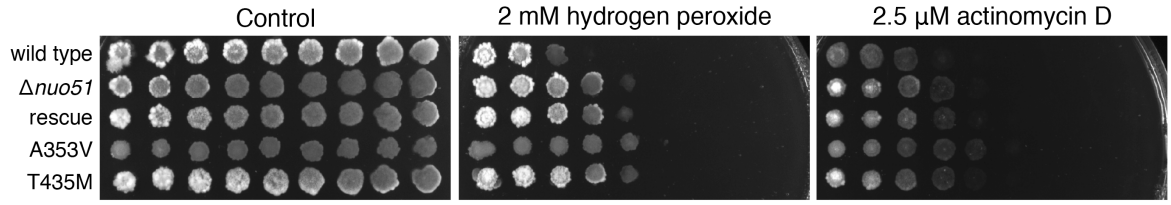

Figure 44 - Disease-related mutant strains A353V and T435M are more resistant than wild type to hydrogen peroxide and actinomycin D.
The spot assay on GFS plates supplemented with hydrogen peroxide and actinomycin D was used to test the sensitivity of the indicated mutant strains.

Due to the effect of inhibiting ER and vacuolar sequestration of Ca^{2+} on the wild type staurosporine Ca^{2+}-signature (Fig. 24C-D), we decided to perform identical experiments in cells lacking *nde-1*. In the Δ*nde-1* mutant, thapsigargin blocked peak "A" due to depletion of Ca^{2+} of the ER preventing its contributing to the cytosolic signal (Fig. 45A-B), as in the wild type (Fig. 24C and 24F-G). Bafilomycin A1, by blocking the vacuolar uptake of Ca^{2+}, slightly augmented the signal in the cytosol, although in the bafilomycin A1 plus staurosporine profile, peaks "A" and "B" were roughly joined (Fig. 45A-B). Also as in the wild type, pre-incubation with thapsigargin and bafilomycin A1 led to a drastic accumulation of cytosolic Ca^{2+} during peak B (Fig. 24D and 24F-G). It is important to emphasize that when exposed to staurosporine alone and compared with wild type, Δ*nde-1* cells lacked peak "B" almost completely. Therefore, the fold increase in the levels of cytosolic Ca^{2+} caused by staurosporine in Δ*nde-1* cells in the presence of thapsigargin and bafilomycin A1 is much higher than in wild type (Fig. 45C). In Δ*nuo51* knockout cells, the response to staurosporine was modulated by thapsigargin and bafilomycin A1 like in Δ*nde-1* cells (Fig. 46A-B). Pre-treatment with these inhibitors resulted in increased levels of cytosolic Ca^{2+} compared with staurosporine alone, namely in peak "B". This may suggest that these Ca^{2+} buffering pathways may be upregulated in the Δ*nde-1* and Δ*nuo51* mutants.

We also measured the accumulation of ROS after treatment with staurosporine in Δ*nde-1* cells. In the wild type strain, a 30-minutes incubation with the drug lead to a ~4.2 fold increase in the formation of ROS relatively to the control (Fig. 45D). Under the same conditions, the fold increase in ROS production in Δ*nde-1* knockout cells was significantly higher (~6.6). The higher levels of ROS induced by staurosporine can be explained by reduced antioxidant capacity or because of a putative upregulation of ROS production in the absence of NDE-1.

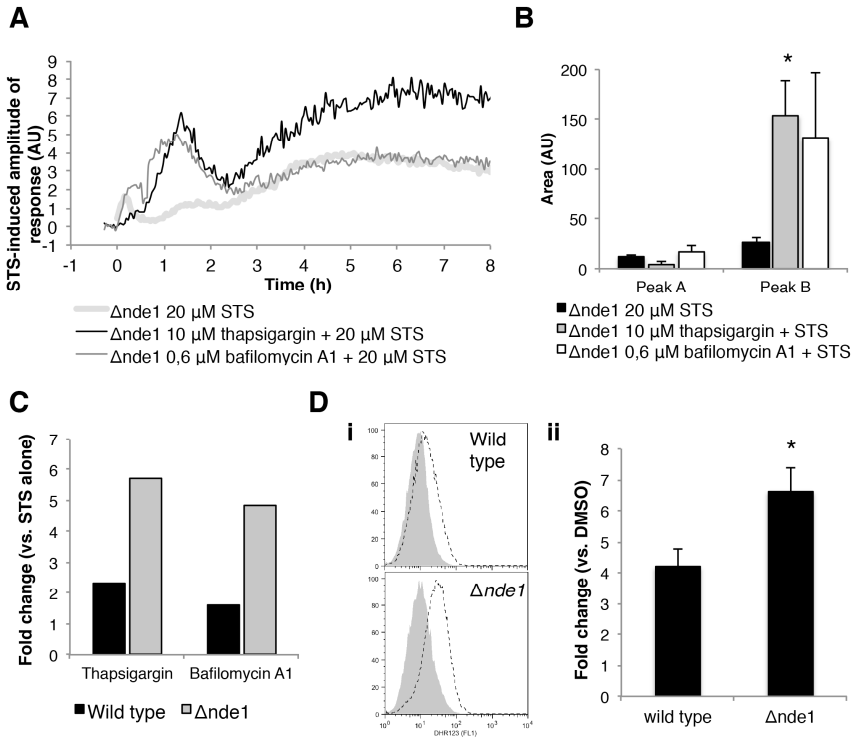

Figure 45 - The absence of NDE-1 leads to abnormal Ca^{2+} fluxes in internal stores and increased ROS accumulation.

A- Cytosolic levels of Ca^{2+} and the amplitude of response were measured after the addition of staurosporine (STS) in aequorin-expressing Δ*nde-1* cells pre-incubated with thapsigargin and bafilomycin A1. B- Quantification (in arbitrary units) of the $[Ca^{2+}]_c$ transients "A" and "B" in (A). *, p-value < 0.05. C- The fold increase in the cytosolic levels of Ca^{2+} in thapsigargin- and bafilomycin A1-pre-treated cells *versus* staurosporine alone was calculated for the wild type and Δ*nde-1* strains. D- Wild type and Δ*nde-1* cells were grown for 4 hours followed by a 30-minute treatment with staurosporine and the accumulation of ROS measured by dihydrorhodamine 123 staining. i) representative histograms and ii) quantification of the fold increase in ROS in staurosporine-treated samples *versus* the control. *, p-value < 0.05.

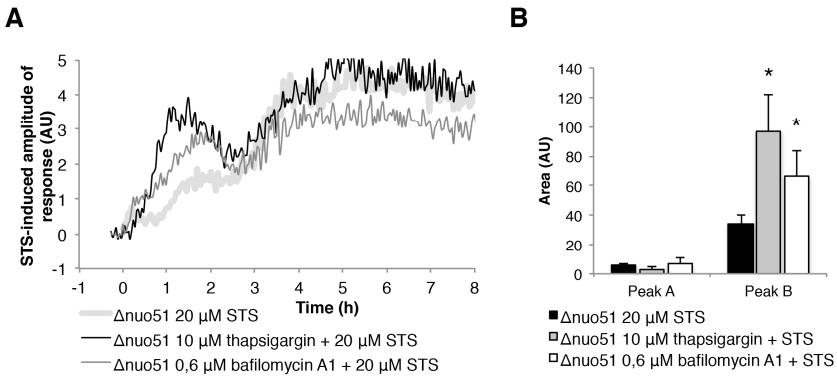

Figure 46 - NUO51 deletion results in altered Ca^{2+} fluxes in intracellular stores.

A- Cytosolic levels of Ca^{2+} and the amplitude of response were measured after the addition of staurosporine (STS) in aequorin-expressing Δ*nuo51* cells pre-incubated with thapsigargin and bafilomycin A1. B- Quantification (in arbitrary units) of the $[Ca^{2+}]_c$ transients "A" and "B" in (A). *, p-value < 0.05.

In *N. crassa*, four alternative NAD(P)H dehydrogenases (NDI-1, NDE-1, NDE-2 and NDE-3) associate with the inner mitochondrial membrane. We examined the sensitivity to staurosporine of a collection of viable double and triple knockout strains for those genes. Several of these strains presented a sensitivity profile distinct from the wild type (Fig. 47). Apart from the aforementioned effect of the deletion of NDE-1, whereas the individual deletion of NDE-2 and NDE-3 resulted in a slight increase in sensitivity and resistance, the individual lack of NDI-1 did not influence tolerance to staurosporine. Interestingly, a combined removal of two or three of these enzymes resulted in moderate to high susceptibility to staurosporine in comparison with the wild type strain. The results support the conclusion that these alternative respiratory systems are important mediators of cell death induced by staurosporine and provide valuable hints for future investigations on the role of these enzymes during cell death.

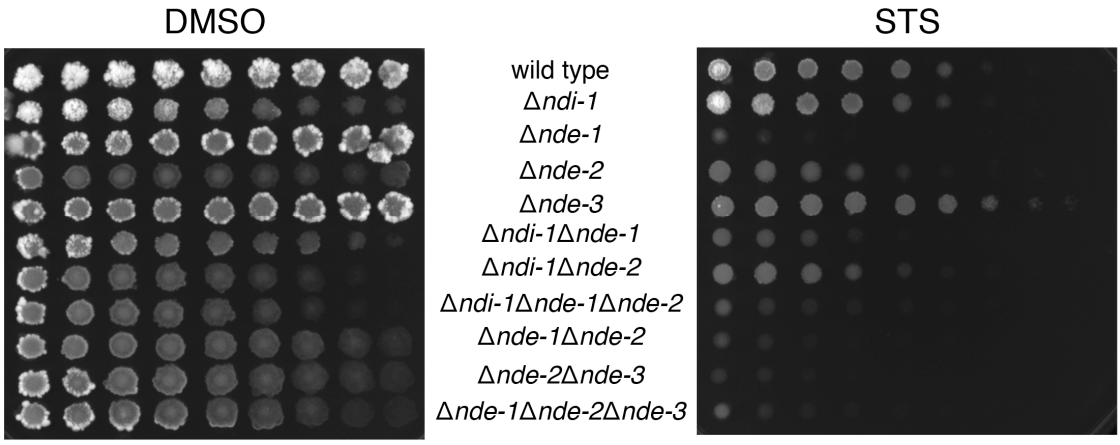

Figure 47 - Disruption of alternative NAD(P)H dehydrogenases leads to altered resistance to staurosporine.
The spot assay on GFS plates supplemented with STS was used to test the sensitivity of the indicated mutant strains for different alternative NAD(P)H dehydrogenases genes.

The genome of N. crassa encodes a mitochondrial Ca^{2+} uniporter that is involved in the response to staurosporine

Mammalian uptake of Ca^{2+} by mitochondria is executed mainly by the MCU (411, 412). An *in silico* study on the evolutionary diversity of this molecule across kingdoms pointed out a putative homologue in *N. crassa*, encoded by NCU08166 (384). Mammalian MCU possesses a conserved domain that encompasses two transmembrane regions intercalated by an acidic loop (411). In line with this,

residues 325 to 381 of *N. crassa* NCU08166 were predicted to include a double transmembrane region (Fig. 48A) and show high level of conservation with human MCU (Fig. 48B), including in residues shown to be crucial for protein activity (412). The staurosporine-induced Ca^{2+}-signature in a Δ*mcu* strain displayed a slight increase in peak "A", whereas signals "B" and "C" were reduced in comparison with wild type (Fig. 42F-H), suggesting a possible involvement of this putative homologue of the mammalian MCU in the *N. crassa* response to staurosporine. We cannot rule out that other proteins can function as mitochondrial Ca^{2+} importers in the absence of MCU. Indeed, preliminary assays in isolated mitochondria from Δ*mcu* cells suggest that some mitochondrial Ca^{2+} uptake can occur even in the absence of the protein (data not shown). The deletion of *mcu* did not affect the sensitivity to staurosporine (Fig. 42I, ii). Despite the fact that our results still raise some questions that need to be addressed, mitochondrial Ca^{2+} dynamics seem to be implicated in the mechanism of action of staurosporine.

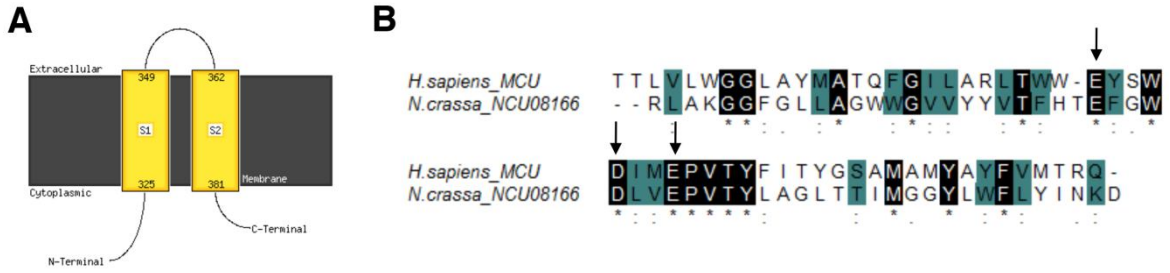

Figure 48 - Comparison between topological and sequence features of NCU08166 and human MCU.

A- Transmembrane domain prediction, with MEMSAT (369), of the NCU08166 region that comprises residues 325 to 381 (Uniprot accession number: Q7S4I4). B- Sequence of alignment of the same region of NCU08166 with its homologue region in the human MCU protein (Q8NE86). Arrows indicate residues that were shown to be required for the Ca^{2+} uptake function of the human MCU (412).

Several members of the Ca^{2+} handling machinery are involved in the fungal response to staurosporine

To further substantiate the crucial role of Ca^{2+} during the *N. crassa* response to staurosporine and to identify mediators of the process we assayed the drug sensitivity profile of approximately 50 deletion strains for members of the Ca^{2+} machinery. Deletion of genes encoding phospholipase C enzymes, especially PLC-2, resulted in resistance to staurosporine (Fig. 27A-B), while strains lacking

the Ca^{2+} channels CCH-1 and MID-1 (Fig. 28E and 29B-D) and the alternative NADPH dehydrogenase NDE-1 (Fig. 42I, i) were hypersensitive. Several other deletion strains, including Ca^{2+}-permeable channels, Ca^{2+}-ATPases and other Ca^{2+} binding molecules involved in cellular signaling presented a resistance phenotype dissimilar from the wild type strain (Fig. 49). A resistance phenotype was particularly strong in knockout mutants for genes encoding the Ca^{2+}-ATPases NCA-2 and PMR-1. The deletion of other Ca^{2+}-ATPases, namely ENA-1, ENA-2 and NCU10143 also led to increased resistance. The disruption of the signaling molecules calmodulin, CAMK-4, and CSE-1 augmented resistance, whereas knockout of STK-16 and PRD-4 resulted in increased susceptibility to staurosporine. Table 11 summarizes the result of the screening of knockout strains. The deletion strains for NCU05360, NCU03804, NCU03833, NCU09871, NCU06347, NCU06617, NCU02411 and NCU09265 were not tested due to strain unavailability or their heterokaryotic nature. This data further stresses the importance and complexity of the fungal response to staurosporine, implicating numerous Ca^{2+}-related proteins of different function and subcellular localization.

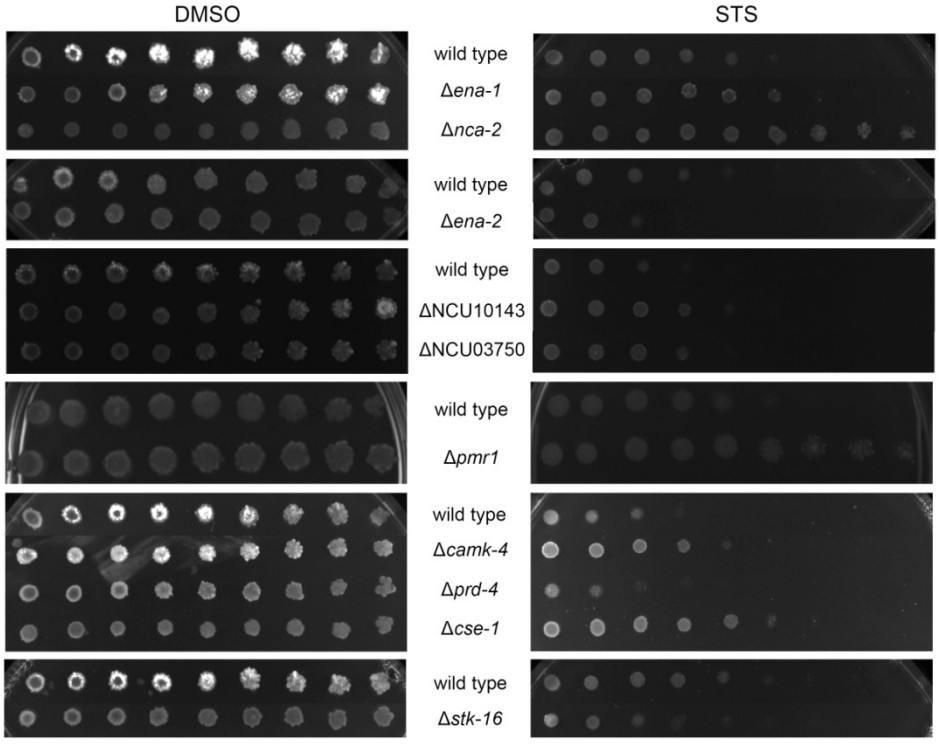

Figure 49 - Several members of the Ca^{2+} handling machinery are involved in the fungal response to staurosporine.

Conidia from the indicated strains were spotted on GFS medium supplemented with staurosporine (STS) and incubated for 3 days.

Table 11 - Ca^{2+}-related knockout strains exhibiting increased sensitivity or resistance to staurosporine when compared with the wild type.

Strain	Gene	Classification	Phenotype
ΔNCU02762	*cch-1*	Ca^{2+}-permeable channel	SS
ΔNCU06703	*mid-1*	Ca^{2+}-permeable channel	SS
ΔNCU04736	*nca-2*	Ca^{2+}-ATPase	RR
ΔNCU05046	*ena-1*	Ca^{2+}-ATPase	R
ΔNCU08147	*ena-2; ph-7*	Ca^{2+}-ATPase	S
ΔNCU10143	-	Ca^{2+}-ATPase	R
ΔNCU03292	*pmr-1*	Ca^{2+}-ATPase	RR
ΔNCU06245	*plc-1*	Phospholipase C (δ-type)	R
ΔNCU01266	*plc-2*	Phospholipase C (δ-type)	RR
ΔNCU09655	*plc-3*	Phospholipase C (δ-type)	R
ΔNCU03750	-	Calmodulin	R
ΔNCU04379	*cse-1*	Ca^{2+} and/or CaM binding protein	R
ΔNCU09212	*camk-4*	Ca^{2+} and/or CaM binding protein	R
ΔNCU00914	*stk-16*	Ca^{2+} and/or CaM binding protein	S
ΔNCU02814	*prd-4*	Ca^{2+} and/or CaM binding protein	S
ΔNCU05225	*nde-1*	Ca^{2+} and/or CaM binding protein	SS

Legend (relative to the wild type): SS: much more sensitive; S: slightly more sensitive; SS: much more resistant; R: slightly more resistant.

3.3) CZT-1 regulates cell death and natural drug resistance

NCU09974/czt-1 is involved in resistance to staurosporine, intracellular Ca^{2+} dynamics and ROS accumulation

Previous DNA microarrays studies in our laboratory identified a group of staurosporine-induced genes (140). Among them, NCU09974 is a highly induced gene that encodes an uncharacterized protein, and so we tested the sensitivity of a ΔNCU09974 deletion strain to staurosporine. We inoculated the wild type and the deletion strain for NCU09974 (ΔNCU09974) on solid Vogel's MM supplemented with staurosporine and observed that the latter was much more affected by the drug (Fig. 50A-B). The same sensitivity to staurosporine was observed when ΔNCU09974 was grown in liquid Vogel's MM (Fig. 50C-D) or spotted on GFS plates (Fig. 50E), indicating that NCU09974 is a key player in resistance to staurosporine-induced cell death.

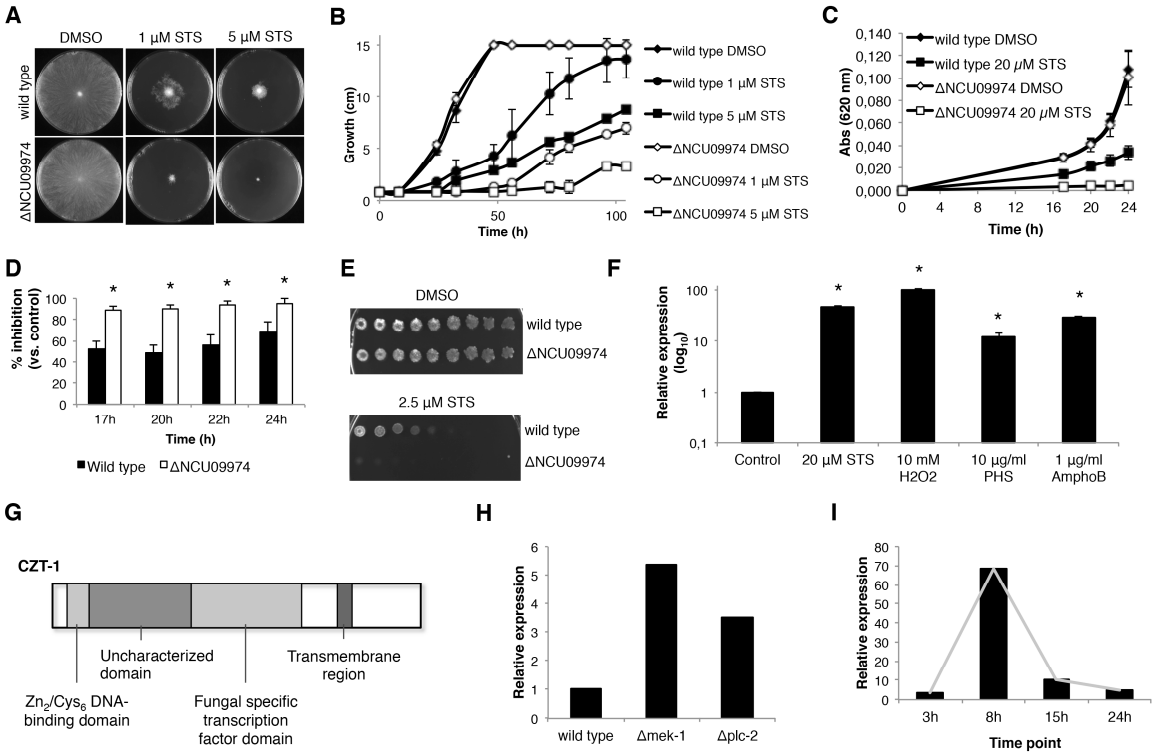

Figure 50 - Deletion of NCU09974/*czt-1* confers sensitivity to staurosporine.

A, B- Conidia from the wild type and ΔNCU09974 strains were inoculated on the center of Petri dishes containing solid Vogel's MM supplemented with staurosporine (STS) or DMSO. Radial growth at 48h (A) and throughout time (B) is shown. C, D- Growth of the strains on liquid Vogel's MM followed by measuring absorbance at 620 nm (C) and percentage of growth inhibition caused by STS (D). *, p-value <0.05. E- Sensitivity of wild type and ΔNCU09974 strains to STS was tested by spotting conidia in GFS medium. F - Relative expression of NCU09974 was quantified by qRT-PCR after exposing wild type cells for to STS, hydrogen peroxide (H_2O_2), phytosphingosine (PHS)

and amphotericin B (AmphoB) for 1 hour. G- Diagram showing the main predicted sequence features of CZT-1. H- *czt-1* expression was evaluated by qRT-PCR in wild type, Δ*mek-1* and Δ*plc-2* strains. I- Time-course relative expression of czt-1 as quantified by qRT-PCR during germination of wild type conidia at 26ºC.

Previous microarray data indicated that expression of NCU09974 is stimulated by exposure to staurosporine (140) and phytosphingosine (116). Indeed, qRT-PCR experiments showed that the gene was not only upregulated by staurosporine and phytosphingosine, but also after the oxidative stress insult with hydrogen peroxide or by the antifungal amphotericin B (Fig. 50F). Furthermore, expression of NCU09974 was also induced upon exposure to menadione (413) and by two novel cell death-inducing compounds currently under characterization in our group (data not shown).

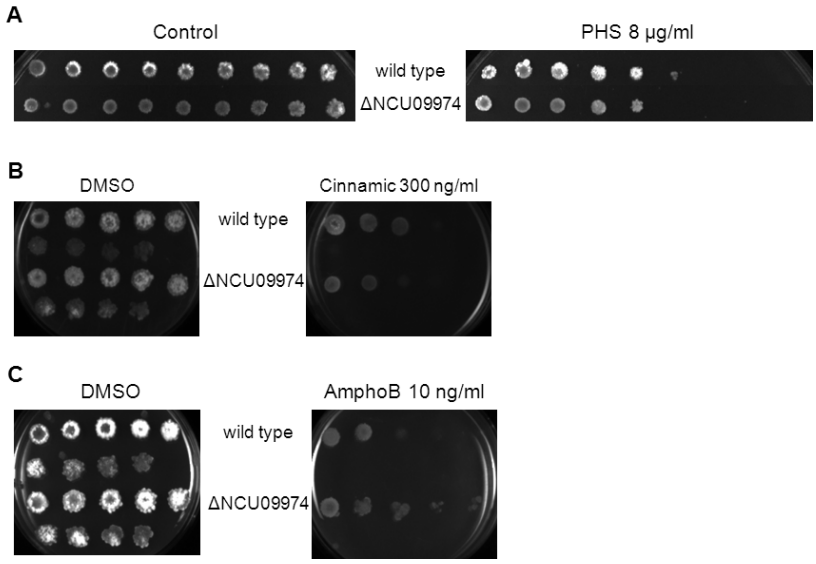

Figure 51 - Sensitivity profile of the wild type and ΔNCU09974 strains to different drugs. Conidia were spotted in GFS medium supplemented with phytosphingosine (PHS) (A), cinnamic acid (B) and amphotericin B (AmphoB) (C).

The sensitivity of ΔNCU09974 to several other chemical compounds was tested with the spot assay. Inhibition of growth of ΔNCU09974 was similar to wild type when the strains were treated with actinomycin D, hydrogen peroxide, deoxycholic acid, acetic acid, ethanol, paraquat, imidazole, cycloheximide, dithiothreitol, 8-hydroxyquinoline, diphenyleneiodonium, menadione, antimycin A, oligomycin or caffeine (data not shown). However, ΔNCU09974 was slightly more sensitive than wild type to phytosphingosine and cinnamic acid (Fig. 51A-B) and more resistant to amphotericin B (Fig. 51C). These data indicate that NCU09974 is

activated by cell death stimuli and its absence is especially crucial for the response to staurosporine, likely because of specific pathways activated by this drug.

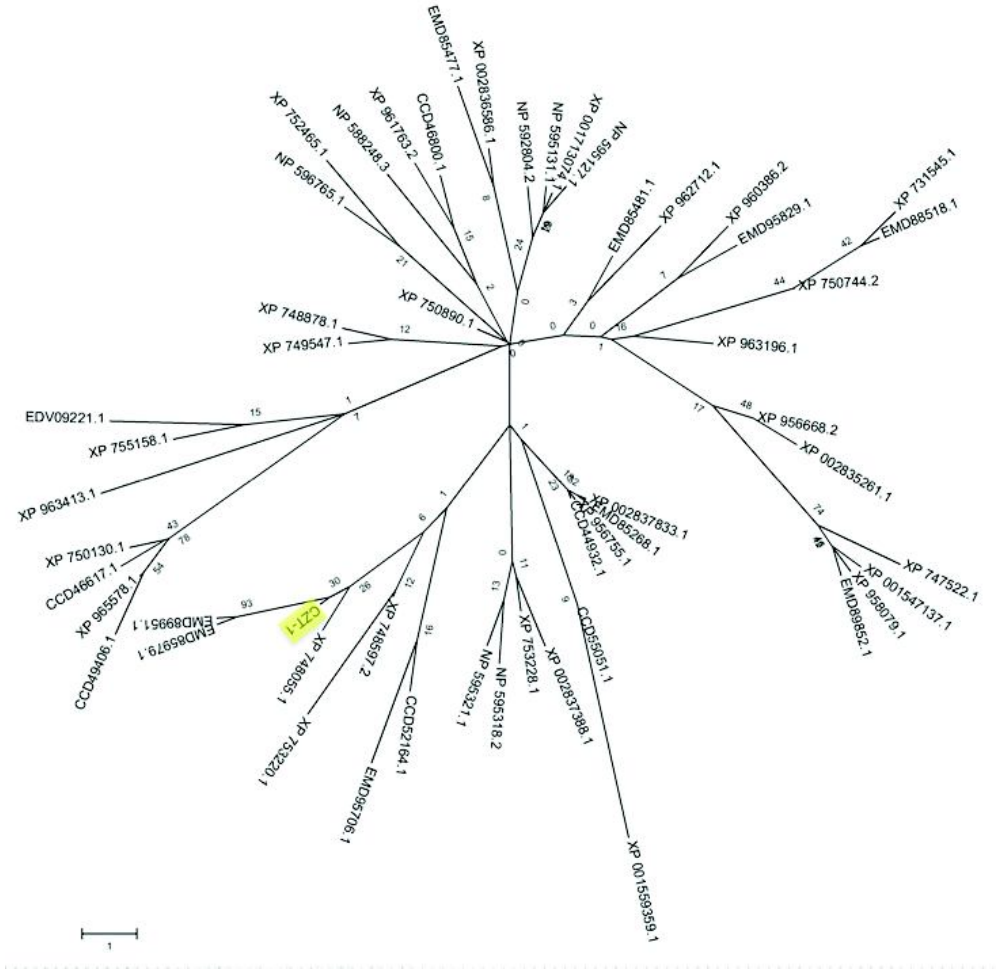

Figure 52 - Maximum likelihood tree illustrating the phylogenetic relationship between CZT-1 and some of its homologues in other fungi.

A maximum likelihood phylogenetic tree was built using the Dayhoff method on a ClustalW2 (367) multiple alignment. The bootstrap test (1000 replications) was applied. Different classes of Ascomycota are represented (one species per class): Sordariomycetes/*Neurospora crassa* (accession numbers: XP_958092.1/CZT-1, XP_956755.1, XP_963196.1, XP_961763.2, XP_958079.1, XP_956668.2, XP_963413.1, XP_960386.2, XP_965578.1, XP_962712.1), Eurotiomycetes/*Aspergillus fumigatus* (XP_748055.1, XP_748597.2, XP_753220.1, XP_753228.1, XP_755158.1, XP_750744.2, XP_731545.1, XP_747522.1, XP_749547.1, XP_750130.1, XP_748878.1, XP_752465.1, XP_750890.1), Dothideomycetes/*Bipolaris maydis* (EMD85979.1, EMD89951.1, EMD85481.1, EMD85477.1, EMD85268.1, EMD89852.1, EMD88518.1, EMD95829.1, EMD95706.1), Pezizomycetes/*Tuber melanosporum* (XP_002837388.1, XP_002837833.1, XP_002836586.1, XP_002835261.1), Leotiomycetes/*Botrytis cinerea* (CCD52164.1, CCD44932.1, CCD46036.1, CCD55051.1, CCD49406.1, CCD46800.1, CCD43955.1, CCD46617.1), Saccharomycetes/*Saccharomyces cerevisiae* (EDV09221.1) and Schizosaccharomycetes/*Schizosaccharomyces pombe* (XP_001713074.1, NP_592804.2, NP_595127.1, NP_596765.1, NP_588248.3, NP_595318.2, NP_595131.1, NP_595321.1). CZT-1 is highlighted with a yellow-shaded box.

Conserved domain prediction on the protein sequence of CZT-1 showed the presence of a Zn_2/Cys_6 DNA-binding domain, characteristic of zinc cluster transcription factors, near the N'-terminal part of the protein and a 'fungal specific transcription factor domain' in the middle of the molecule (Fig. 50G). The function of this fungal-specific 'transcription factor domain' in this family of proteins is unclear. Between these two domains, an 'uncharacterized transcriptional regulatory protein' domain was found. A transmembrane segment was also robustly predicted by several tools. Since NCU09974 displays typical features of zinc cluster transcription factors and our results implicate it as a mediator of the fungal response to cell death, we named it CZT-1 (Cell death-activated Zinc cluster Transcription factor).

In order to analyse phylogenetic relationships between CZT-1 and its homologues in other fungi, we built a maximum likelihood tree (Fig. 52). There was strong homology between CZT-1 and members of the Pezizomycotina, whereas homology was weaker for members of the Saccharomycotina and Taphrinomycotina. Within the same species, it appears that there are two types of zinc cluster proteins: some with strong homology to CZT-1 and others with weak homology. Specific CZT-1 sequence features suggest that it may belong to a novel divergent subfamily of zinc cluster transcription factors.

Because of the important role played by CZT-1 during staurosporine-induced cell death and since the absence of *mek-1* (Fig. 21) and *plc-2* (Fig. 27A) resulted in increased tolerance to staurosporine, we evaluated the expression of the transcription factor in Δ*mek-1* and Δ*plc-2* deletion strains. The absence of both genes led to an increase in the expression of *czt-1* (Fig. 50H; ~5.4 folds for Δ*mek-1* and ~3.5 for Δ*plc-2*). This suggests that the signaling molecules MEK-1 and PLC-2 may be upstream of *czt-1*, regulating its expression. The time-course expression of *czt-1* during *N. crassa* germination in liquid Vogel's is shown in Fig. 50I. *czt-1* showed a maximum level of expression after 8h, in accordance with microarray data that included *czt-1* in the list of differentially expressed genes during asexual development of *N. crassa* (414). Parameters such as aerial hyphae elongation, conidial production, growth rate and germination were not affected by the deletion of *czt-1* (Fig. 53A-F).

Exposure of *N. crassa* to staurosporine elicited a response that includes defined alterations in intracellular Ca^{2+} levels (Fig. 23A) and increased ROS

production (Fig. 18B). We compared these parameters in wild type and Δ*czt-1* strains. We expressed the Ca^{2+} reporter probe aequorin (312) in the cytosol of both strains and compared Ca^{2+} dynamics upon treatment with staurosporine. The Δ*czt-1* mutant showed a Ca^{2+} profile distinct from the wild type (Fig. 54A). The initial peak of cytosolic Ca^{2+} (immediately after addition of staurosporine, lasting 20 minutes) was increased in Δ*czt-1* cells whereas the highest peak, at around 60 minutes after drug treatment was nearly abolished when CZT-1 is absent. The last part of the cytosolic Ca^{2+} response (from about 3 hours after addition of staurosporine) was also amplified in the Δ*czt-1* mutant. Thus, CZT-1 seems to regulate the mobilization or sequestration of the ion by the Ca^{2+} storage compartments.

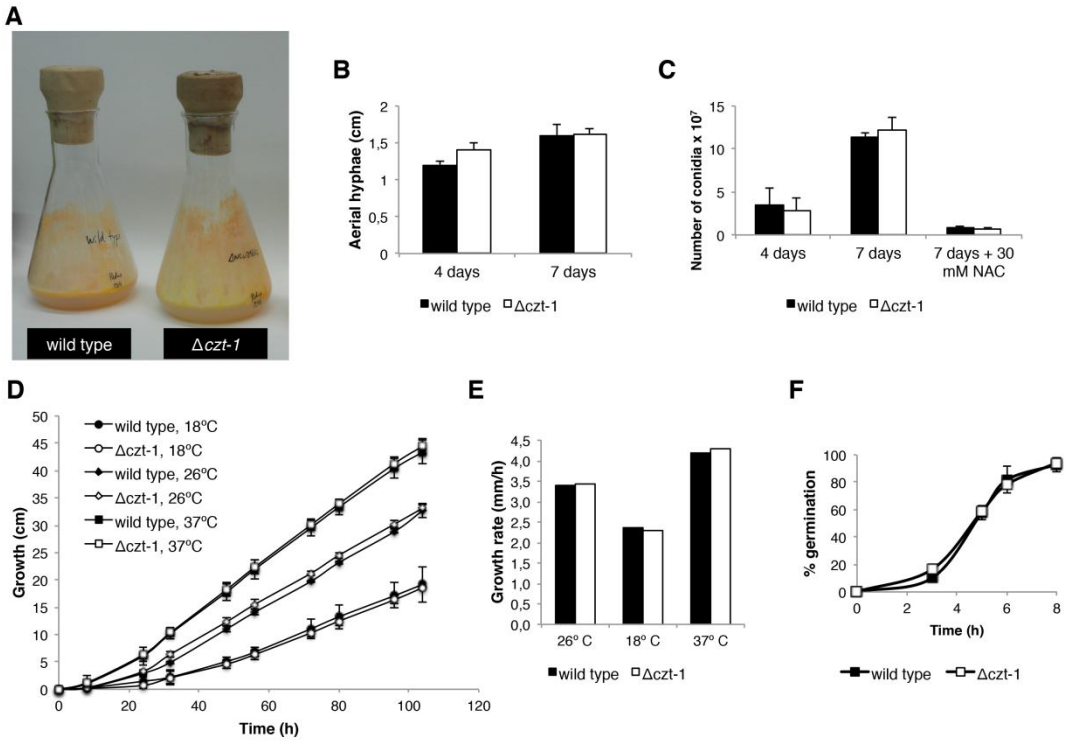

Figure 53 - Growth, hyphal extension and conidiation are not affected by the deletion of *czt-1*.

A- Pictures of Vogel's MM with agar-containing flasks growing for 7 days with wild type or Δ*czt-1* cells. B, C- Aerial hyphae elongation (B) and conidiation (C) were measured after 4 or 7 days of growth in Vogel's MM with agar. In (C), NAC was used as a control, since the generation of ROS is important for conidial production (415). D, E- Growth was evaluated by following the extension of wild type and Δ*czt-1* cells in race tubes incubated at different temperatures (D) and calculating the respective growth rate (E). F- The percentage of germinated cells was determined microscopically as the fraction of cells presenting the typical conidial anastomosis tubes or an hyphal appearance.

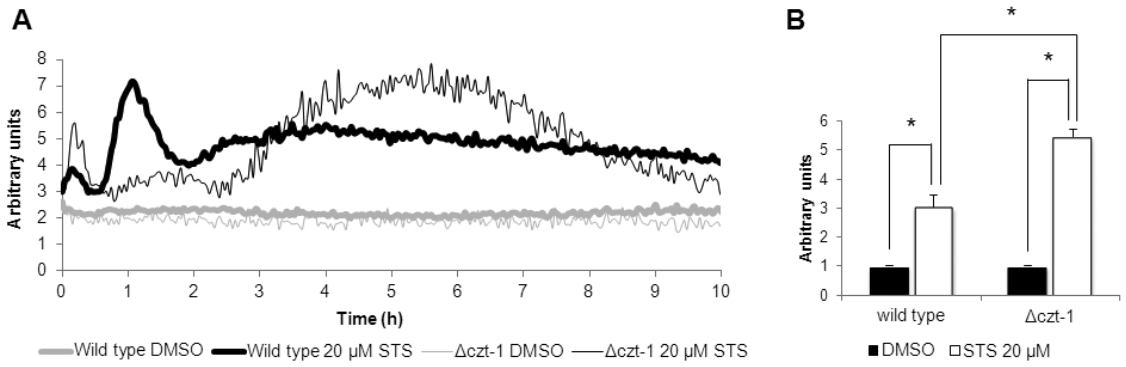

Figure 54 - CZT-1 is a zinc cluster transcription factor involved in the regulation of Ca^{2+} dynamics and ROS accumulation.

A- After 6 hours of growth in liquid Vogel's MM, intracellular Ca^{2+} levels were followed in aequorin-expressing wild type and Δ*czt-1* cells upon treatment with staurosporine (STS) or DMSO. B- Accumulation of ROS was assessed with dihydrorhodamine 123 by staining cells grown in liquid Vogel's MM for 4 hours and treated with STS or DMSO for 30 minutes. *, p-value <0.05.

We observed that the Δ*czt-1* mutant accumulates more ROS than wild type upon insult with staurosporine. ROS accumulation increased about 3 times in the wild type and 5.5 times in the knockout mutant (Fig. 54B). This function of CZT-1 in the control of ROS accumulation is in agreement with its induction by hydrogen peroxide (Fig. 50F). These data suggest a function for CZT-1 in the control of ROS accumulation, although it is unclear if it acts at the level of ROS production or detoxification.

Natural variation to drug resistance in N. crassa

Two natural and divergent populations of *N. crassa* from the region of the Caribbean basin were recently described based on SNP search after whole-transcriptome sequencing (375). We examined the expression levels of *czt-1* in 111 strains from one of these populations (the subtropical Louisiana population) and also on the wild type laboratory strain (FGSC 2489). We observed a minimum, maximum and median RPKM of 10.14, 125.06 and 29.19, respectively (Fig. 55), demonstrating that there is variation in the expression of this gene within a single population of wild isolates. We looked for biogeographic correlations between the expression of *czt-1* and the collection place of the wild strains and although we did not achieve strong statistical significance but considering the relatively small size of the population, some interesting associations were found. This includes a tendency towards high expression of *czt-1* and, consequently, resistance to

staurosporine, for strains collected in Iowa, LA or Elizabeth, LA, east and north of Lake Charles, respectively (Fig. 56).

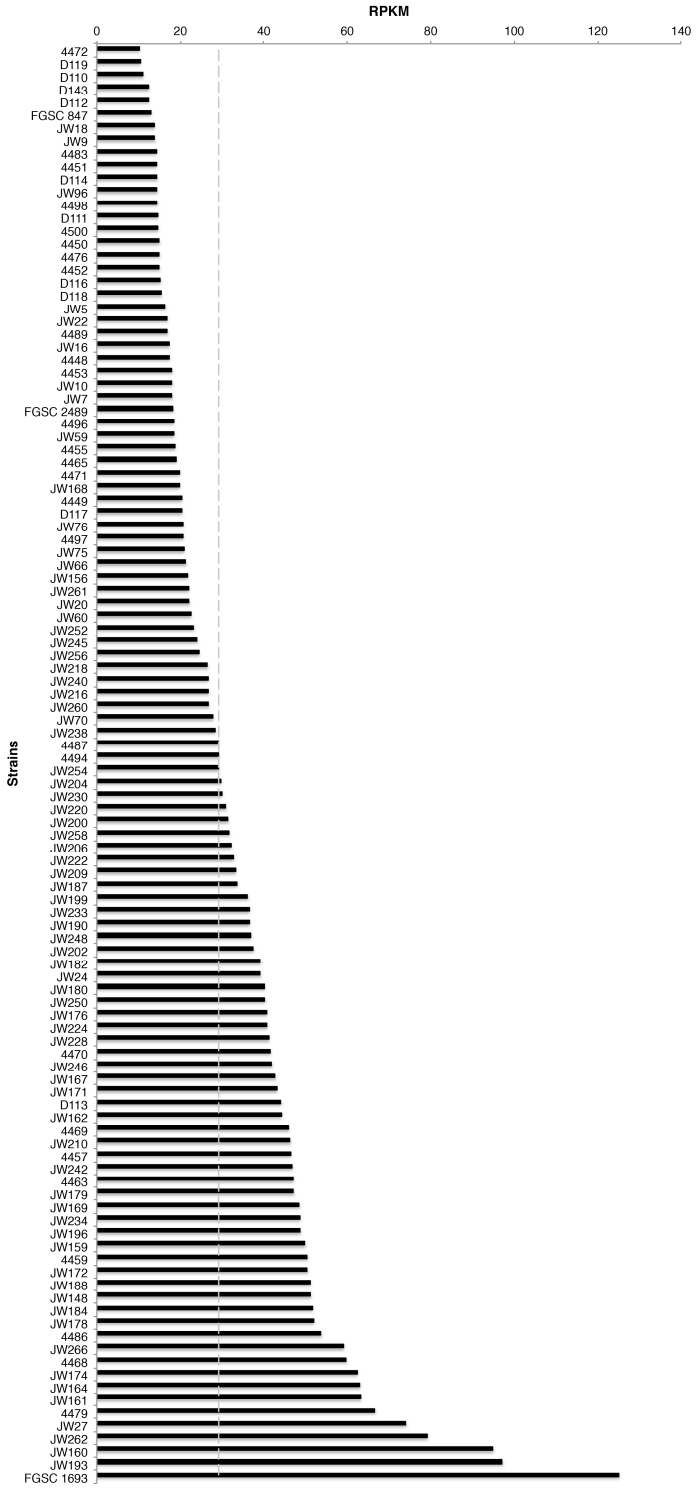

Figure 55 - Expression levels of *czt-1*, expressed as RPKM, in *N. crassa* wild strains collected in the Louisiana state, USA.

The wild type laboratory strain FGSC 2489 is shown for reference. The dashed line represents the median RPKM.

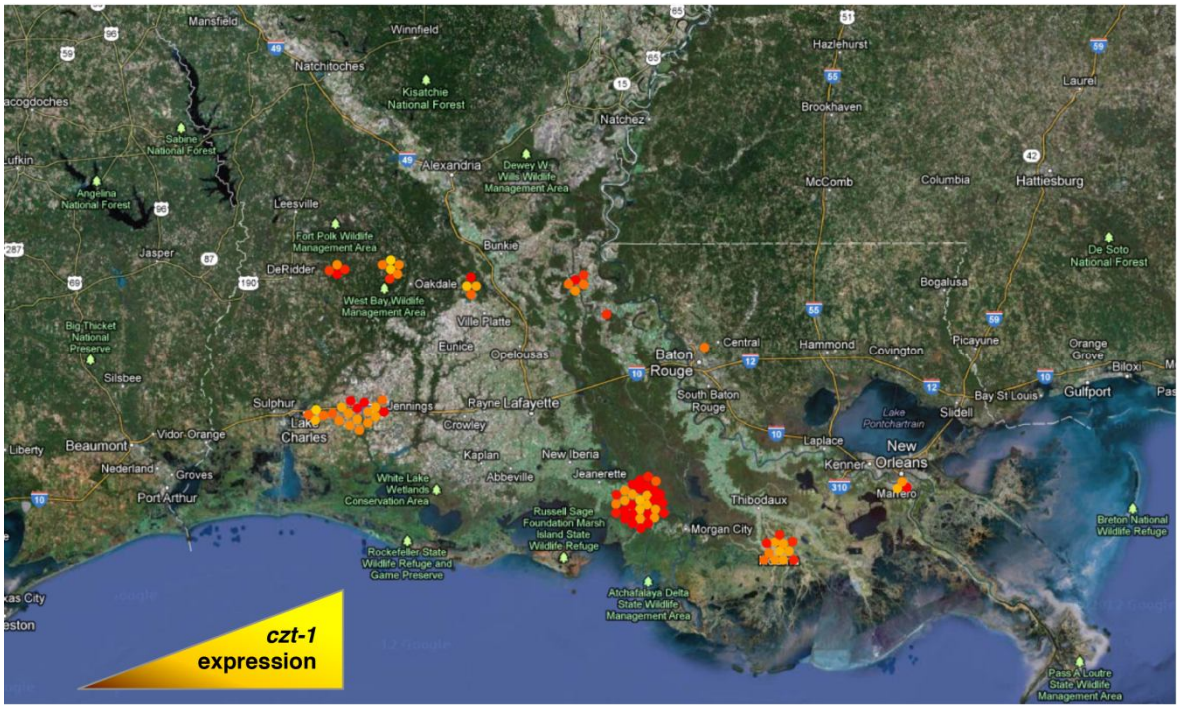

Figure 56 - Correlation between *czt-1* expression and the collection place, within the Louisiana state of the USA, of the wild isolates of *N. crassa* discussed in the text.
Each collection place is identified with a spot. A gradient from red (low *czt-1* expression) to yellow (high *czt-1* expression) is represented.

We recently observed that CZT-1 influences the expression of NCU09975 which encodes the multidrug resistance-related pump ABC-3 (140). Activation of CZT-1 may lead to the upregulation of *abc-3*, so we hypothesized that wild isolates of the Louisiana population with higher levels of *czt-1* would also have higher expression of *abc-3*. We divided the strains in four groups based on the RPKM values for *czt-1* (<25, 25-50, 50-75 and >75) and considered the respective RPKM for *abc-3*. There is a clear correlation between the expression of these two genes (Fig. 57A-B), arguing in favour of a regulatory role of CZT-1 on *abc-3*. Since the lack of *czt-1* (Fig. 50A-E) or *abc-3* (140) leads to hypersensitivity to staurosporine, we hypothesized that, conversely, overexpression of both would lead to drug resistance. This would also support the conclusion that the hypersensitivity of Δ*czt-1* cells (Fig. 50A-E) is indeed due to the lack of CZT-1. In order to test this, we selected some strains representing the four groups of *czt-1* RPKMs and assessed their sensitivity to staurosporine. Indeed, wild isolates with higher levels of expression of *czt-1* and *abc-3* showed increased resistance to the drug (Fig. 57C), arguing in favour of a specific role of CZT-1. FGSC 1693 is an exception, presumably due to alterations in other genes with a role in tolerance to

staurosporine. Some of these strains also showed different sensitivity to oxidative stress with hydrogen peroxide (Fig. 57D). More specifically, JW160 and JW161 were slightly more resistant to hydrogen peroxide, while JW193 and FGSC 1693 were more sensitive. These data indicate that there is natural variation in drug resistance among *N. crassa* wild isolates.

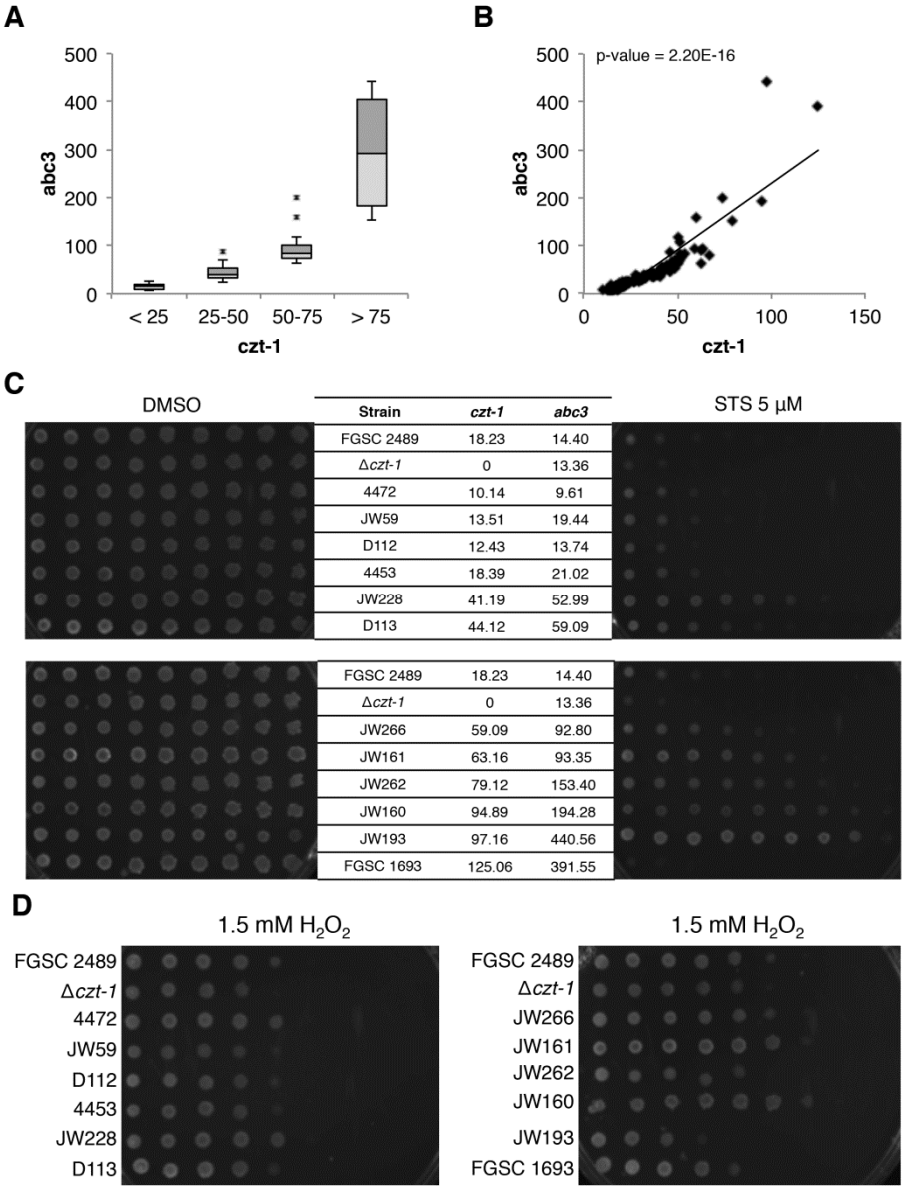

Strain	*czt-1*	*abc3*
FGSC 2489	18.23	14.40
Δ*czt-1*	0	13.36
4472	10.14	9.61
JW59	13.51	19.44
D112	12.43	13.74
4453	18.39	21.02
JW228	41.19	52.99
D113	44.12	59.09

FGSC 2489	18.23	14.40
Δ*czt-1*	0	13.36
JW266	59.09	92.80
JW161	63.16	93.35
JW262	79.12	153.40
JW160	94.89	194.28
JW193	97.16	440.56
FGSC 1693	125.06	391.55

Figure 57 - CZT-1 controls resistance to cell death in wild isolates of N. crassa.
A- Expression levels of *abc-3* in wild strains. The strains were separated in 4 groups based on *czt-1* expression (<25; 25-50; 50-75 and >75 *czt-1* RPKM). B- Correlation between the expression levels of *czt-1* and *abc-3* in a scatter plot. C- Staurosporine (STS) sensitivity of wild strains representing each of the 4 groups presented in (B) was tested by the spot assay on GFS media supplemented with the drug. The laboratory strain FGSC 2489 was used as a reference. The expression levels of *czt-1* and *abc-3* in each strain are indicated. D- The sensitivity of the same strains to hydrogen peroxide (H_2O_2) was also assessed by the spot assay.

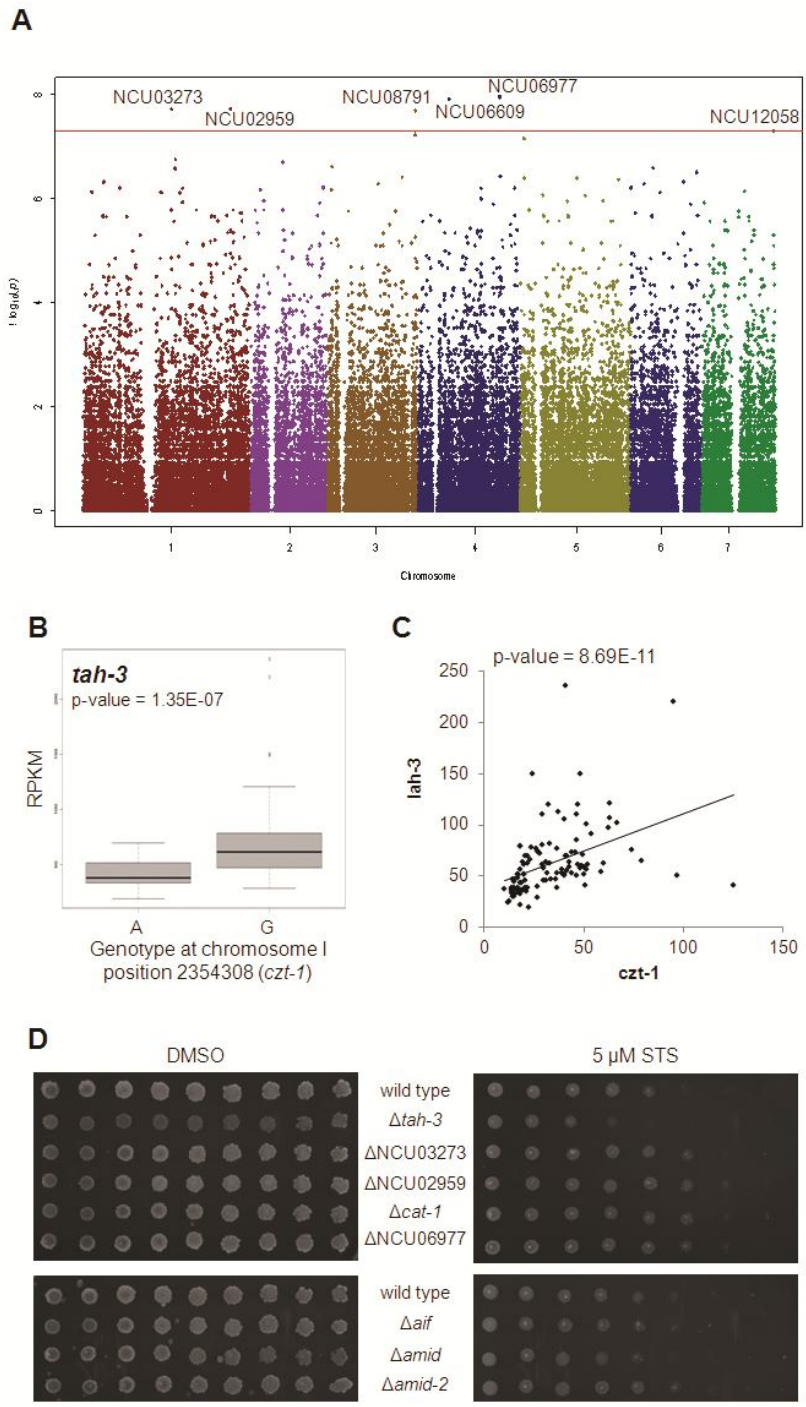

Figure 58 - Genome-wide association studies (GWAS) links CZT-1 to novel putative mediators of cell death in *N. crassa*.

A- Manhattan plot depicting the results of a GWAS between the expression of *czt-1* and the presence of SNPs in the Louisiana population of wild isolates. The dots are the -log of the p-value from the Fisher's exact test for each SNP. Because the strongest associations have the smallest p-values, their negative logarithms are the greatest. The horizontal axis represents the seven chromosomes of *N. crassa*. The red line is the significance cut-off as determined by permutation tests. B- A second GWAS found an association between a SNP (A/G) in *czt-1* and the expression of *tah-3*. C- Correlation between the expression levels of *czt-1* and *tah-3* in a scatter plot. D- The spot assay on GFS plates supplemented with STS was used to test the sensitivity of deletion strains for the genes identified by the GWAS.

Genome-wide association studies (GWAS) allow the analysis of phenotypic traits whose variation is determined by genotypic differences (416). GWAS normally associate traits to quantitative loci, based on SNP analyses. Given the correlation between expression of *czt-1* and resistance to staurosporine, the former was used as a quantitative proxy for drug resistance in a GWAS using the cDNA-sequenced Louisiana population of wild isolates. Six genes with SNPs significantly associated with the expression of *czt-1* were identified (Fig. 58A and Table 12). Of them, NCU08791 and NCU12058 encode CAT-1 and AMID-2, which are known to be involved in the detoxification of ROS during oxidative stress (417) and in the execution of mammalian cell death (196), respectively. A more detailed analysis of all genes showed that the genotype at each SNP locus was significantly associated with altered expression of the respective gene (Fig. 59 and Table 12).

Table 12 - Genes with a single nucleotide polymorphism (SNP) associated with increased expression of *czt-1* in the Louisiana population of wild isolates.

Gene	Gene name	Annotation / Domains	SNP		
			Linkage group	Locus	Genotype
NCU03273	-	NF-X1 finger transcription factor; contains a R3H domain	I	5150086	A, G
NCU02959	-	homologue to RNA-binding proteins from other fungi	I	8577711	C, T
NCU08791	*cat-1*	catalase; antioxidant system	III	5113141	C, T
NCU06609	-	contains a R3H domain	IV	1796142	A, G
NCU06977	-	homology with a subunit of the F0 portion of the mitochondrial ATP synthase	IV	4746463	A, G
NCU12058	*amid-2*	apoptosis-inducing factor-homologous mitochondrion-associated inducer of death 2	VII	4179144	A, G

[a] For all SNPs, a specific allele at the indicated position is associated with increased expression of the respective gene.

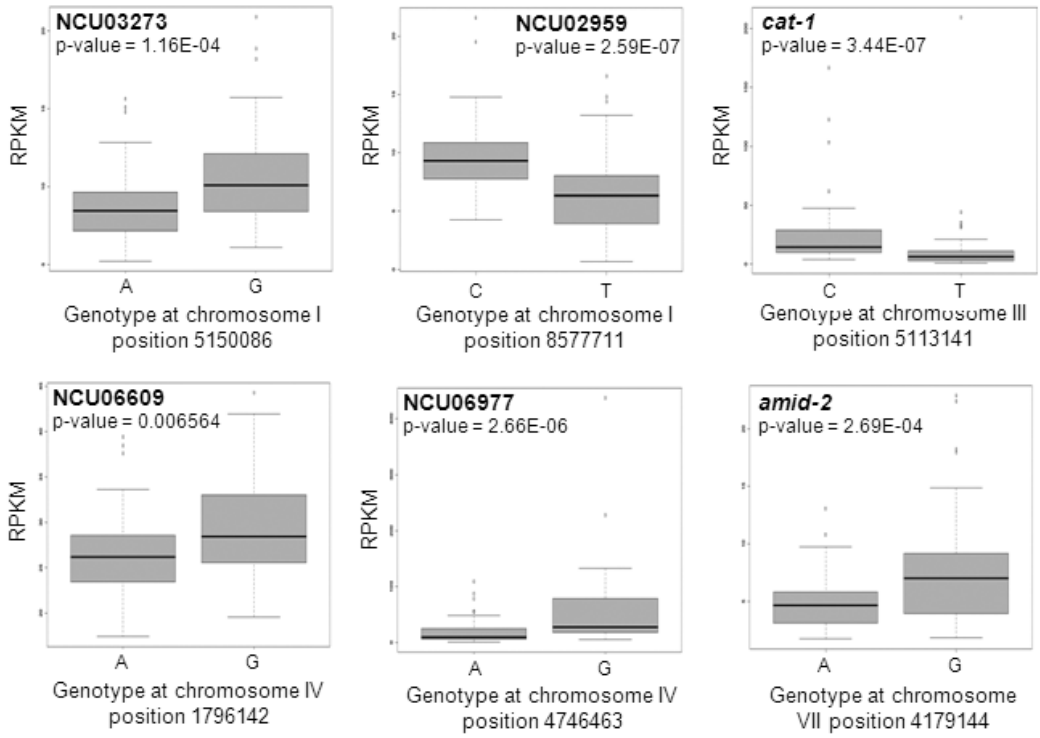

Figure 59 - Box plots showing the relationship between the two found nucleotides for each SNP identified by the GWAS and the expression of the respective gene.

We also performed the reverse GWAS, *i.e.*, we looked at expression of genes linked to SNPs cis to *czt-1*. We identified a SNP (A/G) in *czt-1* that was significantly linked to the expression of NCU03686/*tah-3* (Fig. 58B). The expression of *tah-3* (also designated *lah-3*) correlated well with the expression of *czt-1* (Fig. 58C). TAH-3 is also a Zn_2/Cys_6 binuclear cluster transcription factor as *czt-1* and has been reported to be required for fungal tolerance to a harsh environment caused by an argon plasma jet (418).

The results of both GWAS pointed out genes that, because of their genetic association with *czt-1*, may underlie the natural resistance phenotype observed for the wild strains. Therefore, we next tested the sensitivity profile of the knockout strains for the genes identified by the GWAS (except for ΔNCU06609, unavailable). The Δ*tah-3* deletion mutant was more sensitive to staurosporine than wild type, whereas ΔNCU03273, ΔNCU02959, ΔNCU06977 and Δ*cat-1* were slightly more resistant (Fig. 58D, upper panel). This further implicates these molecules in the cell death response to staurosporine and in the resistance conferred by CZT-1. The deletion strain for *amid-2* is not particularly sensitive or resistant to the drug (Fig. 58D, lower panel), probably due to redundant functions

of its paralog proteins, like amid and AIF (148). Altogether, our data points to the existence of natural variation to drug resistance in wild isolates of *N. crassa* and to the relevance of the CZT-1 transcriptional regulator. The genes that interact genetically with CZT-1, indicated by the GWAS, likely contribute to the resistance phenotype of the strains.

Transcriptional profiling of staurosporine-treated wild type versus Δczt-1

We analysed transcriptional patterns of the *czt-1* deletion strain. Considering basal expression, 8.5% of the genes were altered in the Δ*czt-1* strain in comparison with wild type, corresponding to 605 genes (Fig. 60A, left panel). From these, 58.5% were induced whereas 41.5% were repressed (Fig. 60B, left panel). Enrichment analysis shows, for instance, that, since the mutant showed induction of these genes, CZT-1 negatively regulates 'phosphate metabolism' and 'cAMP/cGMP mediated signal transduction' (Table 13). On the other hand, it seems that CZT-1 is controlling positively the expression of genes involved in 'respiration' and 'alcohol fermentation'.

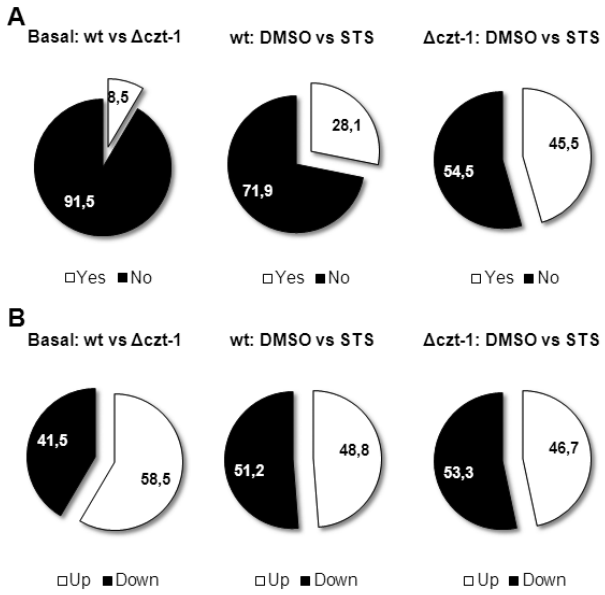

Figure 60 - Summary of the transcriptional response to staurosporine in wild type and Δ*czt-1* cells.

A- The percentage of genes with altered expression is represented by the white portion of the pie chart. The left panel represents the basal gene expression altered in the Δ*czt-1* mutant versus wild type; the other panels represent staurosporine (STS) altered genes in wild type and Δ*czt-1*, respectively. B- Comparison between the percentage of upregulated (white) and downregulated (black) genes.

Table 13 - Functional category enrichment analysis (using FunCat) of genes induced and repressed basally in the Δ*czt-1* strain.

ID	Category	P-value
Induced genes		
01.04	phosphate metabolism	7.37E-05
11.02.03.04	transcriptional control	8.31E-06
30.01.09.07	cAMP/cGMP mediated signal transduction	3.70E-05
36.25.01.13	olfaction	4.57E-05
Repressed genes		
02.13	respiration	3.78E-05
02.16.01	alcohol fermentation	1.72E-05

The response provoked by staurosporine in the Δ*czt-1* mutant was more active than in wild type (Fig. 61), with 45.5% of the genes depicting altered expression (Fig. 60A, right panel). Roughly half of these genes were induced and half were repressed (Fig. 60B, right panel). The transcriptional response to staurosporine was partially independent of CZT-1 (Fig. 62A-B, note the number of shared genes). However, it is also true that CZT-1 is a major regulator of the genetic response to staurosporine, given that more than 1000 genes were only induced or repressed in the mutant strain and not in the wild type (Fig. 62A-B).

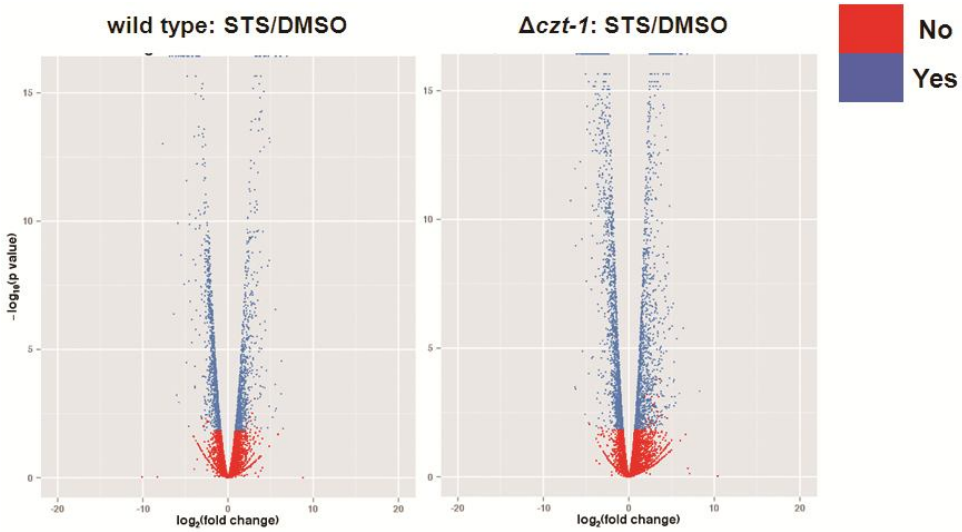

Figure 61 - Volcano plots illustrate the amplification of the response to staurosporine in Δ*czt-1 versus* the wild type strain.

A FunCat enrichment analysis for each group is represented in the Venn diagrams on Fig. 62A and 62B, for induced and repressed genes, respectively. Upon treatment with staurosporine, only wild type cells were able to induce genes involved in several ER-related functions, such as ‘protein folding and stabilization’,

'modification with sugar residues (eg, glycosylation, deglycosylation)', 'ER to Golgi transport' and 'cellular export and secretion' (Fig. 62A), suggesting a ER-mediated stress response that is not induced in Δ*czt-1*. Actually, the 'protein folding and stabilization' category was significantly repressed in the mutant (Fig. 62B). This suggests that CZT-1 affects ER processes which, given the role of the ER as a Ca^{2+} storage organelle, may be related to the differences in Ca^{2+} dynamics observed in the deletion strain (Fig. 62B).

A

wild type and Δ*czt-1* shared, staurosporine-induced genes (538)

ID	Category	P-value
01.01	amino acid metabolism	9.64E-05
01.05.02.07	sugar, glucoside, polyol and carboxylate catabolism	1.93E-05
01.06	lipid, fatty acid and isoprenoid metabolism	3.00E-05

Wild type-specific, staurosporine-induced genes (451)

ID	Category	P-value
14.01	protein folding and stabilization	4.43E-06
14.07.02	modification with sugar residues (eg, glycosylation, deglycosylation)	3.48E-06
20.09.07.03	ER to Golgi transport	1.47E-05
20.09.16	cellular export and secretion	8.82E-05
30.01.09	second messenger mediated signal transduction	8.91E-06
30.01.09.11	polyphosphoinositol mediated signal transduction	1.59E-03

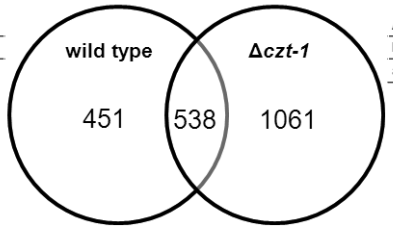

Δ*czt-1*-specific, staurosporine-induced genes (1061)

ID	Category	P-value
a		

B

wild type and Δ*czt-1* shared, staurosporine-repressed genes (810)

ID	Category	P-value
01.05.13	transfer of activated C- groups	1.71E-07
01.05.13.01	S-adenosyl-methionine - homocysteine cycle	9.82E-05
11.02.01	rRNA synthesis	2.67E-15
11.02.02	tRNA synthesis	2.82E-05
11.04.01	rRNA processing	2.61E-50
11.06.01	rRNA modification	1.70E-08
11.06.02	tRNA modification	2.12E-05
12.01	ribosome biogenesis	1.82E-148
12.01.01	ribosomal proteins	3.67E-109
12.04.01	translation initiation	7.32E-12
12.04.02	translation elongation	1.04E-09
12.07	translational control	1.08E-09
16.01	protein binding	9.28E-29
16.03.03	RNA binding	7.32E-38
20.09.04	mitochondrial transport	1.47E-10
42.10.07	nucleolus	4.56E-05
42.16	mitochondrion	7.99E-08

Wild type-specific, staurosporine-repressed genes (228)

ID	Category	P-value
02.11	electron transport and membrane-associated energy conservation	2.06E-10
02.13.03	aerobic respiration	8.81E-08
02.45.15	energy generation (eg, ATP synthase)	1.69E-08
20.01.15	electron transport	3.91E-07
34.01.01.03	homeostasis of protons	1.78E-05

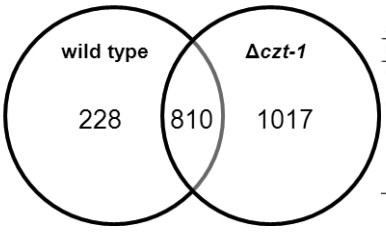

Δ*czt-1*-specific, staurosporine-repressed genes (1017)

ID	Category	P-value
01.01.06.05.01	biosynthesis of methionine	7.60E-05
01.06	lipid, fatty acid and isoprenoid metabolism	6.25E-05
11.02.03	mRNA synthesis	1.79E-05
14.01	protein folding and stabilization	1.39E-07
16.03	nucleic acid binding	7.03E-06

Figure 62 - CZT-1 controls genes involved in ER and mitochondrial functions.
A, B- Venn diagrams showing the number of staurosporine-induced (A) and -repressed (B) genes specifically in the wild type or in the Δ*czt-1* mutant. FunCat functional enrichment analysis (373) for each set of genes is indicated. a, no highly enriched category was found.

Signal transduction seems to be impaired in the deletion strain considering its inability to induce genes in the 'second messenger mediated signal transduction' category, in opposition to the wild type (Fig. 62A). Within this

category, the wild type enrichment analysis included the 'polyphosphoinositol mediated signal transduction' subcategory (p-value = 0.0016), which seems to be regulated by CZT-1. Notably, phosphoinositol-mediated signaling pathways control Ca^{2+} release from the ER (387) and this result may correlate with the altered Ca^{2+} dynamics observed in the mutant (Fig. 54A). As described above, wild type cells downregulated genes involved in the mitochondrial electron transport after treatment with staurosporine (Fig. 62B and Table 7). Interestingly, this was not the case in *czt-1* knockout cells (Fig. 62B).

We looked if there were differences in expression in wild type *versus* Δ*czt-1* strain for the genes identified by the GWAS (Fig. 58A). At basal conditions, Δ*czt-1* showed significant downregulation of *cat-1* and upregulation of *tah-3* (Fig. 63A). Upon treatment with staurosporine, *amid-2* was induced in the wild type but not in the mutant; NCU06977 was induced in Δ*czt-1* but not in the wild type; *tah-3* was repressed in the mutant but not in the wild type; *cat-1* was induced in both strains, although more extensively in Δ*czt-1* (Fig. 63B). The alteration in the expression of *cat-1* is in agreement with the fact that staurosporine induces ROS formation, which is increased in Δ*czt-1* (Fig. 54B). We also looked at expression alterations in the *amid-2* paralogues, namely *amid* and *aif*: *amid* expression was repressed only in the mutant whereas *aif* was induced in both strains. The staurosporine-provoked expression profile for all these genes corroborate their role in cell death and expression differences observed in Δ*czt-1* suggest that they are under the control of the transcription factor.

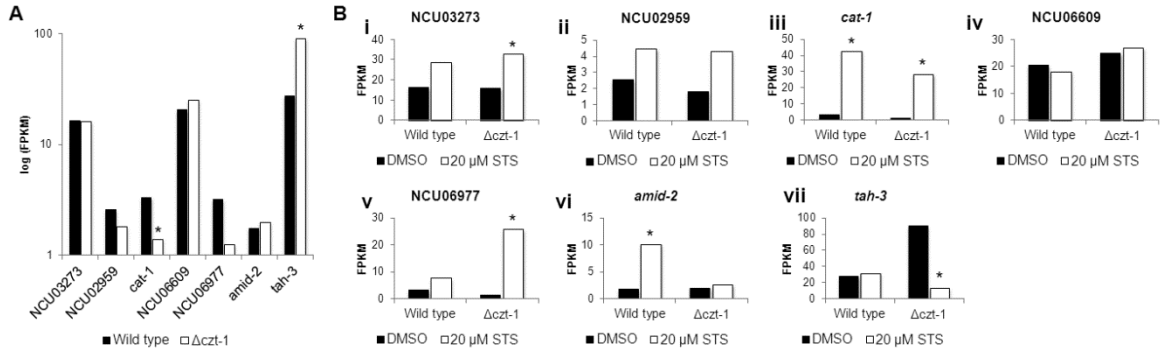

Figure 63 - RNA-seq data support the involvement of genes identified by the GWAS in staurosporine-induced cell death.

A, B- The expression of NCU03273, NCU02959, *cat-1*, NCU06609, NCU06977, *amid-2* and *tah-3*, indicated as FPKMs was compared between wild type and Δ*czt-1* strains in control samples (A) or between staurosporine (STS)- and DMSO-treated samples (B). *, p-value <0.05.

CZT-1 regulates the expression of multiple ABC transporters

Genes encoding members of the ABC (ATP-binding cassette)-transporter family are induced in response to drug treatments and confer resistance to numerous compounds in a process designated multidrug drug resistance or pleotropic drug resistance (419). We compiled a list of genes encoding ABC transporters from the FunCat database and checked their expression in the RNA-seq dataset. Under basal conditions, there was an upregulation of some of these genes in Δ*czt-1* cells (Fig. 64A), including NCU02544, NCU03591, NCU07546, NCU08056/*atrf*, NCU10009/*atrf-2*, NCU07276 and NCU09975/*abc-3*. The latter plays a crucial role during the response of *N. crassa* to staurosporine since it was observed that the cells pump the drug out to the extracellular medium through ABC-3 (140).

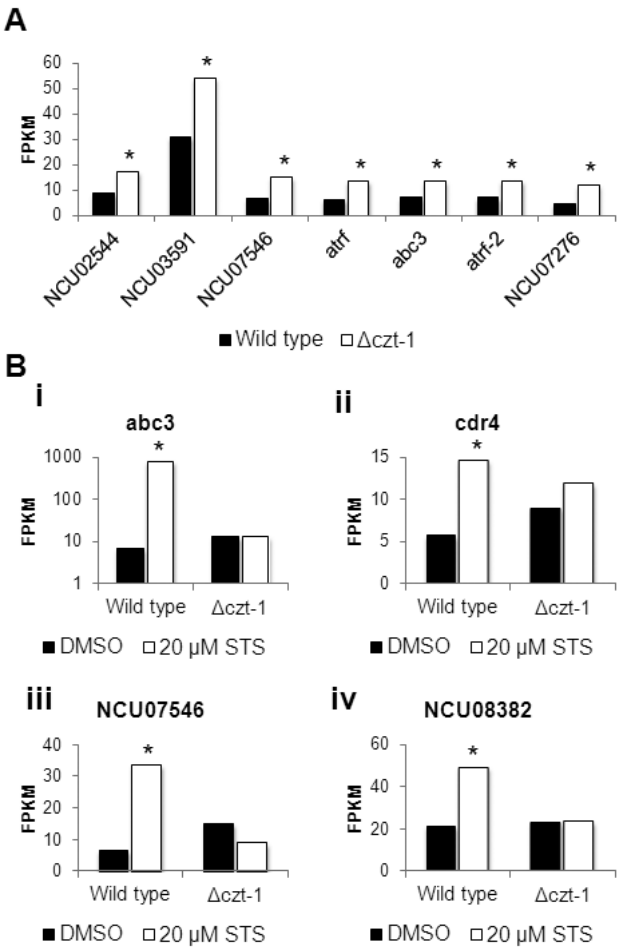

Figure 64 - CZT-1 controls genes encoding ABC transporters.
A- The levels of expression (in FPKMs) of the indicated ABC transporter-encoding genes were compared between wild type and Δ*czt-1* strains under basal conditions. B- Expression of *abc3*, *cdr-4*, NCU07546 and NCU08382, indicated as FPKMs was compared between wild type and Δ*czt-1* strains treated with staurosporine or DMSO. *, p-value <0.05.

The staurosporine-stimulated induction of *abc-3* (NCU09975) in the wild type but not in Δ*czt-1* cells was observed in our RNA-seq data (Fig. 64B, i). Upon treatment of wild type cells with staurosporine, not only *abc-3*, but other ABC transporter genes were induced. These include NCU05591/*cdr-4* (Fig. 64B, ii), NCU07546 (Fig. 64B, iii) and NCU08382 (Fig. 64B, iv). CDR-4 was shown to be involved in resistance to azoles in *N. crassa* (420). Cells lacking CZT-1 were unable to induce these genes, indicating that the expression of several ABC transporters is CZT-1-dependent. Altogether, our data shows that the novel transcription factor CZT-1 is an important regulator of cell death and controls the genetic response to staurosporine in *N. crassa*.

4. Discussion

Our results further confirmed that staurosporine, an archetypal cell death inducer of therapeutic interest, triggers PCD in *N. crassa* as deduced by different morphological and biochemicals signs: loss of viability, permeability to the early apoptosis and late apoptosis/necrosis markers YOPRO-1 and propidium iodide, respectively, increased and indispensable ROS production, loss of ΔΨm, DNA fragmentation (140), GSH export (114), activation of multidrug resistance proteins (140) and altered intracellular Ca^{2+} signaling.

4.1) The role of Ca^{2+} and mitochondrial bioenergetics during staurosporine-induced cell death

Activation of a TRP-like calcium channel in the plasma membrane and calcium release from intracellular stores during phospholipase C-mediated cell death

Staurosporine activates a complex and dynamic intracellular response involving the movement of Ca^{2+} from the external medium and intracellular storage reservoirs to the cytosol. At the molecular level, this is promoted by a putative novel TRP-like channel and a phospholipase C protein (probably PLC-2) that trigger a Ca^{2+} response with a characteristic $[Ca^{2+}]_c$ signature. Some reports have shown an increase in $[Ca^{2+}]_c$ in response to staurosporine (353, 421-425), but the underlying mechanisms remained largely unknown. Recent work showed that staurosporine, as well as its clinically relevant analogue PKC412, induces Ca^{2+} influx through the hyperpolarization-activated cyclic nucleotide-gated channel HCN2 in lung cancer cells and neurons (421). No HCN2 homologues are known in *N. crassa*.

Our data indicate that staurosporine triggers the activation of phospholipase C by a yet unknown mechanism. Possible phospholipase C activation mechanisms include stretch (426), interaction with G-protein-coupled receptors (427) and liberation from phosphorylation by PKC (428). Given that staurosporine

is a powerful inhibitor of PKC (174), it is tempting to propose that it is the alleviation of the phosphorylation of phospholipase C by PKC that prompts the onset of the response. Anyhow, as a consequence of its activation, phospholipase C hydrolyses PIP_2 with three outcomes: depletion of PIP_2, generation of DAG and generation of IP_3, that all affect the activity of TRP channels (325). First of all, the depletion of PIP_2 controls TRP proteins, though the mode of regulation depends on the specific identity of the channel: in animals, the depletion of PIP_2 inhibits TRPC3, TRPC6 and TRPC7 (429) whereas it activates TRPC4 (398). Other channels, like TRPC5 and TRPV1 were shown to be both negatively and positively regulated by PIP_2 depletion, depending on the cellular environment (325). Our results support the hypothesis that phospholipase C depletes PIP_2 and this causes the opening of a channel behaving like TRPC4. Indeed, TRPC4 was shown to be inhibited by PKC (430) and we found that the selective TRPC4 antagonist ML204 partially reduces the $[Ca^{2+}]_c$ response to staurosporine. In the presence of staurosporine, PKC is inhibited (174) and this would relieve and open a TRPC4-like channel. PIP_2 depletion also affects TRPV1 (431), but the existing data is conflicting on whether the reduction in PIP_2 activates or inactivates the channel (325). Secondly, the generation of DAG may not have a significant role in our system, because DAG activates PKC, which is blocked by staurosporine alone (174). We cannot exclude that DAG is acting directly on TRP channels as shown before (430, 432). Nonetheless, it was shown that this PKC-independent direct interaction of DAG with TRP channels is protein specific and does not occur in members of the family such as TRPC4 and TRPC5 (430). If indeed there is a TRPC4-like channel involved in staurosporine-induced cell death, it is more likely that PIP_2 depletion is the major regulatory mechanism. In accordance with our results, inositol starvation triggers ER-mediated cell death in fission yeast (433). The generation of IP_3 after treatment with staurosporine led to the mobilization of Ca^{2+} from internal stores, in line with the observation that during part of the response the ER contributes to the increase in $[Ca^{2+}]_c$.

In *N. crassa*, treatment with the antifungal peptide PAF (126) or with the bacterial metabolite 2,4-diacetylphloroglucinol (394) led to Ca^{2+} influx from the external medium in a CCH-1-independent manner. Ca^{2+} influx induced by 2,4-diacetylphloroglucinol was also shown to be independent of FIG-1, while this was not tested for PAF. Cell survival-associated Ca^{2+} uptake, mediated by an

unidentified channel, was shown to occur in parallel with Ca^{2+} entry via Cch1-Mid1 in yeast treated with tunicamycin, an ER stress agent (359). There is thus evidence for the presence of fungal Ca^{2+} uptake systems in addition to the so far characterized HACS (CCH-1 and MID-1) and LACS (FIG-1) mechanisms (337, 341, 342, 345, 395, 396). Here we describe a putative Ca^{2+}-channel in the plasma membrane with the pharmacological properties of a TRP protein. This represents a novel mechanism for Ca^{2+} influx in fungi and it is conceivable that it may be involved in the some or all of these aforementioned responses. The only TRP channel so far described in *N. crassa* is YVC-1 (314, 315), although a few proteins were recently proposed as putative homologues of the mammalian TRP channels in pathogenic fungi (329). It is not plausible that YVC-1 is the channel activated by staurosporine because the respective knockout mutant does not show major differences from the wild type in terms of the $[Ca^{2+}]_c$ response to staurosporine and furthermore yeast YVC-1 is localized in the vacuole (326). The TRP Ca^{2+} uptake system seems to be more active in the absence of CCH-1. Possibly as a consequence of this upregulation in Ca^{2+} uptake, cells lacking CCH-1 (and MID-1) die more than the wild type when treated with staurosporine as shown by the growth and death assays. This is consistent with the observation that Δ*cch-1* and Δ*mid-1* cells are less tolerant to high levels of Ca^{2+}. In line with our results, lack of CCH-1 and MID-1 renders *S. cerevisiae* and *C. neoformans* cells very sensitive to ER stress with tunicamycin or azole drugs (341, 359, 434).

Extracellular Ca^{2+} modulates staurosporine-induced cell death and triggers unique transcriptional programs

We show that controlling the amount of Ca^{2+} available in the extracellular milieu is enough for a robust modulation of the effects of staurosporine. Cell death is strongly enhanced by Ca^{2+} limitation whereas it is partially supressed in 30-times excess of Ca^{2+}. A similar behavior was observed in *S. cerevisiae* cells treated with miconazole or terbinafine, inhibitors of ergosterol biosynthesis (435), suggesting the presence of common stress-responsive pathways in the two fungi, even when the stimuli have apparently distinct targets. Supplementation of the medium with high Ca^{2+} concentrations (20 mM $CaCl_2$ as used in our study)

protected *N. crassa* cells from PAF-induced toxicity. Interestingly, treatment with PAF, an antifungal protein from *P. chrysogenum*, also disturbs intracellular Ca^{2+} homeostasis. (185). Thus, our results substantiate the view that Ca^{2+} is an important player during cell death in *N. crassa*.

The effects of staurosporine in media containing different amounts of Ca^{2+} are remarkably paralleled by distinct intracellular Ca^{2+} dynamics, in line with our results that show that extracellular Ca^{2+} uptake is required for the development of the cytosolic Ca^{2+} signature induced by the drug. In the presence of 20 mM $CaCl_2$, the massive Ca^{2+} transient immediately after staurosporine addition might be a pro-survival event regulating signaling pathways involved in cell defence. In medium lacking Ca^{2+}, the initial part of the staurosporine-induced cytosolic Ca^{2+} response is completely abolished and cells become more susceptible to the drug. This supports the suggestion that the Ca^{2+} signaling events that occur during approximately 2 hours after addition of the drug (peaks “A” and “B”) have a pro-survival role. However, the intracellular response to staurosporine is very complex and direct conclusions on the susceptibility of the cells based solely on the intracellular Ca^{2+} profile, although tempting, are not possible. For instance, the Δ*plc-2* mutant shows increased resistance to the drug though the intracellular Ca^{2+} response is nearly obliterated. Thus, it seems that events downstream of the cytosolic changes in Ca^{2+} levels ultimately define cell fate in response to staurosporine.

The *N. crassa* transcriptional response to staurosporine is robustly reduced in the presence of 20 mM $CaCl_2$ when compared with standard MM, whereas limited extracellular Ca^{2+} causes alterations in an increased number of genes. Thus, different concentrations of extracellular Ca^{2+} not only lead to distinct intracellular Ca^{2+} dynamics, ROS accumulation and levels of cell death, but also seems to be coupled to unique transcriptional profiles. It appears that when treated with staurosporine in the absence of Ca^{2+}, cells turn off a diverse array of biological processes, because we discovered several enriched functional categories in the set of 0 Ca^{2+}-specific repressed genes. This includes the enriched repression of genes involved in cell cycle, signal transduction, cell growth, anti-apoptosis, cellular polarization, protein fate and the unfolded protein response. It is possible that this inactivation of various intracellular pathways

explains the inability of cells to cope with the staurosporine insult and consequent increased cell death.

Alterations in gene expression are caused simply by extracellular Ca^{2+} limitation or overload alone. Clearly, *N. crassa* translates changes in extracellular Ca^{2+} into a transcriptional response. This likely results from the homeostatic adaptation to the abnormal Ca^{2+} environment, *i.e.*, the observed differences in gene expression might be triggered after the uptake or release of Ca^{2+} to balance the intracellular levels of the ion. Alternatively, these alterations may be secondary to the activity of a surface-localized Ca^{2+} sensor. Although a sequence homologue of the extracellular Ca^{2+}-sensing receptor of animals and plants (318, 319) has not been found so far in *N. crassa*, we cannot exclude that a functional homologue exists. It could sense the lack and excess of Ca^{2+} in the extracellular milieu and trigger a signaling mechanism that would culminate in alterations in gene expression, similarly to the animal and plant Ca^{2+}-sensing receptor. Given the predicted cell surface localization of the two putative novel Ca^{2+}-binding proteins NCU08524 and NCU06607 and the growth phenotype of the respective knockout mutants under Ca^{2+} stress, it is tempting to speculate that they could play role in Ca^{2+} sensing. NCU08524 and NCU06607 possess the Ca^{2+}-binding Dx[DN]xDG motif, but the exact role of this motif is currently elusive.

NDE-1, mitochondrial complex I, MCU and staurosporine-induced cell death

We identified mitochondrial proteins with respiratory activities that mediate cell death induced by staurosporine and whose respective knockout mutants present abnormal Ca^{2+} dynamics in response to the drug. This includes the NADPH dehydrogenase NDE-1 and the complex I subunit NUO51. A previous report has shown that patient-derived fibroblast cells harboring two point mutations in *NDUFV1*, the human *nuo51* homologue, and in other genes for complex I subunits present altered Ca^{2+} homeostasis, including a decrease in the basal levels of cytosolic and ER Ca^{2+} as well as a reduced response to bradykinin (436, 437). It was proposed that the reduced $\Delta\Psi m$ and consequent defective energetic outcome due to the mutations leads to an insufficient supply of ATP to Ca^{2+}-

ATPases required for proper Ca^{2+} dynamics to occur. Additionally, an increase in intracellular Ca^{2+} and defective mitochondrial buffering of Ca^{2+} was observed in cells with a mutation on the mitochondrial-specific leucine tRNA from patients suffering from mitochondrial encephalomyopathy, lactic acidosis, and stroke-like episodes (MELAS) syndrome (438).

We show that a properly working respiratory chain and the accumulation of ROS are required for the staurosporine-induced Ca^{2+} response. It was shown that the drug causes a shift in the redox balance of the cells to a more oxidative intracellular environment driven by the depletion of GSH (114). This facilitates the oxidation of intracellular elements like lipids and proteins, modulates redox signaling and ultimately is toxic to the cells. Replenishment of the glutathione pool by the exogenous addition of GSH (139) or NAC (114) restores cell viability, highlighting the importance of the accumulation of ROS during staurosporine-induced cell death. Our results indicate that the antioxidant effect of these molecules prevent the progress of the cytosolic Ca^{2+} signaling events triggered by staurosporine.

Importantly, the non-proton pumping and rotenone-insensitive NDE-1 protein possesses a Ca^{2+}-binding domain (241) and its activity is Ca^{2+}-dependent (242). It is conceivable that NDE-1 may sense the mitochondrial levels of Ca^{2+} or act as a regulatory partner of a Ca^{2+}-permeable channel like MCU. We emphasized the role of NDE-1, but our data also suggest the involvement of the other alternative NAD(P)H dehydrogenases during cell death. Mechanisms of compensation occur when cells are deficient in one or more alternative NAD(P)H dehydrogenases: double knockout strains for NDE-2 or NDI-1 and complex I are unviable (240, 243) and the absence of NDE-2 affects the activity of NDE-3 (244). In addition, expression analyses revealed that deletion strains for some of these enzymes present altered levels of the genes encoding other members of the family (145, 148). The lack of NDE-1 causes upregulation of *nde-2* (148), which is engaged in the production of ROS (145), consistent with increased ROS formation in the Δ*nde-1* mutant after treatment with staurosporine.

Alternative NAD(P)H dehydrogenases probably have a regulatory role as redox sensors. Different points of view in different organisms converge in the concept that the activation of these enzymes is favoured in situations of substrate overflow or low energy requirement in order to prevent unnecessary electron

transfer through the canonical pathway (234, 250, 285). Uncoupled electron flux by the alternative system avoids excessive use of the respiratory chain and the concomitant production of ATP and ROS, the latter with presumably deleterious effects. In agreement with this, examples exist showing that *S. cerevisiae* Ndi1 overexpression in mammalian cells prevents cell death and oxidative stress resultant from chemical and genetic inhibition of complex I (254, 284). Quite surprisingly, other works show that yeast Ndi1 promotes apoptosis (257, 282) and the external alternative NADH dehydrogenases of *S. cerevisiae* were proposed to be a potential source of superoxide radicals (255). Also, amiodarone-induced cell death in *S. cerevisiae* comprises a rise in the cytosolic levels of Ca^{2+} which causes a burst in respiration attributed to an external NADH dehydrogenase, increased $\Delta\Psi m$ and ROS production (355). *S. cerevisiae* lacks complex I and the alternative system is different from other fungi because there is an apparent specificity for NADH (236, 439). From our data, NDE-1 seems to protect from excessive ROS accumulation induced by staurosporine and it was shown that mitochondria from the Δ*nde-1* mutant produces slightly more ROS than wild type when supplied with NADH, rotenone or paraquat (145). In *A. nidulans*, knockout of the *nde1* homologue *ndeA* renders cells very sensitive to farnesol and this is associated with an increased accumulation of ROS (138). This remarkably parallels the phenotype of the *N. crassa* Δ*nde-1* deletion strain after exposure to staurosporine.

Involvement of the N. crassa Ca^{2+}-handling molecular machinery in the response to staurosporine

The screening of Ca^{2+}-handling mutant strains for sensitivity to staurosporine revealed a number of proteins likely to be involved in the cell death response to the drug. Although further studies are needed to contextualize them in the mechanisms of action of the drug, it is probable that NCA-2, a Ca^{2+}-ATPase whose respective knockout cells are very resistant to staurosporine, is pumping the excess of cytosolic Ca^{2+} to the vacuoles or extracellular space (347, 440). The knockout strain for PMR-1, a Golgi-localized Ca^{2+}-ATPase (441), is also very resistant to staurosporine and in yeast, Δ*PMR1* knockout cells accumulate much less Ca^{2+} in the ER (442). Lack of these functions in Δ*nca-2* and Δ*pmr-1* cells is

likely related to the phenotype of the strains upon treatment with staurosporine, as both the ER and the vacuoles play an important role during the fungal response to staurosporine. It is plausible that the lack of NCA-2 or PMR-1 results in an increased accumulation of Ca^{2+} in the cytosol and this is consistent with the observations that high levels of Ca^{2+} (below a toxicity threshold) protect against the effects of staurosporine. Other Ca^{2+}-related deletion strains present altered resistance to staurosporine, including Δ*cse-1*, Δ*camk-4* and Δ*stk-16*. Knockout of *cse-1* leads to impaired germling communication and fusion (335) as well as increased sensitivity to UV irradiation and Ca^{2+} (443). Thus, increases in the cytosolic levels of Ca^{2+} after treatment with staurosporine could explain the increased susceptibility of Δ*cse-1* cells. In line with our results, a previous study has shown that disruption of *camk-4* results in resistance to benomyl, while disruption of *stk-16* leads to increased sensitivity to fludioxonil, sodium chloride and benomyl (444).

PLC-2 is required for normal hyphal development

The *N. crassa* genome encompasses four putative phospholipase C (δ-type) genes (314, 315, 393). Of them, only PLC-1 was previously characterized and seems to be involved in aspects of cell morphogenesis not involving polarized hyphal growth (324). We observed that the absence of *plc-2* leads to aberrant spore germination and that it plays an important role in hyphal growth. Evidence has been previously presented from studies on *N. crassa* that support IP_3-mediated mobilization of Ca^{2+} from intracellular ER/Golgi-derived vesicles being involved in the maintenance of the tip-high Ca^{2+} gradient reported to be required for hyphal elongation (10). Our results suggest that PLC-2 might be the main phospholipase C engaged in this process. Recent observations in other filamentous fungi, however, have questioned the presence, and thus requirement, of a constant tip-high $[Ca^{2+}]_c$ gradient in continuously growing hyphae (323). The authors showed that transient $[Ca^{2+}]_c$ spikes occur in growing hyphal tips instead, but their role in hyphal elongation and whether PLC-2 is important in generating these spikes, is as yet unclear. Other studies have shown that deletion of

phospholipase C genes in *M. oryzae* results in defects in other morphogenetic processes such as appressorium formation and conidiation (334, 445).

4.2) CZT-1 is a novel transcription factor controlling cell death and natural drug resistance

The protein encoded by NCU09974, now termed CZT-1, was not considered before in transcription factor-related works in *N. crassa*, likely because only a recent genome annotation added a few extra exons to the gene that include a Zn_2/Cys_6 DNA-binding domain. We show that CZT-1 is a crucial mediator of the fungal response to staurosporine both in laboratory strains as well as in wild isolates of *N. crassa*. Transcriptional profiling of the Δ*czt-1* mutant suggests that CZT-1 controls the expression of several genes, affecting diverse processes and organelles, including the mitochondria and the ER. This regulatory role is in accordance with the transcription factor-related sequence features of CZT-1. The presence of a conserved Zn_2/Cys_6 DNA-binding domain at the N'-terminal portion of CZT-1 positions this protein in the zinc cluster family of transcription factors, which was found exclusively in fungi, namely in the Ascomycota phylum (446). CZT-1 homologues from BLAST searches correspond mostly to uncharacterized proteins in diverse fungi, including human pathogens such as *A. fumigatus* or crop pathogens like *M. oryzae* or *Fusarium sp*. Within the same species, it appears that there are two types of zinc cluster proteins: some with strong homology to CZT-1 and others with weak homology. Specific CZT-1 sequence features suggest that it may belong to a novel divergent subfamily of zinc cluster transcription factors. Thus, we consider that our data on the functions of CZT-1 has a broad interest and can be the basis of future studies on the role of this uncharacterized group of proteins that may have an important role in antifungal responses and drug resistance in clinical or economic relevant fungi.

A large number of zinc cluster transcription factors regulate drug resistance, consistent with our observations on the role of CZT-1. Multidrug resistance is highly conserved and commonly activated by microbes or cancer cells upon exposure to cellular insults. It is the consequence of the extrusion of drugs by cells overexpressing pumps of the ABC transporter family or the major facilitator

superfamily (446). In *C. albicans*, the zinc cluster transcription factor Tac1 controls the expression of the ABC transporter genes *CDR1* and *CDR2*, which mediate resistance to azole drugs (447). In *S. cerevisiae*, some of these regulators, including Pdr1, Pdr3, Yrr1 and Stb5, interact as homodimers and heterodimers in order to accomplish their regulatory functions (448, 449).

Stb5 is an oxidative stress-induced transcription factor that regulates multidrug resistance (450) as well as the expression of genes in the pentose phosphate pathway affecting NADPH production (451). This may parallel to some extent the role of CZT-1 in *N. crassa*, since the lack of the protein results in a higher accumulation of ROS upon insult with staurosporine. Indeed, the deletion of *czt-1* results in altered expression of several components of the oxidative stress detoxification machinery, both basally and after addition of the drug (data not shown). In addition, CZT-1 is necessary for the induction of ABC-3, and the ABC-3 homologue in *M. grisea* is important for cell survival during oxidative stress (452). This may also contribute to the increased levels of ROS in Δ*czt-1* cells. Our results indicate that gene regulation by CZT-1 affects other intracellular events, particularly Ca^{2+} signaling. RNA-seq analyses show that diverse genes encoding molecules intervening in intracellular Ca^{2+} handling are altered in *czt-1* mutant cells (data not shown).

We observed that the lack of *czt-1* seems to be particularly important for the response to staurosporine compared to other tested stimuli (the lack of *czt-1* results in a small increase in sensitivity to phytosphingosine and cinnamic acid and resistance to amphotericin B). On the other hand, we tested the susceptibility of Δ*czt-1* to a limited number of drugs and therefore the possibility that CZT-1 is essential to provide resistance to other stresses is an open subject. Indeed, the expression of *czt-1* is induced by a number of compounds and CZT-1 controls different ABC transporters, which are mediators of multidrug resistance. Thus, it is tempting to speculate that the observed variation in resistance to staurosporine for the wild isolates of the fungus may have implications in the response to certain conditions present in their natural habitats.

Natural variation to oxidative stress and drug resistance has been shown in other fungi. In *S. cerevisiae*, clinical and soil isolates from the Pennsylvania (USA) tolerate ROS accumulation better than human-associated brewery and vineyard strains, soil isolates from North Carolina or fruit populations indicating that

response to oxidative stress is an adaptive feature (453). Recently, a GWAS associated a quantitative trait nucleotide in *RDS2* to increased survival upon oxidative stress in a clinical isolate of *S. cerevisiae versus* a laboratory reference strain (454) and *RDS2* encodes a zinc cluster transcription factor (450). In the plant pathogen *B. cinerea*, three natural populations of field isolates from vineyards in France and Germany exhibiting different mechanisms of fungicide resistance were identified (455). In one of these populations, all strains had mutations in a zinc cluster transcription factor-encoding gene, *mrr1*, causing overexpression of the ABC transporter AtrB. Resistance to sterol demethylation inhibitors and strobilurins in field isolates of *Penicillium digitatum* and *Mycosphaerella graminicola*, respectively, was also described (456, 457). Our work on a subtropical wild population of *N. crassa* (335, 375) further supports that natural variation to drug tolerance occurs and seems to be mediated by zinc cluster transcription factors. A GWAS on this population pointed to putative loci involved in the process, including the oxidative stress- and cell death-related proteins CAT-1 and AMID-2, respectively.

We showed that expression of different ABC transporters is CZT-1-dependent. This is likely to be related to the drug resistance regulatory role of the transcription factor. Since the inactivation of *czt-1* leads to deficiency in several drug efflux pumps, it may be a good target to overcome drug resistance. This suggestion makes it relevant to characterize, in future studies, the role of CZT-1 and its homologues in pathogenic organisms.

CHAPTER II

MECHANISMS OF CELL DEATH-INDUCING DRUGS IN THYROID CANCER CELLS

1. Introduction

Albeit an oversimplification, it can be stated that tumorigenesis results from an unbalance between cell death and proliferation and deficiency in PCD is an hallmark of cancer development (458). It is estimated that more than a half of the neoplasms have defects in the apoptotic machinery, from regulators to executioners (459). For instance, mutations in the tumor suppressor gene *TP53* encoding the transcription factor p53, which regulates several forms of cell death, are commonly found in different types of cancer (460). Thus, modulation of cell death in cancer cells can be a powerful strategy for therapy. Indeed, most of the chemotherapeutic agents currently used or in clinical trials for cancer treatment act by inducing apoptosis (459).

Previous work from our group has demonstrated that the combination of staurosporine with either the mitochondrial complex I inhibitor rotenone or the protein tyrosine phosphatase and ATPase inhibitor sodium orthovanadate results in a synergistic growth inhibitory effect against *N. crassa*, *A. fumigatus* and *C. albicans* (139, 140). Thus, it became of particular interest to study the effects of these combinations of drugs as well as to characterize their molecular mechanisms in a cancer cell model. For this purpose, we decided to use thyroid cancer cell lines with different genetic backgrounds, as thyroid papillary carcinoma is the most common endocrine malignancy (461).

We were able to mimic the synergistic interaction between staurosporine and rotenone in thyroid cancer cells and observed that it involves enhanced cell death. The characterization of the mechanisms of rotenone indicated that in addition to its role as a complex I inhibitor, the drug acts as an anti-mitotic agent. Rotenone triggered a plethora of cellular events, including mitotic catastrophe, mitotic slippage, cell death and cellular senescence, in which p53 played a pivotal role. Using cancer cells devoid of mtDNA we confirmed that the cell death-inducing ability of rotenone is ROS-independent and uncoupled to its action in the mitochondria. The mechanisms of sodium orthovanadate on thyroid cancer cells were also studied. Our data indicates that sodium orthovanadate induces typical features of cell death, including including DNA fragmentation, loss of ΔΨm, ROS

production and activation of caspase-3. We also showed that sodium orthovanadate interferes with the PI3K/Akt/mTOR signaling pathway. Three publications resulted from this work and are presented in the following pages.

Involvement of p53 in cell death following cell cycle arrest and mitotic catastrophe induced by rotenone

A. Pedro Gonçalves, Valdemar Máximo, Jorge Lima, Keshav K. Singh, Paula Soares, Arnaldo Videira

Biochimica et Biophysica Acta - Molecular Cell Research (2011) 1813(3):492-9

Biochimica et Biophysica Acta 1813 (2011) 492–499

Contents lists available at ScienceDirect

Biochimica et Biophysica Acta

journal homepage: www.elsevier.com/locate/bbamcr

Involvement of p53 in cell death following cell cycle arrest and mitotic catastrophe induced by rotenone

António Pedro Gonçalves [a,b,*], Valdemar Máximo [c,d], Jorge Lima [c], Keshav K. Singh [e], Paula Soares [c,d], Arnaldo Videira [a,b]

[a] IBMC–Instituto de Biologia Molecular e Celular, Universidade do Porto, Rua do Campo Alegre 823, 4150-180 Porto, Portugal
[b] ICBAS–Instituto de Ciências Biomédicas de Abel Salazar, Universidade do Porto, Largo Prof. Abel Salazar 2, 4099-003 Porto, Portugal
[c] IPATIMUP–Instituto de Patologia e Imunologia Molecular, Universidade do Porto, Rua Dr. Roberto Frias s/n, 4200-465 Porto, Portugal
[d] Faculdade de Medicina, Universidade do Porto, Al. Prof. Hernâni Monteiro, 4200-319 Porto, Portugal
[e] Roswell Park Cancer Institute, Elm and Carlton Streets, Buffalo, NY 14263, USA

ARTICLE INFO

Article history:
Received 22 September 2010
Received in revised form 6 December 2010
Accepted 3 January 2011
Available online 9 January 2011

Keywords:
Cell death
Rotenone
p53
Mitotic catastrophe
Cell cycle

ABSTRACT

In order to investigate the cell death-inducing effects of rotenone, a plant extract commonly used as a mitochondrial complex I inhibitor, we studied cancer cell lines with different genetic backgrounds. Rotenone inhibits cell growth through the induction of cell death and cell cycle arrest, associated with the development of mitotic catastrophe. The cell death inducer staurosporine potentiates the inhibition of cell growth by rotenone in a dose-dependent synergistic manner. The tumor suppressor p53 is involved in rotenone-induced cell death, since the drug treatment results in increased expression, phosphorylation and nuclear localization of the protein. The evaluation of the effects of rotenone on a p53-deficient cell line revealed that although not required for the promotion of mitotic catastrophe, functional p53 appears to be essential for the extensive cell death that occurs afterwards. Our results suggest that mitotic slippage also occurs subsequently to the rotenone-induced mitotic arrest and cells treated with the drug for a longer period become senescent. Treatment of mtDNA-depleted cells with rotenone induces cell death and cell cycle arrest as in cells containing wild-type mtDNA, but not formation of reactive oxygen species. This suggests that the effects of rotenone are not dependent from the production of reactive oxygen species. This work highlights the multiple effects of rotenone in cancer cells related to its action as an anti-mitotic drug.

1. Introduction

In recent years, the highly sophistication of the mechanisms of programmed cell death which guard the organism against unwanted and potentially harmful cells has become evident. The Nomenclature Committee on Cell Death proposed recently unified criteria for the definition of cell death and of its different morphologies [1]. Nevertheless, one may find several terms to define different (or not so different) ways a cell has to die. The balance between cell division and cell death is of supreme importance for the development and maintenance of multicellular organisms. Deregulation of this balance can lead to pathological conditions, like cancer, neurodegenerative and immune system disorders [2].

One of the cell death processes is mitotic catastrophe. There is not a definitive accepted classification of mitotic catastrophe and its significance is still under debate but, currently, the concept refers to a series of events that result from premature or inadequate entry of cells into mitosis and represent an intermediate stage between a prolonged mitotic arrest and the set off of cell death [3]. It can be triggered either by chemical or physical stresses, namely, by drugs that disturb the stability of microtubules [3,4]. The molecular players involved in mitotic catastrophe are another matter of investigation.

Rotenone is a plant compound derived from the Leguminosae family used primarily as a mitochondrial complex I inhibitor. It induces cell death in several types of cells through the generation of reactive oxygen species (ROS) [5–7]. ROS formation is considered crucial, since treatment with antioxidants could abolish rotenone-induced cell death [6,7]. Yet, it was recently shown that complex I inhibition is not enough to explain the rotenone effect [8,9] and earlier studies showed that rotenone has another point of attack within the cells, the mitotic spindle [10]. Later work described that rotenone inhibits the assembly of the mitotic spindle by direct binding to

Abbreviations: ROS, reactive oxygen species; mtDNA, mitochondrial DNA; DMSO, dimethyl sulfoxide; DHE, dihydroethidium; DHR 123, dihydrorhodamine 123; X-gal, 5-bromo-4-chloro-3-indolyl-β-D-galactopyranoside; DAPI, 4′,6-diamidino-2-phenylindole; FITC, fluorescein isothiocyanate; ΔΨm, mitochondrial membrane potential; CI, combination index; DRI, dose reduction index

* Corresponding author. IBMC–Instituto de Biologia Molecular e Celular, Universidade do Porto, Mitochondria Lab, Rua do Campo Alegre 823, 4150-180 Porto, Portugal. Tel.: +351 226 074 900; fax: +351 226 099 157.
E-mail address: apgoncalves@ibmc.up.pt (A.P. Gonçalves).

0167-4889/$ – see front matter © 2011 Elsevier B.V. All rights reserved.
doi:10.1016/j.bbamcr.2011.01.006

tubulin [11–13], but the molecular mechanisms underlying the effects of rotenone remain elusive. Since compounds that inhibit the spindle assembly are inducers of mitotic catastrophe, it is reasonable to presume that rotenone can be such an inducer. Furthermore, studies in animal models of different forms of cancer demonstrated that rotenone possesses *in vivo* anticancer properties [14–17].

This prompted us to further investigate the effects of rotenone in cancer cells with different genetic backgrounds. In this work we show that rotenone induces mitotic catastrophe, mitotic slippage, cell death and cellular senescence in cancer cells and acts by two independent pathways. Our results also emphasize the involvement of p53 on the action of rotenone.

2. Materials and methods

2.1. Cell culture, reagents and antibodies

TPC-1 and 8505-C cells were maintained in RPMI-1640 medium supplemented with 10% fetal bovine serum, 100 U/ml penicillin, 100 μg/ml streptomycin and 1.25 μg/ml amphotericin B (all from Invitrogen). 143B ρ^0 and CMPBR3 cells were maintained in DMEM (Invitrogen) supplemented with 50 μg/ml uridine (Sigma-Aldrich), 10% fetal bovine serum, 100 U/ml penicillin, 100 μg/ml streptomycin and 1.25 μg/ml amphotericin B. The 143B ρ^0 cell line is derived from the parental osteosarcoma cell line 143B after depletion of mitochondrial DNA (mtDNA) using herpes simplex virus [18]. The CMPBR3 cybrid cell line was obtained through the fusion of 143B ρ^0 cells with platelets from a healthy individual, as in reference [19]. All cell lines were kept at 37 °C and 5% CO_2. For the treatments with the drugs, cells were seeded and left to adhere for approximately 24 h. Afterwards, the medium was replaced by fresh medium supplemented with the desired concentrations of the drugs. Stock solutions of rotenone and staurosporine were prepared in dimethyl sulfoxide (DMSO) at 50 and 10 mM, respectively. DMSO was used in all experiments as the vehicle (control).

Rotenone, sulphorhodamine B, propidium iodide, dihydroethidium (DHE) and dihydrorhodamine 123 (DHR123) were purchased from Sigma-Aldrich, DMSO from AppliChem, staurosporine from LC Laboratories, mounting medium with 4′,6-diamidino-2-phenylindole (DAPI) from Vector Laboratories, CMXRos (MitoTracker Red) and rhodamine-phalloidin from Molecular Probes, nonyl acridine orange from PromoKine, 5-bromo-4-chloro-3-indolyl-β-D-galactopyranoside (X-gal) from NZYTech and RNase A from Fermentas. The following antibodies were employed: p53 (clone DO-1) (Oncogene Science), phospho-p53 (Serine 15) (Cell Signaling Technology), SSBP1 (Abnova), OPA1 (BD Biosciences), cytochrome *c* and complex V subunit α (MitoSciences) and actin (Santa Cruz Biotechnology).

2.2. Analysis of cell growth

For the sulphorhodamine B assay, cells were fixed with 10% trichloroacetic acid and stained with 0.1% sulphorhodamine B. The plates were read in a microplate reader (Bio-Rad) at 560 nm. Triplicate wells per condition were evaluated in each experiment. For cell cycle analysis, cells were fixed with ice-cold 70% ethanol for at least 4 h and, after washing with PBS, stained with a solution containing 5 μg/ml propidium iodide and 100 μg/ml RNase A. Flow cytometry was performed in a Epics XL-MCL (Beckman-Coulter) and the results were analyzed using FlowJo software (Tree Star).

The β-galactosidase assay was carried out as previously described [20]. Phase-contrast and β-galactosidase micrographs of cells were taken using a CKX41 (Olympus) inverted microscope.

2.3. Fluorescence microscopy

For observation of nuclei, cells were incubated with 0.075 M KCl (individual chromosomes can be microscopically identified and examined in much greater detail by incubating cells with a hypotonic solution), washed with PBS, fixed (with a 3:1 mixture of methanol and acetic acid at 4 °C) and stained with DAPI. For staining of F-actin, cells growing in coverslips were fixed with 4% paraformaldehyde, washed with PBS, permeabilized with 0.2% Triton X-100 and incubated with phalloidin-rhodamine diluted 1:40 in PBS for 20 min.

For immunostaining for p53, cells were fixed and permeabilized, incubated 1 h with blocking buffer (5% normal rabbit serum and 0.3% Triton X-100 in PBS), 1 h with the primary anti-p53 (DO-1) antibody (1:40 dilution in 10% BSA + 0.3% Triton X-100 in PBS), washed (PBS–0.5% Tween-20–0.05% BSA) and 1 h with the secondary rabbit anti-mouse antibody conjugated with fluorescein isothiocyanate (FITC) (Dako).

The cytochrome *c* release assay was performed according to the protocol provided by the manufacturer (MitoSciences). For observation and analysis, the Axio Imager 2 microscope and the AxioVision LE software (Zeiss) were used.

2.4. Western blotting

Whole lysates of cells were obtained first by incubation with RIPA buffer (50 mM Tris–HCl + 1% NP-40 + 150 mM NaCl + 2 mM EDTA, ph 7.5), a protease inhibitor cocktail (Roche Applied Science) and a phosphatase inhibitor cocktail (Sigma-Aldrich), followed by centrifugation (14000 rpm, 15 min, 4 °C) and collection of the supernatant. The lysates were separated by SDS-PAGE and transferred to a nitrocellulose membrane. The membrane was blocked for 1 h using a 5% non-fat dry milk or bovine serum albumin in PBS–0.5% Tween-20 solution and incubated with the appropriate primary and secondary antibodies. The protein bands were detected by chemiluminescence and X-ray film exposure (GE Healthcare).

2.5. Analysis of mitochondrial parameters

For evaluation of the production of ROS or mitochondrial membrane potential ($\Delta\Psi m$), 5 μM DHE/10 μM DHR123 or 250 nM CMXRos, respectively, was added to the culture medium for 30 min. Then, cells were detached, washed two times and resuspended in PBS. For analysis of the mitochondrial mass, cells were first detached, washed two times and incubated in PBS containing 5 μM nonyl acridine orange. Samples were analyzed by flow cytometry.

For inspection of mitochondrial morphology, cells growing in coverslips were incubated with 250 nM CMXRos for 30 min at 37 °C, fixed with 4% paraformaldehyde, washed twice in PBS and observed by fluorescence microscopy.

2.6. Statistical analysis

For quantification of synergy two measurements were employed – the combination index (CI) and the dose reduction index (DRI) [21] – using CalcuSyn software (Biosoft). The calculation is based on the median-effect equation derived from the mass-action law. Briefly, the median-effect equation describes dose-effect relationships, allows the construction of the median-effect plot and provides parameters for the calculation of CI and DRI. When two or more drugs are combined and the CI is calculated, $CI < 1$, $= 1$, and > 1 indicates synergism, additive effect, and antagonism, respectively. The DRI measures how many folds the dose of each drug in a synergistic combination may be reduced to a given effect level; the greater DRI value indicates a greater dose reduction [21]. The remaining statistical analysis of the data was performed using SPSS 13.0 (SPSS Inc.) by the non-parametric Mann–Whitney test, for comparisons between two groups. *P*-values < 0.05 were considered to be statistically significant.

3. Results

3.1. Rotenone inhibits the growth of cancer cells and induces cell death, cell cycle arrest, mitotic catastrophe and cellular senescence

Treatment of TPC-1 cells for 24 h with rotenone results in growth inhibition, as demonstrated in Supplemental Fig. 1A by phase-contrast micrographs of the cells. This growth inhibition occurred in a dose-dependent manner (Supplemental Fig. 1B). The calculated median-effect dose of the drug or IC_{50} is 26 μM (data not shown). We analyzed the cell cycle of TPC-1 cells treated for 24 h with increasing concentrations of rotenone. Fig. 1A shows two representative histograms of the DNA content of TPC-1 cells treated with a control or with 5 μM rotenone and quantification of the data for the various concentrations tested are represented in Fig. 1B. Rotenone induces cell death, represented by the fraction of sub-G_1 cells (15.78% for 5 μM rotenone vs. 2.86% for the control; $P=0.006$), and also cell cycle arrest, showed by the increase of the percentage of cells with 4 N DNA content, typical of the G_2 and M phases of the cycle (72.38% for 5 μM rotenone vs. 31.83% for the control; $P=0.006$). Thereby, rotenone-induced growth inhibition of TPC-1 cells can be explained by the induction of death and cell cycle arrest.

Evaluation of the nuclear morphology of TPC-1 cells by fluorescence microscopy shows that rotenone induces mitotic catastrophe (Fig. 1C). Scoring of the presence of interphase-like nuclei, mitotic figures, aberrant nuclei and clusters of nuclei typical of mitotic catastrophe (Fig. 1D) denotes a significant alteration in all the types of nuclei scored, including an increase in the number of mitotic figures (20.18% for 5 μM rotenone vs. 1.22% for the control; $P=0.034$ at 24 h) and in the presence of syncytia of nuclei resembling those characteristic of mitotic catastrophe (12.71% for 5 μM rotenone vs. 0% for the control; $P=0.019$ at 24 h). TPC-1 cells treated with rotenone for 5 days display a senescent-like phenotype [22], with a higher size, flattened aspect, numerous vacuoles and foci of heterochromatin (Fig. 2A). Increased expression of β-galactosidase (Fig. 2B and C; 14.41% for 5 μM rotenone vs. 0.18% for the control; $P=0.004$) supports the observation that cells become senescent after prolonged exposure to rotenone. Staining of F-actin with phalloidin revealed overexpression of the filaments and a considerable increase in cell size (Fig. 2D).

3.2. Involvement of p53 in rotenone-induced cell death

Since p53 is a molecule frequently responsive to cell stress, particularly cell cycle insults, we tested if rotenone was altering its state. Western blot analysis revealed that rotenone induces almost a two-fold increase in the levels of p53 (Fig. 3A and B; $P=0.037$). In control-treated cells, p53 was located in the nucleus and dispersed in the cytoplasm (Fig. 3C). Conversely, in rotenone-treated cells, p53 was almost exclusively within the nucleus, including mitotic catastrophe-like nuclei (Fig. 3C). Phosphorylation of p53 at its serine 15 residue is a key step during the p53 activation process [23,24]. Rotenone-treated TPC-1 cells evidenced an increase in the phosphorylation of p53 in serine 15 (Fig. 3D). Therefore, rotenone induces a nuclear accumulation of p53 together with an increase in the levels of the protein and possibly its activation, since its phosphorylation at serine 15 was enhanced by rotenone. We also studied the expression of the cyclin-dependent kinase inhibitor p21, which is a p53 target gene that regulates cell cycle progression at G_1 [25,26]. Treatment with rotenone leads to an increase in the expression of p21 (Fig. 3E). We did not detect alterations in other molecules tested by Western blot, specifically Chk2, Bax, XIAP and cyclin D1 (data not shown).

To further study the involvement of p53, we analyzed the outcome of the treatment with rotenone in 8505-C cells. These cells harbor a point mutation at the DNA-binding domain of *TP53* that translates to the substitution Arg248Gly [27], leading to a non-functional protein [28]. The basal cell cycle profile of TPC-1 and 8505-C cells is similar (Supplemental Fig. 2). The cell cycle of 8505-C cells after 24 h of treatment with 5 μM rotenone is arrested as in TPC-1 cells, as demonstrated by the percentage of cells with a 4 N DNA content (80.75% for 5 μM rotenone vs. 35.28% for the control; $P=0.05$) (Fig. 4A and C). Analysis of the nuclear morphology of rotenone-treated 8505-C cells also revealed the presence of mitotic catastrophe-like clusters (Fig. 4B).

It is currently accepted that mitotic catastrophe is a biological state that precedes cell death [3]. Thereby, we tested if there is induction of cell death after the mitotic catastrophe state induced by the drug. As depicted in Fig. 4C and D, in TPC-1 cells, there was a dramatic increase in the percentage of hypodiploid cells from 24 to 48 h of treatment (15.78% at 24 h vs. 57.70% at 48 h; $P=0.009$) and a decrease in the percentage of cells with a DNA content typical of G_2/M (72.38% at 24 h vs. 18.48% at 48 h; $P=0.009$). In contrast, p53-mutant 8505-C cells remain arrested in the cell cycle after 48 h of treatment and undergo death to a lesser extent than TPC-1 cells (Fig. 4D; TPC-1 vs. 8505-C cells, $P=0.009$ for sub-G_1 cells and $P=0.008$ for G_2/M cells). Taken together, these results suggest that a functional p53, although not required for the rotenone-induced cell cycle arrest and mitotic catastrophe, plays a role in the extensive cell death that occurs afterwards.

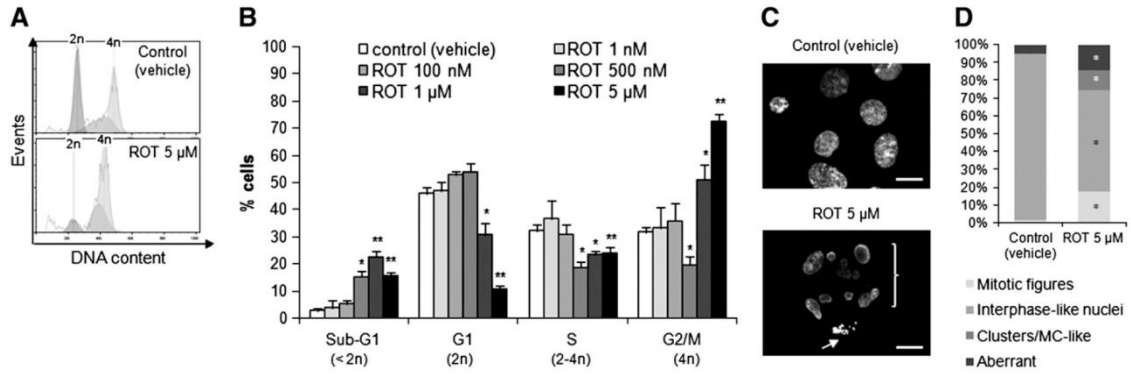

Fig. 1. Rotenone induces cell death, cell cycle arrest and mitotic catastrophe. (A) Representative histograms of the cell cycle analysis by propidium iodide staining of DNA of cells treated with a control (vehicle) (upper panel) or with rotenone (lower panel). (B) Quantification of the data for experiments like the one in (A) for different concentrations of the drug. (C) Nuclear morphology of 5 μM rotenone-treated cells was assessed by staining with DAPI; the bracket indicates a mitotic catastrophe-like cluster and the arrow points to a mitotic figure; scale bar: 10 μm. (D) Stained nuclei were counted and classified in four groups (mitotic figures, interphase-like nuclei, clusters/mitotic catastrophe-like and aberrant) based on their morphological features. All treatments in this figure were 24 h long. Data is representative of at least three independent experiments. Data shown in (B) represents the mean ± standard error of mean (SEM). *, $P<0.05$; **, $P<0.01$.

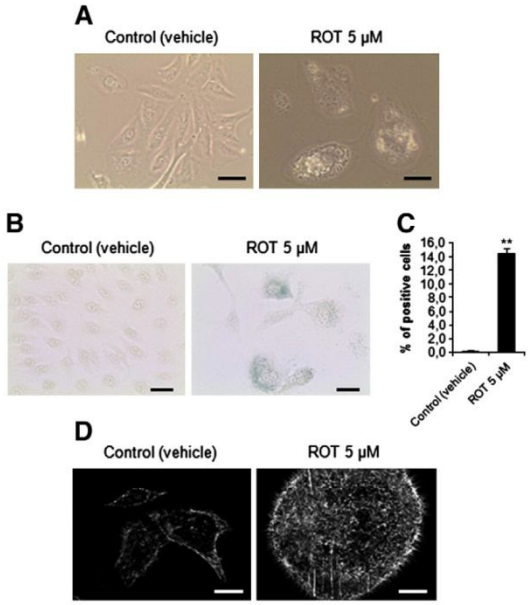

Fig. 2. Long rotenone treatments induce cellular senescence in TPC-1 cells. (A) Phase-contrast micrographs of rotenone (ROT)-treated TPC-1 cells; scale bar: 30 μm. The expression of β-galactosidase was evaluated by staining cells treated with rotenone with X-gal (B; scale bar: 50 μm) and by calculating the ratio of positive cells/total number of cells (C). (D) The F-actin filaments of rotenone-treated cells were stained with phalloidin-rhodamine; scale bar: 10 μm. The cells were exposed to rotenone for 5 days (after 3 days of treatment the above alterations were already observable). Data is representative of at least three independent experiments. Data shown in (C) represents the mean ± SEM. **, $P<0.01$.

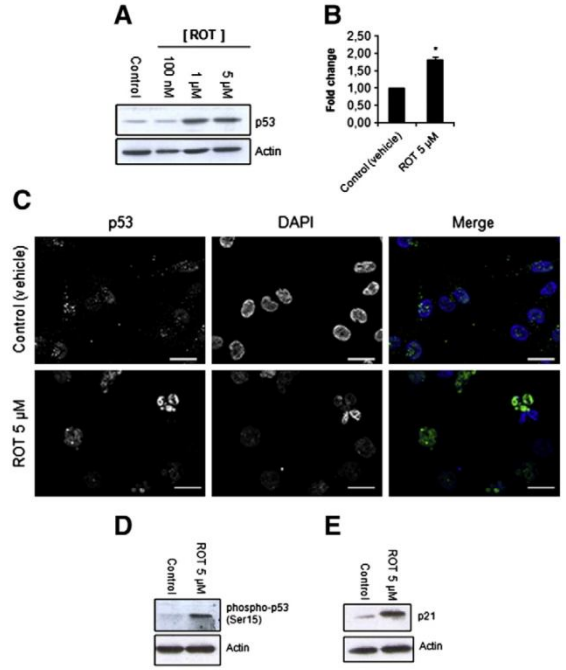

Fig. 3. Rotenone increases the expression, phosphorylation of serine 15 and nuclear accumulation of p53 in TPC-1 cells. (A) Whole lysates of cells treated with rotenone (ROT) were immunoblotted for p53 and quantification of data (B) was determined by relative intensity (normalized to actin). (C) Cells treated with rotenone were stained for p53 (left column and green in the right column) and with DAPI for nuclei (middle column and blue in the right column); scale bar: 10 μm. (D–G) Whole lysates of cells treated with rotenone were immunoblotted for p53 phospho-serine 15 (D) and p21 (E). The rotenone treatments in this figure correspond to a 24 h period. Immunoblotting against actin served as a loading control. Data is representative of at least three independent experiments. Data shown in (B) represents the mean ± SEM. *, $P<0.05$.

There are other differences between these two cell lines. In contrast to TPC-1, in 8505-C cells p53 is already located in the nucleus even without rotenone treatment (Supplemental Fig. 3). 8505-C also undergo cellular senescence after prolonged treatment with rotenone, as evidenced by typical morphological alterations (Supplemental Fig. 4A) and by a significant increase in the number of β-galactosidase-positive cells (2.21% for 5 μM rotenone vs. 0.13% for the control; $P=0.001$; Supplemental Fig. 4B and C). However, the percentage of positive cells is significantly higher in TPC-1 than in the 8505-C cell line (14.41% for TPC-1 cells vs. 2.21% for 8505-C cells; $P=0.021$). These results indicate that p53 is also important for the senescence effect of rotenone.

3.3. Rotenone-induced cell death and cell cycle arrest is independent from the mitochondrial production of ROS

Since oxidative stress induced by rotenone was advanced to be required to trigger cell death [6,7], we evaluated the formation of ROS in rotenone-treated TPC-1 cells. Using DHE (for superoxide detection), the production of ROS showed a significant increase both at 6 h (Fig. 5A and C; 1.25-fold with 5 μM rotenone; $P=0.037$), and at 24 h (Fig. 5B and C; 2.12-fold with 5 μM rotenone; $P=0.037$), in a dose-dependent manner. This effect was not cell type-specific, since 8505-C and HEK293 cells were also stimulated to produce ROS (Supplemental Fig. 5A and B). Detection of ROS with DHR 123 (detects hydrogen peroxide, peroxonitrite and hypoclorous acid) provided similar results (Supplemental Fig. 5C–E).

On the other hand, we checked ROS production in 143B ρ^0 cells (depleted of mtDNA) and in CMPBR3 cells (obtained by fusing the previous cell line with mitochondria from platelets harboring wild-type mtDNA). The results showed a remarkable increase in ROS formation in CMPBR3 cells upon rotenone treatment (Fig. 5D and F; about 2.5-fold with 5 μM rotenone; $P=0.028$), but not in 143B ρ^0 cells (Fig. 5E and F; 1,16-fold with 5 μM rotenone; $P=0.487$).

Analysis of the cell cycle in 143B ρ^0 and CMPBR3 cells treated with 5 μM rotenone for 24 h show that both cell lines displayed a significant increase in the percentage of dead cells (Fig. 5G and H; 23.16% for 5 μM rotenone vs. 3.01% for the control in CMPBR3 cells, $P=0.018$; 17.53% for 5 μM rotenone vs. 1.70% for the control in 143 B ρ^0 cells, $P=0.028$) and in the percentage of cells in G_2/M (64.80% for 5 μM rotenone vs. 34.73% for the control in CMPBR3 cells, $P=0.021$; 53.49% for 5 μM rotenone vs. 27.37% for the control in 143B ρ^0 cells, $P=0.034$), similarly to the results obtained with TPC-1 and 8505-C cells. Thus, it appears that cell death and cell cycle arrest induced by rotenone is independent from the mitochondrial production of ROS, at least in this model. In addition, the fact that 143B cells harbor a point mutation at the DNA-binding domain of *TP53* that translates to the substitution Arg156Pro [29], leading to a non-functional protein [28], further corroborates that a functional p53 is not required for the rotenone-induced cell cycle arrest.

3.4. Treatment with rotenone leads to alterations in ΔΨm, biogenesis and morphology

We assessed mitochondrial function in TPC-1 cells treated with rotenone by estimation of different parameters. A dual effect on the ΔΨm was observed (Fig. 6A and B). There is a fraction of cells with loss of ΔΨm (21.25% for 5 μM rotenone vs. control; $P=0.014$) and a

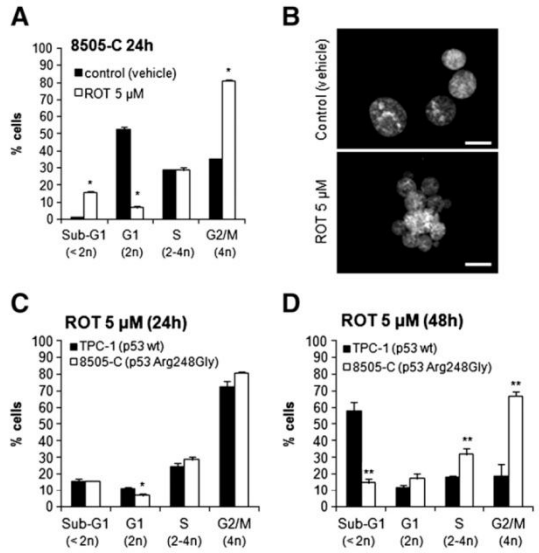

Fig. 4. Comparison of the rotenone effects in 8505-C and TPC-1 cells. (A) Quantification of data regarding the cell cycle analysis of 8505-C cells by DNA staining with propidium iodide after a 24 h treatment with 5 μM rotenone. (B) Nuclear morphology of control (vehicle)-treated (upper panel) or 5 μM rotenone-treated 8505-C cells was assessed by staining with DAPI; scale bar: 10 μm. (C and D) Comparison of the cell cycle of TPC-1 and 8505-C cell lines upon treatment with 5 μM rotenone for 24 h (C) or 48 h (D). Data is representative of at least three independent experiments. Data shown in (A), (C) and (D) represents the mean ± SEM. *, $P<0.05$; **, $P<0.01$.

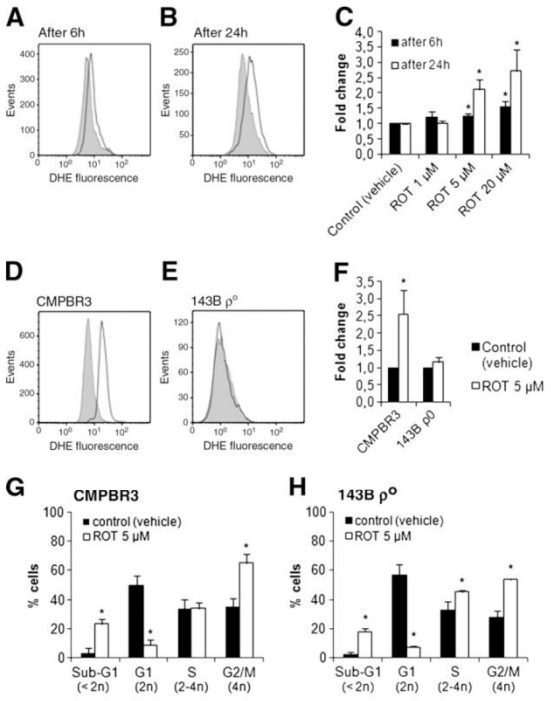

Fig. 5. Rotenone-induced cell death and cell cycle arrest is independent from the mitochondrial production of ROS. (A–F) The production of superoxide was measured using dihydroethidium as a probe; (A) and (B) are representative flow cytometry histograms of TPC-1 cells after treatment with rotenone (ROT) and quantification of the data is presented in (C); (D) and (E) are representative flow cytometry histograms of CMPBR3 (D) and 143B ρ^0 (E) cells after treatment with rotenone for 24 h and quantification of the data is presented in (F). In the histograms presented in (A), (B), (D) and (E), the gray areas correspond to control (vehicle) and the white areas represent treatment with 5 μM rotenone. (G and H) Cell cycle analysis of CMPBR3 (G) and 143B ρ^0 (H) cells by staining with propidium iodide after treatment with control (vehicle) or 5 μM rotenone for 24 h. Data is representative of at least three independent experiments. Data shown in (C), (F), (G) and (H) represents the mean ± SEM. *, $P<0.05$.

second population of cells with gain of $\Delta\Psi m$ (7.82% for 5 μM rotenone vs. control; $P=0.014$) after treatment with rotenone for 24 h. The population of cells with loss of $\Delta\Psi m$ likely corresponds to those that are in the process of cell death. The observed hyperpolarization may result from an increase in mitochondrial mass [30]. In fact, there is a significant 1.5-fold increase in the number of mitochondria (Fig. 6C and D; $P=0.037$), suggesting that the drug is stimulating mitochondrial biogenesis. Concordantly, we observed an increase in the expression of SSBP1 (Fig. 6E), a protein that is upregulated during mitochondrial biogenesis [31]. Thus, the gain of $\Delta\Psi m$ may be a consequence of the increase in the number of mitochondria. Rotenone treatment also leads to the presence of cells with a giant nucleus surrounded by a massive network of fused mitochondria (Fig. 6G). This correlates with an increase in the expression of the pro-fusion protein OPA1 (Fig. 6F). Integrity of mitochondria seems to be maintained since we did not observe release of cytochrome *c* to the cytoplasm (Supplemental Fig. 6).

The growth of HEK293 cells, which are derived from non-neoplastic embryonic kidney tissue, is also inhibited by rotenone and the other effects described above for TPC-1 cells, such as cell cycle arrest followed by massive cell death induction, increased expression of p53 and p21 and production of ROS are also observed (data not shown).

3.5. Rotenone and staurosporine act synergistically in inhibiting the growth of thyroid cancer cells in a dose-dependent manner

Synergistic combinations of drugs represent a good strategy to treat diseases, namely cancer, because they offer several advantages such as increasing the efficacy of the treatment, decreasing the dose of the compounds and slowing down the development of drug resistance [21]. Hence, we decided to evaluate whether rotenone could interact synergistically with staurosporine, a potent cell death inducer, as observed recently in the filamentous fungus *Neurospora crassa* [9]. In fact, there is an increase in the percentage of inhibition of cell growth when the drugs were combined vs. either drug used alone (Fig. 7A). The median-effect dose of the 1:1000 (staurosporine:rotenone) combination was 2 nM/μM, meaning a more powerful effect when compared with the median-effect doses of 23 nM and 26 μM, for staurosporine or rotenone alone, respectively) (data not shown). To quantify the synergistic interaction between the drugs we used the combination index (CI), which is based on the median-effect equation and according which there is synergy when CI<1 [21]. As depicted in Fig. 7B, despite the presence of 4 points with CI>1, there is a dose-dependent tendency to have experimental points falling into the CI<1 region, as illustrated by the trend line presented in the graph. Another index calculated using the same data, the dose reduction index (DRI), further supports our conclusions. DRI is a measure of how many folds the dose of each drug in a synergistic combination may be reduced at a given effect level compared with the doses of each drug alone [21]. In this case the greater DRI (DRI>1) value indicates a greater dose reduction for a given therapeutic effect [21]. The DRI calculations (Fig. 7C) for almost all doses of the drugs are greater than 1.

4. Discussion

A deregulation in the normal processes of cell death and cell cycle is a common feature of cancer cells [32]. Rotenone was previously

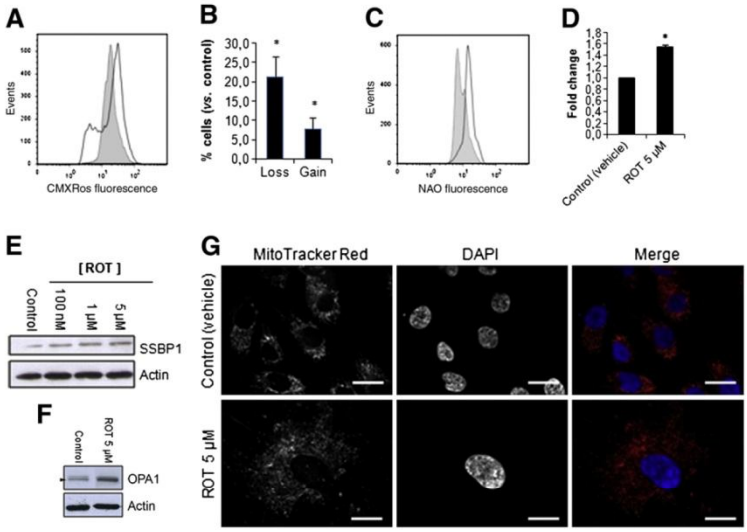

Fig. 6. Rotenone leads to alterations in mitochondrial transmembrane potential, biogenesis and morphology of TPC-1 cells. The mitochondrial membrane potential was determined by incubating cells with CMXRos followed by analysis through flow cytometry histograms (A) and quantification of the data (B). The mitochondrial mass was assessed by staining cells with nonyl acridine orange followed by analysis through flow cytometry histograms (C) and quantification of the data (D). In the histograms presented in (A) and (C), the gray areas correspond to control (vehicle) and the white areas represent treatment with 5 μM rotenone. Whole lysates of cells treated with the indicated concentrations of rotenone (ROT) were immunoblotted against SSBP1 (E) and OPA1 (F); in (F), the arrow head points to the mature form of OPA1. (G) The morphology of mitochondria was evaluated by microscopy after treatment of cells with 5 μM rotenone and incubation with CMXRos (left column and red in the right column) and staining with DAPI for nuclei (middle column and blue in the right column); scale bar: 10 μm. Data is representative of at least three independent experiments. Data shown in (B) and (D) represents the mean ± SEM. *, $P<0.05$

shown to possess anti-tumoral properties by its capacity to induce cell death, both *in vitro* and *in vivo* [5–7,14–17,33]. Here we show that rotenone-induced inhibition of the growth of cancer cells is potentiated by the death inducer staurosporine in a dose-dependent manner. A similar synergistic effect of this drug combination was observed in cells of the filamentous fungus *Neurospora crassa* [9]. Because the administration of drugs to cells usually elicit collateral toxic effects, a strategy to minimize them could be decreasing the dose of the drug applied and this may be achieved by using drug combinations as we report. Future experiments are required in order to evaluate the possible translation of the results to *in vivo* models.

Since rotenone is an inhibitor of respiratory chain complex I [6], we evaluated its effect on mitochondria. The mitochondrial network morphology was modified but the organelles seemed intact and we did not observe release of cytochrome *c*. As expected, a significant percentage of the cells lost their ΔΨm. Yet, other cells exhibited an increase of ΔΨm, which may be explained by some stimulation of mitochondrial biogenesis by rotenone. The observed higher number of mitochondria may account for the increase in the potential per cell, as already proposed [30]. It was proposed recently that p53 regulates mitochondrial biogenesis and mtDNA copy number [34,35], in line with our findings that the effects of rotenone involve p53. Rotenone treatment also increased ROS production. Nevertheless, ROS do not appear to be essential for rotenone-induced cell death in our model. Cells with depleted mtDNA are not stimulated to produce ROS, but become arrested in the cell cycle and undergo death to a similar

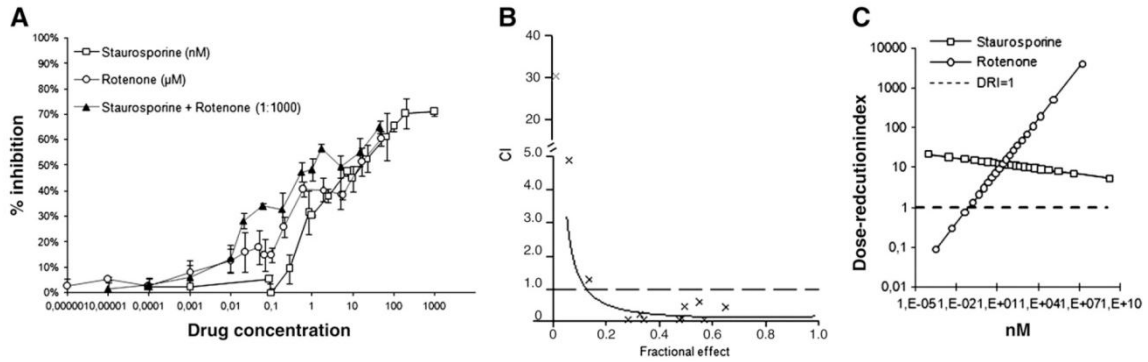

Fig. 7. Staurosporine and rotenone have a synergistic effect against the growth of TPC-1 cells. (A) Growth inhibition was determined by the sulphorhodamine B assay, after 24 h of treatment, for the indicated concentrations of staurosporine, rotenone or the combination of both drugs. Synergy was evaluated according to the combination index (B) and the dose reduction index (C) using the software CalcuSyn; in (B) the crosses correspond to experimental values and the curve is a trend line; in (C) the dashed line corresponds to DRI = 1. Data is representative of at least three independent experiments.

extent as cells containing wild-type mtDNA. This is in agreement with reports that rotenone-induced apoptosis does not depend directly on inhibition of the mitochondrial respiratory chain [8,9].

We found that treatment with rotenone induces cell cycle arrest in the G_2/M phases, as previously shown [5,7]. Further, we could observe morphological features of mitotic catastrophe, in particular the appearance of typical giant clusters of nuclei along with micronucleation and multinucleation [3,4]. Other observations support the idea that rotenone induces mitotic catastrophe. Mitotic catastrophe can be triggered upon microtubule instability leading to an abnormal mitotic checkpoint [3,4], and rotenone binding to tubulin results in the inhibition of the spindle assembly and thus in an anomalous spindle checkpoint [10–13]. In addition, rotenone can induce endoreduplication [36], a process through which successive rounds of DNA replication take place without mitosis, which may facilitate the polyploidization of cells [37].

Treatment of TPC-1 cells with rotenone increased the levels of p53 together with its phosphorylation at serine 15 and its nuclear accumulation. These three consequences are common responses to DNA or spindle damage [24], suggesting the involvement of the protein in rotenone-induced cell death. Cells arrested in response to spindle assembly inhibition eventually bypass the block and exit mitosis without an appropriate division, in a phenomenon known as mitotic slippage [3,4,38]. Consequently, cells enter in G_1 with a 4 N DNA content and this abnormality leads to the activation of the G_1 checkpoint [3,4,38]. This halt is mediated by p53 and p21 appears to be a crucial p53-target gene in this postmitotic checkpoint [25,26]. Moreover, serine 15 phosphorylation stimulates p53 transactivation and is required for this postmitotic checkpoint [23,39]. Similarly, we observed p53 increase and phosphorylation and upregulation of p21 following rotenone exposure. An increase in the levels of p53 after treatment with microtubule disruptors occurring only after tetraploid cells exit mitotic arrest and progress to interphase was also demonstrated [26].

On the other hand, functional p53 is not an absolute requirement for the rotenone-induced cell cycle arrest and mitotic catastrophe because cells harboring a mutation in the DNA-binding domain of the molecule still become arrested and display polyploidy after treatment with the drug. This is consistent with evidence that in the absence of p53, cells have the ability to activate alternative pathways to halt the cell cycle [3]. However, our results stress that the extensive cell death occurring after the mitotic catastrophe state is p53-dependent. The majority of the cells with wild-type p53 overrides the cell cycle blockage and dies after 48 h of rotenone treatment, whereas cells with mutant p53 remain arrested in the cell cycle in the same period and do not show extensive cell death. Kato et al. showed that the mutation present in the 8505-C cell line (Arg248Gly) leads to a total absence of the capacity of p53 to transactivate key players of cell death execution such as Bax, NOXA and Apoptosis-inducing Protein 1 [40]. This may explain why 8505-C cells are less prone to die upon treatment with rotenone.

Our results also suggest involvement of p53 in rotenone-induced cellular senescence, a phenomenon that can occur as a consequence of mitotic catastrophe [41–43]. We observed that when treated for a longer period with rotenone, cells exhibit a senescent-like phenotype. Cells possessing non-functional p53 display significantly less senescence than cells harboring the wild-type protein, suggesting that the rotenone-induced cellular senescence occurs through a p53-pathway. In fact, p53 and p16 are the initiators of two independent senescence pathways [22] and we did not observe increase in the expression of p16 (data not shown).

In summary, we show that rotenone induces a panoply of effects, including mitotic catastrophe, mitotic slippage, cell death and cellular senescence. Our results are in agreement with findings that rotenone may act by at least two different pathways [5,7,8,12,13]: acting directly on mitochondria and in the nucleus. The tumor suppressor protein p53 is involved in these processes, especially regarding the extensive cell death that occurs following a polyploidy state.

Acknowledgments

We thank Joana Nunes (IPATIMUP) for the help with the ρ^0 and cybrid cell lines. A.P.G. was recipient of a fellowship from Fundação Calouste Gulbenkian (reference 104210). K.K.S. was supported by a NIH grant (RO1-121904). This work was supported by Fundação para a Ciência e Tecnologia.

Appendix A. Supplementary data

Supplementary materials related to this article can be found online at doi:10.1016/j.bbamcr.2011.01.006.

References

[1] G. Kroemer, L. Galluzzi, P. Vandenabeele, J. Abrams, E.S. Alnemri, E.H. Baehrecke, M.V. Blagosklonny, W.S. El-Deiry, P. Golstein, D.R. Green, M. Hengartner, R.A. Knight, S. Kumar, S.A. Lipton, W. Malorni, G. Nunez, M.E. Peter, J. Tschopp, J. Yuan, M. Piacentini, B. Zhivotovsky, G. Melino, Classification of cell death: recommendations of the Nomenclature Committee on Cell Death 2009, Cell Death Differ. 16 (2009) 3–11.
[2] R.S. Hotchkiss, A. Strasser, J.E. McDunn, P.E. Swanson, Cell death, N. Engl. J. Med. 361 (2009) 1570–1583.
[3] H. Vakifahmetoglu, M. Olsson, B. Zhivotovsky, Death through a tragedy: mitotic catastrophe, Cell Death Differ. 15 (2008) 1153–1162.
[4] M. Castedo, J.L. Perfettini, T. Roumier, K. Andreau, R. Medema, G. Kroemer, Cell death by mitotic catastrophe: a molecular definition, Oncogene 23 (2004) 2825–2837.
[5] J.S. Armstrong, B. Hornung, P. Lecane, D.P. Jones, S.J. Knox, Rotenone-induced G2/M cell cycle arrest and apoptosis in a human B lymphoma cell line PW, Biochem. Biophys. Res. Commun. 289 (2001) 973–978.
[6] N. Li, K. Ragheb, G. Lawler, J. Sturgis, B. Rajwa, J.A. Melendez, J.P. Robinson, Mitochondrial complex I inhibitor rotenone induces apoptosis through enhancing mitochondrial reactive oxygen species production, J. Biol. Chem. 278 (2003) 8516–8525.
[7] J. Lee, M.S. Huang, I.C. Yang, T.C. Lai, J.L. Wang, V.F. Pang, M. Hsiao, M.Y. Kuo, Essential roles of caspases and their upstream regulators in rotenone-induced apoptosis, Biochem. Biophys. Res. Commun. 371 (2008) 33–38.
[8] W.S. Choi, S.E. Kruse, R.D. Palmiter, Z. Xia, Mitochondrial complex I inhibition is not required for dopaminergic neuron death induced by rotenone, MPP+, or paraquat, Proc. Natl Acad. Sci. USA 105 (2008) 15136–15141.
[9] A. Castro, C. Lemos, A. Falcao, A.S. Fernandes, N.L. Glass, A. Videira, Rotenone enhances the antifungal properties of staurosporine, Eukaryot. Cell 9 (2010) 906–914.
[10] H.M. Meisner, L. Sorensen, Metaphase arrest of Chinese hamster cells with rotenone, Exp. Cell Res. 42 (1966) 291–295.
[11] B.R. Brinkley, S.S. Barham, S.C. Barranco, G.M. Fuller, Rotenone inhibition of spindle microtubule assembly in mammalian cells, Exp. Cell Res. 85 (1974) 41–46.
[12] Y. Ren, W. Liu, H. Jiang, Q. Jiang, J. Feng, Selective vulnerability of dopaminergic neurons to microtubule depolymerization, J. Biol. Chem. 280 (2005) 34105–34112.
[13] P. Srivastava, D. Panda, Rotenone inhibits mammalian cell proliferation by inhibiting microtubule assembly through tubulin binding, FEBS J. 274 (2007) 4788–4801.
[14] M.L. Cunningham, M.S. Soliman, M.Z. Badr, H.B. Matthews, Rotenone, an anticarcinogen, inhibits cellular proliferation but not peroxisome proliferation in mouse liver, Cancer Lett. 95 (1995) 93–97.
[15] C. Gerhauser, W. Mar, S.K. Lee, N. Suh, Y. Luo, J. Kosmeder, L. Luyengi, H.H. Fong, A.D. Kinghorn, R.M. Moriarty, et al., Rotenoids mediate potent cancer chemopreventive activity through transcriptional regulation of ornithine decarboxylase, Nat. Med. 1 (1995) 260–266.
[16] S.I. Yoshitani, T. Tanaka, H. Kohno, S. Takashima, Chemoprevention of azoxymethane-induced rat colon carcinogenesis by dietary capsaicin and rotenone, Int. J. Oncol. 19 (2001) 929–939.
[17] T. Tanaka, H. Kohno, K. Sakata, Y. Yamada, Y. Hirose, S. Sugie, H. Mori, Modifying effects of dietary capsaicin and rotenone on 4-nitroquinoline 1-oxide-induced rat tongue carcinogenesis, Carcinogenesis 23 (2002) 1361–1367.
[18] H.A. Saffran, J.M. Pare, J.A. Corcoran, S.K. Weller, J.R. Smiley, Herpes simplex virus eliminates host mitochondrial DNA, EMBO Rep. 8 (2007) 188–193.
[19] M. Kulawiec, K.M. Owens, K.K. Singh, mtDNA G10398A variant in African-American women with breast cancer provides resistance to apoptosis and promotes metastasis in mice, J. Hum. Genet. 54 (2009) 647–654.
[20] G.P. Dimri, X. Lee, G. Basile, M. Acosta, G. Scott, C. Roskelley, E.E. Medrano, M. Linskens, I. Rubelj, O. Pereira-Smith, et al., A biomarker that identifies senescent human cells in culture and in aging skin in vivo, Proc. Natl Acad. Sci. USA 92 (1995) 9363–9367.
[21] T.C. Chou, Theoretical basis, experimental design, and computerized simulation of synergism and antagonism in drug combination studies, Pharmacol. Rev. 58 (2006) 621–681.
[22] J. Campisi, F. d'Adda di Fagagna, Cellular senescence: when bad things happen to good cells, Nat. Rev. Mol. Cell Biol. 8 (2007) 729–740.
[23] N. Dumaz, D.W. Meek, Serine15 phosphorylation stimulates p53 transactivation but does not directly influence interaction with HDM2, EMBO J. 18 (1999) 7002–7010.
[24] G.S. Jimenez, F. Bryntesson, M.I. Torres-Arzayus, A. Priestley, M. Beeche, S. Saito, K. Sakaguchi, E. Appella, P.A. Jeggo, G.E. Taccioli, G.M. Wahl, M. Hubank, DNA-

dependent protein kinase is not required for the p53-dependent response to DNA damage, Nature 400 (1999) 81–83.
[25] J.S. Lanni, T. Jacks, Characterization of the p53-dependent postmitotic checkpoint following spindle disruption, Mol. Cell. Biol. 18 (1998) 1055–1064.
[26] P.R. Andreassen, O.D. Lohez, F.B. Lacroix, R.L. Margolis, Tetraploid state induces p53-dependent arrest of nontransformed mammalian cells in G1, Mol. Biol. Cell 12 (2001) 1315–1328.
[27] A.M. Meireles, A. Preto, A.S. Rocha, A.P. Rebocho, V. Maximo, I. Pereira-Castro, S. Moreira, T. Feijao, T. Botelho, R. Marques, V. Trovisco, L. Cirnes, C. Alves, S. Velho, P. Soares, M. Sobrinho-Simoes, Molecular and genotypic characterization of human thyroid follicular cell carcinoma-derived cell lines, Thyroid 17 (2007) 707–715.
[28] A. Petitjean, E. Mathe, S. Kato, C. Ishioka, S.V. Tavtigian, P. Hainaut, M. Olivier, Impact of mutant p53 functional properties on TP53 mutation patterns and tumor phenotype: lessons from recent developments in the IARC TP53 database, Hum. Mutat. 28 (2007) 622–629.
[29] L. Ottaviano, K.L. Schaefer, M. Gajewski, W. Huckenbeck, S. Baldus, U. Rogel, C. Mackintosh, E. de Alava, O. Myklebost, S.H. Kresse, L.A. Meza-Zepeda, M. Serra, A.M. Cleton-Jansen, P.C. Hogendoorn, H. Buerger, T. Aigner, H.E. Gabbert, C. Poremba, Molecular characterization of commonly used cell lines for bone tumor research: a trans-European EuroBoNet effort, Genes Chromosom. Cancer 49 (2010) 40–51.
[30] J.C. Reed, J.M. Jurgensmeier, S. Matsuyama, Bcl-2 family proteins and mitochondria, Biochim. Biophys. Acta 1366 (1998) 127–137.
[31] R.A. Schultz, S.J. Swoap, L.D. McDaniel, B. Zhang, E.C. Koon, D.J. Garry, K. Li, R.S. Williams, Differential expression of mitochondrial DNA replication factors in mammalian tissues, J. Biol. Chem. 273 (1998) 3447–3451.
[32] D. Hanahan, R.A. Weinberg, The hallmarks of cancer, Cell 100 (2000) 57–70.
[33] Y. Chen, E. McMillan-Ward, J. Kong, S.J. Israels, S.B. Gibson, Mitochondrial electron-transport-chain inhibitors of complexes I and II induce autophagic cell death mediated by reactive oxygen species, J. Cell Sci. 120 (2007) 4155–4166.
[34] M. Kulawiec, V. Ayyasamy, K.K. Singh, p53 regulates mtDNA copy number and mitocheckpoint pathway, J. Carcinog. 8 (2009) 8.
[35] M.A. Lebedeva, J.S. Eaton, G.S. Shadel, Loss of p53 causes mitochondrial DNA depletion and altered mitochondrial reactive oxygen species homeostasis, Biochim. Biophys. Acta 1787 (2009) 328–334.
[36] K. Matsumoto, T. Ohta, Rotenone induces aneuploidy, polyploidy and endoreduplication in cultured Chinese hamster cells, Mutat. Res. 263 (1991) 173–177.
[37] H.O. Lee, J.M. Davidson, R.J. Duronio, Endoreplication: polyploidy with purpose, Genes Dev. 23 (2009) 2461–2477.
[38] K.E. Gascoigne, S.S. Taylor, How do anti-mitotic drugs kill cancer cells? J. Cell Sci. 122 (2009) 2579–2585.
[39] A. Tritarelli, E. Oricchio, M. Ciciarello, R. Mangiacasale, A. Palena, P. Lavia, S. Soddu, E. Cundari, p53 localization at centrosomes during mitosis and postmitotic checkpoint are ATM-dependent and require serine 15 phosphorylation, Mol. Biol. Cell 15 (2004) 3751–3757.
[40] S. Kato, S.Y. Han, W. Liu, K. Otsuka, H. Shibata, R. Kanamaru, C. Ishioka, Understanding the function-structure and function-mutation relationships of p53 tumor suppressor protein by high-resolution missense mutation analysis, Proc. Natl Acad. Sci. USA 100 (2003) 8424–8429.
[41] Y.W. Eom, M.A. Kim, S.S. Park, M.J. Goo, H.J. Kwon, S. Sohn, W.H. Kim, G. Yoon, K.S. Choi, Two distinct modes of cell death induced by doxorubicin: apoptosis and cell death through mitotic catastrophe accompanied by senescence-like phenotype, Oncogene 24 (2005) 4765–4777.
[42] X. Huang, T. Tran, L. Zhang, R. Hatcher, P. Zhang, DNA damage-induced mitotic catastrophe is mediated by the Chk1-dependent mitotic exit DNA damage checkpoint, Proc. Natl Acad. Sci. USA 102 (2005) 1065–1070.
[43] S. Li, A. Szymborski, M.J. Miron, R. Marcellus, O. Binda, J.N. Lavoie, P.E. Branton, The adenovirus E4orf4 protein induces growth arrest and mitotic catastrophe in H1299 human lung carcinoma cells, Oncogene 28 (2009) 390–400.

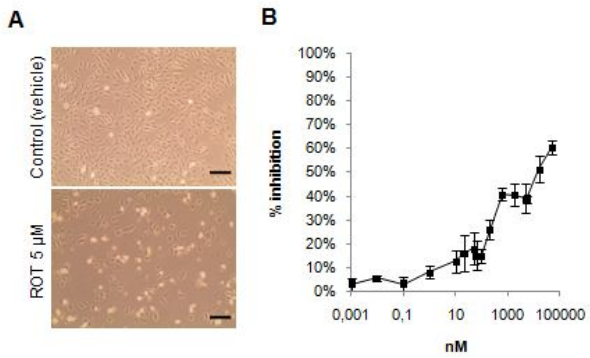

Supplemental Figure 1 – Rotenone inhibits the growth of TPC-1 cells. (A) Phase-contrast micrographs of cells cultured in the absence (upper panel) or in the presence of 5 µM rotenone (ROT, lower panel); scale bar: 100 µm. (B) Growth inhibition was determined by the sulphorhodamine B assay for the indicated concentrations of rotenone. Data is representative of at least three independent experiments. Data shown in (B) represents the mean ± s.e.m.

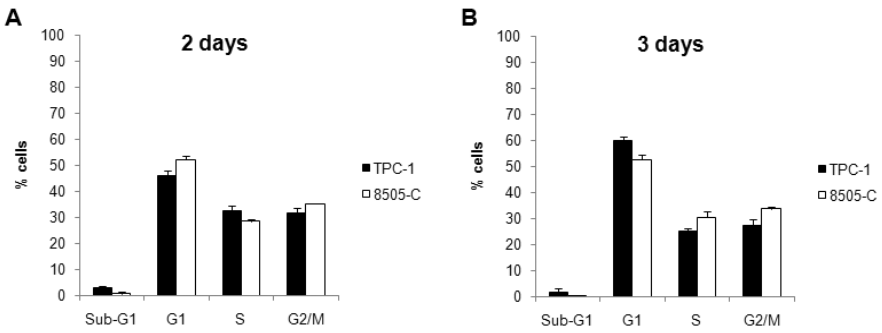

Supplemental Figure 2 – Basal percentages of cells in each phase of the cell cycle of TPC-1 and 8505-C cells. Quantification of the cell cycle analysis by propidium iodide staining of DNA of cells cultured for two (A) or three (B) days. Data is representative of at least three independent experiments. Data shown represents the mean ± s.e.m.

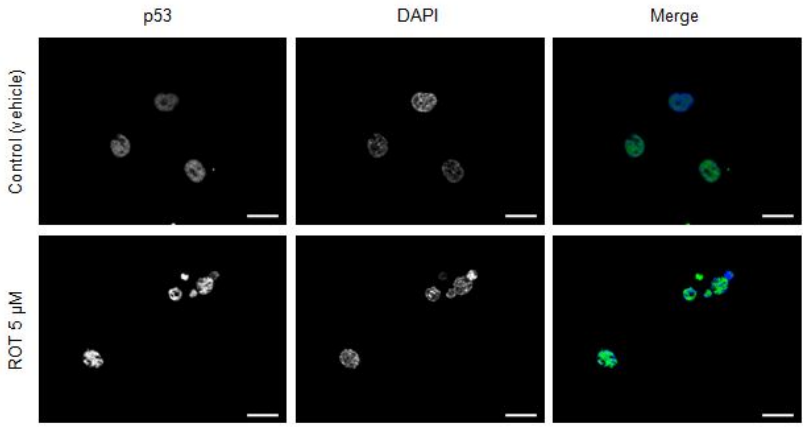

Supplemental Figure 3 – Subcellular localization of p53 in 8505-C cells. Cells treated with rotenone were stained for p53 (left column and green in the right column) and with DAPI for nuclei (middle column and blue in the right column); scale bar: 10 µm. Data is representative of at least three independent experiments.

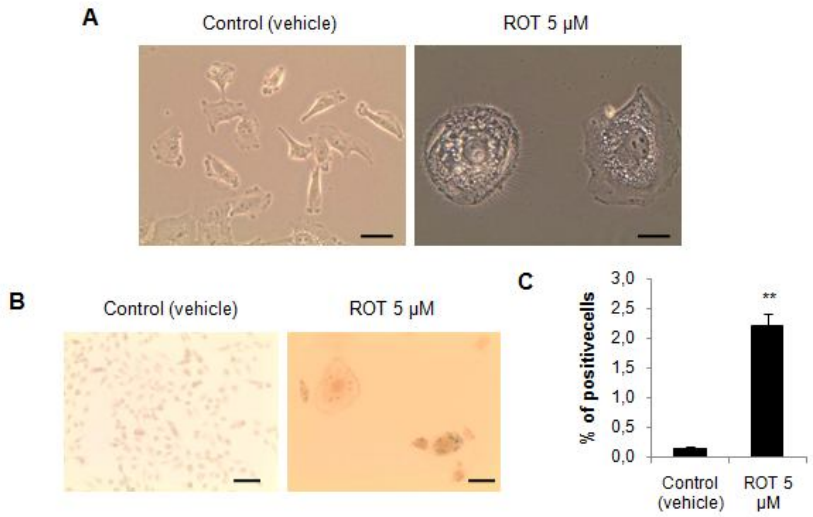

Supplemental Figure 4 - Long rotenone treatments induce lower levels of cellular senescence in 8505-C than in TPC-1 cells. (A) Phase-contrast micrographs of rotenone (ROT)-treated; scale bar: 30 µm. The expression of β-galactosidase was evaluated by staining cells treated with rotenone with X-gal (B; scale bar: 50 µm) and by calculating the ratio of positive cells/total number of cells (C). The cells were exposed to rotenone for 5 days. Data is representative of at least three independent experiments. Data shown in (C) represents the mean ± s.e.m. **, $P < 0.01$.

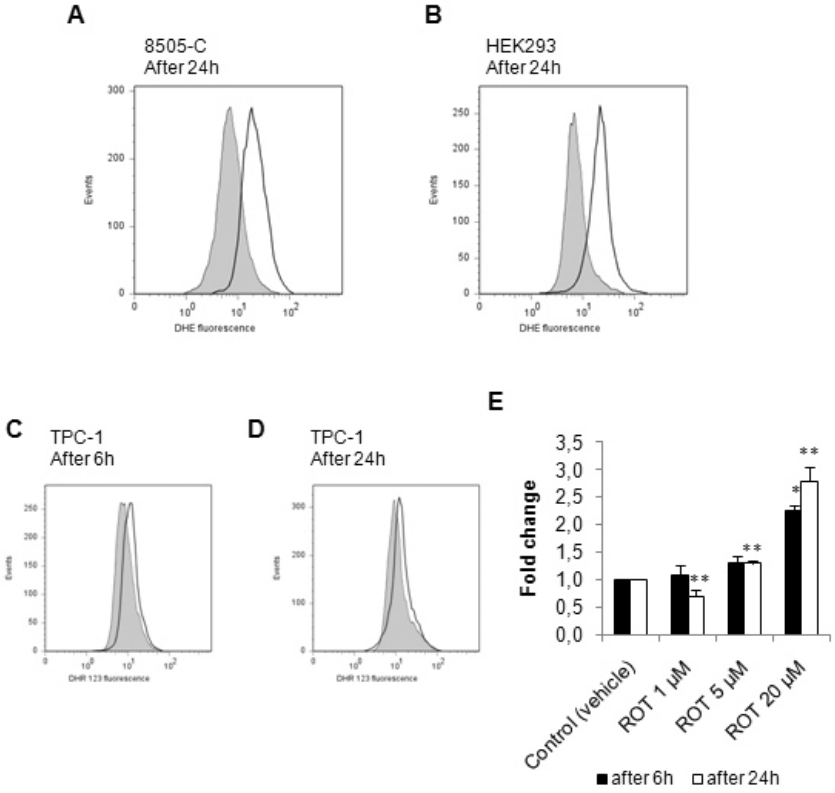

Supplemental Figure 5 – Rotenone stimulates the production of ROS. (A-C) The production of superoxide was measured using dyhydroethidium as a probe; presented are representative flow cytometry histograms of 8505-C (A) and HEK293T (B) cells, respectively, after a 24 hours treatment with rotenone (ROT). (C-E) The production of hydrogen peroxide, peroxinitrite and hypochlorous acid was measured using dihydrorhodamine 123 as a probe; (C) and (D) are representative flow cytometry histograms of TPC-1 cells after treatment with rotenone (ROT) and quantification of the data is presented in (E). In the histograms presented in (A), (B), (C) and (D), the gray areas correspond to control (vehicle) and the white areas represent treatment with 5 µM rotenone. Data is representative of at least three independent experiments. Data shown in (C) represents the mean ± s.e.m. *, $P < 0.05$; **, $P < 0.01$.

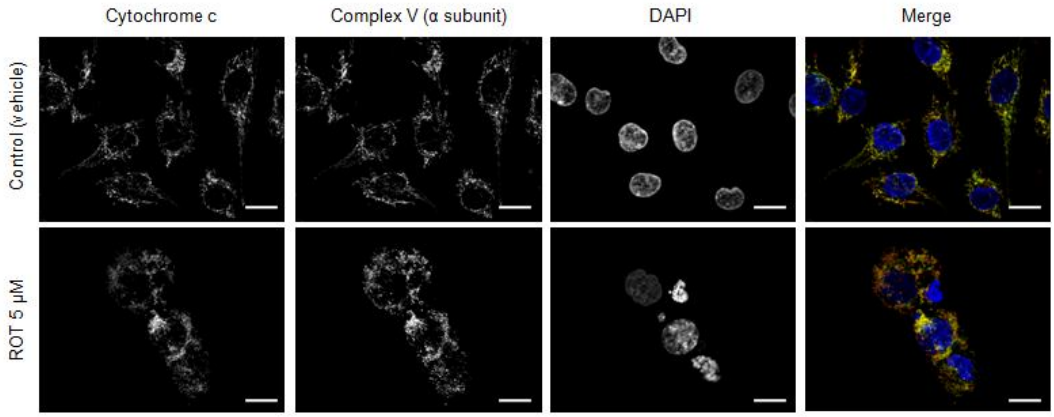

Supplemental Figure 6 – Mitochondrial integrity is maintained after treatment with rotenone. Cells treated with 5 µM rotenone were fixed and stained for cytochrome c (left column and green in the right column), α subunit of complex V (second column and red in the right column) and DAPI (third column and blue in the right column); scale bar: 10 µm. Data is representative of at least three independent experiments.

Synergistic growth inhibition of cancer cells harboring the RET/PTC1 oncogene by staurosporine and rotenone involves enhanced cell death

A. Pedro Gonçalves, Arnaldo Videira, Valdemar Máximo, Paula Soares

Journal of Biosciences (2011) 36(4):639-48

Synergistic growth inhibition of cancer cells harboring the *RET/PTC1* oncogene by staurosporine and rotenone involves enhanced cell death

ANTÓNIO PEDRO GONÇALVES[1,2,*], ARNALDO VIDEIRA[1,2], VALDEMAR MÁXIMO[3,4] and PAULA SOARES[3,4]

[1]*Instituto de Biologia Molecular e Celular, Universidade do Porto, Rua do Campo Alegre 823, 4150-180 Porto, Portugal*

[2]*Instituto de Ciências Biomédicas de Abel Salazar, Universidade do Porto, Largo Prof Abel Salazar 2, 4099-003 Porto, Portugal*

[3]*Instituto de Patologia e Imunologia Molecular, Universidade do Porto, Rua Dr Roberto Frias s/n, 4200-465 Porto, Portugal*

[4]*Faculdade de Medicina, Universidade do Porto, Al Prof Hernâni Monteiro, 4200-319 Porto, Portugal*

**Corresponding author (Fax, +351-226-099157; Email, apgoncalves@ibmc.up.pt)*

TPC-1 is a highly proliferative thyroid papillary carcinoma-derived cell line. These cells express the RET/PTC1 fusion protein, whose isoforms are characterized in this work. The bacterial alkaloid staurosporine and the plant extract rotenone are death-inducing drugs that have an inhibitory synergistic effect on the growth of TPC-1 cells. We show that this synergism is accompanied by an enhancement of the induction of cell death. Staurosporine alone induces cell cycle arrest in G_1, whereas rotenone induces arrest in G_2/M. We suggest that this additive pressure may drive cells to die, resulting in the synergistic interaction of the drug combination. These data emphasize the potential use of the staurosporine plus rotenone combination as an anticancer tool.

[Gonçalves AP, Videira A, Máximo V and Soares P 2011 Synergistic growth inhibition of cancer cells harboring the *RET/PTC1* oncogene by staurosporine and rotenone involves enhanced cell death. *J. Biosci.* **36** 639–648] **DOI** 10.1007/s12038-011-9100-7

1. Introduction

Cancer arises from an anomalous behaviour of cells under different circumstances. Using an oversimplification, it can be stated that carcinogenesis results from an unbalance between cell death and proliferation, and therefore, therapeutic strategies aim to influence these processes. For that reason, stimulation of cell death became one of the main approaches to treat neoplastic diseases (Reed 2006).

Thyroid papillary carcinoma is the most frequent endocrine malignancy (Santoro *et al.* 2004). This type of tumours are molecularly characterized by the presence of chromosomal rearrangements that cause the recombination of the receptor *RET* with other genes, generating the *RET/PTC* oncogenes (Grieco *et al.* 1990; Santoro *et al.* 2004). RET is a receptor comprising extracellular, transmembrane and intracellular domains. In its intracellular part RET holds several docking residues that are responsible for triggering signalling pathways that regulate cell proliferation, migration, differentiation and death (Santoro *et al.* 2004). From these, tyrosine 1062 was shown to be particularly important (Besset *et al.* 2000; Buckwalter *et al.* 2002; Coulpier *et al.* 2002). It is known that alternative splicing of *RET* occurs, leading to three isoforms of the protein differing in the sequence following a C-terminal splice site: RET9, RET43 and RET51 (Myers *et al.* 1995). At least 10 RET/PTC rearrangements were already described, RET/PTC1 and RET/PTC3 being the

Keywords. Cell cycle; cell death; RET/PTC1; rotenone; staurosporine; TPC-1

Supplementary materials pertaining to this article are available on the *Journal of Biosciences* Website at *http://www.ias.ac.in/jbiosci/Sep2011/pp639–648/suppl.pdf*

most frequent ones (Nikiforov 2002). RET/PTC1 involves the fusion of the N-terminal portion of *H4* (a gene also known as *D10S170*) with the C-terminal part of RET (Fusco *et al.* 1987; Grieco *et al.* 1990). Because of the formation of this fusion gene, the tyrosine 1062 of wild-type *RET* corresponds to the tyrosine 451 of the produced protein. The phosphorylation of the tyrosine 451 and concomitant downstream signalling was shown to be required to sustain the mitogenesis of a carcinoma cell line harboring RET/PTC1 (Salvatore *et al.* 2000). In addition, phosphorylation of tyrosine 451 is involved in RET/PTC1-mediated apoptosis (Castellone *et al.* 2003). These data underlines the importance of RET/PTC1 as a regulator of cell fate and survival. The TPC-1 cell line is derived from a thyroid papillary carcinoma and harbors *RET/PTC1* (Meireles *et al.* 2007).

The bacterial alkaloid staurosporine is a well-established cell death inducer. It is classically considered to be a protein kinase C inhibitor, although current evidence shows that it has a broad activity against serine/threonine kinases (Gescher 2000). Its analogue 7-hydroxystaurosporine (UCN-01) is currently being tested in several clinical trials (Perez *et al.* 2006; Sampath *et al.* 2006; Jimeno *et al.* 2008). Rotenone is another cell-death-inducing drug commonly used as a mitochondrial complex I inhibitor. Recent data pointed out that cell death induction by rotenone is independent of complex I inhibition and that the mechanism underlying its toxicity is associated with a cell cycle insult and generation of a mitotic catastrophe-like phenotype (Choi *et al.* 2008; Gonçalves *et al.* 2011).

We have previously shown that staurosporine and rotenone interact synergistically in the inhibition of growth of TPC-1 cells (Gonçalves *et al.* 2011). In this work, we studied the response of this cell line to staurosporine in terms of cell growth and cell cycle. Furthermore, we demonstrate that the synergism between staurosporine and rotenone is associated with an enhanced capacity of inducing cell death. In addition, we show that TPC-1 cells express both the RET9 and RET51 isoforms of RET/PTC1 and are constitutively phosphorylated on tyrosine 451.

2. Materials and methods

2.1 *Cell culture*

TPC-1 cells were maintained at 37°C and 5% CO_2 in RPMI-1640 medium supplemented with 10% fetal bovine serum, 100 U/ml penicillin, 100 µg/ml streptomycin and 1.25 µg/ml amphotericin B (all from Invitrogen, California, USA). XTC.UC1 cells were maintained at 37°C and 5% CO_2 in 1:1 DMEM/Ham's F-12 supplemented with 10% fetal bovine serum, 100 U/ml penicillin, 1.25 µg/ml amphotericin B (all from Invitrogen), 10 µg/ml insulin and 10 mU/ml thyroid-stimulating hormone (both from Sigma-Aldrich, Missouri, USA).

2.2 *Chemicals and antibodies*

For the treatments with chemicals, cells were seeded and left to adhere for approximately 24 h. Afterwards, the medium was replaced by fresh medium supplemented with different concentrations of the desired compound. Staurosporine was purchased from LC Laboratories (Massachusetts, USA) and rotenone from Sigma-Aldrich. The RET (C-19), RET (C-20) and phospho-RET (tyrosine 1062) antibodies were purchased from Santa Cruz Biotechnology (California, USA).

2.3 *Western blotting and immunofluorescence*

Whole lysates of cells were obtained first by incubation with RIPA buffer (50 mM Tris-HCl+1% NP-40+150 mM NaCl +2 mM EDTA, ph 7.5), a protease inhibitor cocktail (Roche Applied Science, Mannheim, Germany) and a phosphatase inhibitor cocktail (Sigma-Aldrich), followed by centrifugation (14000 rpm, 15 min, 4°C) and collection of the supernatant. The lysates were separated by SDS-PAGE and transferred to a nitrocellulose membrane. The membrane was blocked for 1 h using a 5% non-fat dry milk or bovine serum albumin in PBS 0.5%, Tween-20 solution and incubated with the appropriate primary and secondary antibodies. The protein bands were detected by chemiluminescence and X-ray film exposure (GE Healthcare, Chalfont St Giles, UK).

For immunostaining of phospho-RET, cells were fixed and permeabilized, incubated for 1 hour with blocking buffer (5% normal rabbit serum and 0.3% Triton X-100 in PBS), 1 hour with the primary anti-phospho-RET (tyrosine 1062) antibody (1:50 dilution in 10% BSA+0.3% Triton X-100 in PBS), washed (PBS 0.5%, Tween-20 0.05% BSA) and incubated for 1 hour with the secondary rabbit anti-mouse antibody conjugated with fluorescein isothiocyanate (FITC) (Dako, Glostrup, Denmark).

2.4 *Analysis of cell growth*

For the determination of the population doubling time, the number of cells was counted 96 h after seeding using an hemocytometer and the following formula was applied: $r=(3.32\times(\log(n_2)-\log(n_1))/96)\times 24$, where r is the multiplication rate per 24 h, and n_1 and n_2 are the number of cells at the beginning of the experiment and after 96 h, respectively. Then, the population doubling time (PDT), expressed in hours, was obtained by the formula: $PDT=1/r$ (Davis 2001).

For the sulphorhodamine B assay, cells were fixed with 10% trichloroacetic acid, stained with 0.1% sulphorhodamine B (Sigma-Aldrich) and then the plates were read in a microplate reader (Bio-Rad, California, USA) at 560 nm. Triplicate wells per condition were evaluated in each experiment.

For quantification of synergy the combination index (CI) was measured (Chou 2006) using CalcuSyn (Biosoft, Cambridge, UK). When two or more drugs are combined and the CI is calculated, CI<1, =1 and >1 indicates synergism, additive effect and antagonism, respectively.

2.5 *Flow cytometry*

For cell cycle analysis, cells were fixed with ice-cold 70% ethanol for at least 4 h and, after washing with PBS, stained with a solution containing 5 µg/ml propidium iodide (Sigma-Aldrich) and 100 µg/ml RNase A (Fermentas, St Leon-Rot, Germany). For evaluation of the mitochondrial membrane potential ($\Delta\Psi$m), 250 nM CMXRos (Molecular Probes, Oregon, USA) was added to the culture medium for 30 min. Then, cells were detached, washed two times and ressuspended in PBS. The results were analysed using FlowJo (Tree Star, Oregon, USA) and WinMDI 2.9 (The Scripps Research Institute, California, USA). For quantifications of $\Delta\Psi$m, the geometric mean of fluorescence of control- or staurosporine-treated cells was determined in each experiments and the percentage of the control $\Delta\Psi$m was calculated for staurosporine treatments.

2.6 *Statistical analysis*

Statistical analysis of the data was performed using SPSS 13.0 (SPSS Inc., Illinois, USA) by the non-parametric Mann–Whitney test, for comparisons between two groups. *P*-values≤0.05 were considered to be statistical significant.

3. Results

3.1 *Characterization of the isoforms of RET/PTC1 expressed in TPC-1 cells*

TPC-1 cells are derived from a thyroid papillary carcinoma and carry the RET/PTC1 rearrangement (Meireles *et al.* 2007). The TPC-1 cell line presents a fibroblast-like morphology (supplementary figure 1) and has a population doubling time of 21.4 h (figure 1A), meaning a high multiplication rate. For comparison, we also evaluated the thyroid oncocytoma-derived cell line XTC.UC1. XTC.UC1 cells display a population doubling time of 98.4 h (figure 1A). XTC.UC1 cells do not harbor any of the mutations or chromosomal rearrangements that are commonly involved in thyroid carcinogenesis, rather having alterations in mitochondrial DNA and function. This suggests that the oncogenic events in TPC-1 cells (namely the presence of RET/PTC1) have a stronger proliferation effect.

Alternative splicing of *RET* generates three isoforms, which contain 51 (RET51), 43 (RET43) or 9 (RET9) amino acids in the C-terminal tail (Myers *et al.* 1995). RET43 has not yet been characterized. We used antibodies that bind to different isoforms of RET to characterize the TPC-1 cell line, by Western blot. RET51/PTC1 has 520 amino acids and a predicted molecular weight of 64 kDa,

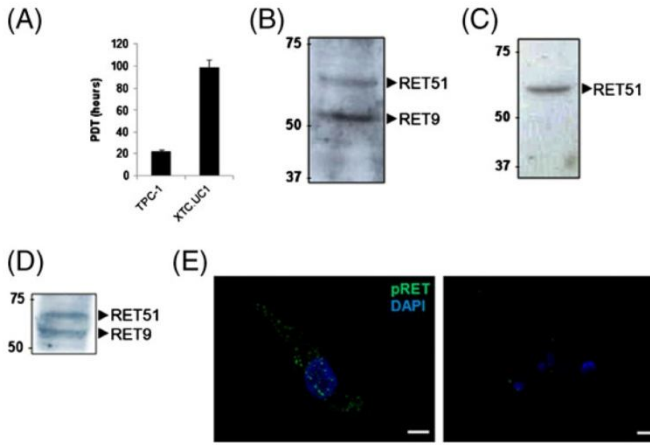

Figure 1. TPC-1 cells possess both the RET9 and RET51 isoforms of RET/PTC1 and are constitutively phosphorylated in tyrosine 451 of the protein. (**A**) The population doubling time of TPC-1 and XTC.UC1 cells was determined after cell counting with an hemocytometer. (**B**–**D**) Whole lysates of TPC-1 cells were immunoblotted using the RET C-19 (**B**), RET C-20 (**C**) and phospho-RET (tyrosine 451; **D**). (**E**) TPC-1 cells were stained for phospho-RET (tyrosine 451) and with DAPI for nuclei (left panel; scale bar: 10 µm); as a negative control, anti-phospho-RET was omitted in the procedure (right panel; scale bar: 31.5 µm).

whereas RET9/PTC1 has 477 amino acids and a predicted molecular weight of 57 kDa. The RET (C-19) antibody binds to RET9 and, to a lesser extent, to RET51, whereas the RET (C-20) antibody detects RET51. Incubation with RET (C-19) detects a strong band above the 50 kDa marker and a less intense band with a higher molecular weight (figure 1B), probably corresponding to RET9/PTC1 and RET51/PTC1, respectively. Incubation with RET (C-20) only detects one band with the predicted molecular weight of RET51/PTC1 (figure 1C). We also observe that unstimulated TPC-1 cells display phosphorylation of the tyrosine 451 (the same as tyrosine 1062 in wild-type RET) of RET/PTC1 (figure 1D–E), which is an important residue for triggering signalling pathways (Buckwalter *et al.* 2002). Previous work from our group (data not shown) and other authors validates the use of these antibodies to distinguish different splicing variants of RET and the phosphorylated form of the protein (either the wild type RET or RET/PTC1) (Oppenheimer *et al.* 2007; Encinas *et al.* 2008). Therefore, TPC-1 cells possess both the RET9 and RET51 isoforms of RET/PTC1 and are constitutively phosphorylated on tyrosine 451.

3.2 *Staurosporine inhibits growth of TPC-1 cells by cell cycle arrest and induction of cell death*

We evaluated the growth of TPC-1 cells exposed for 24 h to staurosporine. Concentrations of staurosporine above ~0.5 nM induced significant cell growth inhibition (figure 2A). Using the CalcuSyn software we calculated the median-effect plot and its parameters (figure 2B). Treatment with staurosporine results in a median-effect dose or IC_{50} of 23.2 nM. This measurement indicates that this drug displays a potent inhibitory effect against TPC-1 cells, taking into account that we obtained, in the same cell line, an IC_{50} of 26 µM and 50 µM for two other death inducers, rotenone (Gonçalves *et al.* 2011a) and sodium orthovanadate (Gonçalves *et al.* 2011b), respectively.

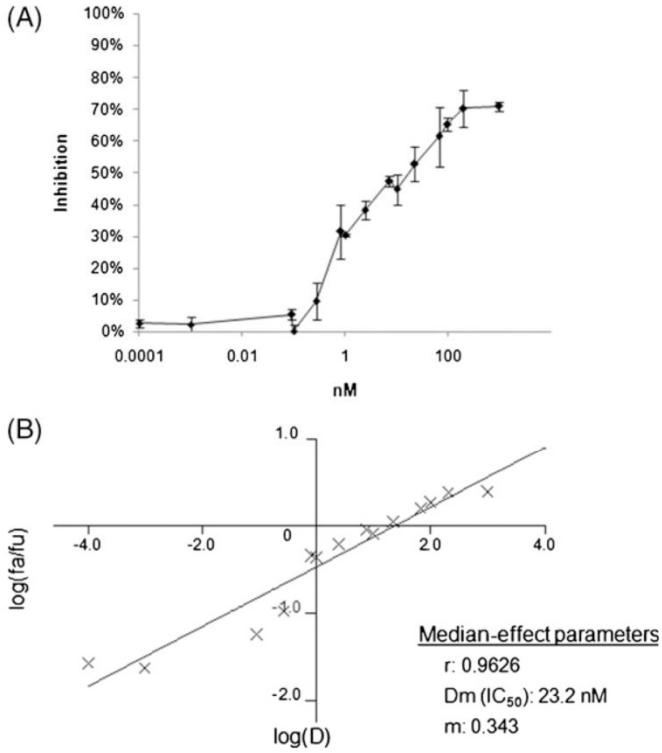

Figure 2. Staurosporine inhibits the growth of TPC-1 cells. (**A**) Growth inhibition was determined by the sulphorhodamine B assay for the indicated concentrations of staurosporine. (**B**) CalcuSyn software was used for obtaining the median-effect plot and its parameters: 'fa/fu' is the ratio between affected and unaffected cell fractions; 'D' is the dose of the drug; 'r' is the linear correlation coefficient of the plot; 'Dm' is median-effect dose and equal to the IC_{50}; 'm' is a measurement of the sigmoidicity of the dose-effect curve. Data is representative of at least three independent experiments. Data shown represents the mean±s.e.m.

We then tested the effects of staurosporine on the cell cycle of TPC-1 cells treated for 24 h. At 0.1 nM staurosporine has no significant consequence on the cell cycle (figure 3A–B), but at 1 nM there is a significant G_1 arrest (G_1 fraction of 64.06% *vs* 48.76% for the control; P=0.039; figure 3A–B) and presence of cells with a sub-G_1 DNA content, indicative of cell death (7.64% *vs* 3.09% for the control; P=0.020; figure 3A–B). At 10 nM staurosporine, these effects are also observed, both the G_1 arrest (68.45% *vs* 48.76% for the control; P=0.020; figure 3A–B) and cell death (18.29% *vs* 3.09% for the control; P=0.020; figure 3A–B). At 100 nM staurosporine, the G_1 arrest is lost and there is a considerable induction of cell death (43.40% *vs* 3.09% for the control; P=0.020; figure 3A–B). We determined the effects of staurosporine in the mitochondrial membrane potential ($\Delta\Psi$m) as another marker of cell death. Staurosporine at 1 nM (84.62% of $\Delta\Psi$m of the control) and 10 nM (61.32% of $\Delta\Psi$m of the control) induces loss of

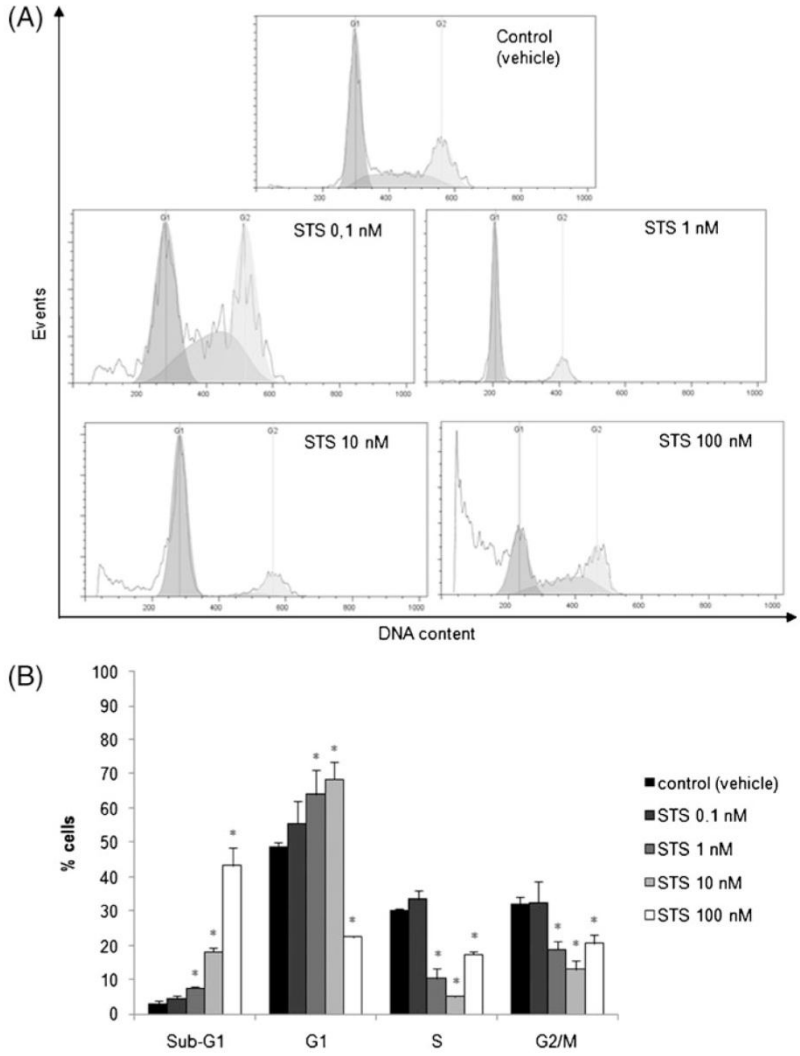

Figure 3. Staurosporine induces a G_1 cell cycle arrest and cell death. (**A**) Representative histograms of the cell cycle analysis by propidium iodide staining of DNA of cells treated for 24 h with the indicated concentrations of staurosporine (STS). Quantification of the data is presented in (**B**). Data is representative of at least three independent experiments. Data shown represents the mean±s.e.m. *, P<0.05.

ΔΨm (figure 4A–B), being statistically significant for 10 nM (P=0.006). These data show that staurosporine causes a dose-dependent effect on the cell cycle of TPC-1 cells that includes induction of cell death and G_1 arrest.

3.3 *The synergistic interaction between staurosporine and rotenone involves an increase in cell death*

We have previously reported that staurosporine and rotenone interact in a synergistic way to inhibit the growth of the filamentous fungus *Neurospora crassa* (Castro *et al.* 2010) and TPC-1 cells (Gonçalves *et al.* 2011). Previously, synergy was accomplished in TPC-1 cells when staurosporine and rotenone were combined in a constant ratio of 1:1000 (staurosporine:rotenone) (Gonçalves *et al.* 2011). This conclusion was based on the calculation of the combination index (CI), according which there is synergy when CI<1 (Chou 2006). We have now applied this calculation to other combination ratios of the two drugs. The combination of staurosporine and rotenone in a constant ratio of 1:333 also leads to a synergistic inhibitory effect (figure 5A), as well as when varying concentrations of staurosporine are combined with an unchanging concentration (50 nM) of rotenone (figure 5B). In both cases, although there are two experimental points with a CI>1, there is a clear tendency for synergy when the drugs are combined (figure 5A–B).

In order to evaluate if the synergistic growth inhibition was due to alterations on the cell cycle and induction of cell death, TPC-1 cells were treated for 24 h with two combinations of staurosporine plus rotenone (0.5 nM+ 500 nM and 10 nM+5 μM). When used alone, 0.5 nM staurosporine induces cell death and G_1 arrest (figure 6A-B). Rotenone at 500 nM concentration induces cell death (15.27% for 500 nM rotenone *vs* 3.09% for the control; P=0.046; figure 6A–B). At 5 μM concentration, besides cell death induction (14.93% *vs* 3.09% for the control; P=0.020; figure 6C–D), there is a notorious G_2/M increase (72.73% *vs* 32.08% for the control; P=0.020; figure 6C–D).

When 500 nM rotenone is added together with 0.5 nM staurosporine, there is a significant increase in the percentage of cell death (6.11% for 0.5 nM staurosporine *vs* 22.19% for the combination; P=0.034; figure 6A–B). Regarding the combination 10 nM staurosporine plus 5 μM rotenone, all phases of the cell cycle were altered in comparison with staurosporine alone (figure 6C–D). Interestingly, the G_1 arrest is diminished (68.45% for 10 nM staurosporine *vs* 19.35% for the combination; P=0.050) and an increase of dead cells is observed (18.29% for 10 nM staurosporine *vs* 40.00% for the combination; P=0.050). The G_2/M arrest caused by rotenone is also diminished (72.73% for 5 μM rotenone *vs* 33.98% for the combination; P=0.050). These results suggest that the synergistic inhibitory effect of the drug combination staurosporine plus rotenone is related to an increase in cell death induction.

4. Discussion

TPC-1 is a thyroid papillary carcinoma-derived cell line that harbors the RET/PTC1 rearrangement (Meireles *et al.* 2007). Because alternative splicing generates different isoforms of *RET* (Myers *et al.* 1995), we sought to study what are the RET/PTC1 isoforms present in these cells, which was unknown. We show that TPC-1 cells express both the RET51/PTC1 and RET9/PTC1 isoforms and also present constitutive phosphorylation of tyrosine 451, which is an important residue for triggering different signalling pathways that control cell fate (Buckwalter *et al.* 2002).

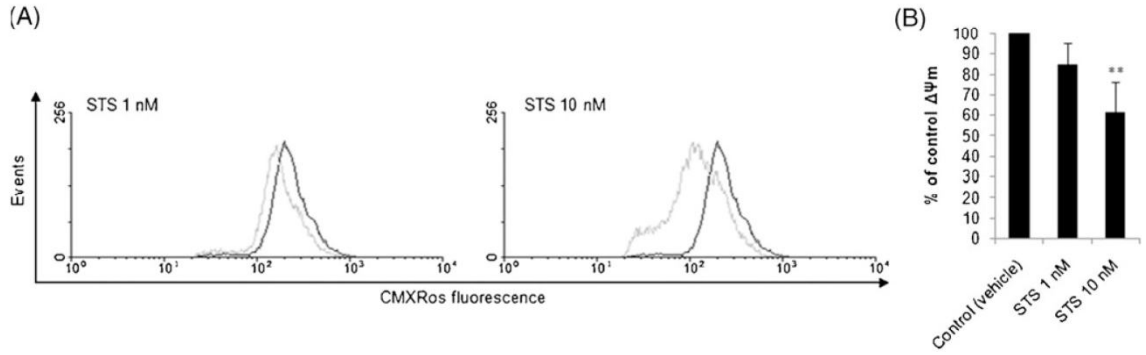

Figure 4. Staurosporine induces loss of mitochondrial membrane potential (ΔΨm). (**A**) Representative histograms of the ΔΨm analysis using CMXRos for the indicated concentrations of staurosporine (STS); the black line corresponds to control (vehicle) and the grey lines represent treatment with staurosporine. Quantification of the data is presented in (**B**). Data is representative of at least three independent experiments. Data shown represents the mean±s.e.m. **, P<0.01.

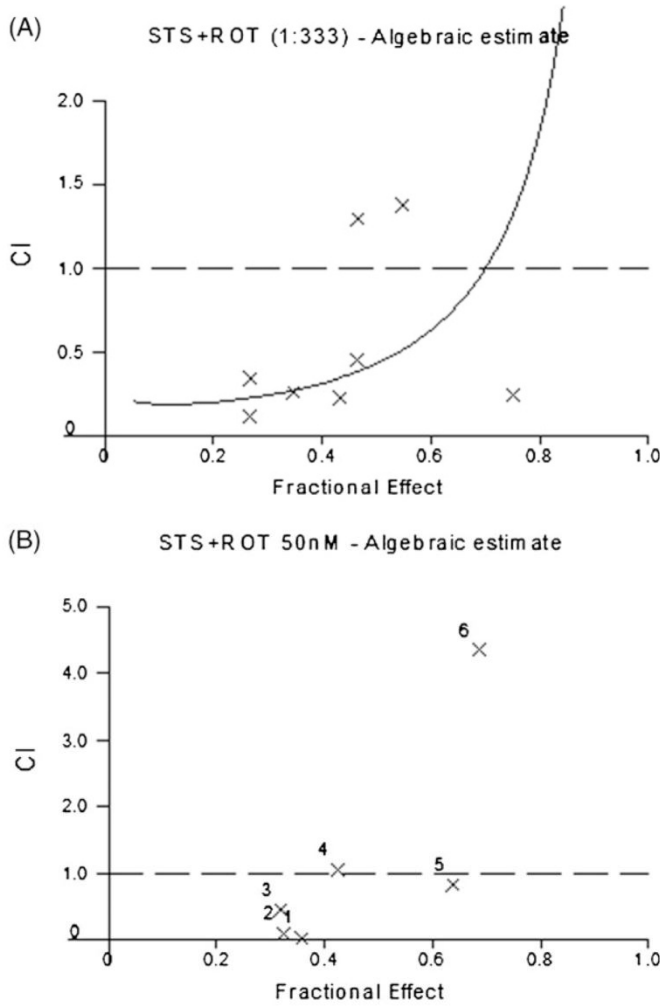

Figure 5. The synergistic interaction of staurosporine and rotenone on the growth of TPC-1 cells occurs when the drugs are combined in different ratios. Growth inhibition was determined by the sulphorhodamine B assay, after 24 h of treatment, for several concentrations of staurosporine (STS), rotenone (ROT) or the combination of both drugs. Synergy was evaluated according to the combination index (CI); the crosses correspond to experimental values and the curve is a trend line. (**A**) represents a constant ratio combination of 1:333 (staurosporine:rotenone) whereas (**B**) represents a non-constant ratio combination in which the concentration of staurosporine is variable and the concentration of rotenone remains unchanged (50 nM). Data is representative of at least three independent experiments.

Staurosporine is a well-known cell death inducer, mainly through the mitochondrial pathway (Bertrand *et al.* 1994; Gescher 2000). Because of its potency to induce apoptosis, it became a very attractive hypothesis to test against cancer cells, and so analogues were synthesized and their usefulness tested in several models (Gescher 2000). From these, UCN-01 provided good results and is currently being tested in clinical trials as an anticancer agent (Perez *et al.* 2006; Sampath *et al.* 2006; Jimeno *et al.* 2008). In the TPC-1 cell line, staurosporine powerfully inhibited cell growth, with an IC_{50} of 23 nM. At low but effective concentrations (1–10 nM), the drug induced a marked G_1 cell cycle arrest, indicating that this is likely the main reason for growth inhibition, as observed in other models (Nishi *et al.* 1998; Orr *et al.* 1998; McGahren-Murray *et al.* 2006). Growth inhibition observed at higher concentrations (100 nM) is caused mainly by the induction of cell death. These results are in line with the finding that the effects of staurosporine

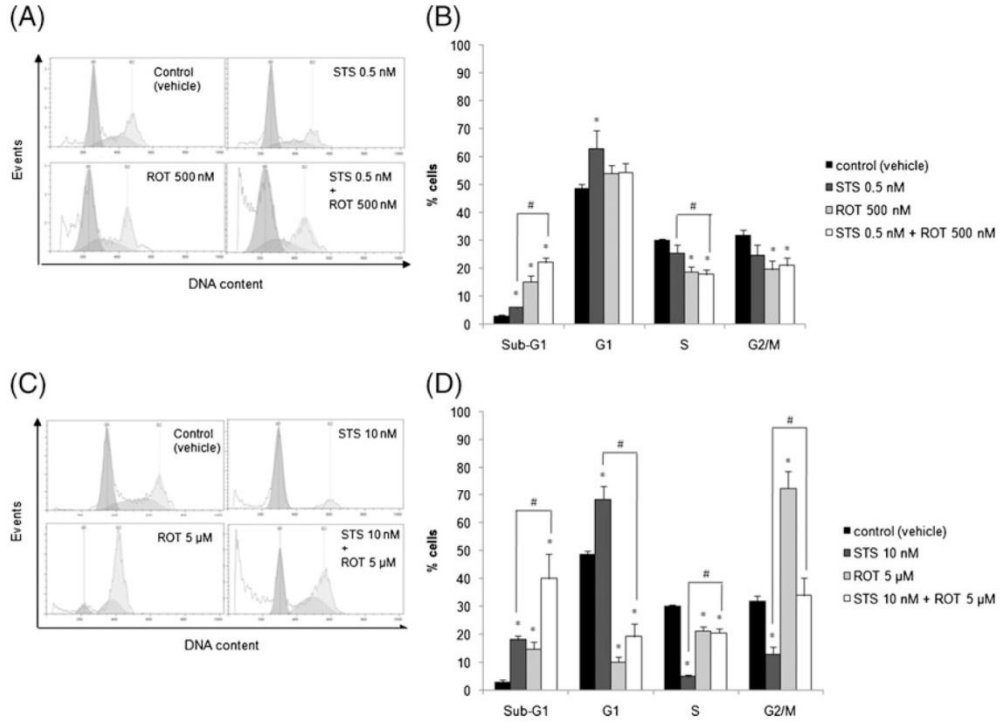

Figure 6. The combination of staurosporine with rotenone results in an enhancement of the induction of cell death. (**A**, **C**) Representative histograms of the cell cycle analysis by propidium iodide staining of DNA of cells treated for 24 h with the indicated concentrations of staurosporine (STS), rotenone (ROT) or the combination of both. Quantification of the data is presented in (**B**, **D**). Data is representative of at least three independent experiments. Data shown represents the mean±s.e.m. *, $P<0.05$ for comparisons between drug-treated samples and the control; #, $P<0.05$ for comparisons between drug-treated samples.

on the cell cycle are dose-dependent (Schnier *et al.* 1996). Further experiments need to be performed, but because RET/PTC1 has a major impact on the survival of these cells, we hypothesize that it may be implicated in the effects of staurosporine and rotenone in TPC-1 cells.

We showed that the cell death inducers staurosporine and rotenone have a synergistic effect on the inhibition of cell growth (Castro *et al.* 2010; Gonçalves *et al.* 2011). In the filamentous fungus *Neurospora crassa* this synergistic interaction is independent of inhibition of mitochondrial complex I by rotenone and probably results from increased glutathione depletion (Castro *et al.* 2010). synergism is not fungal-specific, since it is also observed in TPC-1 cells (Gonçalves *et al.* 2011). When used alone, staurosporine and rotenone induce G_1 and mitotic accumulation (Gonçalves *et al.* 2011), respectively. When the drugs are combined, there is a reduction of the percentage of cells in each of these phases when compared with the drugs alone, but there is a significant increase in the fraction of dead cells. Thus, we hypothesize that the combination of both causes a double pressure that may lead to cell death enhancement. The complementary cell cycle arrests caused by staurosporine and rotenone may be behind the synergism. This conclusion is supported by other drug combination studies where compounds with different consequences on the cell cycle profile have a synergistic anti-tumoural activity (Nehme *et al.* 2001; Lambert *et al.* 2008; Sei *et al.* 2009).

Anticancer therapy with drug combinations provides several advantages. First of all, drug combinations offer the possibility of affecting different targets or subpopulations of cells, as exemplified in this study with two drugs that arrest cells in different phases of the cell cycle. In addition, synergistic combinations can increase the therapeutic efficacy and allow the decrease of drug concentrations, potentially avoiding problems with high doses-associated collateral toxicity (Chou 2006). We provide more *in vitro* data towards the comprehension of the potential of combining staurosporine and rotenone as an anticancer tool. *In vivo* studies are needed to substantiate this possibility.

Acknowledgements

We thank Vitor Trovisco. APG was recipient of a fellowship from Fundação Calouste Gulbenkian (reference 104210). IBMC and IPATIMUP are Associated Laboratories of the Portuguese Ministry of Science, Technology and Higher Education, and is partially supported by from the Portuguese Foundation for Science and Technology.

References

Bertrand R, Solary E, O'Connor P, Kohn KW and Pommier Y 1994 Induction of a common pathway of apoptosis by staurosporine. *Exp. Cell Res.* **211** 314–321

Besset V, Scott RP and Ibanez CF 2000 Signaling complexes and protein-protein interactions involved in the activation of the Ras and phosphatidylinositol 3-kinase pathways by the c-Ret receptor tyrosine kinase. *J. Biol. Chem.* **275** 39159–39166

Buckwalter TL, Venkateswaran A, Lavender M, La Perle KM, Cho JY, Robinson ML and Jhiang SM 2002 The roles of phosphotyrosines-294, -404, and −451 in RET/PTC1-induced thyroid tumor formation. *Oncogene* **21** 8166–8172

Castellone MD, Cirafici AM, De Vita G, De Falco V, Malorni L, Tallini G, Fagin JA, Fusco A, *et al.* 2003 Ras-mediated apoptosis of PC CL 3 rat thyroid cells induced by RET/PTC oncogenes. *Oncogene* **22** 246–255

Castro A, Lemos C, Falcao A, Fernandes AS, Glass NL and Videira A 2010 Rotenone enhances the antifungal properties of staurosporine. *Eukaryot. Cell* **9** 906–914

Choi WS, Kruse SE, Palmiter RD and Xia Z 2008 Mitochondrial complex I inhibition is not required for dopaminergic neuron death induced by rotenone, MPP+, or paraquat. *Proc. Natl. Acad. Sci. USA* **105** 15136–15141

Chou TC 2006 Theoretical basis, experimental design, and computerized simulation of synergism and antagonism in drug combination studies. *Pharmacol. Rev.* **58** 621–681

Coulpier M, Anders J and Ibanez CF 2002 Coordinated activation of autophosphorylation sites in the RET receptor tyrosine kinase: importance of tyrosine 1062 for GDNF mediated neuronal differentiation and survival. *J. Biol. Chem.* **277** 1991–1999

Davis JM 2001 B*asic cell culture: A practical approach* (Oxford: Oxford University Press)

Encinas M, Rozen EJ, Dolcet X, Jain S, Comella JX, Milbrandt J and Johnson EM Jr. 2008 Analysis of Ret knockin mice reveals a critical role for IKKs, but not PI 3-K, in neurotrophic factor-induced survival of sympathetic neurons. *Cell Death Differ.* **15** 1510–1521

Fusco A, Grieco M, Santoro M, Berlingieri MT, Pilotti S, Pierotti MA, Della Porta G and Vecchio G 1987 A new oncogene in human thyroid papillary carcinomas and their lymph-nodal metastases. *Nature (London)* **328** 170–172

Gescher A 2000 Staurosporine analogues - pharmacological toys or useful antitumour agents? *Crit. Rev. Oncol. Hematol.* **34** 127–135

Gonçalves AP, Máximo V, Lima J, Singh KK, Soares P and Videira A 2011a Involvement of p53 in cell death following cell cycle arrest and mitotic catastrophe induced by rotenone. *Biochim. Biophys. Acta* **1813** 492–499

Gonçalves AP, Videira A, Soares P and Máximo V 2011b Orthovanadate-induced cell death in RET/PTC1-harboring cancer cells involves the activation of caspases and altered signaling through PI3K/Akt/mTOR. *Life Sci.* doi:10.1016/j.lfs.2011.07.004

Grieco M, Santoro M, Berlingieri MT, Melillo RM, Donghi R, Bongarzone I, Pierotti MA, Della Porta G, *et al.* 1990 PTC is a novel rearranged form of the ret proto-oncogene and is frequently detected *in vivo* in human thyroid papillary carcinomas. *Cell* **60** 557–563

Jimeno A, Rudek MA, Purcell T, Laheru DA, Messersmith WA, Dancey J, Carducci MA, Baker SD, *et al.* 2008 Phase I and pharmacokinetic study of UCN-01 in combination with irinotecan in patients with solid tumors. *Cancer Chemother. Pharmacol.* **61** 423–433

Lambert LA, Qiao N, Hunt KK, Lambert DH, Mills GB, Meijer L and Keyomarsi K 2008 Autophagy: a novel mechanism of synergistic cytotoxicity between doxorubicin and roscovitine in a sarcoma model. *Cancer Res.* **68** 7966–7974

McGahren-Murray M, Terry NH and Keyomarsi K 2006 The differential staurosporine-mediated G1 arrest in normal *versus* tumor cells is dependent on the retinoblastoma protein. *Cancer Res.* **66** 9744–9753

Meireles AM, Preto A, Rocha AS, Rebocho AP, Maximo V, Pereira-Castro I, Moreira S, Feijao T, *et al.* 2007 Molecular and genotypic characterization of human thyroid follicular cell carcinoma-derived cell lines. *Thyroid* **17** 707–715

Myers SM, Eng C, Ponder BA and Mulligan LM 1995 Characterization of RET proto-oncogene 3' splicing variants and polyadenylation sites: a novel C-terminus for RET. *Oncogene* **11** 2039–2045

Nehme A, Varadarajan P, Sellakumar G, Gerhold M, Niedner H, Zhang Q, Lin X and Christen RD 2001 Modulation of docetaxel-induced apoptosis and cell cycle arrest by all-trans retinoic acid in prostate cancer cells. *Br. J. Cancer* **84** 1571–1576

Nikiforov YE 2002 RET/PTC rearrangement in thyroid tumors. *Endocr. Pathol.* **13** 3–16

Nishi K, Schnier JB and Bradbury EM 1998 The accumulation of cyclin-dependent kinase inhibitor p27kip1 is a primary response to staurosporine and independent of G1 cell cycle arrest. *Exp. Cell Res.* **243** 222–231

Oppenheimer O, Cheung NK and Gerald WL 2007 The RET oncogene is a critical component of transcriptional programs associated with retinoic acid-induced differentiation in neuroblastoma. *Mol. Cancer Ther.* **6** 1300–1309

Orr MS, Reinhold W, Yu L, Schreiber-Agus N and O'Connor PM 1998 An important role for the retinoblastoma protein in staurosporine-induced G1 arrest in murine embryonic fibroblasts. *J. Biol. Chem.* **273** 3803–3807

Perez RP, Lewis LD, Beelen AP, Olszanski AJ, Johnston N, Rhodes CH, Beaulieu B, Ernstoff MS, *et al.* 2006 Modulation of cell cycle progression in human tumors: a pharmacokinetic and tumor molecular pharmacodynamic study of cisplatin plus the Chk1 inhibitor UCN-01 (NSC 638850). *Clin. Cancer Re.s* **12** 7079–7085

Reed JC 2006 Drug insight: cancer therapy strategies based on restoration of endogenous cell death mechanisms. *Nat. Clin. Pract. Oncol.* **3** 388–398

Salvatore D, Barone MV, Salvatore G, Melillo RM, Chiappetta G, Mineo A, Fenzi G, Vecchio G *et al.* 2000 Tyrosines 1015 and 1062 are *in vivo* autophosphorylation sites in ret and ret-derived oncoproteins. *J. Clin. Endocrinol. Metab.* **85** 3898–3907

Sampath D, Cortes J, Estrov Z, Du M, Shi Z, Andreeff M, Gandhi V and Plunkett W 2006 Pharmacodynamics of cytarabine alone and in combination with 7-hydroxystaurosporine (UCN-01) in AML blasts *in vitro* and during a clinical trial. *Blood* **107** 2517–2524

Santoro M, Carlomagno F, Melillo RM and Fusco A 2004 Dysfunction of the RET receptor in human cancer. *Cell Mol. Life Sci.* **61** 2954–2964

Schnier JB, Nishi K, Goodrich DW and Bradbury EM 1996 G1 arrest and down-regulation of cyclin E/cyclin-dependent kinase 2 by the protein kinase inhibitor staurosporine are dependent on the retinoblastoma protein in the bladder carcinoma cell line 5637. *Proc. Natl. Acad. Sci. USA* **93** 5941–5946

Sei S, Mussio JK, Yang QE, Nagashima K, Parchment RE, Coffey MC, Shoemaker RH and Tomaszewski JE 2009 Synergistic antitumor activity of oncolytic reovirus and chemotherapeutic agents in non-small cell lung cancer cells. *Mol. Cancer* **8** 47

MS received 10 February 2011; accepted 30 May 2011

*e*Publication: 16 August 2011

Corresponding editor: RITA MULHERKAR

Synergistic growth inhibition of cancer cells harboring the *RET/PTC1* oncogene by staurosporine and rotenone involves enhanced cell death

António Pedro Gonçalves, Arnaldo Videira, Valdemar Máximo and Paula Soares

J. Biosci. 36(4), September 2011, 639-648, © Indian Academy of Sciences

Supplementary material

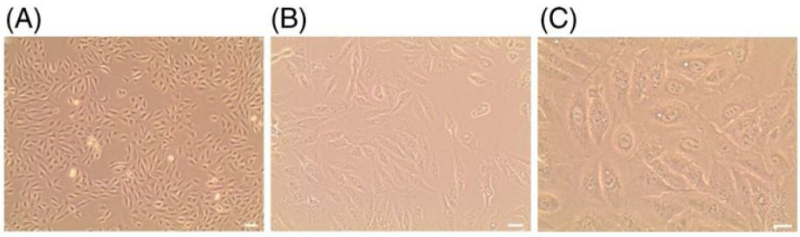

Supplemental figure 1. TPC-1 cells display a fibroblast-like morphology. Phase-contrast micrographs of TPC-1 cells; scale bars: 100μm (**A**), 50μm (**B**) and 30μm (**C**).

Orthovanadate-induced cell death in RET/PTC1-harboring cancer cells involves the activation of caspases and altered signaling through PI3K/Akt/mTOR

A. Pedro Gonçalves, Arnaldo Videira, Paula Soares, Valdemar Máximo

Life Sciences (2011) 89(11-12):371-7

Life Sciences 89 (2011) 371–377

Contents lists available at ScienceDirect

Life Sciences

journal homepage: www.elsevier.com/locate/lifescie

Orthovanadate-induced cell death in RET/PTC1-harboring cancer cells involves the activation of caspases and altered signaling through PI3K/Akt/mTOR

António Pedro Gonçalves [a,b], Arnaldo Videira [a,b], Paula Soares [c,d,*], Valdemar Máximo [c,d]

[a] IBMC—Instituto de Biologia Molecular e Celular, Universidade do Porto, Rua do Campo Alegre 823, 4150-180 Porto, Portugal
[b] ICBAS—Instituto de Ciências Biomédicas de Abel Salazar, Universidade do Porto, Largo Prof. Abel Salazar 2, 4099-003 Porto, Portugal
[c] IPATIMUP—Instituto de Patologia e Imunologia Molecular, Universidade do Porto, Rua Dr. Roberto Frias s/n, 4200-465 Porto, Portugal
[d] Faculdade de Medicina, Universidade do Porto, Al. Prof. Hernâni Monteiro, 4200-319 Porto, Portugal

ARTICLE INFO

Article history:
Received 13 March 2011
Accepted 6 July 2011

Keywords:
Apoptosis
PI3K/Akt/mTOR signaling pathway
RET/PTC1
Orthovanadate
Vanadium

ABSTRACT

Aims: Oncogenic *RET/PTC1* chromosomal rearrangements are hallmarks of thyroid papillary carcinoma. The resulting protein, mainly through tyrosine 451, is responsible for the activation of pathways controlling cell survival, including the PI3K/Akt/mTOR cascade. Vanadium compounds were shown to have anti-neoplastic potential. However, reports about their mechanism of action are contradictory, particularly in what concerns the signaling mediators that are involved. Here, the aim was to characterize the effects of orthovanadate in thyroid cancer cells harboring *RET/PTC1*.

Main methods: Growth behavior of orthovanadate-treated cells was evaluated by the sulphorhodamine B assay, cell cycle analysis and Terminal Transferase dUTP Nick End Labeling (TUNEL). Mitochondrial parameters such as the transmembrane potential and production of reactive oxygen species (ROS) were also assessed. Western blot was used to study cellular signaling.

Key findings: Low doses of the compound induce a pro-proliferative response. In contrast, treatment with inhibitory concentrations of orthovanadate results in increased phosphorylation of tyrosine 451 of RET/PTC1 and activation of the mTOR/S6R branch of the PI3K/Akt signaling pathway. These concentrations of the drug also induce typical features of apoptosis including DNA fragmentation, loss of mitochondrial membrane potential, production of ROS and activation of caspase-3. Addition of the glial cell line-derived neutrophic factor, a pro-survival stimulator that acts through RET, could not completely block orthovanadate-induced growth inhibition and cell death.

Significance: In this model, orthovanadate induces caspase-dependent apoptosis and interferes with the PI3K/Akt/mTOR cascade. This work provides characterization of the effects of orthovanadate and underlines the possibility of its usefulness as a cell death modulator.

Introduction

Although relatively uncommon in comparison with other types of neoplasias, the incidence of thyroid cancer has been increasing very quickly in the last years and it is more common in women but more aggressive in men (Nucera et al., 2009). In fact, thyroid papillary carcinoma is the most common endocrine malignancy (Nucera et al., 2009). Some hallmark genetic features are found during the tumorigenic process of the disease. One of them is a point mutation in the exon 15 of *BRAF* ($BRAF^{V600E}$), which is particularly present in aggressive subtypes (Trovisco et al., 2006; Xing, 2007; Nucera et al., 2010). Another genetic hallmarkis chromosomal rearrangements involving the proto-oncogene *RET* (REarranged during Transfection), which encodes a receptor tyrosine kinase (Santoro et al., 2004). *RET/PTC1* involves the fusion of the *RET* C-terminal region containing the tyrosine kinase domain with the N-terminal region of *H4* (Fusco et al., 1987; Grieco et al., 1990; Pierotti et al., 1992). The RET/PTC1 protein has been shown to be constitutively activated in the cytoplasm and able to induce a transformed phenotype (Ishizaka et al., 1992; Lanzi et al., 1992; Santoro et al., 1993).

Ligand binding to RET triggers receptor dimerization, autophosphorylation of tyrosine residues within its intracellular domain and activation of downstream signaling (Santoro et al., 2004; Plaza-Menacho et al., 2006). The tyrosine 1062 residue (Y1062) is a multidocking site for several adaptor and effector proteins and has been shown to be crucial for RET-mediated signaling, including the phosphatidylinositol 3-kinase (PI3K)/Akt/mammalian target of

* Corresponding author at: IPATIMUP, Cancer Biology; Rua Dr. Roberto Frias, s/n; 4200-465 Porto, Portugal. Tel.: +351 225570700; fax: +351 225570799.
E-mail address: psoares@ipatimup.pt (P. Soares).

0024-3205/$ – see front matter © 2011 Elsevier Inc. All rights reserved.
doi:10.1016/j.lfs.2011.07.004

rapamycin (mTOR) pathway (Besset et al., 2000; Hayashi et al., 2000; Melillo et al., 2001). The PI3K/Akt signaling cascade has a crucial role in the control of cell survival, metabolism and motility and inappropriate signals through this pathway occur frequently in cancer (Courtney et al., 2010). In multiple endocrine neoplasia type 2A, phosphorylation of RET Y1062 is necessary for the activation of PI3K and promotion of cell survival depends on the PI3K/Akt pathway (De Vita et al., 2000; Segouffin-Cariou and Billaud, 2000). In RET/PTC1, signaling mediated by Y451 (corresponding to Y1062 in the wild type protein) is not essential for tumor formation, although it was significantly reduced in transgenic mice when this tyrosine was substituted (Buckwalter et al., 2002). Also, Y451-mediated signaling together with Met activation promote invasiveness (Cassinelli et al., 2009). RET/PTC1 signaling is required to maintain the mitogenesis of a human carcinoma cell line expressing RET/PTC1 (Salvatore et al., 2000). Importantly, a recent work pointed out that the presence of RET/PTC1 confers more sensitivity to cells when they are exposed to inhibitors of components of the PI3K/Akt/mTOR pathway (Liu et al., 2009).

The cleavage of RET by caspases (namely caspase-3) exposes a pro-apoptotic domain, leading to cell death (Bordeaux et al., 2000), directly implicating RET in apoptosis. RET-induced apoptosis, in the absence of its ligand, the glial cell line-derived neutrophic factor (GDNF), is associated with the formation of a complex consisting of the cytoplasmic portion of RET, caspase-3 and protein kinase C δ and this complex is disrupted in the presence of the ligand through the activation of Akt (Canibano et al., 2007). It is not known if the RET/PTC1 rearranged form presents this feature of RET. However, the expression of *RET/PTC1* in wild type *RET* thyroid cells resulted in Y451-mediated apoptosis (Castellone et al., 2003).

Vanadium is a transition metal that belongs to the group of micronutrients essential for a normal metabolism. Vanadium compounds are protein tyrosine phosphatase inhibitors (Evangelou, 2002). These compounds have a promising potential to be used as anti-neoplastic agents since they are able to reduce proliferation and tumor incidence, induce cell death, inhibit invasion and metastasis and overcome the drug resistance of cancer cells (Evangelou, 2002). Notably, in some models, vanadium compounds were also shown to inhibit apoptosis (Morita et al., 2006; Ohi et al., 2006; Kang et al., 2007).

In this work we show that the vanadium compound sodium orthovanadate induces cell death with activation of caspases in thyroid cancer cells harboring *RET/PTC1*. It also induces alterations in the PI3K/Akt/mTOR signaling pathway. The phosphorylation of the important tyrosine 451 of RET/PTC1 is increased in response to the drug.

Materials and methods

Cell culture, reagents and antibodies

Papillary thyroid carcinoma-derived TPC-1 cells (for a detailed characterization please check references (Meireles et al., 2007; Ribeiro et al., 2008; Gonçalves et al., in press) were maintained at 37 °C and 5% CO_2 in RPMI-1640 medium supplemented with 10% fetal bovine serum, 100 U/ml penicillin, 100 μg/ml streptomycin and 1.25 μg/ml amphotericin B (all from Invitrogen, California, USA). For the treatments with chemicals, cells were seeded and left to adhere for approximately 24 h. Afterwards, the medium was replaced by fresh medium supplemented with the desired concentrations of the compound. The following compounds were used for treatments: sodium orthovanadate and GDNF from Sigma-Aldrich (Missouri, USA), Z-VAD-FMK from Calbiochem (New Jersey, USA) and staurosporine from LC Laboratories (Massachusetts, USA).

The following antibodies were employed: phospho-Tyr, phospho-RET (Tyr 1062), RET (C-19), PI3K (p110α), p27 and actin were from Santa Cruz Biotechnology (California, USA); PTEN, Akt, phospho-Akt (Ser 473 and Thr 308), mTOR, phospho-mTOR (Ser 2448), S6R, phospho-S6R (Ser 235/236) and cleaved caspase-3 (Asp 175) were from Cell Signaling Techonology (Massachusetts, USA); cyclin D1 was from Lab Vision (California, USA); p21 was from Calbiochem. Phase-contrast micrographs of cells were taken using a CKX41 (Olympus, New York, USA) inverted microscope.

Analysis of cell growth and cell death

For the sulphorhodamine B assay, cells were fixed with 10% trichloroacetic acid, stained with 0.1% sulphorhodamine B (Sigma-Aldrich) and then the plates were read in a microplate reader (Bio-Rad, California, USA) at 560 nm. Triplicate wells per condition were evaluated in each experiment.

For cell cycle analysis, cells were fixed with ice-cold 70% ethanol for at least 4 h and, after washing with PBS, stained with a solution containing 5 μg/ml propidium iodide (Sigma-Aldrich) and 100 μg/ml RNase A (Fermentas, St. Leon-Rot, Germany). For the detection of cell death by the Terminal Transferase dUTP Nick End Labeling (TUNEL) assay, cells were fixed with 4% paraformaldehyde, washed with PBS, permeabilized with 0.1% Triton X-100 in 0.1% sodium citrate and incubated with a staining solution prepared from the In Situ Cell Death Detection Kit, Fluorescein (Roche Applied Science, Mannheim, Germany). For both methods, flow cytometry was performed in an Epics XL-MCL (Beckman-Coulter, California, USA) and the results analyzed using FlowJo software (Tree Star, Oregon, USA).

For the determination of the multiplication rate per 24 h (r), the number of cells was counted 96 h after seeding using a hemocytometer and the following formula was applied: $r = (3.32\ (\mathrm{LOG}(n_2) - \mathrm{LOG}(n_1))/96)\ 24$, where n_1 and n_2 are the number of cells at the beginning of the experiment and after 96 h, respectively (Davis, 2001).

Western blotting

Whole lysates were obtained by cell lysis followed by centrifugation as previously described (Gonçalves et al., 2011). The lysates were separated by SDS-PAGE and transferred to a nitrocellulose membrane. The membrane was blocked for 1 h using a 5% non-fat dry milk or bovine serum albumin in PBS-0.5% Tween-20 solution and incubated with the appropriate primary and secondary antibodies. The protein bands were detected by chemiluminescence and X-ray film exposure.

Immunofluorescence

For the bromodeoxyuridine (BrdU) proliferation assay, after 1 h of exposition to 10 μM BrdU (Sigma-Aldrich) in the culture medium, cells were fixed with 4% paraformaldehyde, washed with PBS-0.5% Tween 20 and incubated with 2 M HCl for DNA denaturation. Cells were then incubated 1 h with the primary anti-BrdU antibody (Dako, Glostrup, Denmark; 1:10 dilution in 1% BSA + 0.01% Triton X-100 in PBS), washed, 1 h with the secondary anti-mouse antibody conjugated with FITC (Dako) and analyzed by fluorescence microscopy.

Analysis of mitochondrial parameters

For evaluation of the mitochondrial membrane potential ($\Delta\Psi m$) or the production of reactive oxygen species (ROS), 250 nM CMXRos (Molecular Probes, Oregon, USA) or 10 μM dihydrorhodamine 123 (DHR123; Sigma-Aldrich), respectively, were added to the culture medium for 30 min. Then, cells were detached, washed two times and resuspended in PBS. Samples were analyzed by flow cytometry, as above.

Statistical analysis

Statistical analysis of the data was performed using SPSS 13.0 (SPSS Inc., Illinois, USA) by the non-parametric Mann–Whitney test,

for comparisons between two groups. *P*-values ≤0.05 were considered to be statistically significant.

Results

The effects of sodium orthovanadate in the growth of TPC-1 cells

Sodium orthovanadate exhibits a dual-effect on the growth of TPC-1 cells, since it causes a little stimulation of proliferation at small doses and inhibits cell growth at higher concentrations, resulting in a median-effect dose of the drug or IC_{50} of about 50 μM (Fig. 1A). The pro-proliferative effect of the compound at low concentrations involves an increase in the number of proliferating cells (Fig. 1B) and in the multiplication rate (Fig. 1C). TPC-1 cells treated with pro-proliferative doses of the drug present a cell cycle profile similar to the control (data not shown). We decided to focus the work in the inhibitory effects of sodium orthovanadate. The shape of the cells is altered by 10 μM sodium orthovanadate, since they became more narrow and elongated (Fig. 2A). At the cell cycle level, treatment with 10 μM sodium orthovanadate leads to the presence of cells with hypodiploid or sub-G1 content, indicating cell death (22.21% for 10 μM sodium orthovanadate vs 2.86% for the control; $P=0.011$) and to a reduction in the percentage of cells in the G_1 phase (31.51% for 10 μM sodium orthovanadate vs 46.08% for the control; $P=0.011$; Fig. 2B,C). Analysis of the expression of proteins that regulate the progression through the cell cycle upon treatment with sodium orthovanadate revealed that the drug decreases the expression of cyclin D1 and increases the expression of p21, whereas p27 remains unaltered (Fig. 2D).

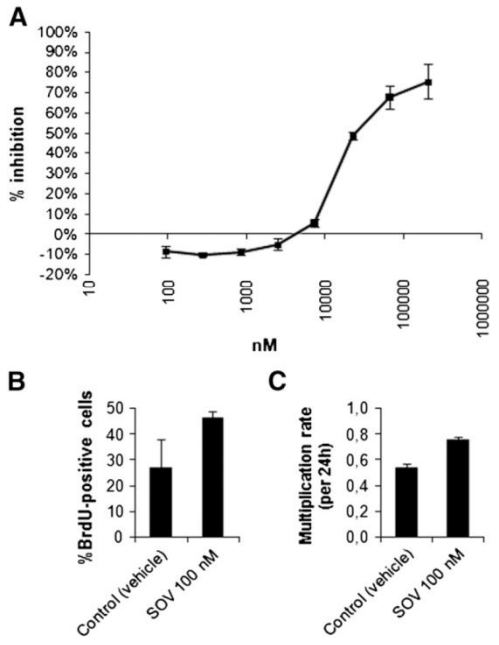

Fig. 1. Sodium orthovanadate elicits a dual effect in the growth of TPC-1 cells. (A) Growth inhibition was determined by the sulphorhodamine B assay for the indicated concentrations of sodium orthovanadate. (B) The BrdU assay was performed in 100 nM sodium orthovanadate-treated cells and the ratio of positive nuclei versus the total number of nuclei calculated (at least 200 nuclei were counted in each experiment). (C) The multiplication rate per 24 h of 100 nM sodium orthovanadate-treated cells was determined after cell counting with a hemocytometer. All treatments in this figure were 24 hours long. Data shown represents the mean ± SEM.

Sodium orthovanadate enhances the phosphorylation of tyrosine 451 of RET/PTC1 and interferes with the PI3K/Akt/mTOR signaling pathway

Because sodium orthovanadate inhibits the growth of TPC-1 cells, we sought to analyze the status of a key proliferation regulator of this cell line – RET/PTC1 (Meireles et al., 2007) – and also a signaling cascade that regulates cell growth — the PI3K/Akt pathway. Treatment of TPC-1 cells for 24 h with 10 μM sodium orthovanadate results in an overall increase in tyrosine phosphorylation, as demonstrated by the use of a pan-tyrosine antibody (Fig. 3A). Consistently, there is an increase in the phosphorylation of the tyrosine 451 residue of RET/PTC1 upon treatment with sodium orthovanadate (Fig. 3B) and in the total levels of the protein (Fig. 3C).

Regarding the PI3K/Akt pathway, treatment with 10 μM sodium orthovanadate decreases the expression of PTEN (Fig. 4A), which was expected since sodium orthovanadate is a tyrosine phosphatase inhibitor. However, whereas the phosphorylation of threonine 308 and expression of the total form of Akt are unaltered by the drug (Fig. 4A), phosphorylation of serine 473 is downregulated by sodium orthovanadate (Fig. 4A). These results indicate that PTEN down-regulation by sodium orthovanadate is not sufficient to activate Akt, probably because of the upstream decrease in the activity and expression of PI3K (Fig. 4A).

Downstream in the pathway, we studied the expression of mTOR and its effectors. Although the expression of the total form of mTOR was unaltered (Fig. 4B), 10 μM sodium orthovanadate induces an increase in the phosphorylation of its serine 2448 (Fig. 4B). The activity of mTOR is also stimulated because there is an increase in the phosphorylation of serine 235/236 of S6R (Fig. 4B), which is a readout of the activity of mTORC1. The total form of S6R remains unaffected (Fig. 4B). The expression of the other substrate of mTOR, 4E-BP1, is not altered upon treatment with sodium orthovanadate (data not shown). These results indicate that sodium orthovanadate attenuates the PI3K/Akt branch but stimulates the mTOR/S6R branch of the signaling cascade.

Sodium orthovanadate induces apoptosis through the participation of caspases

The PI3K/Akt pathway is a major regulator of cell survival and its downregulation or the absence of PI3K can lead to apoptosis (Yao and Cooper, 1995; Courtney et al., 2010). Moreover, it was shown that RET/PTC1 is able to transmit both mitogenic and pro-apoptotic signals in thyroid cells following phosphorylation of Y451 (Castellone et al., 2003). The effects of sodium orthovanadate on both RET/PTC1 and the PI3K/Akt/mTOR pathway led us to analyze DNA fragmentation through the TUNEL assay to determine if the drug was inducing apoptosis, given that the cell cycle evaluation indicated the presence of dead cells. At 10 μM, sodium orthovanadate causes an increase in apoptosis (1.36 fold change vs control; $P=0.005$), which is significantly abrogated when cells are pre-treated with the multicaspase inhibitor Z-VAD-FMK (Fig. 5A,B). Treatment with 10 μM sodium orthovanadate results in a significant loss of the mitochondrial membrane potential ($\Delta\Psi m$) (14.1%; $P=0.014$; Fig. 5C,D). Increasing concentrations of the drug stimulate the production of ROS ($P=0.003$; Fig. 5E,F), which is thought to be important for the action of vanadium compounds (Evangelou, 2002). Using an antibody that specifically detects the activated form of caspase-3, we observed that caspase-3 is activated in response to sodium orthovanadate exposure (Fig. 5G). These results indicate that the induction of apoptosis by sodium orthovanadate occurs through the stimulation of caspases and involves the mitochondria.

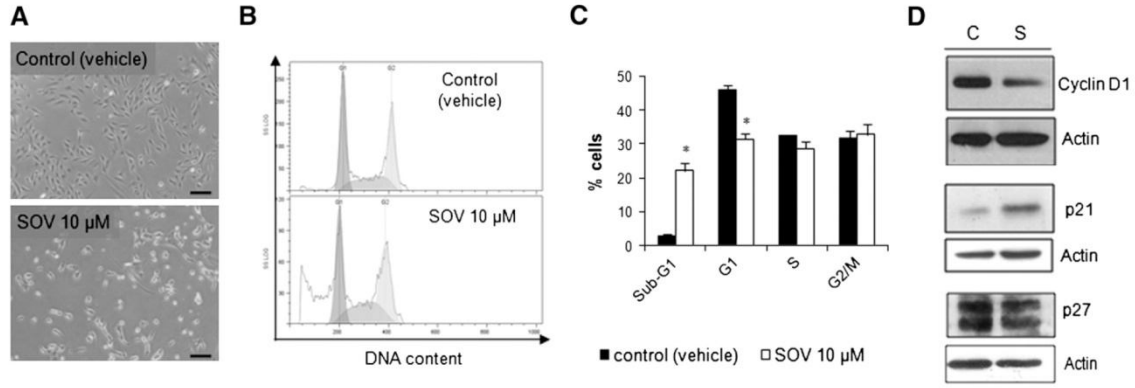

Fig. 2. Sodium orthovanadate-induced growth inhibition is associated with an increase in cell death and alterations in cell cycle regulators. (A) Phase-contrast micrographs of cells cultured in the absence or in the presence of 10 μM sodium orthovanadate (SOV); scale bar: 100 μm. (B) Representative histograms of cell cycle analysis by propidium iodide staining of DNA of treated cells and quantification of the data (C). (D) Whole lysates of cells treated with a vehicle control (C) or 10 μM sodium orthovanadate (S) were immunoblotted for cyclin D1, p21 and p27. Immunoblotting against actin served as a loading control. All treatments in this figure were 24 hours long. Data shown in (C) represents the mean ± standard error of mean (SEM). *, $P \leq 0.05$.

Sodium orthovanadate-induced growth inhibition is not abrogated by GDNF

Since sodium orthovanadate elicits an inhibitory response at 10 μM and RET/PTC1 is one of the molecules affected, we studied if its effects could be counteracted by the addition of the ligand GDNF, considering that RET-triggered cell death is suppressed when GDNF is present (Bordeaux et al., 2000; Canibano et al., 2007). Addition of 50 ng/ml GDNF has an innocuous effect on the growth of TPC-1 cells (0.6% of inhibition for 50 ng/ml GDNF vs the control; $P = 1.000$; Fig. 6A). Growth inhibition resulting from the treatment with 10 μM sodium orthovanadate alone is similar to the same dose in combination with 50 ng/ml GDNF (15.7% of inhibition for 10 μM sodium orthovanadate vs 15.9% for the combination; $P = 0.083$; Fig. 6A). Likewise, treatment with 50 ng/ml GDNF results in apoptotic levels equivalent to the control (1.03 fold change vs control; $P = 1.000$; Fig. 6B,C). Treatment with 50 ng/ml GDNF in combination with 10 μM sodium orthovanadate only mildly prevents apoptosis caused by sodium orthovanadate alone (1.12 and 1.36 fold change vs control, respectively; $P = 0.245$; Fig. 6B,C). This data suggests that although RET/PTC1 is affected by sodium orthovanadate, there are additional targets for the drug.

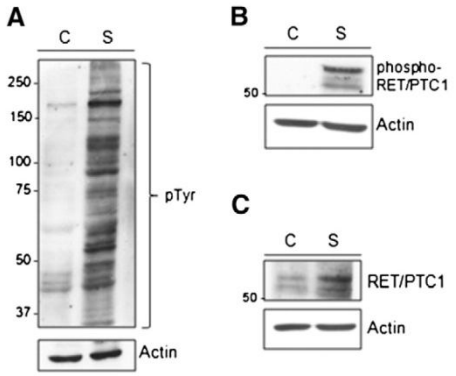

Fig. 3. Sodium orthovanadate increases the overall tyrosine phosphorylation of TPC-1 cells and the specific phosphorylation of Y451 of RET/PTC1. Whole lysates of cells treated for 24 h with a vehicle control (C) or 10 μM sodium orthovanadate (S) were immunoblotted for phospho-Tyr (A), phospho-RET/PTC1 (Y451; B) and RET/PTC1 (C). Immunoblotting against actin served as a loading control.

Discussion

Our results show that treatment with sodium orthovanadate, a vanadium compound with anti-cancer potential, induces growth inhibition and apoptosis with activation of caspase-3 and production of ROS in TPC-1 cells. The levels of phosphorylation of Y451 of RET/PTC1 are

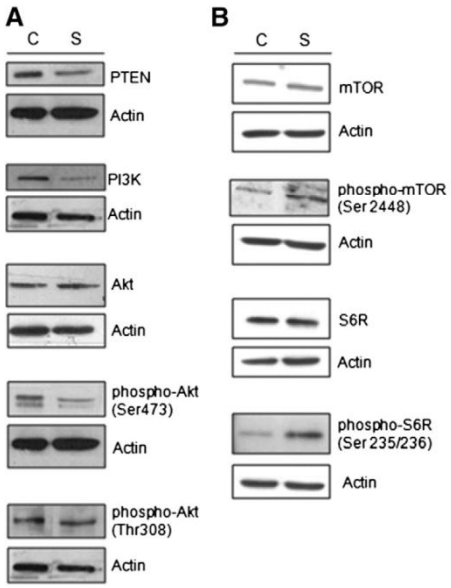

Fig. 4. Treatment with sodium orthovanadate interferes with the PI3K/Akt/mTOR signaling pathway. Whole lysates of cells treated for 24 h with a vehicle control (C) or 10 μM sodium orthovanadate (S) were immunoblotted for PTEN, PI3K (p110α), Akt and phospho-Akt (Ser 473 and Thr 308) (A) and for mTOR, phospho-mTOR (Ser 2448), S6R and phospho-S6R (Ser 235/236) (B). Immunoblotting against actin served as a loading control.

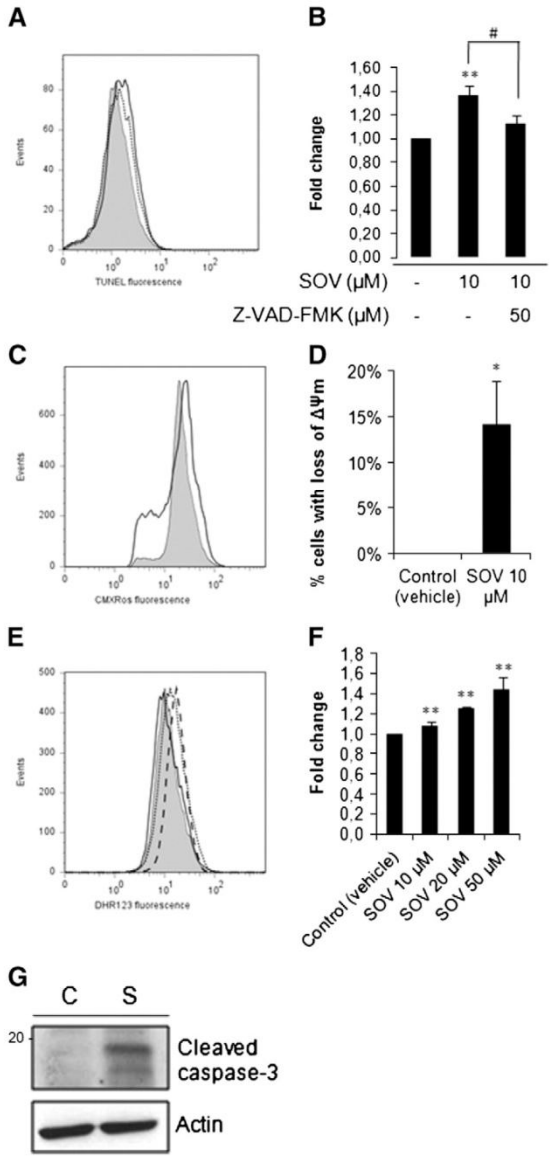

Fig. 5. Sodium orthovanadate induces apoptosis with activation of caspases, loss of mitochondrial membrane potential (ΔΨm) and formation of ROS. (A) Representative histogram of apoptosis analysis by TUNEL of cells treated with a control (vehicle) (shaded), 10 μM sodium orthovanadate (SOV; solid line) and 10 μM sodium orthovanadate preceded by a 1 hour treatment with 50 μM Z-VAD-FMK (dotted line) and quantification of the data (B). (C) Representative histogram of ΔΨm analysis by CMXRos staining of cells treated with a control (vehicle) (shaded) and 10 μM sodium orthovanadate (solid line) and quantification of the data (D). (E) Representative histogram of ROS analysis by DHR123 staining of cells treated with a control (vehicle) (shaded), 10 μM (solid line), 20 μM (dotted line) and 50 μM (dashed line) sodium orthovanadate and quantification of the data (F). (G) Whole lysates of cells treated with a vehicle control (C) or 10 μM sodium orthovanadate (S) were immunoblotted for cleaved caspase-3. Immunoblotting against actin served as a loading control. All treatments in this figure were 24 hours long. Data shown in (B), (D) and (F) represents the mean ± SEM. *, $P \leq 0.05$ and **, $P \leq 0.01$ for comparisons between drug-treated samples and the control; #, $P \leq 0.05$ for comparisons between drug-treated samples.

markedly increased in response to sodium orthovanadate. Despite this, this rearranged form of the RET receptor cannot be an absolute requirement for the effects in cell growth caused by the drug, because it inhibited other cell lines with wild type *RET* (Gonçalves et al., in press; Ray et al., 2007). However, in papillary thyroid carcinomas, the RET/PTC1 abnormality is frequent and plays a central role in the etiopathogenesis of the disease and in the proliferative behavior of cells (Santoro et al., 2004). Hence, we hypothesize that, because of the importance of this genetic event, the action of sodium orthovanadate on RET/PTC1 may be significant for the observed effects in TPC-1 cells. In fact, Y451 of RET/PTC1 was previously associated with the induction of apoptosis in rat thyroid cells through the activation of the Ras/ERK pathway (Castellone et al., 2003).

Concordant with the fact that vanadium compounds may affect different pathways (Chen and Shi, 2002; Evangelou, 2002), GDNF could not completely block sodium orthovanadate-induced inhibition. This is unsurprising since orthovanadate is a non-specific tyrosine phosphatase inhibitor and may affect several molecules, principally if they rely on the phosphorylation of tyrosine residues to operate. However, this work highlights the usefulness of phosphatase inhibitors as cell death modulators. We focused the study in the PI3K/Akt signaling pathway, as the TPC-1 cell line is a good model to study this cascade, because besides the presence of RET/PTC1 (Meireles et al., 2007) and a four times higher content of the insulin receptor (Vella et al., 2002), which are activators of the pathway, the cells possess wild type forms of *PI3KCA* and *PTEN* (Meireles et al., 2007; Leboeuf et al., 2008). One study showed a *PIK3CA* mutation (H1047R) in TPC-1 cells (Nucera et al., 2011), but it may be due to culture conditions, since our previous works of characterization of thyroid cell lines (Meireles et al., 2007; Ribeiro et al., 2008) consistently show no alterations in this region of *PIK3CA* in aliquots of TPC-1 cells from different sources. It is possible that different batches of TPC-1 growing independently in different laboratories for long term have acquired diverse additional genetic alterations.

Despite the increase in phosphorylation of Y451 of RET/PTC1 caused by sodium orthovanadate, we observed that PI3K levels and Akt phosphorylation at serine 473 were attenuated. Apparently, depending on the model used, vanadium compounds can stimulate or inhibit cell growth. Some reports of vanadium-stimulated cell survival show activation of PI3K and Akt, both in vitro and in vivo (Gao et al., 2002; Hasegawa et al., 2006; Wu et al., 2006), though the drug was also described to act without activation of Akt (Yan and Wenner, 2001). In opposition, other works denote that, like in our situation, this group of drugs can prompt apoptosis, although the exact mechanisms behind it are still not well understood (Huang et al., 2000; Ray et al., 2007; Markopoulou et al., 2009). Importantly, in rat models of mammary tumors, the induction of apoptosis may account for the anticancer activity of the drug (Ray et al., 2007). The disparity of data found in the literature is hard to explain. The different effects caused by different forms of vanadium compounds or the genetic background of the cells used are possible explanations. Another important factor to consider is the dose of the drug applied, since sodium orthovanadate seems to exert a positive effect in proliferation when the compound is at low concentrations and exert a cytotoxic effect when at higher concentrations. In fact, we have observed this dual effect in our model suggesting that the dose may be the key factor.

The downregulation of PI3K also highlights that the inhibition of PTEN by sodium orthovanadate cannot account by itself for the effects observed, since this phosphatase works downstream of PI3K. We observed that treatment with sodium orthovanadate results in an increase in the phosphorylation of mTOR and its downstream effector S6R, indicating a boost of activity in this part of the signaling pathway. While this remains to be proved, we consider that the main reason for the reduction of PI3K owes to this activation of the downstream mTOR/S6R branch of the pathway, because it is well established that PI3K and Akt can be inhibited by mTOR through a negative feedback regulatory loop involving the serine phosphorylation and downregulation of insulin

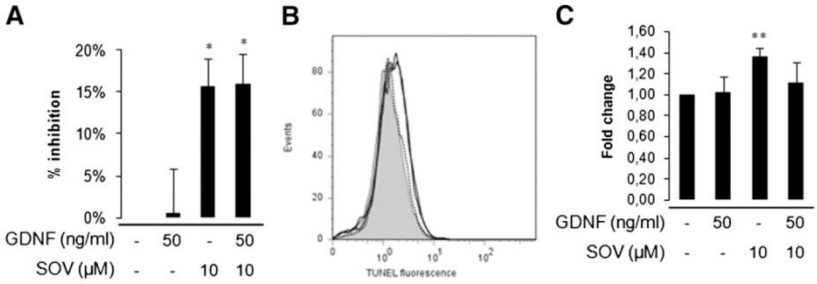

Fig. 6. Sodium orthovanadate-induced RET/PTC1-mediated growth inhibition is not abrogated by GDNF. (A) Growth inhibition was determined by the sulphorhodamine B assay for 50 ng/ml GDNF, 10 μM sodium orthovanadate (SOV) or the combination of both. (B) Representative histogram of apoptosis analysis by TUNEL of cells treated with a control (vehicle) (shaded), 10 μM sodium orthovanadate (solid line), 50 ng/ml GDNF (dotted line) and the combination of both (dashed line) and quantification of the data (C). All treatments in this figure were 24 hours long. Data shown in (A) and (C) represents the mean ± SEM. *, $P \leq 0.05$ and **, $P \leq 0.01$ for comparisons between drug-treated samples and the control.

receptor substrate-1 (IRS-1) (Hay, 2005). Also, the reduction in PI3K can explain the lower expression of phospho-Akt473, because PI3K phosphorylates Akt. Consistently, vanadium compounds are insulin-mimetics (Srivastava and Mehdi, 2005) and it was shown that mTOR regulates insulin-dependent IRS-1 degradation and that serine phosphorylation of IRS-1 inhibits insulin signaling (Hartman et al., 2001; Pederson et al., 2001). Although mTOR is canonically activated by Akt, this does not seem to be the case when cells are treated with sodium orthovanadate, because Akt is negatively affected by the drug. Supporting this, it is known that mTOR activation can occur through other signals (Memmott and Dennis, 2009), although we could not find the specific mediators for sodium orthovanadate-induced mTOR phosphorylation. Through its downstream effectors, S6K1/S6R and 4E-BP1, mTOR regulates the G_1-phase progression during the cell cycle (Fingar et al., 2004). Hence, sodium orthovanadate-induced alterations in mTOR/S6R may be related to the decrease in the number of cells in G_1. Our observation that molecular mediators of G_1 cyclin D1 and p21 were altered by the drug is in line with previous observations that treatment with sodium orthovanadate leads to cyclin D1 degradation and phosphorylation of p70S6K without activation of Akt (Yan and Wenner, 2001).

Conclusion

Inappropriate signals through the PI3K/Akt pathway occur frequently in cancer, namely in the thyroid gland (Courtney et al., 2010; Saji and Ringel, 2010). Importantly, because of the presence of RET/PTC1, TPC-1 cells are particularly sensitive to inhibitors of this signaling cascade (Liu et al., 2009). We provide in vitro data demonstrating that the effects of the apoptosis-inducer sodium orthovanadate include alterations in the PI3K/Akt/mTOR signaling pathway. Further studies are needed to clarify the relevance of these results in vivo.

Conflict of interest statement

The authors declare that there are no conflicts of interest.

Acknowledgments

A.P.G. was recipient of a fellowship from Fundação Calouste Gulbenkian (reference 104210). IPATIMUP and IBMC are Associated Laboratories of the Portuguese Ministry of Science, Technology and Higher Education and are partially supported by the Portuguese Foundation for Science and Technology.

References

Besset V, Scott RP, Ibanez CF. Signaling complexes and protein–protein interactions involved in the activation of the Ras and phosphatidylinositol 3-kinase pathways by the c-Ret receptor tyrosine kinase. J Biol Chem 2000;275(50):39159–66.
Bordeaux MC, Forcet C, Granger L, Corset V, Bidaud C, Billaud M, et al. The RET proto-oncogene induces apoptosis: a novel mechanism for Hirschsprung disease. EMBO J 2000;19(15):4056–63.
Buckwalter TL, Venkateswaran A, Lavender M, La Perle KM, Cho JY, Robinson ML, et al. The roles of phosphotyrosines-294, -404, and -451 in RET/PTC1-induced thyroid tumor formation. Oncogene 2002;21(53):8166–72.
Canibano C, Rodriguez NL, Saez C, Tovar S, Garcia-Lavandeira M, Borrello MG, et al. The dependence receptor Ret induces apoptosis in somatotrophs through a Pit-1/p53 pathway, preventing tumor growth. EMBO J 2007;26(8):2015–28.
Cassinelli G, Favini E, Degl'Innocenti D, Salvi A, De Petro G, Pierotti MA, et al. RET/PTC1-driven neoplastic transformation and proinvasive phenotype of human thyrocytes involve Met induction and beta-catenin nuclear translocation. Neoplasia 2009;11(1):10–21.
Castellone MD, Cirafici AM, De Vita G, De Falco V, Malorni L, Tallini G, et al. Ras-mediated apoptosis of PC CL 3 rat thyroid cells induced by RET/PTC oncogenes. Oncogene 2003;22(2):246–55.
Chen F, Shi X. Intracellular signal transduction of cells in response to carcinogenic metals. Crit Rev Oncol Hematol 2002;42(1):105–21.
Courtney KD, Corcoran RB, Engelman JA. The PI3K pathway as drug target in human cancer. J Clin Oncol 2010;28(6):1075–83.
Davis JM. Basic cell culture: a practical approach. Second Edition. Oxford: Oxford University Press; 2001.
De Vita G, Melillo RM, Carlomagno F, Visconti R, Castellone MD, Bellacosa A, et al. Tyrosine 1062 of RET-MEN2A mediates activation of Akt (protein kinase B) and mitogen-activated protein kinase pathways leading to PC12 cell survival. Cancer Res 2000;60(14):3727–31.
Evangelou AM. Vanadium in cancer treatment. Crit Rev Oncol Hematol 2002;42(3):249–65.
Fingar DC, Richardson CJ, Tee AR, Cheatham L, Tsou C, Blenis J. mTOR controls cell cycle progression through its cell growth effectors S6K1 and 4E-BP1/eukaryotic translation initiation factor 4E. Mol Cell Biol 2004;24(1):200–16.
Fusco A, Grieco M, Santoro M, Berlingieri MT, Pilotti S, Pierotti MA, et al. A new oncogene in human thyroid papillary carcinomas and their lymph-nodal metastases. Nature 1987;328(6126):170–2.
Gao N, Ding M, Zheng JZ, Zhang Z, Leonard SS, Liu KJ, et al. Vanadate-induced expression of hypoxia-inducible factor 1 alpha and vascular endothelial growth factor through phosphatidylinositol 3-kinase/Akt pathway and reactive oxygen species. J Biol Chem 2002;277(35):31963–71.
Gonçalves AP, Maximo V, Lima J, Singh KK, Soares P, Videira A. Involvement of p53 in cell death following cell cycle arrest and mitotic catastrophe induced by rotenone. Biochim Biophys Acta 2011;1813(3):492–9.
Gonçalves AP, Videira A, Máximo V, Soares P. The synergistic growth inhibition of cancer cells harboring the RET/PTC1 oncogene by staurosporine and rotenone involves enhanced cell death. J Biosci (in press).
Grieco M, Santoro M, Berlingieri MT, Melillo RM, Donghi R, Bongarzone I, et al. PTC is a novel rearranged form of the ret proto-oncogene and is frequently detected in vivo in human thyroid papillary carcinomas. Cell 1990;60(4):557–63.
Hartman ME, Villela-Bach M, Chen J, Freund GG. Frap-dependent serine phosphorylation of IRS-1 inhibits IRS-1 tyrosine phosphorylation. Biochem Biophys Res Commun 2001;280(3):776–81.
Hasegawa Y, Morioka M, Hasegawa S, Matsumoto J, Kawano T, Kai Y, et al. Therapeutic time window and dose dependence of neuroprotective effects of sodium orthovanadate following transient middle cerebral artery occlusion in rats. J Pharmacol Exp Ther 2006;317(2):875–81.
Hay N. The Akt-mTOR tango and its relevance to cancer. Cancer Cell 2005;8(3):179–83.
Hayashi H, Ichihara M, Iwashita T, Murakami H, Shimono Y, Kawai K, et al. Characterization of intracellular signals via tyrosine 1062 in RET activated by glial cell line-derived neurotrophic factor. Oncogene 2000;19(39):4469–75.

Huang C, Zhang Z, Ding M, Li J, Ye J, Leonard SS, et al. Vanadate induces p53 transactivation through hydrogen peroxide and causes apoptosis. J Biol Chem 2000;275(42):32516–22.
Ishizaka Y, Shima H, Sugimura T, Nagao M. Detection of phosphorylated retTPC oncogene product in cytoplasm. Oncogene 1992;7(7):1441–4.
Kang SG, Brown AL, Chung JH. Oxygen tension regulates the stability of insulin receptor substrate-1 (IRS-1) through caspase-mediated cleavage. J Biol Chem 2007;282(9): 6090–7.
Lanzi C, Borrello MG, Bongarzone I, Migliazza A, Fusco A, Grieco M, et al. Identification of the product of two oncogenic rearranged forms of the RET proto-oncogene in papillary thyroid carcinomas. Oncogene 1992;7(11):2189–94.
Leboeuf R, Baumgartner JE, Benezra M, Malaguarnera R, Solit D, Pratilas CA, et al. BRAFV600E mutation is associated with preferential sensitivity to mitogen-activated protein kinase kinase inhibition in thyroid cancer cell lines. J Clin Endocrinol Metab 2008;93(6):2194–201.
Liu D, Hou P, Liu Z, Wu G, Xing M. Genetic alterations in the phosphoinositide 3-kinase/Akt signaling pathway confer sensitivity of thyroid cancer cells to therapeutic targeting of Akt and mammalian target of rapamycin. Cancer Res 2009;69(18):7311–9.
Markopoulou S, Kontargiris E, Batsi C, Tzavaras T, Trougakos I, Boothman DA, et al. Vanadium-induced apoptosis of HaCaT cells is mediated by c-fos and involves nuclear accumulation of clusterin. FEBS J 2009;276(14):3784–99.
Meireles AM, Preto A, Rocha AS, Rebocho AP, Maximo V, Pereira-Castro I, et al. Molecular and genotypic characterization of human thyroid follicular cell carcinoma-derived cell lines. Thyroid 2007;17(8):707–15.
Melillo RM, Carlomagno F, De Vita G, Formisano P, Vecchio G, Fusco A, et al. The insulin receptor substrate (IRS)-1 recruits phosphatidylinositol 3-kinase to Ret: evidence for a competition between Shc and IRS-1 for the binding to Ret. Oncogene 2001;20(2): 209–18.
Memmott RM, Dennis PA. Akt-dependent and -independent mechanisms of mTOR regulation in cancer. Cell Signal 2009;21(5):656–64.
Morita A, Zhu J, Suzuki N, Enomoto A, Matsumoto Y, Tomita M, et al. Sodium orthovanadate suppresses DNA damage-induced caspase activation and apoptosis by inactivating p53. Cell Death Differ 2006;13(3):499–511.
Nucera C, Goldfarb M, Hodin R, Parangi S. Role of B-Raf(V600E) in differentiated thyroid cancer and preclinical validation of compounds against B-Raf(V600E). Biochim Biophys Acta 2009;1795(2):152–61.
Nucera C, Porrello A, Antonello ZA, Mekel M, Nehs MA, Giordano TJ, et al. B-Raf(V600E) and thrombospondin-1 promote thyroid cancer progression. Proc Natl Acad Sci USA 2010;107(23):10649–54.
Nucera C, Nehs MA, Nagarkatti SS, Sadow PM, Mekel M, Fischer AH, et al. Targeting BRAFV600E with PLX4720 displays potent antimigratory and anti-invasive activity in preclinical models of human thyroid cancer. Oncologist 2011;16(3):296–309.
Ohi N, Nishikawa Y, Tokairin T, Yamamoto Y, Doi Y, Omori Y, et al. Maintenance of Bad phosphorylation prevents apoptosis of rat hepatic sinusoidal endothelial cells in vitro and in vivo. Am J Pathol 2006;168(4):1097–106.
Pederson TM, Kramer DL, Rondinone CM. Serine/threonine phosphorylation of IRS-1 triggers its degradation: possible regulation by tyrosine phosphorylation. Diabetes 2001;50(1):24–31.
Pierotti MA, Santoro M, Jenkins RB, Sozzi G, Bongarzone I, Grieco M, et al. Characterization of an inversion on the long arm of chromosome 10 juxtaposing D10S170 and RET and creating the oncogenic sequence RET/PTC. Proc Natl Acad Sci USA 1992;89(5): 1616–20.
Plaza-Menacho I, Burzynski GM, de Groot JW, Eggen BJ, Hofstra RM. Current concepts in RET-related genetics, signaling and therapeutics. Trends Genet 2006;22(11):627–36.
Ray RS, Ghosh B, Rana A, Chatterjee M. Suppression of cell proliferation, induction of apoptosis and cell cycle arrest: chemopreventive activity of vanadium in vivo and in vitro. Int J Cancer 2007;120(1):13–23.
Ribeiro FR, Meireles AM, Rocha AS, Teixeira MR. Conventional and molecular cytogenetics of human non-medullary thyroid carcinoma: characterization of eight cell line models and review of the literature on clinical samples. BMC Cancer 2008;8:371.
Saji M, Ringel MD. The PI3K-Akt-mTOR pathway in initiation and progression of thyroid tumors. Mol Cell Endocrinol 2010;321(1):20–8.
Salvatore D, Barone MV, Salvatore G, Melillo RM, Chiappetta G, Mineo A, et al. Tyrosines 1015 and 1062 are in vivo autophosphorylation sites in ret and ret-derived oncoproteins. J Clin Endocrinol Metab 2000;85(10):3898–907.
Santoro M, Melillo RM, Grieco M, Berlingieri MT, Vecchio G, Fusco A. The TRK and RET tyrosine kinase oncogenes cooperate with ras in the neoplastic transformation of a rat thyroid epithelial cell line. Cell Growth Differ 1993;4(2):77–84.
Santoro M, Carlomagno F, Melillo RM, Fusco A. Dysfunction of the RET receptor in human cancer. Cell Mol Life Sci 2004;61(23):2954–64.
Segouffin-Cariou C, Billaud M. Transforming ability of MEN2A-RET requires activation of the phosphatidylinositol 3-kinase/AKT signaling pathway. J Biol Chem 2000;275(5): 3568–76.
Srivastava AK, Mehdi MZ. Insulino-mimetic and anti-diabetic effects of vanadium compounds. Diabet Med 2005;22(1):2–13.
Trovisco V, Soares P, Sobrinho-Simoes M. B-RAF mutations in the etiopathogenesis, diagnosis, and prognosis of thyroid carcinomas. Hum Pathol 2006;37(7):781–6.
Vella V, Pandini G, Sciacca L, Mineo R, Vigneri R, Pezzino V, et al. A novel autocrine loop involving IGF-II and the insulin receptor isoform-A stimulates growth of thyroid cancer. J Clin Endocrinol Metab 2002;87(1):245–54.
Wu DN, Pei DS, Wang Q, Zhang GY. Down-regulation of PTEN by sodium orthovanadate inhibits ASK1 activation via PI3-K/Akt during cerebral ischemia in rat hippocampus. Neurosci Lett 2006;404(1–2):98–102.
Xing M. BRAF mutation in papillary thyroid cancer: pathogenic role, molecular bases, and clinical implications. Endocr Rev 2007;28(7):742–62.
Yan S, Wenner CE. Modulation of cyclin D1 and its signaling components by the phorbol ester TPA and the tyrosine phosphatase inhibitor vanadate. J Cell Physiol 2001;186(3):338–49.
Yao R, Cooper GM. Requirement for phosphatidylinositol-3 kinase in the prevention of apoptosis by nerve growth factor. Science 1995;267(5206):2003–6.

CONCLUDING REMARKS AND FUTURE PERSPECTIVES

Concluding remarks

Simple organisms can be very useful as models for the study of complex biological processes, provided that they possess the necessary molecular machinery to execute them. In the absence of that machinery, an organism may be useful as well, as it can be used as a “clean model” to study the mechanisms of specific molecules. With respect to PCD, evidence is accumulating that shows that fungi, namely filamentous species, undergo regulated forms of death (46-48). This study confirms that the filamentous *Neurospora crassa* has such an ability, despite the fact that much of its molecular mechanisms involved in cell death are still unclear. The work presented in this dissertation addresses part of this lack of knowledge.

In this study, staurosporine was used as the main cell death stimulus. The drug is a widely used tool in cell death research and a prototype for anticancer drugs (177). Thus, characterization of its mechanism of action may impact future studies on the fundamental aspects of cell death signaling and on the development of therapeutic treatments for fungal infections and cancer. A substantial part of this work was devoted to the role of Ca^{2+} dynamics during staurosporine-induced cell death. We observed that staurosporine triggers well defined alteration in the levels of cytosolic Ca^{2+} that involve internal Ca^{2+} reservoirs such as the ER, vacuoles and mitochondria as well as Ca^{2+} uptake from the extracellular medium. In line with the latter, we showed that staurosporine-induced cell death is robustly modulated by the amount of extracellularly available Ca^{2+}, as it affects intracellular events like Ca^{2+} signaling or ROS production. At the molecular level, we emphasized the role of phospholipase C as a pivotal player during staurosporine-induced cell death. In the absence of PLC-2, one of the four phospolipase C genes encoded by the *N. crassa* genome, cells exhibit increased survival and the staurosporine-induced Ca^{2+} signature is abolished. Additionally, we found that PLC-2 is important for proper hyphal development. Our results with specific inhibitors of the phospholipase C-IP_3 signaling pathway suggest the existence of an IP_3 receptor in *N. crassa*, despite the fact that *in silico* predictions have failed to identify such a protein so far (314, 315). We were able to prove that a Ca^{2+} influx mechanism distinct from the hitherto reported high-affinity (CCH-

1/MID-1) and low-affinity (FIG-1) Ca^{2+} uptake systems. Our pharmacological approach indicates that, in response to staurosporine, one (or more) channel(s) with properties of the transient receptor potential family is (are) activated to perform Ca^{2+} influx.

We characterized the role of a novel zinc cluster transcription factor, herein termed CZT-1 (Cell death-activated Zinc cluster Transcription factor), that is induced during staurosporine-induced cell death. CZT-1 controls the expression of several proteins that influence different organelles, such as the mitochondria and the ER, as well as different cellular activities, including Ca^{2+} signaling and ROS accumulation. Through its transcriptional regulation, CZT-1 confers resistance to staurosporine-induced cell death in laboratory strains and in wild isolates of *N. crassa*.

In order to assess the transcriptional response to stauroporine in a high-throughput manner, we employed the recent RNA-seq technology. The results of these experiments contributed not only to the understanding of the molecular pathways involved in the fungal response to staurosporine, but we also anticipate that our RNA-seq dataset will be useful as a resource for investigations on different aspects of fungal biology. For example, a few genes with altered expression in culture medium lacking Ca^{2+} that may function in cell fusion were revealed (Palma-Guerrero J, Gonçalves AP, unpublished results).

A model illustrating the mechanisms involved in staurosporine-induced and phospholipase C-mediated cell death is presented in Fig. 65. We propose that after the increase in the $[Ca^{2+}]_c$ caused by continuous Ca^{2+} influx from the external medium and release of Ca^{2+} from the ER, the vacuoles readily sequester the excess of cytosolic Ca^{2+}, which may have deleterious effects to the cells. This sequestration can occur by means of a Ca^{2+}/H^+ antiport system that can be indirectly blocked by disruption of the membrane proton gradient when the vacuolar H^+-ATPase is inhibited with bafilomycin A1 (383, 462). Sequestration of Ca^{2+} through this system seems to eventually saturate, since bafilomycin A1 does not block the “C” phase of the staurosporine-induced Ca^{2+} signature. Interestingly, recent reports demonstrated that the vacuolar H^+/ATPase is a central mediator of cell death in fungal (463, 464) and cancer (465) cells. In *S. cerevisiae*, cells lacking vacuolar ATPase activity are very sensitive even to brief elevations of

$[Ca^{2+}]_c$ (466). In future studies, it will be interesting to determine the role of the vacuolar H^+-ATPase in *N. crassa* cell death.

Mitochondrial fluxes of Ca^{2+} also seem to be involved in the response to staurosporine. The initial alteration in cytosolic Ca^{2+} accumulation profile when the MCU is inhibited with Ru360 suggests that mitochondria play an early role in Ca^{2+} sequestration. However, Ca^{2+} peaks "B" and "C" are reduced in the presence of Ru360, suggesting that mitochondria are not restricted to sequestration but also release Ca^{2+} directly to the cytosol or the ER through the so-called microdomains of contact between the two organelles (289). Interestingly, thapsigargin-treated cells generated an opposite response to those treated with Ru360 because the amplitudes of the $[Ca^{2+}]_c$ transients are higher during phases 'B" and "C". These results can be explained by the hypothesis that mitochondria and ER exhibit Ca^{2+} crosstalk over long periods by transporting Ca^{2+} ions between them. The apparent paradoxical conclusion that the ER is releasing Ca^{2+} through an IP_3-activated channel but sequestering the ion at the same time (especially during phase "B", see the staurosporine-induced cytosolic $[Ca^{2+}]_c$ transient in thapsigargin-treated cells) could then be explained by a tunneling mechanism by which the ER can load with Ca^{2+} via contact spots between mitochondria and ER and almost instantaneously release Ca^{2+} from regions of the ER rich in IP_3-activated channels (467). Extracellular Ca^{2+} uptake continues throughout the whole length of the response to staurosporine, as deduced from the experiments involving treatment with the Ca^{2+} chelator BAPTA at different times.

Our model also illustrates that the extent of staurosporine-induced cell death is controlled by the activity of the staurosporine-exporting ABC transporter ABC-3 (140). The expression of ABC-3 is in turn controlled by the transcription factor CZT-1, which also regulates other ABC transporters, as well as intracellular Ca^{2+} signaling and ROS accumulation. ROS accumulation, which is facilitated by the efflux of GSH, is required for staurosporine-induced cell death (114, 139). Within mitochondria, alternative NAD(P)H dehydrogenases (particularly NDE-1) and specific subunits of the mitochondrial complex I (particularly NUO51, NUO14, NUO30.4 and NUO9.8 (139)) are important mediators of staurosporine-induced cell death. NDE-1 regulates ROS accumulation and favours cell survival in the presence of staurosporine. NDE-1 binds Ca^{2+}, required for its NADPH oxidase activity (241, 242), and could possibly behave as a mitochondrial Ca^{2+} sensor.

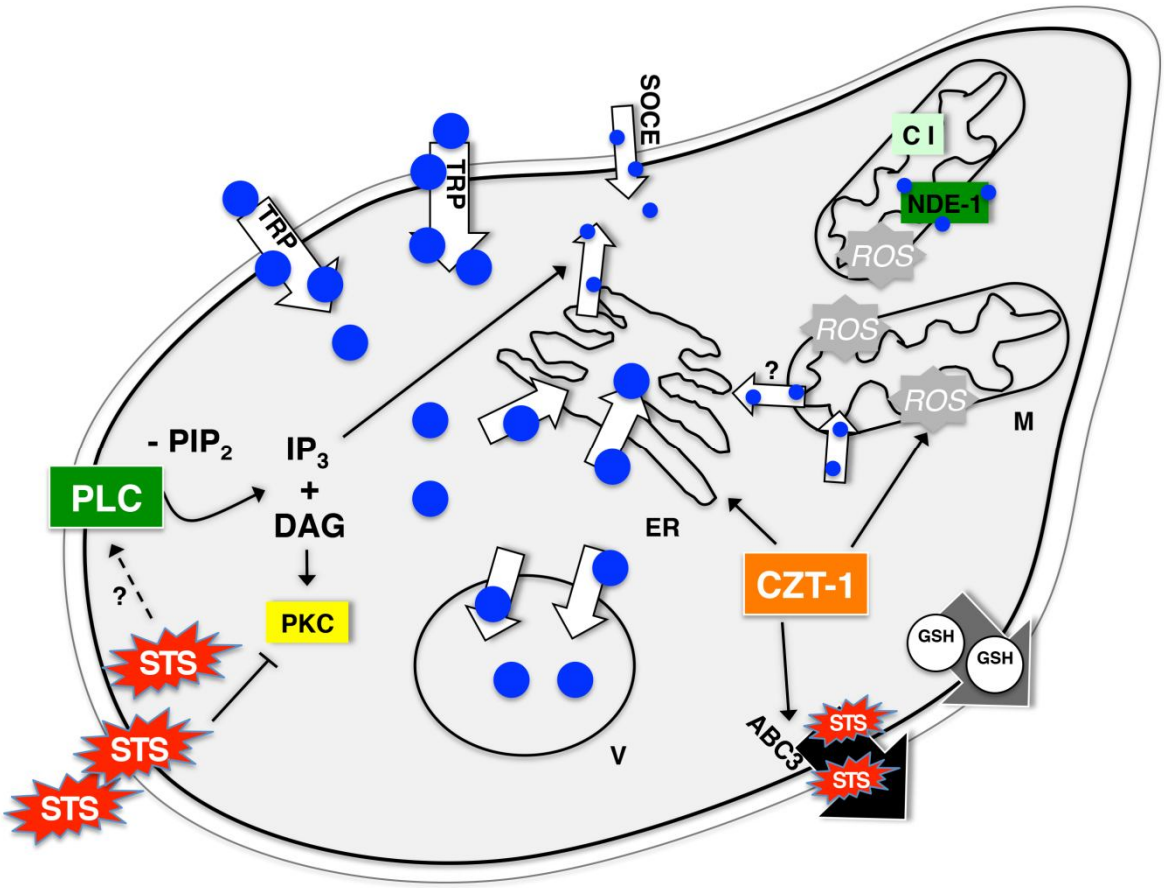

Figure 65 - Proposed model for the action of staurosporine in *N. crassa*.
See text for details. M: mitochondria; ER: endoplasmic reticulum; V: vacuoles; ROS: reactive oxygen species; GSH: reduced glutathione; C I: mitochondrial complex I; SOCE: store-operated Ca^{2+} entry.

Using cancer cell lines, the mechanisms of action of staurosporine, sodium orthovanadate and rotenone were characterized. In particular, our results indicate that rotenone, albeit normally used as mitochondrial complex I inhibitor, is also a potent mitotic disruptor. In thyroid cancer cells, we observed that rotenone triggers a wide range of effects including mitotic catastrophe, mitotic slippage and cellular senescence. The tumor suppressor protein p53 is especially involved in these rotenone-induced processes, especially in the extensive cell death that occurs following a polyploidy state.

Future perspectives

Our group is very interested in studying how the mitochondrion is involved in *N. crassa* cell death. Given that intracellular Ca^{2+} is a crucial mediator of staurosporine-induced cell death, a mitochondria-targeted version of the Ca^{2+} reporter aequorin has meanwhile been developed and recently transformed into a few strans. The mitochondrial targeting of aequorin (mitoAeq) was already confirmed by western blots of mitochondrial and cytosolic cellular fractions and by functional assays. Preliminary experiments indicated that wild type mitoAeq-expressing cells accumulate Ca^{2+} in the mitochondria upon treatment with staurosporine. More experiments need to be performed in order to correlate mitochondrial and cytosolic Ca^{2+} dynamics in staurosporine-treated cells. Relevant deletion strains such as those lacking the mitochondrial proteins NDE-1 and MCU are among the strains transformed with mitoAeq and we intend to understand if the altered cytosolic staurosporine-induced Ca^{2+} signatures on these strains are associated with abnormal mitochondrial Ca^{2+} fluxes. Another aspect of our work was the identification of a cell surface channel with properties resembling those of the TRP channels. Although our pharmacological approach indicates that a TRP-like channel promotes the influx of Ca^{2+} from the external medium, we were not able to determine the molecular identity of such a protein. However, we have now a few candidate genes that can be screened for deficiency in Ca^{2+} influx in response to staurosporine.

We observed that expression of different ABC transporters is CZT-1-dependent. This is likely related to the drug resistance regulatory role of the transcription factor. Since inactivation of *czt-1* leads to deficiency in several drug efflux pumps, it may be a good target to overcome drug resistance. This suggestion makes it relevant to characterize, in future studies, the role of CZT-1 and its homologues in pathogenic organisms. Sequence homology analyses suggest that CZT-1 belongs to a novel and divergent subfamily of zinc cluster transcription factors. Because of the conservation between CZT-1 and uncharacterized proteins from human and crop pathogens it will be interesting to extend the characterization of these molecules.

Overall, along the way of this PhD project, other remaining “loose ends” deserve deeper investigation in the future. For example, we performed screenings of numerous deletion strains for sensitivity to cell death-inducing drugs and several strains with a phenotype distinct from the wild type have been identified. Since these strains lack putative mediators of cell death, it would be certainly interesting to perform additional studies in order to clarify how are these elements implicated in the molecular mechanisms of PCD in *N. crassa*.

REFERENCES

1. Payen A (1843) Extrain d'un rapport addressé à M. Le Maréchal Duc de Dalmatie, Ministre de la Guerre, Président du Conseil, sur une altération extraordinaire du pain de munition. *Ann Chim Phys* 9:5-21.

2. Borkovich KA*, et al.* (2004) Lessons from the genome sequence of Neurospora crassa: tracing the path from genomic blueprint to multicellular organism. *Microbiol Mol Biol Rev* 68(1):1-108.

3. Shear CL & Dodge BO (1927) Life histories and heterothallism of the red bread-mold fungi of the Monilia sitophila group. *Journal of Agricultural Research* 34:1019-1042.

4. Beadle GW & Tatum EL (1941) Genetic Control of Biochemical Reactions in Neurospora. *Proc Natl Acad Sci U S A* 27(11):499-506.

5. Srb AM & Horowitz NH (1944) The Ornithine Cycle in Neurospora and its Genetic Control. *J Biol Chem* 154:129-139.

6. Davis RH & Perkins DD (2002) Timeline: Neurospora: a model of model microbes. *Nat Rev Genet* 3(5):397-403.

7. Hibbett DS*, et al.* (2007) A higher-level phylogenetic classification of the Fungi. *Mycol Res* 111(Pt 5):509-547.

8. Fitzpatrick DA, Logue ME, Stajich JE, & Butler G (2006) A fungal phylogeny based on 42 complete genomes derived from supertree and combined gene analysis. *BMC Evol Biol* 6:99.

9. Silverman-Gavrila LB & Lew RR (2001) Regulation of the tip-high [Ca2+] gradient in growing hyphae of the fungus Neurospora crassa. *Eur J Cell Biol* 80(6):379-390.

10. Silverman-Gavrila LB & Lew RR (2002) An IP3-activated Ca2+ channel regulates fungal tip growth. *J Cell Sci* 115(Pt 24):5013-5025.

11. Silverman-Gavrila LB & Lew RR (2003) Calcium gradient dependence of Neurospora crassa hyphal growth. *Microbiology* 149(Pt 9):2475-2485.

12. Mishra NC (1977) Genetics and biochemistry of morphogenesis in Neurospora. *Adv Genet* 19:341-405.

13. Vogel HJ (1956) A convenient growth medium for Neurospora (Medium N). *Microbial Genet Bull* 13:42-43.

14. Videira A & Duarte M (2001) On complex I and other NADH:ubiquinone reductases of Neurospora crassa mitochondria. *J Bioenerg Biomembr* 33(3):197-203.

15. Videira A & Duarte M (2002) From NADH to ubiquinone in Neurospora mitochondria. *Biochim Biophys Acta* 1555(1-3):187-191.

16. Lambowitz AM & Slayman CW (1971) Cyanide-resistant respiration in Neurospora crassa. *J Bacteriol* 108(3):1087-1096.

17. Li Q*, et al.* (1996) Cloning and analysis of the alternative oxidase gene of Neurospora crassa. *Genetics* 142(1):129-140.

18. Jacobson DJ*, et al.* (2006) New findings of Neurospora in Europe and comparisons of diversity in temperate climates on continental scales. *Mycologia* 98(4):550-559.

19. Perkins DD & Turner BC (1988) Neurospora from natural populations: Toward the population biology of a haploid eukaryote. *Exptl Mycol* 12(2):91-131.

20. Turner BC, Perkins DD, & Fairfield A (2001) Neurospora from natural populations: a global study. *Fungal Genet Biol* 32(2):67-92.

21. Davis RH (2000) *Neurospora: Contributions of a Model Organism* (Oxford University Press, New York City NY, USA).

22. Springer ML (1993) Genetic control of fungal differentiation: the three sporulation pathways of Neurospora crassa. *Bioessays* 15(6):365-374.

23. Maheshwari R (1999) Microconidia of Neurospora crassa. *Fungal Genet Biol* 26(1):1-18.

24. Westergaard M & Mitchell HK (1947) Neurospora-V - a Synthetic Medium Favoring Sexual Reproduction. *American Journal of Botany* 34(10):573-577.

25. Bistis GN (1983) Evidence for Diffusible, Mating-Type-Specific Trichogyne Attractants in Neurospora-Crassa. *Experimental Mycology* 7(3):292-295.

26. Raju NB (1992) Genetic-Control of the Sexual Cycle in Neurospora. *Mycological Research* 96:241-262.

27. Iyengar GA, Deka PC, Kundu SC, & Sen SK (1977) DNA syntheses in course of meiotic development in Neurospora crassa. *Genet Res* 29(1):1-8.

28. Galagan JE*, et al.* (2003) The genome sequence of the filamentous fungus Neurospora crassa. *Nature* 422(6934):859-868.

29. Colot HV*, et al.* (2006) A high-throughput gene knockout procedure for Neurospora reveals functions for multiple transcription factors. *Proc Natl Acad Sci U S A* 103(27):10352-10357.

30. Dunlap JC*, et al.* (2007) Enabling a community to dissect an organism: overview of the Neurospora functional genomics project. *Adv Genet* 57:49-96.

31. McCluskey K, Wiest A, & Plamann M (2010) The Fungal Genetics Stock Center: a repository for 50 years of fungal genetics research. *J Biosci* 35(1):119-126.

32. Fuchs Y & Steller H (2011) Programmed cell death in animal development and disease. *Cell* 147(4):742-758.

33. Galluzzi L*, et al.* (2012) Molecular definitions of cell death subroutines: recommendations of the Nomenclature Committee on Cell Death 2012. *Cell Death Differ* 19(1):107-120.

34. Vanden Berghe T, Linkermann A, Jouan-Lanhouet S, Walczak H, & Vandenabeele P (2014) Regulated necrosis: the expanding network of non-apoptotic cell death pathways. *Nat Rev Mol Cell Biol* 15(2):135-147.

35. Boya P, Reggiori F, & Codogno P (2013) Emerging regulation and functions of autophagy. *Nat Cell Biol* 15(7):713-720.

36. Xie Z & Klionsky DJ (2007) Autophagosome formation: core machinery and adaptations. *Nat Cell Biol* 9(10):1102-1109.

37. Kerr JF, Wyllie AH, & Currie AR (1972) Apoptosis: a basic biological phenomenon with wide-ranging implications in tissue kinetics. *Br J Cancer* 26(4):239-257.

38. Taylor RC, Cullen SP, & Martin SJ (2008) Apoptosis: controlled demolition at the cellular level. *Nat Rev Mol Cell Biol* 9(3):231-241.

39. Tait SW & Green DR (2010) Mitochondria and cell death: outer membrane permeabilization and beyond. *Nat Rev Mol Cell Biol* 11(9):621-632.

40. Chipuk JE, Moldoveanu T, Llambi F, Parsons MJ, & Green DR (2010) The BCL-2 family reunion. *Mol Cell* 37(3):299-310.

41. Madeo F, Frohlich E, & Frohlich KU (1997) A yeast mutant showing diagnostic markers of early and late apoptosis. *J Cell Biol* 139(3):729-734.

42. Sato T*, et al.* (1994) Interactions among members of the Bcl-2 protein family analyzed with a yeast two-hybrid system. *Proc Natl Acad Sci U S A* 91(20):9238-9242.

43. Xu Q & Reed JC (1998) Bax inhibitor-1, a mammalian apoptosis suppressor identified by functional screening in yeast. *Mol Cell* 1(3):337-346.

44. Longo VD, Ellerby LM, Bredesen DE, Valentine JS, & Gralla EB (1997) Human Bcl-2 reverses survival defects in yeast lacking superoxide dismutase and delays death of wild-type yeast. *J Cell Biol* 137(7):1581-1588.

45. Polcic P & Forte M (2003) Response of yeast to the regulated expression of proteins in the Bcl-2 family. *Biochem J* 374(Pt 2):393-402.

46. Sharon A, Finkelstein A, Shlezinger N, & Hatam I (2009) Fungal apoptosis: function, genes and gene function. *FEMS Microbiol Rev* 33(5):833-854.

47. Shlezinger N, Goldfinger N, & Sharon A (2012) Apoptotic-like programed cell death in fungi: the benefits in filamentous species. *Front Oncol* 2:97.

48. Ramsdale M (2012) Programmed cell death in the cellular differentiation of microbial eukaryotes. *Curr Opin Microbiol* 15(6):646-652.

49. Carmona-Gutierrez D*, et al.* (2010) Apoptosis in yeast: triggers, pathways, subroutines. *Cell Death Differ* 17(5):763-773.

50. Wlodkowic D, Telford W, Skommer J, & Darzynkiewicz Z (2011) Apoptosis and beyond: cytometry in studies of programmed cell death. *Methods Cell Biol* 103:55-98.

51. Skulachev VP (1999) Phenoptosis: programmed death of an organism. *Biochemistry (Mosc)* 64(12):1418-1426.

52. Palkova Z & Vachova L (2006) Life within a community: benefit to yeast long-term survival. *FEMS Microbiol Rev* 30(5):806-824.

53. Vopalenska I, Hulkova M, Janderova B, & Palkova Z (2005) The morphology of Saccharomyces cerevisiae colonies is affected by cell adhesion and the budding pattern. *Res Microbiol* 156(9):921-931.

54. Longo VD, Mitteldorf J, & Skulachev VP (2005) Programmed and altruistic ageing. *Nat Rev Genet* 6(11):866-872.

55. Sukhanova EI, Rogov AG, Severin FF, & Zvyagilskaya RA (2012) Phenoptosis in yeasts. *Biochemistry (Mosc)* 77(7):761-775.

56. Severin FF, Meer MV, Smirnova EA, Knorre DA, & Skulachev VP (2008) Natural causes of programmed death of yeast Saccharomyces cerevisiae. *Biochim Biophys Acta* 1783(7):1350-1353.

57. Laun P*, et al.* (2001) Aged mother cells of Saccharomyces cerevisiae show markers of oxidative stress and apoptosis. *Mol Microbiol* 39(5):1166-1173.

58. Herker E*, et al.* (2004) Chronological aging leads to apoptosis in yeast. *J Cell Biol* 164(4):501-507.

59. Buttner S*, et al.* (2006) Why yeast cells can undergo apoptosis: death in times of peace, love, and war. *J Cell Biol* 175(4):521-525.

60. Fabrizio P*, et al.* (2004) Superoxide is a mediator of an altruistic aging program in Saccharomyces cerevisiae. *J Cell Biol* 166(7):1055-1067.

61. Vachova L & Palkova Z (2005) Physiological regulation of yeast cell death in multicellular colonies is triggered by ammonia. *J Cell Biol* 169(5):711-717.

62. Severin FF & Hyman AA (2002) Pheromone induces programmed cell death in S. cerevisiae. *Curr Biol* 12(7):R233-235.

63. Eastwood MD, Cheung SW, Lee KY, Moffat J, & Meneghini MD (2012) Developmentally programmed nuclear destruction during yeast gametogenesis. *Dev Cell* 23(1):35-44.

64. Semighini CP, Averette AF, Perfect JR, & Heitman J (2011) Deletion of Cryptococcus neoformans AIF ortholog promotes chromosome aneuploidy and fluconazole-resistance in a metacaspase-independent manner. *PLoS Pathog* 7(11):e1002364.

65. Ratcliff WC, Denison RF, Borrello M, & Travisano M (2012) Experimental evolution of multicellularity. *Proc Natl Acad Sci U S A* 109(5):1595-1600.

66. Dementhon K, Iyer G, & Glass NL (2006) VIB-1 is required for expression of genes necessary for programmed cell death in Neurospora crassa. *Eukaryot Cell* 5(12):2161-2173.

67. Glass NL & Dementhon K (2006) Non-self recognition and programmed cell death in filamentous fungi. *Curr Opin Microbiol* 9(6):553-558.

68. Glass NL, Grotelueschen J, & Metzenberg RL (1990) Neurospora crassa A mating-type region. *Proc Natl Acad Sci U S A* 87(13):4912-4916.

69. Glass NL & Kaneko I (2003) Fatal attraction: nonself recognition and heterokaryon incompatibility in filamentous fungi. *Eukaryot Cell* 2(1):1-8.

70. Hutchison E, Brown S, Tian C, & Glass NL (2009) Transcriptional profiling and functional analysis of heterokaryon incompatibility in Neurospora crassa reveals that reactive oxygen species, but not metacaspases, are associated with programmed cell death. *Microbiology* 155(Pt 12):3957-3970.

71. Hutchison EA, Bueche JA, & Glass NL (2012) Diversification of a protein kinase cascade: IME-2 is involved in nonself recognition and programmed cell death in Neurospora crassa. *Genetics* 192(2):467-482.

72. Jacobson DJ, Beurkens K, & Klomparens KL (1998) Microscopic and Ultrastructural Examination of Vegetative Incompatibility in Partial Diploids Heterozygous at het Loci in Neurospora crassa. *Fungal Genet Biol* 23(1):45-56.

73. Kaneko I, Dementhon K, Xiang Q, & Glass NL (2006) Nonallelic interactions between het-c and a polymorphic locus, pin-c, are essential for nonself recognition and programmed cell death in Neurospora crassa. *Genetics* 172(3):1545-1555.

74. Lafontaine DL & Smith ML (2012) Diverse interactions mediate asymmetric incompatibility by the het-6 supergene complex in Neurospora crassa. *Fungal Genet Biol* 49(1):65-73.

75. Micali CO & Smith ML (2006) A nonself recognition gene complex in Neurospora crassa. *Genetics* 173(4):1991-2004.

76. Newmeyer D (1970) A suppressor of the heterokaryon-incompatibility associated with mating type in Neurospora crassa. *Can J Genet Cytol* 12(4):914-926.

77. Pittenger TH (1957) The mating type alleles and heterokaryon formation in *Neurospora crassa*. *Microbiol Genet Bull* 15:21-22.

78. Sarkar S, Iyer G, Wu J, & Glass NL (2002) Nonself recognition is mediated by HET-C heterocomplex formation during vegetative incompatibility. *EMBO J* 21(18):4841-4850.

79. Shiu PK & Glass NL (1999) Molecular characterization of tol, a mediator of mating-type-associated vegetative incompatibility in Neurospora crassa. *Genetics* 151(2):545-555.

80. Xiang Q & Glass NL (2002) Identification of vib-1, a locus involved in vegetative incompatibility mediated by het-c in Neurospora crassa. *Genetics* 162(1):89-101.

81. Dufour E, Boulay J, Rincheval V, & Sainsard-Chanet A (2000) A causal link between respiration and senescence in Podospora anserina. *Proc Natl Acad Sci U S A* 97(8):4138-4143.

82. Lorin S, Dufour E, & Sainsard-Chanet A (2006) Mitochondrial metabolism and aging in the filamentous fungus Podospora anserina. *Biochim Biophys Acta* 1757(5-6):604-610.

83. Osiewacz HD (2011) Mitochondrial quality control in aging and lifespan control of the fungal aging model Podospora anserina. *Biochem Soc Trans* 39(5):1488-1492.

84. Osiewacz HD & Borghouts C (2000) Mitochondrial oxidative stress and aging in the filamentous fungus Podospora anserina. *Ann N Y Acad Sci* 908:31-39.

85. Shlezinger N*, et al.* (2011) Anti-apoptotic machinery protects the necrotrophic fungus Botrytis cinerea from host-induced apoptotic-like cell death during plant infection. *PLoS Pathog* 7(8):e1002185.

86. Kershaw MJ & Talbot NJ (2009) Genome-wide functional analysis reveals that infection-associated fungal autophagy is necessary for rice blast disease. *Proc Natl Acad Sci U S A* 106(37):15967-15972.

87. Liu XH, Lu JP, & Lin FC (2007) Autophagy during conidiation, conidial germination and turgor generation in Magnaporthe grisea. *Autophagy* 3(5):472-473.

88. Veneault-Fourrey C, Barooah M, Egan M, Wakley G, & Talbot NJ (2006) Autophagic fungal cell death is necessary for infection by the rice blast fungus. *Science* 312(5773):580-583.

89. Wilson RA & Talbot NJ (2009) Under pressure: investigating the biology of plant infection by Magnaporthe oryzae. *Nat Rev Microbiol* 7(3):185-195.

90. Pinan-Lucarre B, Balguerie A, & Clave C (2005) Accelerated cell death in Podospora autophagy mutants. *Eukaryot Cell* 4(11):1765-1774.

91. Hamann A, Brust D, & Osiewacz HD (2007) Deletion of putative apoptosis factors leads to lifespan extension in the fungal ageing model Podospora anserina. *Mol Microbiol* 65(4):948-958.

92. Raju NB & Perkins DD (2000) Programmed ascospore death in the homothallic ascomycete Coniochaeta tetraspora. *Fungal Genet Biol* 30(3):213-221.

93. Lu BC, Gallo N, & Kues U (2003) White-cap mutants and meiotic apoptosis in the basidiomycete Coprinus cinereus. *Fungal Genet Biol* 39(1):82-93.

94. Umar MH & Griensven van LJLD (1997) Morphogenetic cell death in developing primordia of *Agaricus bisporus*. *Mycologia* 89:274-277.

95. Thrane C, Kaufmann U, Stummann BM, & Olsson S (2004) Activation of caspase-like activity and poly (ADP-ribose) polymerase degradation during sporulation in Aspergillus nidulans. *Fungal Genet Biol* 41(3):361-368.

96. Rizet G (1953) [Impossibility of obtaining uninterrupted and unlimited multiplication of the ascomycete Podospora anserina]. *C R Hebd Seances Acad Sci* 237(15):838-840.

97. Jones EY, Tormo J, Reid SW, & Stuart DI (1998) Recognition surfaces of MHC class I. *Immunol Rev* 163:121-128.

98. Biella S, Smith ML, Aist JR, Cortesi P, & Milgroom MG (2002) Programmed cell death correlates with virus transmission in a filamentous fungus. *Proc Biol Sci* 269(1506):2269-2276.

99. Debets AJM & Griffiths AJF (1998) Polymorphism of het-genes prevents resource plundering in *Neurospora crassa*. *Mycol Res* 102:1343-1349.

100. Debets F, Yang X, & Griffiths AJ (1994) Vegetative incompatibility in Neurospora: its effect on horizontal transfer of mitochondrial plasmids and senescence in natural populations. *Curr Genet* 26(2):113-119.

101. van Diepeningen AD, Debets AJ, & Hoekstra RF (1997) Heterokaryon incompatibility blocks virus transfer among natural isolates of black Aspergilli. *Curr Genet* 32(3):209-217.

102. Marek SM, Wu J, Louise Glass N, Gilchrist DG, & Bostock RM (2003) Nuclear DNA degradation during heterokaryon incompatibility in Neurospora crassa. *Fungal Genet Biol* 40(2):126-137.

103. Wichmann G, Sun J, Dementhon K, Glass NL, & Lindow SE (2008) A novel gene, phcA from Pseudomonas syringae induces programmed cell death in the filamentous fungus Neurospora crassa. *Mol Microbiol* 68(3):672-689.

104. Pinan-Lucarre B, Paoletti M, Dementhon K, Coulary-Salin B, & Clave C (2003) Autophagy is induced during cell death by incompatibility and is essential for differentiation in the filamentous fungus Podospora anserina. *Mol Microbiol* 47(2):321-333.

105. Dementhon K*, et al.* (2003) Rapamycin mimics the incompatibility reaction in the fungus Podospora anserina. *Eukaryot Cell* 2(2):238-246.

106. Paoletti M & Clave C (2007) The fungus-specific HET domain mediates programmed cell death in Podospora anserina. *Eukaryot Cell* 6(11):2001-2008.

107. Finkelshtein A, Shlezinger N, Bunis O, & Sharon A (2011) Botrytis cinerea BcNma is involved in apoptotic cell death but not in stress adaptation. *Fungal Genet Biol* 48(6):621-630.

108. Roze LV & Linz JE (1998) Lovastatin triggers an apoptosis-like cell death process in the fungus Mucor racemosus. *Fungal Genet Biol* 25(2):119-133.

109. Ito S*, et al.* (2007) alpha-Tomatine, the major saponin in tomato, induces programmed cell death mediated by reactive oxygen species in the fungal pathogen Fusarium oxysporum. *FEBS Lett* 581(17):3217-3222.

110. Brandwagt BF*, et al.* (2000) A longevity assurance gene homolog of tomato mediates resistance to Alternaria alternata f. sp. lycopersici toxins and fumonisin B1. *Proc Natl Acad Sci U S A* 97(9):4961-4966.

111. Cheng J, Park TS, Chio LC, Fischl AS, & Ye XS (2003) Induction of apoptosis by sphingoid long-chain bases in Aspergillus nidulans. *Mol Cell Biol* 23(1):163-177.

112. Plesofsky NS, Levery SB, Castle SA, & Brambl R (2008) Stress-induced cell death is mediated by ceramide synthesis in Neurospora crassa. *Eukaryot Cell* 7(12):2147-2159.

113. Castro A, Lemos C, Falcao A, Glass NL, & Videira A (2008) Increased resistance of complex I mutants to phytosphingosine-induced programmed cell death. *J Biol Chem* 283(28):19314-19321.

114. Fernandes AS, Castro A, & Videira A (2013) Reduced glutathione export during programmed cell death of Neurospora crassa. *Apoptosis* 18(8):940-948.

115. Li L*, et al.* (2012) The translin-TRAX complex (C3PO) is a ribonuclease in tRNA processing. *Nat Struct Mol Biol* 19(8):824-830.

116. Videira A*, et al.* (2009) Transcriptional analysis of the response of Neurospora crassa to phytosphingosine reveals links to mitochondrial function. *Microbiology* 155(Pt 9):3134-3141.

117. Mousavi SA & Robson GD (2004) Oxidative and amphotericin B-mediated cell death in the opportunistic pathogen Aspergillus fumigatus is associated with an apoptotic-like phenotype. *Microbiology* 150(Pt 6):1937-1945.

118. Bowman JC*, et al.* (2002) The antifungal echinocandin caspofungin acetate kills growing cells of Aspergillus fumigatus in vitro. *Antimicrob Agents Chemother* 46(9):3001-3012.

119. Shirazi F & Kontoyiannis DP (2013) The calcineurin pathway inhibitor tacrolimus enhances the in vitro activity of azoles against mucorales via apoptosis. *Eukaryot Cell* 12(9):1225-1234.

120. Shirazi F & Kontoyiannis DP (2013) Mitochondrial respiratory pathways inhibition in Rhizopus oryzae potentiates activity of posaconazole and itraconazole via apoptosis. *PLoS One* 8(5):e63393.

121. Palma-Guerrero J*, et al.* (2009) Chitosan permeabilizes the plasma membrane and kills cells of Neurospora crassa in an energy dependent manner. *Fungal Genet Biol* 46(8):585-594.

122. Kretschmer M, Klose J, & Kronstad JW (2012) Defects in mitochondrial and peroxisomal beta-oxidation influence virulence in the maize pathogen Ustilago maydis. *Eukaryot Cell* 11(8):1055-1066.

123. Franco FP*, et al.* (2014) The Sugarcane Defense Protein SUGARWIN2 Causes Cell Death in Colletotrichum falcatum but Not in Non-Pathogenic Fungi. *PLoS One* 9(3):e91159.

124. Tian J*, et al.* (2012) The mechanism of antifungal action of essential oil from dill (Anethum graveolens L.) on Aspergillus flavus. *PLoS One* 7(1):e30147.

125. Fujita KI, Tatsumi M, Ogita A, Kubo I, & Tanaka T (2014) Anethole induces apoptotic cell death accompanied by reactive oxygen species production and DNA fragmentation in Aspergillus fumigatus and Saccharomyces cerevisiae. *FEBS J*.

126. Binder U, Chu M, Read ND, & Marx F (2010) The antifungal activity of the Penicillium chrysogenum protein PAF disrupts calcium homeostasis in Neurospora crassa. *Eukaryot Cell* 9(9):1374-1382.

127. Leiter E*, et al.* (2005) Antifungal protein PAF severely affects the integrity of the plasma membrane of Aspergillus nidulans and induces an apoptosis-like phenotype. *Antimicrob Agents Chemother* 49(6):2445-2453.

128. Shi M*, et al.* (2012) Antimicrobial peptaibols from Trichoderma pseudokoningii induce programmed cell death in plant fungal pathogens. *Microbiology* 158(Pt 1):166-175.

129. Krizsan K*, et al.* (2010) Effect of the sesterterpene-type metabolites, ophiobolins A and B, on zygomycetes fungi. *FEMS Microbiol Lett* 313(2):135-140.

130. Cheng CH, Yang CA, & Peng KC (2012) Antagonism of Trichoderma harzianum ETS 323 on Botrytis cinerea mycelium in culture conditions. *Phytopathology* 102(11):1054-1063.

131. de Castro Pimentel Figueiredo B, de Castro PA, Dinamarco TM, Goldman MH, & Goldman GH (2011) The Aspergillus nidulans nucA(EndoG) homologue is not involved in cell death. *Eukaryot Cell* 10(2):276-283.

132. Liu P*, et al.* (2010) Farnesol induces apoptosis and oxidative stress in the fungal pathogen Penicillium expansum. *Mycologia* 102(2):311-318.

133. Savoldi M*, et al.* (2008) Farnesol induces the transcriptional accumulation of the Aspergillus nidulans Apoptosis-Inducing Factor (AIF)-like mitochondrial oxidoreductase. *Mol Microbiol* 70(1):44-59.

134. Semighini CP, Hornby JM, Dumitru R, Nickerson KW, & Harris SD (2006) Farnesol-induced apoptosis in Aspergillus nidulans reveals a possible mechanism for antagonistic interactions between fungi. *Mol Microbiol* 59(3):753-764.

135. Semighini CP, Savoldi M, Goldman GH, & Harris SD (2006) Functional characterization of the putative Aspergillus nidulans poly(ADP-ribose) polymerase homolog PrpA. *Genetics* 173(1):87-98.

136. Semighini CP, Murray N, & Harris SD (2008) Inhibition of Fusarium graminearum growth and development by farnesol. *FEMS Microbiol Lett* 279(2):259-264.

137. Colabardini AC*, et al.* (2010) Involvement of the Aspergillus nidulans protein kinase C with farnesol tolerance is related to the unfolded protein response. *Mol Microbiol* 78(5):1259-1279.

138. Dinamarco TM*, et al.* (2010) The roles played by Aspergillus nidulans apoptosis-inducing factor (AIF)-like mitochondrial oxidoreductase (AifA) and NADH-ubiquinone oxidoreductases (NdeA-B and NdiA) in farnesol resistance. *Fungal Genet Biol* 47(12):1055-1069.

139. Castro A*, et al.* (2010) Rotenone enhances the antifungal properties of staurosporine. *Eukaryot Cell* 9(6):906-914.

140. Fernandes AS*, et al.* (2011) Modulation of fungal sensitivity to staurosporine by targeting proteins identified by transcriptional profiling. *Fungal Genet Biol* 48(12):1130-1138.

141. Qi G*, et al.* (2010) Lipopeptide induces apoptosis in fungal cells by a mitochondria-dependent pathway. *Peptides* 31(11):1978-1986.

142. Munoz A, Marcos JF, & Read ND (2012) Concentration-dependent mechanisms of cell penetration and killing by the de novo designed antifungal hexapeptide PAF26. *Mol Microbiol* 85(1):89-106.

143. Munoz A*, et al.* (2013) Two functional motifs define the interaction, internalization and toxicity of the cell-penetrating antifungal peptide PAF26 on fungal cells. *PLoS One* 8(1):e54813.

144. Barbu EM*, et al.* (2013) An antimicrobial peptidomimetic induces mucorales cell death through mitochondria-mediated apoptosis. *PLoS One* 8(10):e76981.

145. Carneiro P, Duarte M, & Videira A (2012) Disruption of alternative NAD(P)H dehydrogenases leads to decreased mitochondrial ROS in Neurospora crassa. *Free Radic Biol Med* 52(2):402-409.

146. Chen C & Dickman MB (2005) Proline suppresses apoptosis in the fungal pathogen Colletotrichum trifolii. *Proc Natl Acad Sci U S A* 102(9):3459-3464.

147. Duarte M & Videira A (2012) Defective valyl-tRNA synthetase hampers the mitochondrial respiratory chain in Neurospora crassa. *Biochem J* 448(3):297-306.

148. Carneiro P, Duarte M, & Videira A (2012) Characterization of apoptosis-related oxidoreductases from Neurospora crassa. *PLoS One* 7(3):e34270.

149. Duarte M & Videira A (2009) Effects of mitochondrial complex III disruption in the respiratory chain of Neurospora crassa. *Mol Microbiol* 72(1):246-258.

150. Azevedo MM, Almeida B, Ludovico P, & Cassio F (2009) Metal stress induces programmed cell death in aquatic fungi. *Aquat Toxicol* 92(4):264-270.

151. Savi GD, Vitorino V, Bortoluzzi AJ, & Scussel VM (2013) Effect of zinc compounds on Fusarium verticillioides growth, hyphae alterations, conidia, and fumonisin production. *J Sci Food Agric* 93(13):3395-3402.

152. Gaddameedi RR, Burgula S, Sairam M, & Singh SS (2011) Role of insulin in Cr(VI)-mediated genotoxicity in Neurospora crassa. *Lett Appl Microbiol* 53(1):14-21.

153. Adam AL, Kohut G, & Hornok L (2008) Fphog1, a HOG-type MAP kinase gene, is involved in multistress response in Fusarium proliferatum. *J Basic Microbiol* 48(3):151-159.

154. Baltazar Lde M*, et al.* (2013) Photodynamic inhibition of Trichophyton rubrum: in vitro activity and the role of oxidative and nitrosative bursts in fungal death. *J Antimicrob Chemother* 68(2):354-361.

155. Richie DL*, et al.* (2007) The Aspergillus fumigatus metacaspases CasA and CasB facilitate growth under conditions of endoplasmic reticulum stress. *Mol Microbiol* 63(2):591-604.

156. Mousavi SA & Robson GD (2003) Entry into the stationary phase is associated with a rapid loss of viability and an apoptotic-like phenotype in the opportunistic pathogen Aspergillus fumigatus. *Fungal Genet Biol* 39(3):221-229.

157. Emri T, Molnar Z, & Pocsi I (2005) The appearances of autolytic and apoptotic markers are concomitant but differently regulated in carbon-starving Aspergillus nidulans cultures. *FEMS Microbiol Lett* 251(2):297-303.

158. Nitsche BM, Jorgensen TR, Akeroyd M, Meyer V, & Ram AF (2012) The carbon starvation response of Aspergillus niger during submerged cultivation: insights from the transcriptome and secretome. *BMC Genomics* 13:380.

159. Krohn NG*, et al.* (2014) The Aspergillus nidulans ATM Kinase Regulates Mitochondrial Function, Glucose Uptake and the Carbon Starvation Response. *G3 (Bethesda)* 4(1):49-62.

160. Munkres KD (1976) Ageing of Neurospora crassa. III. Induction of cellular death and clonal senescence of an inositol-less mutant by inositol starvation and the protective effect of dietary antioxidants. *Mech Ageing Dev* 5(3):163-169.

161. Strauss BS (1958) Cell death and unbalanced growth in Neurospora. *J Gen Microbiol* 18(3):658-669.

162. Li H*, et al.* (2007) Glycosylphosphatidylinositol (GPI) anchor is required in Aspergillus fumigatus for morphogenesis and virulence. *Mol Microbiol* 64(4):1014-1027.

163. Yan J*, et al.* (2013) Transcriptome and biochemical analysis reveals that suppression of GPI-anchor synthesis leads to autophagy and possible necroptosis in Aspergillus fumigatus. *PLoS One* 8(3):e59013.

164. Tao L, Gao N, Chen S, & Yu JH (2010) The choC gene encoding a putative phospholipid methyltransferase is essential for growth and development in Aspergillus nidulans. *Curr Genet* 56(3):283-296.

165. Bok JW, Ishida K, & Griffiths AJ (2003) Ultrastructural changes in Neurospora cells undergoing senescence induced by kalilo plasmids. *Mycologia* 95(3):500-505.

166. Griffiths AJ & Bertrand H (1984) Unstable cytoplasms in Hawaiian strains of Neurospora intermedia. *Curr Genet* 8(5):387-398.

167. Barhoom S & Sharon A (2007) Bcl-2 proteins link programmed cell death with growth and morphogenetic adaptations in the fungal plant pathogen Colletotrichum gloeosporioides. *Fungal Genet Biol* 44(1):32-43.

168. Plesofsky-Vig N & Brambl R (1995) Disruption of the gene for hsp30, an alpha-crystallin-related heat shock protein of Neurospora crassa, causes defects in thermotolerance. *Proc Natl Acad Sci U S A* 92(11):5032-5036.

169. Silar P (2005) Peroxide accumulation and cell death in filamentous fungi induced by contact with a contestant. *Mycol Res* 109(Pt 2):137-149.

170. Morales A, Lee H, Goni FM, Kolesnick R, & Fernandez-Checa JC (2007) Sphingolipids and cell death. *Apoptosis* 12(5):923-939.

171. Jenkins GM*, et al.* (1997) Involvement of yeast sphingolipids in the heat stress response of Saccharomyces cerevisiae. *J Biol Chem* 272(51):32566-32572.

172. Yamagata M, Obara K, & Kihara A (2013) Unperverted synthesis of complex sphingolipids is essential for cell survival under nitrogen starvation. *Genes Cells* 18(8):650-659.

173. Nagiec MM*, et al.* (1997) Sphingolipid synthesis as a target for antifungal drugs. Complementation of the inositol phosphorylceramide synthase defect in a mutant strain of Saccharomyces cerevisiae by the AUR1 gene. *J Biol Chem* 272(15):9809-9817.

174. Omura S*, et al.* (1977) A new alkaloid AM-2282 OF Streptomyces origin. Taxonomy, fermentation, isolation and preliminary characterization. *J Antibiot (Tokyo)* 30(4):275-282.

175. Karaman MW*, et al.* (2008) A quantitative analysis of kinase inhibitor selectivity. *Nat Biotechnol* 26(1):127-132.

176. Yoshida S, Ikeda E, Uno I, & Mitsuzawa H (1992) Characterization of a staurosporine- and temperature-sensitive mutant, stt1, of Saccharomyces cerevisiae: STT1 is allelic to PKC1. *Mol Gen Genet* 231(3):337-344.

177. Gani OA & Engh RA (2010) Protein kinase inhibition of clinically important staurosporine analogues. *Nat Prod Rep* 27(4):489-498.

178. Breier A, Barancik M, Sulova Z, & Uhrik B (2005) P-glycoprotein--implications of metabolism of neoplastic cells and cancer therapy. *Curr Cancer Drug Targets* 5(6):457-468.

179. Yoshida S & Anraku Y (2000) Characterization of staurosporine-sensitive mutants of Saccharomyces cerevisiae: vacuolar functions affect staurosporine sensitivity. *Mol Gen Genet* 263(5):877-888.

180. Yoshida S, Ohya Y, Goebl M, Nakano A, & Anraku Y (1994) A novel gene, STT4, encodes a phosphatidylinositol 4-kinase in the PKC1 protein kinase pathway of Saccharomyces cerevisiae. *J Biol Chem* 269(2):1166-1172.

181. Yoshida S, Ohya Y, Nakano A, & Anraku Y (1994) Genetic interactions among genes involved in the STT4-PKC1 pathway of Saccharomyces cerevisiae. *Mol Gen Genet* 242(6):631-640.

182. Hegedus N*, et al.* (2011) The small molecular mass antifungal protein of Penicillium chrysogenum--a mechanism of action oriented review. *J Basic Microbiol* 51(6):561-571.

183. Marx F, Binder U, Leiter E, & Pocsi I (2008) The Penicillium chrysogenum antifungal protein PAF, a promising tool for the development of new antifungal therapies and fungal cell biology studies. *Cell Mol Life Sci* 65(3):445-454.

184. Szappanos H*, et al.* (2005) The Penicillium chrysogenum-derived antifungal peptide shows no toxic effects on mammalian cells in the intended therapeutic concentration. *Naunyn Schmiedebergs Arch Pharmacol* 371(2):122-132.

185. Binder U, Oberparleiter C, Meyer V, & Marx F (2010) The antifungal protein PAF interferes with PKC/MPK and cAMP/PKA signalling of Aspergillus nidulans. *Mol Microbiol* 75(2):294-307.

186. Dinamarco TM, Goldman MH, & Goldman GH (2011) Farnesol-induced cell death in the filamentous fungus Aspergillus nidulans. *Biochem Soc Trans* 39(5):1544-1548.

187. Joo JH & Jetten AM (2010) Molecular mechanisms involved in farnesol-induced apoptosis. *Cancer Lett* 287(2):123-135.

188. Hornby JM*, et al.* (2001) Quorum sensing in the dimorphic fungus Candida albicans is mediated by farnesol. *Appl Environ Microbiol* 67(7):2982-2992.

189. Fedorova ND, Badger JH, Robson GD, Wortman JR, & Nierman WC (2005) Comparative analysis of programmed cell death pathways in filamentous fungi. *BMC Genomics* 6:177.

190. Shlezinger N, Doron A, & Sharon A (2011) Apoptosis-like programmed cell death in the grey mould fungus Botrytis cinerea: genes and their role in pathogenicity. *Biochem Soc Trans* 39(5):1493-1498.

191. Buttner S*, et al.* (2011) A yeast BH3-only protein mediates the mitochondrial pathway of apoptosis. *EMBO J* 30(14):2779-2792.

192. Ludovico P*, et al.* (2002) Cytochrome c release and mitochondria involvement in programmed cell death induced by acetic acid in Saccharomyces cerevisiae. *Mol Biol Cell* 13(8):2598-2606.

193. Pereira C, Camougrand N, Manon S, Sousa MJ, & Corte-Real M (2007) ADP/ATP carrier is required for mitochondrial outer membrane permeabilization and cytochrome c release in yeast apoptosis. *Mol Microbiol* 66(3):571-582.

194. Vahsen N*, et al.* (2004) AIF deficiency compromises oxidative phosphorylation. *EMBO J* 23(23):4679-4689.

195. Wissing S*, et al.* (2004) An AIF orthologue regulates apoptosis in yeast. *J Cell Biol* 166(7):969-974.

196. Wu M, Xu LG, Li X, Zhai Z, & Shu HB (2002) AMID, an apoptosis-inducing factor-homologous mitochondrion-associated protein, induces caspase-independent apoptosis. *J Biol Chem* 277(28):25617-25623.

197. Brust D, Hamann A, & Osiewacz HD (2010) Deletion of PaAif2 and PaAmid2, two genes encoding mitochondrial AIF-like oxidoreductases of Podospora anserina, leads to increased stress tolerance and lifespan extension. *Curr Genet* 56(3):225-235.

198. Cote J & Ruiz-Carrillo A (1993) Primers for mitochondrial DNA replication generated by endonuclease G. *Science* 261(5122):765-769.

199. Burhans WC & Weinberger M (2007) Yeast endonuclease G: complex matters of death, and of life. *Mol Cell* 25(3):323-325.

200. Fahrenkrog B, Sauder U, & Aebi U (2004) The S. cerevisiae HtrA-like protein Nma111p is a nuclear serine protease that mediates yeast apoptosis. *J Cell Sci* 117(Pt 1):115-126.

201. Alnemri ES*, et al.* (1996) Human ICE/CED-3 protease nomenclature. *Cell* 87(2):171.

202. Fuentes-Prior P & Salvesen GS (2004) The protein structures that shape caspase activity, specificity, activation and inhibition. *Biochem J* 384(Pt 2):201-232.

203. Pop C & Salvesen GS (2009) Human caspases: activation, specificity, and regulation. *J Biol Chem* 284(33):21777-21781.

204. Uren AG*, et al.* (2000) Identification of paracaspases and metacaspases: two ancient families of caspase-like proteins, one of which plays a key role in MALT lymphoma. *Mol Cell* 6(4):961-967.

205. Carmona-Gutierrez D, Frohlich KU, Kroemer G, & Madeo F (2010) Metacaspases are caspases. Doubt no more. *Cell Death Differ* 17(3):377-378.

206. Enoksson M & Salvesen GS (2010) Metacaspases are not caspases--always doubt. *Cell Death Differ* 17(8):1221.

207. Vercammen D, Declercq W, Vandenabeele P, & Van Breusegem F (2007) Are metacaspases caspases? *J Cell Biol* 179(3):375-380.

208. Sundstrom JF*, et al.* (2009) Tudor staphylococcal nuclease is an evolutionarily conserved component of the programmed cell death degradome. *Nat Cell Biol* 11(11):1347-1354.

209. Coll NS*, et al.* (2010) Arabidopsis type I metacaspases control cell death. *Science* 330(6009):1393-1397.

210. Vercammen D*, et al.* (2004) Type II metacaspases Atmc4 and Atmc9 of Arabidopsis thaliana cleave substrates after arginine and lysine. *J Biol Chem* 279(44):45329-45336.

211. Vercammen D*, et al.* (2006) Serpin1 of Arabidopsis thaliana is a suicide inhibitor for metacaspase 9. *J Mol Biol* 364(4):625-636.

212. Watanabe N & Lam E (2005) Two Arabidopsis metacaspases AtMCP1b and AtMCP2b are arginine/lysine-specific cysteine proteases and activate apoptosis-like cell death in yeast. *J Biol Chem* 280(15):14691-14699.

213. Tamura K*, et al.* (2011) MEGA5: molecular evolutionary genetics analysis using maximum likelihood, evolutionary distance, and maximum parsimony methods. *Mol Biol Evol* 28(10):2731-2739.

214. Madeo F*, et al.* (2002) A caspase-related protease regulates apoptosis in yeast. *Mol Cell* 9(4):911-917.

215. Dantzer F*, et al.* (2000) Base excision repair is impaired in mammalian cells lacking Poly(ADP-ribose) polymerase-1. *Biochemistry* 39(25):7559-7569.

216. Strobel I & Osiewacz HD (2013) Poly(ADP-ribose) polymerase is a substrate recognized by two metacaspases of Podospora anserina. *Eukaryot Cell* 12(6):900-912.

217. Alberts B*, et al.* (2008) *Molecular Biology of the Cell* (Garland Science, Taylor and Francis Group, New York City NY, USA) 5th Edition Ed.

218. Dudkina NV, Kouril R, Peters K, Braun HP, & Boekema EJ (2010) Structure and function of mitochondrial supercomplexes. *Biochim Biophys Acta* 1797(6-7):664-670.

219. Lenaz G & Genova ML (2010) Structure and organization of mitochondrial respiratory complexes: a new understanding of an old subject. *Antioxid Redox Signal* 12(8):961-1008.

220. Marques I, Dencher NA, Videira A, & Krause F (2007) Supramolecular organization of the respiratory chain in Neurospora crassa mitochondria. *Eukaryot Cell* 6(12):2391-2405.

221. Wittig I, Carrozzo R, Santorelli FM, & Schagger H (2006) Supercomplexes and subcomplexes of mitochondrial oxidative phosphorylation. *Biochim Biophys Acta* 1757(9-10):1066-1072.

222. Videira A (1998) Complex I from the fungus Neurospora crassa. *Biochim Biophys Acta* 1364(2):89-100.

223. Buschges R, Bahrenberg G, Zimmermann M, & Wolf K (1994) NADH: ubiquinone oxidoreductase in obligate aerobic yeasts. *Yeast* 10(4):475-479.

224. Zickermann V*, et al.* (2009) Architecture of complex I and its implications for electron transfer and proton pumping. *Biochim Biophys Acta* 1787(6):574-583.

225. Carroll J*, et al.* (2006) Bovine complex I is a complex of 45 different subunits. *J Biol Chem* 281(43):32724-32727.

226. Marques I, Duarte M, Assuncao J, Ushakova AV, & Videira A (2005) Composition of complex I from Neurospora crassa and disruption of two "accessory" subunits. *Biochim Biophys Acta* 1707(2-3):211-220.

227. Brandt U (2006) Energy converting NADH:quinone oxidoreductase (complex I). *Annu Rev Biochem* 75:69-92.

228. Pereira B, Videira A, & Duarte M (2013) Novel insights into the role of Neurospora crassa NDUFAF2, an evolutionarily conserved mitochondrial complex I assembly factor. *Mol Cell Biol* 33(13):2623-2634.

229. Lenaz G*, et al.* (2006) Mitochondrial Complex I: structural and functional aspects. *Biochim Biophys Acta* 1757(9-10):1406-1420.

230. Koopman WJ*, et al.* (2010) Mammalian mitochondrial complex I: biogenesis, regulation, and reactive oxygen species generation. *Antioxid Redox Signal* 12(12):1431-1470.

231. Pagniez-Mammeri H*, et al.* (2012) Mitochondrial complex I deficiency of nuclear origin I. Structural genes. *Mol Genet Metab* 105(2):163-172.

232. Duarte M, Schulte U, Ushakova AV, & Videira A (2005) Neurospora strains harboring mitochondrial disease-associated mutations in iron-sulfur subunits of complex I. *Genetics* 171(1):91-99.

233. Melo AM, Bandeiras TM, & Teixeira M (2004) New insights into type II NAD(P)H:quinone oxidoreductases. *Microbiol Mol Biol Rev* 68(4):603-616.

234. Rasmusson AG, Geisler DA, & Moller IM (2008) The multiplicity of dehydrogenases in the electron transport chain of plant mitochondria. *Mitochondrion* 8(1):47-60.

235. De Vries S, Van Witzenburg R, Grivell LA, & Marres CA (1992) Primary structure and import pathway of the rotenone-insensitive NADH-ubiquinone oxidoreductase of mitochondria from Saccharomyces cerevisiae. *Eur J Biochem* 203(3):587-592.

236. Luttik MA*, et al.* (1998) The Saccharomyces cerevisiae NDE1 and NDE2 genes encode separate mitochondrial NADH dehydrogenases catalyzing the oxidation of cytosolic NADH. *J Biol Chem* 273(38):24529-24534.

237. Dong CK*, et al.* (2009) Type II NADH dehydrogenase of the respiratory chain of Plasmodium falciparum and its inhibitors. *Bioorg Med Chem Lett* 19(3):972-975.

238. Biagini GA, Viriyavejakul P, O'Neill P M, Bray PG, & Ward SA (2006) Functional characterization and target validation of alternative complex I of Plasmodium falciparum mitochondria. *Antimicrob Agents Chemother* 50(5):1841-1851.

239. Matus-Ortega MG*, et al.* (2011) The alternative NADH dehydrogenase is present in mitochondria of some animal taxa. *Comp Biochem Physiol Part D Genomics Proteomics* 6(3):256-263.

240. Duarte M, Peters M, Schulte U, & Videira A (2003) The internal alternative NADH dehydrogenase of Neurospora crassa mitochondria. *Biochem J* 371(Pt 3):1005-1011.

241. Melo AM, Duarte M, & Videira A (1999) Primary structure and characterisation of a 64 kDa NADH dehydrogenase from the inner membrane of Neurospora crassa mitochondria. *Biochim Biophys Acta* 1412(3):282-287.

242. Melo AM*, et al.* (2001) The external calcium-dependent NADPH dehydrogenase from Neurospora crassa mitochondria. *J Biol Chem* 276(6):3947-3951.

243. Carneiro P, Duarte M, & Videira A (2004) The main external alternative NAD(P)H dehydrogenase of Neurospora crassa mitochondria. *Biochim Biophys Acta* 1608(1):45-52.

244. Carneiro P, Duarte M, & Videira A (2007) The external alternative NAD(P)H dehydrogenase NDE3 is localized both in the mitochondria and in the cytoplasm of Neurospora crassa. *J Mol Biol* 368(4):1114-1121.

245. Elhafez D*, et al.* (2006) Characterization of mitochondrial alternative NAD(P)H dehydrogenases in Arabidopsis: intraorganelle location and expression. *Plant Cell Physiol* 47(1):43-54.

246. Rasmusson AG, Svensson AS, Knoop V, Grohmann L, & Brennicke A (1999) Homologues of yeast and bacterial rotenone-insensitive NADH dehydrogenases in higher eukaryotes: two enzymes are present in potato mitochondria. *Plant J* 20(1):79-87.

247. Carrie C*, et al.* (2008) Type II NAD(P)H dehydrogenases are targeted to mitochondria and chloroplasts or peroxisomes in Arabidopsis thaliana. *FEBS Lett* 582(20):3073-3079.

248. Grandier-Vazeille X*, et al.* (2001) Yeast mitochondrial dehydrogenases are associated in a supramolecular complex. *Biochemistry* 40(33):9758-9769.

249. Guerrero-Castillo S, Vazquez-Acevedo M, Gonzalez-Halphen D, & Uribe-Carvajal S (2009) In Yarrowia lipolytica mitochondria, the alternative NADH dehydrogenase interacts specifically with the cytochrome complexes of the classic respiratory pathway. *Biochim Biophys Acta* 1787(2):75-85.

250. Guerrero-Castillo S, Cabrera-Orefice A, Vazquez-Acevedo M, Gonzalez-Halphen D, & Uribe-Carvajal S (2012) During the stationary growth phase, Yarrowia lipolytica prevents the overproduction of reactive oxygen species by activating an uncoupled mitochondrial respiratory pathway. *Biochim Biophys Acta* 1817(2):353-362.

251. Michalecka AM, Agius SC, Moller IM, & Rasmusson AG (2004) Identification of a mitochondrial external NADPH dehydrogenase by overexpression in transgenic Nicotiana sylvestris. *Plant J* 37(3):415-425.

252. Geisler DA, Broselid C, Hederstedt L, & Rasmusson AG (2007) Ca2+-binding and Ca2+-independent respiratory NADH and NADPH dehydrogenases of Arabidopsis thaliana. *J Biol Chem* 282(39):28455-28464.

253. Rasmusson AG & Wallstrom SV (2010) Involvement of mitochondria in the control of plant cell NAD(P)H reduction levels. *Biochem Soc Trans* 38(2):661-666.

254. Seo BB, Marella M, Yagi T, & Matsuno-Yagi A (2006) The single subunit NADH dehydrogenase reduces generation of reactive oxygen species from complex I. *FEBS Lett* 580(26):6105-6108.

255. Fang J & Beattie DS (2003) External alternative NADH dehydrogenase of Saccharomyces cerevisiae: a potential source of superoxide. *Free Radic Biol Med* 34(4):478-488.

256. Davidson JF & Schiestl RH (2001) Mitochondrial respiratory electron carriers are involved in oxidative stress during heat stress in Saccharomyces cerevisiae. *Mol Cell Biol* 21(24):8483-8489.

257. Li W*, et al.* (2006) Yeast AMID homologue Ndi1p displays respiration-restricted apoptotic activity and is involved in chronological aging. *Mol Biol Cell* 17(4):1802-1811.

258. Seo BB*, et al.* (1998) Molecular remedy of complex I defects: rotenone-insensitive internal NADH-quinone oxidoreductase of Saccharomyces cerevisiae mitochondria restores the NADH oxidase activity of complex I-deficient mammalian cells. *Proc Natl Acad Sci U S A* 95(16):9167-9171.

259. Seo BB, Nakamaru-Ogiso E, Flotte TR, Matsuno-Yagi A, & Yagi T (2006) In vivo complementation of complex I by the yeast Ndi1 enzyme. Possible application for treatment of Parkinson disease. *J Biol Chem* 281(20):14250-14255.

260. Marella M*, et al.* (2008) Protection by the NDI1 gene against neurodegeneration in a rotenone rat model of Parkinson's disease. *PLoS One* 3(1):e1433.

261. Marella M, Seo BB, Thomas BB, Matsuno-Yagi A, & Yagi T (2010) Successful amelioration of mitochondrial optic neuropathy using the yeast NDI1 gene in a rat animal model. *PLoS One* 5(7):e11472.

262. Santidrian AF*, et al.* (2013) Mitochondrial complex I activity and NAD+/NADH balance regulate breast cancer progression. *J Clin Invest* 123(3):1068-1081.

263. Angell JE, Lindner DJ, Shapiro PS, Hofmann ER, & Kalvakolanu DV (2000) Identification of GRIM-19, a novel cell death-regulatory gene induced by the interferon-beta and retinoic acid combination, using a genetic approach. *J Biol Chem* 275(43):33416-33426.

264. Fearnley IM*, et al.* (2001) GRIM-19, a cell death regulatory gene product, is a subunit of bovine mitochondrial NADH:ubiquinone oxidoreductase (complex I). *J Biol Chem* 276(42):38345-38348.

265. Huang G*, et al.* (2004) GRIM-19, a cell death regulatory protein, is essential for assembly and function of mitochondrial complex I. *Mol Cell Biol* 24(19):8447-8456.

266. Huang G, Chen Y, Lu H, & Cao X (2007) Coupling mitochondrial respiratory chain to cell death: an essential role of mitochondrial complex I in the interferon-beta and retinoic acid-induced cancer cell death. *Cell Death Differ* 14(2):327-337.

267. Reeves MB, Davies AA, McSharry BP, Wilkinson GW, & Sinclair JH (2007) Complex I binding by a virally encoded RNA regulates mitochondria-induced cell death. *Science* 316(5829):1345-1348.

268. Moreira S, Correia M, Soares P, & Maximo V (2011) GRIM-19 function in cancer development. *Mitochondrion* 11(5):693-699.

269. Martinvalet D, Dykxhoorn DM, Ferrini R, & Lieberman J (2008) Granzyme A cleaves a mitochondrial complex I protein to initiate caspase-independent cell death. *Cell* 133(4):681-692.

270. Ricci JE*, et al.* (2004) Disruption of mitochondrial function during apoptosis is mediated by caspase cleavage of the p75 subunit of complex I of the electron transport chain. *Cell* 117(6):773-786.

271. Ricci JE, Gottlieb RA, & Green DR (2003) Caspase-mediated loss of mitochondrial function and generation of reactive oxygen species during apoptosis. *J Cell Biol* 160(1):65-75.

272. Ladha JS, Tripathy MK, & Mitra D (2005) Mitochondrial complex I activity is impaired during HIV-1-induced T-cell apoptosis. *Cell Death Differ* 12(11):1417-1428.

273. Lartigue L*, et al.* (2009) Caspase-independent mitochondrial cell death results from loss of respiration, not cytotoxic protein release. *Mol Biol Cell* 20(23):4871-4884.

274. Dey R & Moraes CT (2000) Lack of oxidative phosphorylation and low mitochondrial membrane potential decrease susceptibility to apoptosis and do not modulate the protective effect of Bcl-x(L) in osteosarcoma cells. *J Biol Chem* 275(10):7087-7094.

275. Chen ZX & Pervaiz S (2007) Bcl-2 induces pro-oxidant state by engaging mitochondrial respiration in tumor cells. *Cell Death Differ* 14(9):1617-1627.

276. Lemarie A, Huc L, Pazarentzos E, Mahul-Mellier AL, & Grimm S (2011) Specific disintegration of complex II succinate:ubiquinone oxidoreductase links pH changes to oxidative stress for apoptosis induction. *Cell Death Differ* 18(2):338-349.

277. Zubovych IO, Straud S, & Roth MG (2010) Mitochondrial dysfunction confers resistance to multiple drugs in Caenorhabditis elegans. *Mol Biol Cell* 21(6):956-969.

278. Li D*, et al.* (2011) Enzymatic dysfunction of mitochondrial complex I of the Candida albicans goa1 mutant is associated with increased reactive oxidants and cell death. *Eukaryot Cell* 10(5):672-682.

279. Sun N*, et al.* (2013) Azole susceptibility and transcriptome profiling in Candida albicans mitochondrial electron transport chain complex I mutants. *Antimicrob Agents Chemother* 57(1):532-542.

280. Matsuyama S, Xu Q, Velours J, & Reed JC (1998) The Mitochondrial F0F1-ATPase proton pump is required for function of the proapoptotic protein Bax in yeast and mammalian cells. *Mol Cell* 1(3):327-336.

281. Wang C*, et al.* (2014) Protective Effects of ETC Complex III and Cytochrome c against Hydrogen Peroxide-Induced Apoptosis in Yeast. *Free Radic Res*.

282. Cui Y, Zhao S, Wu Z, Dai P, & Zhou B (2012) Mitochondrial release of the NADH dehydrogenase Ndi1 induces apoptosis in yeast. *Mol Biol Cell* 23(22):4373-4382.

283. Marella M, Seo BB, Matsuno-Yagi A, & Yagi T (2007) Mechanism of cell death caused by complex I defects in a rat dopaminergic cell line. *J Biol Chem* 282(33):24146-24156.

284. Park JS, Li YF, & Bai Y (2007) Yeast NDI1 improves oxidative phosphorylation capacity and increases protection against oxidative stress and cell death in cells carrying a Leber's hereditary optic neuropathy mutation. *Biochim Biophys Acta* 1772(5):533-542.

285. Voulgaris I, O'Donnell A, Harvey LM, & McNeil B (2012) Inactivating alternative NADH dehydrogenases: enhancing fungal bioprocesses by improving growth and biomass yield? *Sci Rep* 2:322.

286. O'Donnell A, Harvey LM, & McNeil B (2011) The roles of the alternative NADH dehydrogenases during oxidative stress in cultures of the filamentous fungus Aspergillus niger. *Fungal Biol* 115(4-5):359-369.

287. Li W*, et al.* (2005) Yeast model uncovers dual roles of mitochondria in action of artemisinin. *PLoS Genet* 1(3):e36.

288. Emadi A, Ross AE, Cowan KM, Fortenberry YM, & Vuica-Ross M (2010) A chemical genetic screen for modulators of asymmetrical 2,2'-dimeric naphthoquinones cytotoxicity in yeast. *PLoS One* 5(5):e10846.

289. Clapham DE (2007) Calcium signaling. *Cell* 131(6):1047-1058.

290. Berridge MJ, Lipp P, & Bootman MD (2000) The versatility and universality of calcium signalling. *Nat Rev Mol Cell Biol* 1(1):11-21.

291. Carafoli E (2002) Calcium signaling: a tale for all seasons. *Proc Natl Acad Sci U S A* 99(3):1115-1122.

292. Cerella C, Diederich M, & Ghibelli L (2010) The dual role of calcium as messenger and stressor in cell damage, death, and survival. *Int J Cell Biol* 2010:546163.

293. Iida H, Yagawa Y, & Anraku Y (1990) Essential role for induced Ca2+ influx followed by [Ca2+]i rise in maintaining viability of yeast cells late in the mating pheromone response pathway. A study of [Ca2+]i in single Saccharomyces cerevisiae cells with imaging of fura-2. *J Biol Chem* 265(22):13391-13399.

294. Miller AJ, Vogg G, & Sanders D (1990) Cytosolic calcium homeostasis in fungi: roles of plasma membrane transport and intracellular sequestration of calcium. *Proc Natl Acad Sci U S A* 87(23):9348-9352.

295. Halachmi D & Eilam Y (1989) Cytosolic and vacuolar Ca2+ concentrations in yeast cells measured with the Ca2+-sensitive fluorescence dye indo-1. *FEBS Lett* 256(1-2):55-61.

296. Carafoli E (1987) Intracellular calcium homeostasis. *Annu Rev Biochem* 56:395-433.

297. Malhó R (1998) Spatial characteristics to calcium signalling; the calcium wave as a basic unit in plant cell calcium signalling. *Philos Trans R Soc Lond B Biol Sci* 353(1374):1463-1473.

298. Thomas AP, Bird GS, Hajnoczky G, Robb-Gaspers LD, & Putney JW, Jr. (1996) Spatial and temporal aspects of cellular calcium signaling. *FASEB J* 10(13):1505-1517.

299. Berridge MJ (1995) Capacitative calcium entry. *Biochem J* 312 (Pt 1):1-11.

300. J OU, Pan S, & Sheu SS (2012) Perspectives on: SGP symposium on mitochondrial physiology and medicine: molecular identities of mitochondrial Ca2+ influx mechanism: updated passwords for accessing mitochondrial Ca2+-linked health and disease. *J Gen Physiol* 139(6):435-443.

301. De Stefani D*, et al.* (2012) VDAC1 selectively transfers apoptotic Ca2+ signals to mitochondria. *Cell Death Differ* 19(2):267-273.

302. McCormack JG, Halestrap AP, & Denton RM (1990) Role of calcium ions in regulation of mammalian intramitochondrial metabolism. *Physiol Rev* 70(2):391-425.

303. Robb-Gaspers LD*, et al.* (1998) Coupling between cytosolic and mitochondrial calcium oscillations: role in the regulation of hepatic metabolism. *Biochim Biophys Acta* 1366(1-2):17-32.

304. Moller IM, Johnston SP, & Palmer JM (1981) A specific role for Ca2+ in the oxidation of exogenous NADH by Jerusalem-artichoke (Helianthus tuberosus) mitochondria. *Biochem J* 194(2):487-495.

305. Zhou Y*, et al.* (2006) Prediction of EF-hand calcium-binding proteins and analysis of bacterial EF-hand proteins. *Proteins* 65(3):643-655.

306. Santamaria-Hernando S, Krell T, & Ramos-Gonzalez MI (2012) Identification of a novel calcium binding motif based on the detection of sequence insertions in the animal peroxidase domain of bacterial proteins. *PLoS One* 7(7):e40698.

307. Rigden DJ, Woodhead DD, Wong PW, & Galperin MY (2011) New structural and functional contexts of the Dx[DN]xDG linear motif: insights into evolution of calcium-binding proteins. *PLoS One* 6(6):e21507.

308. Rigden DJ & Galperin MY (2004) The DxDxDG motif for calcium binding: multiple structural contexts and implications for evolution. *J Mol Biol* 343(4):971-984.

309. Rigden DJ, Jedrzejas MJ, Moroz OV, & Galperin MY (2003) Structural diversity of calcium-binding proteins in bacteria: single-handed EF-hands? *Trends Microbiol* 11(7):295-297.

310. Naested H*, et al.* (2000) Caleosins: Ca2+-binding proteins associated with lipid bodies. *Plant Mol Biol* 44(4):463-476.

311. Cioci G*, et al.* (2006) Beta-propeller crystal structure of Psathyrella velutina lectin: an integrin-like fungal protein interacting with monosaccharides and calcium. *J Mol Biol* 357(5):1575-1591.

312. Nelson G*, et al.* (2004) Calcium measurement in living filamentous fungi expressing codon-optimized aequorin. *Mol Microbiol* 52(5):1437-1450.

313. Chiesa A*, et al.* (2001) Recombinant aequorin and green fluorescent protein as valuable tools in the study of cell signalling. *Biochem J* 355(Pt 1):1-12.

314. Tamuli R, Kumar R, Srivastava DA, & Deka R (2013) Calcium signalling. *Neurospora: Genomics and Molecular Biology*, eds Kasbekar DP & McCluskey K (Caister Academic Press, Norfolk, UK), pp 209-226.

315. Zelter A, Bencina M, Bowman BJ, Yarden O, & Read ND (2004) A comparative genomic analysis of the calcium signaling machinery in Neurospora crassa, Magnaporthe grisea, and Saccharomyces cerevisiae. *Fungal Genet Biol* 41(9):827-841.

316. Cornelius G, Gebauer G, & Techel D (1989) Inositol trisphosphate induces calcium release from Neurospora crassa vacuoles. *Biochem Biophys Res Commun* 162(2):852-856.

317. Lakin-Thomas PL (1993) Effects of inositol starvation on the levels of inositol phosphates and inositol lipids in Neurospora crassa. *Biochem J* 292 (Pt 3):805-811.

318. Brown EM*, et al.* (1993) Cloning and characterization of an extracellular Ca(2+)-sensing receptor from bovine parathyroid. *Nature* 366(6455):575-580.

319. Han S, Tang R, Anderson LK, Woerner TE, & Pei ZM (2003) A cell surface receptor mediates extracellular Ca(2+) sensing in guard cells. *Nature* 425(6954):196-200.

320. Lew RR (1999) Comparative analysis of Ca2+ and H+ flux magnitude and location along growing hyphae of Saprolegnia ferax and Neurospora crassa. *Eur J Cell Biol* 78(12):892-902.

321. Torralba S, Heath IB, & Ottensmeyer FP (2001) Ca(2+) shuttling in vesicles during tip growth in Neurospora crassa. *Fungal Genet Biol* 33(3):181-193.

322. Levina NN & Lew RR (2006) The role of tip-localized mitochondria in hyphal growth. *Fungal Genet Biol* 43(2):65-74.

323. Kim HS*, et al.* (2012) Expression of the Cameleon calcium biosensor in fungi reveals distinct Ca(2+) signatures associated with polarized growth, development, and pathogenesis. *Fungal Genet Biol* 49(8):589-601.

324. Gavric O, dos Santos DB, & Griffiths A (2007) Mutation and divergence of the phospholipase C gene in Neurospora crassa. *Fungal Genet Biol* 44(4):242-249.

325. Rohacs T (2013) Regulation of transient receptor potential channels by the phospholipase C pathway. *Adv Biol Regul* 53(3):341-355.

326. Palmer CP*, et al.* (2001) A TRP homolog in Saccharomyces cerevisiae forms an intracellular Ca(2+)-permeable channel in the yeast vacuolar membrane. *Proc Natl Acad Sci U S A* 98(14):7801-7805.

327. Su Z, Zhou X, Loukin SH, Saimi Y, & Kung C (2009) Mechanical force and cytoplasmic Ca(2+) activate yeast TRPY1 in parallel. *J Membr Biol* 227(3):141-150.

328. Dong XP*, et al.* (2010) PI(3,5)P(2) controls membrane trafficking by direct activation of mucolipin Ca(2+) release channels in the endolysosome. *Nat Commun* 1:38.

329. Prole DL & Taylor CW (2012) Identification and analysis of cation channel homologues in human pathogenic fungi. *PLoS One* 7(8):e42404.

330. Shaw BD & Hoch HC (2001) Biology of the fungal cell. *The Mycota VIII*, eds Howard RJ & Gow NAR (Springer-Verlag KG, Berlin), pp 73-89.

331. Cortes JC, Katoh-Fukui R, Moto K, Ribas JC, & Ishiguro J (2004) Schizosaccharomyces pombe Pmr1p is essential for cell wall integrity and is required for polarized cell growth and cytokinesis. *Eukaryot Cell* 3(5):1124-1135.

332. Dinamarco TM*, et al.* (2012) Functional characterization of an Aspergillus fumigatus calcium transporter (PmcA) that is essential for fungal infection. *PLoS One* 7(5):e37591.

333. Kmetzsch L*, et al.* (2010) The vacuolar Ca(2)(+) exchanger Vcx1 is involved in calcineurin-dependent Ca(2)(+) tolerance and virulence in Cryptococcus neoformans. *Eukaryot Cell* 9(11):1798-1805.

334. Rho HS, Jeon J, & Lee YH (2009) Phospholipase C-mediated calcium signalling is required for fungal development and pathogenicity in Magnaporthe oryzae. *Mol Plant Pathol* 10(3):337-346.

335. Palma-Guerrero J*, et al.* (2013) Genome wide association identifies novel loci involved in fungal communication. *PLoS Genet* 9(8):e1003669.

336. Fan Y, Ortiz-Urquiza A, Kudia RA, & Keyhani NO (2012) A fungal homologue of neuronal calcium sensor-1, Bbcsa1, regulates extracellular acidification and contributes to virulence in the entomopathogenic fungus Beauveria bassiana. *Microbiology* 158(Pt 7):1843-1851.

337. Cavinder B & Trail F (2012) Role of Fig1, a component of the low-affinity calcium uptake system, in growth and sexual development of filamentous fungi. *Eukaryot Cell* 11(8):978-988.

338. Cavinder B, Hamam A, Lew RR, & Trail F (2011) Mid1, a mechanosensitive calcium ion channel, affects growth, development, and ascospore discharge in the filamentous fungus Gibberella zeae. *Eukaryot Cell* 10(6):832-841.

339. Bormann J & Tudzynski P (2009) Deletion of Mid1, a putative stretch-activated calcium channel in Claviceps purpurea, affects vegetative growth, cell wall synthesis and virulence. *Microbiology* 155(Pt 12):3922-3933.

340. Iida H, Nakamura H, Ono T, Okumura MS, & Anraku Y (1994) MID1, a novel Saccharomyces cerevisiae gene encoding a plasma membrane protein, is required for Ca2+ influx and mating. *Mol Cell Biol* 14(12):8259-8271.

341. Martin DC*, et al.* (2011) New regulators of a high affinity Ca2+ influx system revealed through a genome-wide screen in yeast. *J Biol Chem* 286(12):10744-10754.

342. Muller EM, Locke EG, & Cunningham KW (2001) Differential regulation of two Ca(2+) influx systems by pheromone signaling in Saccharomyces cerevisiae. *Genetics* 159(4):1527-1538.

343. Kanzaki M*, et al.* (1999) Molecular identification of a eukaryotic, stretch-activated nonselective cation channel. *Science* 285(5429):882-886.

344. Lew RR, Abbas Z, Anderca MI, & Free SJ (2008) Phenotype of a mechanosensitive channel mutant, mid-1, in a filamentous fungus, Neurospora crassa. *Eukaryot Cell* 7(4):647-655.

345. Muller EM, Mackin NA, Erdman SE, & Cunningham KW (2003) Fig1p facilitates Ca2+ influx and cell fusion during mating of Saccharomyces cerevisiae. *J Biol Chem* 278(40):38461-38469.

346. Groppi S, Belotti F, Brandao RL, Martegani E, & Tisi R (2011) Glucose-induced calcium influx in budding yeast involves a novel calcium transport system and can activate calcineurin. *Cell Calcium* 49(6):376-386.

347. Bowman BJ, Abreu S, Margolles-Clark E, Draskovic M, & Bowman EJ (2011) Role of four calcium transport proteins, encoded by nca-1, nca-2, nca-3, and cax, in maintaining intracellular calcium levels in Neurospora crassa. *Eukaryot Cell* 10(5):654-661.

348. Cornelius G & Nakashima H (1987) Vacuoles play a decisive role in calcium homeostasis in *Neurospora crassa*. *J Gen Microbiol* 133:2341-2347.

349. Naveena Lavanya Latha J & Maruthi Mohan P (2011) Role of cell wall bound calcium in Neurospora crassa. *Microbiol Res* 166(5):419-429.

350. Putney JW (2009) Capacitative calcium entry: from concept to molecules. *Immunol Rev* 231(1):10-22.

351. Rizzuto R, De Stefani D, Raffaello A, & Mammucari C (2012) Mitochondria as sensors and regulators of calcium signalling. *Nat Rev Mol Cell Biol* 13(9):566-578.

352. Giorgio V*, et al.* (2013) Dimers of mitochondrial ATP synthase form the permeability transition pore. *Proc Natl Acad Sci U S A* 110(15):5887-5892.

353. Norberg E*, et al.* (2008) An increase in intracellular Ca2+ is required for the activation of mitochondrial calpain to release AIF during cell death. *Cell Death Differ* 15(12):1857-1864.

354. Zhang Y, Muend S, & Rao R (2012) Dysregulation of ion homeostasis by antifungal agents. *Front Microbiol* 3:133.

355. Pozniakovsky AI*, et al.* (2005) Role of mitochondria in the pheromone- and amiodarone-induced programmed death of yeast. *J Cell Biol* 168(2):257-269.

356. Rao A, Zhang Y, Muend S, & Rao R (2010) Mechanism of antifungal activity of terpenoid phenols resembles calcium stress and inhibition of the TOR pathway. *Antimicrob Agents Chemother* 54(12):5062-5069.

357. Roberts SK, McAinsh M, & Widdicks L (2012) Cch1p mediates Ca2+ influx to protect Saccharomyces cerevisiae against eugenol toxicity. *PLoS One* 7(9):e43989.

358. Gupta SS*, et al.* (2003) Antifungal activity of amiodarone is mediated by disruption of calcium homeostasis. *J Biol Chem* 278(31):28831-28839.

359. Bonilla M, Nastase KK, & Cunningham KW (2002) Essential role of calcineurin in response to endoplasmic reticulum stress. *EMBO J* 21(10):2343-2353.

360. Davis RH & de Serres FJ (1970) Genetic and microbiological research techniques for Neurospora crassa. *Meth Enzymol* 17:79-143.

361. Fecke W, Sled VD, Ohnishi T, & Weiss H (1994) Disruption of the gene encoding the NADH-binding subunit of NADH: ubiquinone oxidoreductase in Neurospora crassa. Formation of a partially assembled enzyme without FMN and the iron-sulphur cluster N-3. *Eur J Biochem* 220(2):551-558.

362. Harkness TA*, et al.* (1995) Disruption of the gene encoding the 78-kilodalton subunit of the peripheral arm of complex I in Neurospora crassa by repeat induced point mutation (RIP). *Curr Genet* 27(4):339-350.

363. Alberghina FA (1973) Growth regulation in Neurospora crassa. Effects of nutrients and of temperature. *Arch Mikrobiol* 89(2):83-94.

364. Livak KJ & Schmittgen TD (2001) Analysis of relative gene expression data using real-time quantitative PCR and the 2(-Delta Delta C(T)) Method. *Methods* 25(4):402-408.

365. Altschul SF, Gish W, Miller W, Myers EW, & Lipman DJ (1990) Basic local alignment search tool. *J Mol Biol* 215(3):403-410.

366. Altschul SF*, et al.* (1997) Gapped BLAST and PSI-BLAST: a new generation of protein database search programs. *Nucleic Acids Res* 25(17):3389-3402.

367. Larkin MA*, et al.* (2007) Clustal W and Clustal X version 2.0. *Bioinformatics* 23(21):2947-2948.

368. Quevillon E*, et al.* (2005) InterProScan: protein domains identifier. *Nucleic Acids Res* 33(Web Server issue):W116-120.

369. Jones DT (2007) Improving the accuracy of transmembrane protein topology prediction using evolutionary information. *Bioinformatics* 23(5):538-544.

370. Krogh A, Larsson B, von Heijne G, & Sonnhammer EL (2001) Predicting transmembrane protein topology with a hidden Markov model: application to complete genomes. *J Mol Biol* 305(3):567-580.

371. Horton P*, et al.* (2007) WoLF PSORT: protein localization predictor. *Nucleic Acids Res* 35(Web Server issue):W585-587.

372. Trapnell C*, et al.* (2012) Differential gene and transcript expression analysis of RNA-seq experiments with TopHat and Cufflinks. *Nat Protoc* 7(3):562-578.

373. Ruepp A*, et al.* (2004) The FunCat, a functional annotation scheme for systematic classification of proteins from whole genomes. *Nucleic Acids Res* 32(18):5539-5545.

374. Li H, Ruan J, & Durbin R (2008) Mapping short DNA sequencing reads and calling variants using mapping quality scores. *Genome Res* 18(11):1851-1858.

375. Ellison CE*, et al.* (2011) Population genomics and local adaptation in wild isolates of a model microbial eukaryote. *Proc Natl Acad Sci U S A* 108(7):2831-2836.

376. Chin LS*, et al.* (1997) 4-Aminopyridine causes apoptosis and blocks an outward rectifier K+ channel in malignant astrocytoma cell lines. *J Neurosci Res* 48(2):122-127.

377. Takahashi M*, et al.* (2010) An AP-1-like transcription factor, NAP-1, regulates expression of the glutathione S-transferase and NADH:flavin oxidoreductase genes in Neurospora crassa. *Biosci Biotechnol Biochem* 74(4):746-752.

378. Leung YM (2010) Voltage-gated K+ channel modulators as neuroprotective agents. *Life Sci* 86(21-22):775-780.

379. Wulff H, Castle NA, & Pardo LA (2009) Voltage-gated potassium channels as therapeutic targets. *Nat Rev Drug Discov* 8(12):982-1001.

380. Wang Z, Gerstein M, & Snyder M (2009) RNA-Seq: a revolutionary tool for transcriptomics. *Nat Rev Genet* 10(1):57-63.

381. Kruger A*, et al.* (2011) The pentose phosphate pathway is a metabolic redox sensor and regulates transcription during the antioxidant response. *Antioxid Redox Signal* 15(2):311-324.

382. Thastrup O, Cullen PJ, Drobak BK, Hanley MR, & Dawson AP (1990) Thapsigargin, a tumor promoter, discharges intracellular Ca2+ stores by specific inhibition of the endoplasmic reticulum Ca2(+)-ATPase. *Proc Natl Acad Sci U S A* 87(7):2466-2470.

383. Cordeiro JM, Boda B, Goncalves PP, & Dunant Y (2013) Synaptotagmin 1 is required for vesicular Ca(2)(+)/H(+)-antiport activity. *J Neurochem* 126(1):37-46.

384. Bick AG, Calvo SE, & Mootha VK (2012) Evolutionary diversity of the mitochondrial calcium uniporter. *Science* 336(6083):886.

385. Zazueta C, Sosa-Torres ME, Correa F, & Garza-Ortiz A (1999) Inhibitory properties of ruthenium amine complexes on mitochondrial calcium uptake. *J Bioenerg Biomembr* 31(6):551-557.

386. Wick SM & Hepler PK (1982) Selective localization of intracellular Ca2+ with potassium antimonate. *J Histochem Cytochem* 30(11):1190-1204.

387. Berridge MJ (2009) Inositol trisphosphate and calcium signalling mechanisms. *Biochim Biophys Acta* 1793(6):933-940.

388. Smith RJ*, et al.* (1990) Receptor-coupled signal transduction in human polymorphonuclear neutrophils: effects of a novel inhibitor of phospholipase C-dependent processes on cell responsiveness. *J Pharmacol Exp Ther* 253(2):688-697.

389. Berridge MJ & Irvine RF (1989) Inositol phosphates and cell signalling. *Nature* 341(6239):197-205.

390. Gafni J*, et al.* (1997) Xestospongins: potent membrane permeable blockers of the inositol 1,4,5-trisphosphate receptor. *Neuron* 19(3):723-733.

391. Clapham DE, Julius D, Montell C, & Schultz G (2005) International Union of Pharmacology. XLIX. Nomenclature and structure-function relationships of transient receptor potential channels. *Pharmacol Rev* 57(4):427-450.

392. Zitt C*, et al.* (2004) Potent inhibition of Ca2+ release-activated Ca2+ channels and T-lymphocyte activation by the pyrazole derivative BTP2. *J Biol Chem* 279(13):12427-12437.

393. Jung OJ, Lee EJ, Kim JW, Chung YR, & Lee CW (1997) Identification of putative phosphoinositide-specific phospholipase C genes in filamentous fungi. *Mol Cells* 7(2):192-199.

394. Troppens DM*, et al.* (2013) The bacterial secondary metabolite 2,4-diacetylphloroglucinol impairs mitochondrial function and affects calcium homeostasis in Neurospora crassa. *Fungal Genet Biol* 56:135-146.

395. Hong MP*, et al.* (2013) Activity of the calcium channel pore Cch1 is dependent on a modulatory region of the subunit Mid1 in Cryptococcus neoformans. *Eukaryot Cell* 12(1):142-150.

396. Locke EG, Bonilla M, Liang L, Takita Y, & Cunningham KW (2000) A homolog of voltage-gated Ca(2+) channels stimulated by depletion of secretory Ca(2+) in yeast. *Mol Cell Biol* 20(18):6686-6694.

397. Guinamard R, Simard C, & Del Negro C (2013) Flufenamic acid as an ion channel modulator. *Pharmacol Ther* 138(2):272-284.

398. Zhang C, Bosch MA, Ronnekleiv OK, & Kelly MJ (2013) Kisspeptin activation of TRPC4 channels in female GnRH neurons requires PIP2 depletion and cSrc kinase activation. *Endocrinology* 154(8):2772-2783.

399. Miller M*, et al.* (2011) Identification of ML204, a novel potent antagonist that selectively modulates native TRPC4/C5 ion channels. *J Biol Chem* 286(38):33436-33446.

400. Herwig C, Doerries C, Marison I, & von Stockar U (2001) Quantitative analysis of the regulation scheme of invertase expression in Saccharomyces cerevisiae. *Biotechnol Bioeng* 76(3):247-258.

401. Ziv C, Gorovits R, & Yarden O (2008) Carbon source affects PKA-dependent polarity of Neurospora crassa in a CRE-1-dependent and independent manner. *Fungal Genet Biol* 45(2):103-116.

402. Lee DB & Free SJ (1984) Isolation and characterization of Neurospora mutants affected in invertase synthesis. *Genetics* 106(4):591-599.

403. Rodicio R & Heinisch JJ (2010) Together we are strong--cell wall integrity sensors in yeasts. *Yeast* 27(8):531-540.

404. Ochiai A*, et al.* (2007) A novel structural fold in polysaccharide lyases: Bacillus subtilis family 11 rhamnogalacturonan lyase YesW with an eight-bladed beta-propeller. *J Biol Chem* 282(51):37134-37145.

405. Wilson MA & Brunger AT (2000) The 1.0 A crystal structure of Ca(2+)-bound calmodulin: an analysis of disorder and implications for functionally relevant plasticity. *J Mol Biol* 301(5):1237-1256.

406. Xu AJ & Springer TA (2012) Calcium stabilizes the von Willebrand factor A2 domain by promoting refolding. *Proc Natl Acad Sci U S A* 109(10):3742-3747.

407. Aldieri E*, et al.* (2008) Classical inhibitors of NOX NAD(P)H oxidases are not specific. *Curr Drug Metab* 9(8):686-696.

408. Majander A, Finel M, & Wikstrom M (1994) Diphenyleneiodonium inhibits reduction of iron-sulfur clusters in the mitochondrial NADH-ubiquinone oxidoreductase (Complex I). *J Biol Chem* 269(33):21037-21042.

409. Roberts TH, Fredlund KM, & Moller IM (1995) Direct evidence for the presence of two external NAD(P)H dehydrogenases coupled to the electron transport chain in plant mitochondria. *FEBS Lett* 373(3):307-309.

410. Schuelke M*, et al.* (1999) Mutant NDUFV1 subunit of mitochondrial complex I causes leukodystrophy and myoclonic epilepsy. *Nat Genet* 21(3):260-261.

411. De Stefani D, Raffaello A, Teardo E, Szabo I, & Rizzuto R (2011) A forty-kilodalton protein of the inner membrane is the mitochondrial calcium uniporter. *Nature* 476(7360):336-340.

412. Baughman JM*, et al.* (2011) Integrative genomics identifies MCU as an essential component of the mitochondrial calcium uniporter. *Nature* 476(7360):341-345.

413. Zhu J*, et al.* (2013) Transcriptomic profiling-based mutant screen reveals three new transcription factors mediating menadione resistance in Neurospora crassa. *Fungal Biol* 117(6):422-430.

414. Greenwald CJ*, et al.* (2010) Temporal and spatial regulation of gene expression during asexual development of Neurospora crassa. *Genetics* 186(4):1217-1230.

415. Hansberg W, de Groot H, & Sies H (1993) Reactive oxygen species associated with cell differentiation in Neurospora crassa. *Free Radic Biol Med* 14(3):287-293.

416. McCarthy MI*, et al.* (2008) Genome-wide association studies for complex traits: consensus, uncertainty and challenges. *Nat Rev Genet* 9(5):356-369.

417. Chary P & Natvig DO (1989) Evidence for three differentially regulated catalase genes in Neurospora crassa: effects of oxidative stress, heat shock, and development. *J Bacteriol* 171(5):2646-2652.

418. Park G, Ryu YH, Hong YJ, Choi EH, & Uhm HS (2012) Cellular and molecular responses of Neurospora crassa to non-thermal plasma at atmospheric pressure. *Applied Physics Letters* 100(6).

419. Gulshan K & Moye-Rowley WS (2007) Multidrug resistance in fungi. *Eukaryot Cell* 6(11):1933-1942.

420. Zhang Y*, et al.* (2012) CDR4 is the major contributor to azole resistance among four Pdr5p-like ABC transporters in Neurospora crassa. *Fungal Biol* 116(7):848-854.

421. Norberg E*, et al.* (2010) Critical role for hyperpolarization-activated cyclic nucleotide-gated channel 2 in the AIF-mediated apoptosis. *EMBO J* 29(22):3869-3878.

422. Dezaki K, Maeno E, Sato K, Akita T, & Okada Y (2012) Early-phase occurrence of K+ and Cl- efflux in addition to Ca 2+ mobilization is a prerequisite to apoptosis in HeLa cells. *Apoptosis* 17(8):821-831.

423. Himpens B, De Smedt H, & Casteels R (1993) Staurosporine induced Ca2+ increase in DDT1MF-2 smooth muscle cells. *Am J Physiol* 264(3 Pt 1):C544-551.

424. Kruman I, Guo Q, & Mattson MP (1998) Calcium and reactive oxygen species mediate staurosporine-induced mitochondrial dysfunction and apoptosis in PC12 cells. *J Neurosci Res* 51(3):293-308.

425. Seo SR & Seo JT (2009) Calcium overload is essential for the acceleration of staurosporine-induced cell death following neuronal differentiation in PC12 cells. *Exp Mol Med* 41(4):269-276.

426. Kinnunen PK (2000) Lipid bilayers as osmotic response elements. *Cell Physiol Biochem* 10(5-6):243-250.

427. Werry TD, Wilkinson GF, & Willars GB (2003) Mechanisms of cross-talk between G-protein-coupled receptors resulting in enhanced release of intracellular Ca2+. *Biochem J* 374(Pt 2):281-296.

428. Ryu SH*, et al.* (1990) Feedback regulation of phospholipase C-beta by protein kinase C. *J Biol Chem* 265(29):17941-17945.

429. Lemonnier L, Trebak M, & Putney JW, Jr. (2008) Complex regulation of the TRPC3, 6 and 7 channel subfamily by diacylglycerol and phosphatidylinositol-4,5-bisphosphate. *Cell Calcium* 43(5):506-514.

430. Venkatachalam K, Zheng F, & Gill DL (2003) Regulation of canonical transient receptor potential (TRPC) channel function by diacylglycerol and protein kinase C. *J Biol Chem* 278(31):29031-29040.

431. Chuang HH*, et al.* (2001) Bradykinin and nerve growth factor release the capsaicin receptor from PtdIns(4,5)P2-mediated inhibition. *Nature* 411(6840):957-962.

432. Hofmann T*, et al.* (1999) Direct activation of human TRPC6 and TRPC3 channels by diacylglycerol. *Nature* 397(6716):259-263.

433. Guerin R, Beauregard PB, Leroux A, & Rokeach LA (2009) Calnexin regulates apoptosis induced by inositol starvation in fission yeast. *PLoS One* 4(7):e6244.

434. Hong MP, Vu K, Bautos J, & Gelli A (2010) Cch1 restores intracellular Ca2+ in fungal cells during endoplasmic reticulum stress. *J Biol Chem* 285(14):10951-10958.

435. Edlind T, Smith L, Henry K, Katiyar S, & Nickels J (2002) Antifungal activity in Saccharomyces cerevisiae is modulated by calcium signalling. *Mol Microbiol* 46(1):257-268.

436. Visch HJ*, et al.* (2004) Inhibition of mitochondrial Na+-Ca2+ exchange restores agonist-induced ATP production and Ca2+ handling in human complex I deficiency. *J Biol Chem* 279(39):40328-40336.

437. Willems PH*, et al.* (2008) Mitochondrial Ca2+ homeostasis in human NADH:ubiquinone oxidoreductase deficiency. *Cell Calcium* 44(1):123-133.

438. Moudy AM*, et al.* (1995) Abnormal calcium homeostasis and mitochondrial polarization in a human encephalomyopathy. *Proc Natl Acad Sci U S A* 92(3):729-733.

439. Tarrio N, Diaz Prado S, Cerdan ME, & Gonzalez Siso MI (2005) The nuclear genes encoding the internal (KlNDI1) and external (KlNDE1) alternative NAD(P)H:ubiquinone oxidoreductases of mitochondria from Kluyveromyces lactis. *Biochim Biophys Acta* 1707(2-3):199-210.

440. Bowman BJ, Draskovic M, Freitag M, & Bowman EJ (2009) Structure and distribution of organelles and cellular location of calcium transporters in Neurospora crassa. *Eukaryot Cell* 8(12):1845-1855.

441. Bowman BJ, Abreu S, Johl JK, & Bowman EJ (2012) The pmr gene, encoding a Ca2+-ATPase, is required for calcium and manganese homeostasis and normal development of hyphae and conidia in Neurospora crassa. *Eukaryot Cell* 11(11):1362-1370.

442. Strayle J, Pozzan T, & Rudolph HK (1999) Steady-state free Ca(2+) in the yeast endoplasmic reticulum reaches only 10 microM and is mainly controlled by the secretory pathway pump pmr1. *EMBO J* 18(17):4733-4743.

443. Deka R, Kumar R, & Tamuli R (2011) Neurospora crassa homologue of Neuronal Calcium Sensor-1 has a role in growth, calcium stress tolerance, and ultraviolet survival. *Genetica* 139(7):885-894.

444. Park G*, et al.* (2011) Global analysis of serine-threonine protein kinase genes in Neurospora crassa. *Eukaryot Cell* 10(11):1553-1564.

445. Choi J, Kim KS, Rho HS, & Lee YH (2011) Differential roles of the phospholipase C genes in fungal development and pathogenicity of Magnaporthe oryzae. *Fungal Genet Biol* 48(4):445-455.

446. MacPherson S, Larochelle M, & Turcotte B (2006) A fungal family of transcriptional regulators: the zinc cluster proteins. *Microbiol Mol Biol Rev* 70(3):583-604.

447. Coste AT, Karababa M, Ischer F, Bille J, & Sanglard D (2004) TAC1, transcriptional activator of CDR genes, is a new transcription factor involved in the regulation of Candida albicans ABC transporters CDR1 and CDR2. *Eukaryot Cell* 3(6):1639-1652.

448. Akache B, MacPherson S, Sylvain MA, & Turcotte B (2004) Complex interplay among regulators of drug resistance genes in Saccharomyces cerevisiae. *J Biol Chem* 279(27):27855-27860.

449. Mamnun YM, Pandjaitan R, Mahe Y, Delahodde A, & Kuchler K (2002) The yeast zinc finger regulators Pdr1p and Pdr3p control pleiotropic drug resistance (PDR) as homo- and heterodimers in vivo. *Mol Microbiol* 46(5):1429-1440.

450. Akache B & Turcotte B (2002) New regulators of drug sensitivity in the family of yeast zinc cluster proteins. *J Biol Chem* 277(24):21254-21260.

451. Larochelle M, Drouin S, Robert F, & Turcotte B (2006) Oxidative stress-activated zinc cluster protein Stb5 has dual activator/repressor functions required for pentose phosphate pathway regulation and NADPH production. *Mol Cell Biol* 26(17):6690-6701.

452. Sun CB, Suresh A, Deng YZ, & Naqvi NI (2006) A multidrug resistance transporter in Magnaporthe is required for host penetration and for survival during oxidative stress. *Plant Cell* 18(12):3686-3705.

453. Diezmann S & Dietrich FS (2009) Saccharomyces cerevisiae: population divergence and resistance to oxidative stress in clinical, domesticated and wild isolates. *PLoS One* 4(4):e5317.

454. Diezmann S & Dietrich FS (2011) Oxidative stress survival in a clinical Saccharomyces cerevisiae isolate is influenced by a major quantitative trait nucleotide. *Genetics* 188(3):709-722.

455. Kretschmer M*, et al.* (2009) Fungicide-driven evolution and molecular basis of multidrug resistance in field populations of the grey mould fungus Botrytis cinerea. *PLoS Pathog* 5(12):e1000696.

456. Nakaune R*, et al.* (1998) A novel ATP-binding cassette transporter involved in multidrug resistance in the phytopathogenic fungus Penicillium digitatum. *Appl Environ Microbiol* 64(10):3983-3988.

457. Roohparvar R, Mehrabi R, Van Nistelrooy JG, Zwiers LH, & De Waard MA (2008) The drug transporter MgMfs1 can modulate sensitivity of field strains of the fungal wheat pathogen Mycosphaerella graminicola to the strobilurin fungicide trifloxystrobin. *Pest Manag Sci* 64(7):685-693.

458. Hanahan D & Weinberg RA (2011) Hallmarks of cancer: the next generation. *Cell* 144(5):646-674.

459. Hotchkiss RS, Strasser A, McDunn JE, & Swanson PE (2009) Cell death. *N Engl J Med* 361(16):1570-1583.

460. Vazquez A, Bond EE, Levine AJ, & Bond GL (2008) The genetics of the p53 pathway, apoptosis and cancer therapy. *Nat Rev Drug Discov* 7(12):979-987.

461. Santoro M, Carlomagno F, Melillo RM, & Fusco A (2004) Dysfunction of the RET receptor in human cancer. *Cell Mol Life Sci* 61(23):2954-2964.

462. Cordeiro J, Goncalves PP, & Dunant Y (2011) Synaptic vesicles control the time course of neurotransmitter secretion via a Ca(2)+/H+ antiport. *J Physiol* 589(Pt 1):149-167.

463. Kim H, Kim A, & Cunningham KW (2012) Vacuolar H+-ATPase (V-ATPase) promotes vacuolar membrane permeabilization and nonapoptotic death in stressed yeast. *J Biol Chem* 287(23):19029-19039.

464. Zhang YQ*, et al.* (2010) Requirement for ergosterol in V-ATPase function underlies antifungal activity of azole drugs. *PLoS Pathog* 6(6):e1000939.

465. von Schwarzenberg K*, et al.* (2013) Mode of cell death induction by pharmacological vacuolar H+-ATPase (V-ATPase) inhibition. *J Biol Chem* 288(2):1385-1396.

466. Forster C & Kane PM (2000) Cytosolic Ca2+ homeostasis is a constitutive function of the V-ATPase in Saccharomyces cerevisiae. *J Biol Chem* 275(49):38245-38253.

467. Petersen OH & Verkhratsky A (2007) Endoplasmic reticulum calcium tunnels integrate signalling in polarised cells. *Cell Calcium* 42(4-5):373-378.

APPENDIX

Modulation of fungal sensitivity to staurosporine by targeting proteins identified by transcriptional profiling

Andreia S. Fernandes, A. Pedro Gonçalves, Ana Castro, Telma A. Lopes, Rui Gardner, N. Louise Glass, Arnaldo Videira

Fungal Genetics and Biology (2011) 48(12):1130-8

Fungal Genetics and Biology 48 (2011) 1130–1138

Contents lists available at SciVerse ScienceDirect

Fungal Genetics and Biology

journal homepage: www.elsevier.com/locate/yfgbi

Modulation of fungal sensitivity to staurosporine by targeting proteins identified by transcriptional profiling

Andreia S. Fernandes [a], A. Pedro Gonçalves [a], Ana Castro [a], Telma A. Lopes [b], Rui Gardner [b], N. Louise Glass [c], Arnaldo Videira [a,d,*]

[a] IBMC – Instituto de Biologia Molecular e Celular, Portugal
[b] Instituto Gulbenkian de Ciência, Oeiras, Portugal
[c] Department of Plant and Microbial Biology, University of California, Berkeley, United States
[d] ICBAS – Instituto de Ciências Biomédicas de Abel Salazar, Universidade do Porto, Portugal

ARTICLE INFO

Article history:
Received 25 August 2011
Accepted 29 September 2011
Available online 5 October 2011

Keywords:
Staurosporine
Cell death
Transcriptional profiling
ABC transporter
Neurospora crassa

ABSTRACT

An analysis of the time-dependent genetic response to the death-inducer staurosporine was performed in *Neurospora crassa* by transcriptional profiling. Staurosporine induced two major genes encoding an ABC transporter and a protein with similarity to regulatory subunits of potassium channels. The transcriptional response is dependent on the activity of a novel transcription factor. Deletion mutants in differentially expressed genes displayed altered sensitivity to staurosporine, underscoring significant proteins involved in the response to the drug. A null-mutant of the ABC transporter (abc3) is extremely sensitive to staurosporine, accumulates more staurosporine than the wild type strain and is defective in energy-dependent export of the drug, indicating that the ABC3 protein is the first described staurosporine transporter. It was located in the plasma membrane by immunofluorescence microscopy. The combination of inhibitors of ABC transporters or of potassium channels with staurosporine leads to an enhanced activity against *N. crassa* and pathogenic fungi paving the way to the development of more potent and specific antifungals. Our results highlight the general use of transcriptional profiling for the identification of novel proteins involved in cell death and their potential use as drug targets.

1. Introduction

Programmed cell death (PCD) is a process of cell suicide essential for the development and survival of the organism. The process was firstly described in higher eukaryotes, but more recently found to occur in fungi as well (Madeo et al., 1997). Interference with PCD has had increasing relevance in public health issues due to the fact that its stimulation may prove to be fundamental in cancer treatments and in the control of infectious diseases (Ramsdale, 2008; Reed, 2006; Sharon et al., 2009). Thus, an understanding of the complex networks that ultimately lead to cell death is necessary. It is anticipated that modulation of PCD can be achieved by the identification and targeting of key components regulating the process.

PCD can be induced with drugs like staurosporine (STS), an alkaloid from microbial origin firstly described as antibacterial and antifungal (Omura et al., 1977). STS has been widely used as a protein kinase inhibitor or as a PCD-inducing agent (Gescher, 2000). The STS concentration needed to induce PCD (100 nM–10 μM) is much higher than the k_i for inhibition of protein kinases (~5 nM), indicating that STS interferes with other cellular functions (Jarvis et al., 1994). Although STS effects on apoptosis have been largely studied, nothing is known so far about its trafficking and transport. Several STS analogs are in advanced clinical trials as anticancer agents (Osman et al., 2010).

The filamentous fungus *Neurospora crassa* has been a valuable research model organism (Davis and Perkins, 2002), particularly following its genome sequencing (Galagan et al., 2003) and targeted disruption (Colot et al., 2006). It undergoes PCD following the addition of external pro-apoptotic drugs (Castro et al., 2008, 2010; Videira et al., 2009) or as a consequence of heterokaryon incompatibility (Glass and Dementhon, 2006). Specific mutants of respiratory chain complex I are particularly sensitive to STS (Castro et al., 2010). In this work, we performed a transcriptomic analysis of *N. crassa* exposed to STS in order to identify novel mechanisms associated with PCD. We further showed that targeting specifically identified proteins by chemical means allows modulation of *N. crassa* sensitivity to STS and this effect could be extended to the pathogenic fungi *Aspergillus fumigatus* and *Candida albicans*. The

Abbreviations: PCD, programmed cell death; STS, staurosporine.

* Corresponding author. Address: IBMC – Instituto de Biologia Molecular e Celular, Rua Campo Alegre 823, 4150-180 Porto, Portugal. Fax: +351 226099157.
E-mail address: avideira@ibmc.up.pt (A. Videira).

1087-1845/$ - see front matter © 2011 Elsevier Inc. All rights reserved.
doi:10.1016/j.fgb.2011.09.004

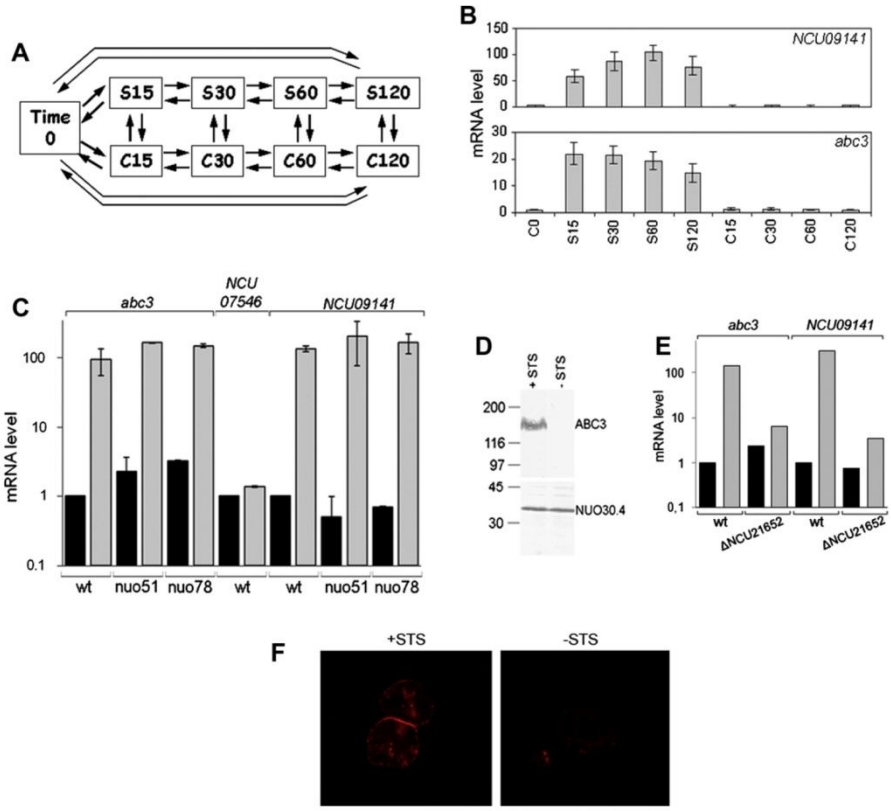

Fig. 1. Expression levels and protein localization after STS treatment. (A) Scheme of the microarray experiment. *N. crassa* conidia were germinated in minimal medium for 5 h (time 0) and then incubated in the absence (C) or in the presence of 12.5 μM STS (S). Samples were withdrawn at the indicated time points (min) and used for di-swap microarray hybridizations (arrows, with the arrowhead pointing the sample labeled with Cy5) and quantification of gene expression levels. (B) Time-course relative expression levels of the genes encoding NCU09141 (upper panel) and ABC3 (lower panel). (C) Quantification by RT-PCR of relative expression levels of the genes encoding ABC3, NCU07546 and NCU09141 performed in the wild type strain (wt) and the complex I mutants (nuo51 and nuo78) following 5-h germination and 30 min incubation in the absence (black bars) or presence of STS (gray bars). (D) Western blots of total protein extracts from 16 h-grown fungal cells exposed to 12.5 μM STS for 3 h or untreated-cells using antiserum against ABC3 and antiserum against the constitutive 30.4 kDa subunit of complex I, as control. Standard molecular weights (kDa) are indicated on the left. (E) Quantification by RT-PCR of relative expression levels of the genes encoding NCU09975 (*abc3*) and NCU09141 (shown above) performed in the wild type strain and the ΔNCU21652 mutant (shown below) following 5-h germination and 30 minutes incubation in the absence (black bars) or presence of STS (gray bars). (F) Localization of the ABC3 protein by immunofluorescence using confocal microscopy in the *N. crassa* slime mutant after 16 h of growth followed by 3 h in the presence (left) or absence (right) of 12.5 μM STS.

higher activity of STS when combined with specific protein inhibitors against pathogenic fungi has potential medical implications.

2. Material and methods

2.1. Strains, growth techniques and chemicals

Wild type *N. crassa* (FGSC 2489), the cell wall-less slime mutant (FGSC 4761), and several deletion strains generated by the Neurospora Genome Project (Dunlap et al., 2007), were obtained from the Fungal Genetics Stock Center (McCluskey, 2003). The mitochondrial complex I nuo mutants have been reviewed (Marques et al., 2005). Standard procedures were employed for growth and handling of *N. crassa*, *A. fumigatus* ATCC 46645 and *C. albicans* SC5314 strains (Castro et al., 2010; Davis and de Serres, 1970). *N. crassa* conidial germination was evaluated by optical microscopy. For spot assays, serial 3-fold dilutions of cellular suspensions from all fungi were spotted on agar plates (GFS for *N. crassa* (Davis and de Serres, 1970), Sabouraud for *A. fumigatus* and *C. albicans*) containing drugs, so that the last spot contained ~50 cells, and incubated at 26 °C (37 °C for *A. fumigatus*). We prepared stock solutions of 10.7 mM STS/DMSO (LC-Laboratories), 50 mM Verapamil/ethanol (Sigma–Aldrich), 1 M sodium orthovanadate (Sigma–Aldrich) and 100 mM 4-aminopyridine (Sigma–Aldrich).

2.2. Microarray experiments and data analysis

Closed-circuit designs were employed for microarray comparisons (Fig. 1A), because they are statistically robust and provide a higher resolution in identifying differentially expressed genes than designs that use a universal reference (Townsend, 2003). *N. crassa* conidia obtained from cultures grown for 7 days at 25 °C under constant light (Kasuga et al., 2005) were germinated in Vogel's minimal medium (10^7 cells/ml) at 30 °C with strong agitation. STS (12.5 μM) was added after 5 h. At different times, mycelium samples were collected by quick filtration, frozen in liquid nitrogen and kept at −70 °C.

The isolation of RNA with TRIzol (Invitrogen Life Technologies) and its purification with the RNeasy kit (Qiagen), cDNA synthesis and labeling with either Cy3 or Cy5 dyes (Amersham) and hybridization (Pronto kit, Corning) with gamma amino propyl silane slides printed with 70-mer oligonucleotides, which include the 10526 ORFs predicted in the Neurospora genome, have been detailed before (Kasuga et al., 2005; Videira et al., 2009). Each hybridization was duplicated, labeling one cDNA sample with Cy3 and the other with Cy5, and *vice-versa* (di-swap).

The hybridization images were obtained with a GenePix 4000B scanner and the signals were quantified with the GenePix Pro6 software, which automatically flagged low-quality spots. Then, slides were also inspected manually. Spots with a mean fluorescence intensity for at least one of the Cy3 or Cy5 dyes that was greater than the mean background intensity plus three standard deviations were selected for further analysis if less than 0.02% of the pixels were saturated.

Normalized ratio data were analyzed with the Bayesian Analysis of Gene Expression Levels (BAGEL) software in order to calculate a relative expression level and a credible interval for each gene in each sample (Townsend and Hartl, 2002). The genes were associated with functional categories using the FunCat catalog created by MIPS (Ruepp et al., 2004). Microarray data have been deposited at the NCBI gene expression and hybridization array data repository (GEO, http://www.ncbi.nlm.nih.gov/geo/, accession No. GSE32451). Table S1 in the Supplemental material lists mRNA profiling results and functional annotations.

2.3. Quantification of gene expression by real time RT-PCR

RNA was extracted with Ilustra RNAspin Mini kit (GE Healthcare) from hyphae grown in the same conditions used for microarray experiments, quantified with the ND 1000 spectrophotometer (Nanodrop) and used to produce cDNA with SuperScript First-Strand Synthesis System kit (Invitrogen). Specific oligonucleotide primers (Table S2), an iCycler iQ5 and SYBR Green Supermix kit (Bio-Rad) were used for qRT-PCR. Triplicate data was obtained in each qRT-PCR experiment and threshold cycle values within an interval of ±0.5 cycle in the same experiment were accepted. Gene concentration was determined by the $2^{-\Delta\Delta Ct}$ method (Livak and Schmittgen, 2001). Relative quantifications employed the NCU04173 gene (actin) as control and the wild type *N. crassa* not exposed to STS as calibrator. Two independent experiments were performed.

2.4. Polyclonal antisera and western blotting

A 905 bp fragment of the 3′-end of the *NCU09975* (*abc3*) cDNA (corresponding to the C-terminal 301 aminoacid residues) was amplified by PCR with specific primers (Table S2) from a first strand cDNA obtained as described in the previous section, ligated in the pCRII-TOPO vector (Invitrogen) and cloned in *Escherichia coli* DH5α. DNA sequencing confirmed the correct sequence. The fragment was then excised with *Bam*HI and *Nde*I, ligated in the pET19b expression vector and cloned in *E. coli* BL21(DE3) (Novagen). The protein was expressed following induction with IPTG, solubilized from cellular inclusion bodies with 8 M urea, purified by Ni^{2+}-affinity chromatography HisTrap HP (GE Healthcare), precipitated with TCA, quantified with the Bio-Rad Protein Assay kit and used for rat immunization by established procedures at IBMC animal house by following the European Directive 86/609/EEC for animal experimentation and the guidelines on antibody production of the Canadian Council on Animal Care. The collected rat antisera was diluted 1/1000 for use in western blots of total protein extracts of *N. crassa* resolved by SDS–PAGE in 12% acrylamide gels (Zauner et al., 1985).

2.5. Immunofluorescence microscopy

The cell wall-less slime mutant was grown for 3 h in SeM medium (Schulte and Scarborough, 1975) from an initial concentration of 5×10^6 cell/ml in the presence or absence of 5 μM STS. Cells were suspended in PBS, fixed in 2% paraformaldehyde for 1 h, washed, and permeabilized with 0.1% Triton X-100, 0.1% sodium citrate for 2 min. They were sequentially incubated with 0.1% BSA for 1 h, 1/250 diluted rat antisera (see above) for 16 h, and 1/1000 diluted secondary antibody conjugated with Alexa Fluor 594 (Invitrogen) for 1 h. The slides were mounted in Vecta Shield (Vector Laboratories) and observed under a Laser Scanning Confocal Microscope Leica SP2 AOBS SE.

2.6. Staurosporine determination by flow cytometry and UV–vis absorption spectroscopy

STS absorbs radiation in the UV region of the spectrum and, when excited in this region, it fluoresces in the range 370–410 nm (Iyer et al., 2008). These spectroscopic properties allowed its intra- and extracellular quantification. For the determination of STS concentration in the extracellular medium, and in order to observe variations, the experiments employed 50-fold more concentrated cellular suspensions (2.5×10^8 cells/ml). Conidial cells, previously incubated in liquid media containing STS, were collected by centrifugation. STS concentration in supernatants (extracellular medium) was measured by visible absorption spectroscopy at A_{372} *minus* A_{395} in a Shimaduzu UV-160A spectrophotometer and normalized with the absorption of a standard STS solution. The cell pellet was washed with PBS and intracellular STS concentration was measured by flow cytometry as detailed in Fig. S1.

2.7. TUNEL assay

DNA strand breaks were analyzed by terminal deoxynucleotidyl transferase biotin-dUTP nick end labeling (TUNEL) using the *in situ* cell death detection kit fluorescein (Roche Applied Science), as described previously (Castro et al., 2008). *N. crassa* conidia were incubated in minimal medium in the presence or absence or 12.5 μM STS for 3 h and washed in PBS. Spheroplasts were prepared (Duarte et al., 1995), and fixation was performed 4.5 h after treatment with the drug. Flow cytometry analysis was performed in a FACSCalibur (BD Biosciences). Twenty-thousand cells per sample were analyzed. Data were acquired with CELLQuest PRO 3.3 (BD Biosciences).

3. Results

3.1. Analysis of gene expression patterns following staurosporine treatment

Staurosporine induces programmed cell death in many organisms, including *N. crassa* (Castro et al., 2010). In order to identify molecular pathways associated with the response to STS, we analyzed gene expression patterns after treatment with the drug during a time-course and utilizing full genome microarrays available for *N. crassa* (Fig. 1A). Conidial cells were germinated in liquid medium during 5 h and further incubated in the presence of STS for a period of 2 h. Samples collected at different time points were used to prepare fungal RNA for evaluation of relative expression levels using full genome *N. crassa* microarrays.

In these experiments, we obtained statistical support for expression levels for 4596 genes, representing about half of the fungal genome (Table S1). Genes that displayed no expression under these conditions or that only displayed expression in some samples were eliminated during BAGEL analyses (Townsend and

Hartl, 2002). Individual scrutiny of the time-course profiles of gene expression patterns revealed 135 genes (~3%) that, under our conditions, display differential expression in the presence or absence of STS. Most genes show increased expression levels in the presence of the drug indicating an active transcriptional response. Assignment of functional categories, as defined by the FunCat catalog (Ruepp et al., 2004), revealed that this set of affected genes is highly enriched in the "Metabolism" category (~50%). About 1/3 of the genes affected by STS treatment have no attributable function (Table S1). The list of genes differentially expressed point at putative novel mechanisms involved in the drug response.

In this work, we focused on two genes, *NCU09141* and *NCU09975* (*abc3*), which show a higher-fold induction 30–60 min upon STS treatment as compared to basal levels of expression (Fig. 1B). Quantification of gene expression by qRT-PCR confirmed that the expression of both genes is highly induced when *N. crassa* cells are exposed to STS (Fig. 1C). The expression of *NCU07546*, a paralog of *NCU09975* (Fig. S2A) was used as control, and showed similar expression levels in the presence or absence of STS. Because specific mutants of respiratory chain complex I are particularly sensitive to STS (Castro et al., 2010), we tested the expression of *NCU09141* and *NCU09975* in complex I mutants. However, the expression response of *NCU09141* and *NCU09975* in the complex I mutants was similar to that of the wild type strain following STS treatment (Fig. 1C). Western blots of total fungal protein extracts with a rat antiserum against NCU09975 (ABC3) show undetectable basal levels of the protein, but which is readily induced by treatment of *N. crassa* with STS (Fig. 1D), confirming the results of gene expression experiments. The use of this antiserum with immunofluorescence microscopy showed that the protein distributes at the cell surface in a pattern compatible with a plasma membrane localization (Fig. 1F), thus supporting the assigned function NCU09975 as a member of the ABC transporter superfamily (see below).

In order to further investigate the involvement of the NCU09141 and NCU09975 proteins in mediating the effects of STS, we checked the drug sensitivity of mutant strains carrying deletions in the respective genes. The ΔNCU09975, hereafter designated abc3 mutant, is extremely sensitive to STS in comparison to wild type, as observed by its growth in GFS solid medium, which induces colonial growth (Fig. 2A), and a marked impairment of germination in liquid medium (Fig. S3A), which is also reflected by a higher impairment of cell size increase over time as measured by the forward scatter parameter in flow cytometry (Fig. S3B). This sensitivity is rather specific since the strain is not particularly sensitive to another cell-death inducer such as phytosphingosine nor to reactive oxygen species, like hydrogen peroxide or those generated by treatment with paraquat. Moreover, STS induces much higher chromatin fragmentation in the abc3 mutant than in the wild type strain, a PCD hallmark detected by the TUNEL assay (Fig. 2D). The ΔNCU09141 mutant is only slightly more sensitive to STS than wild type (Fig. 2B), possibly due to the presence of redundant cellular functions.

We also investigated the reaction to STS of other mutants carrying deletions in genes whose expression is affected by exposure of fungal cells to the drug (Table S3). As controls, we used in these assays the complex I deletion mutants nuo51 and nuo21.3c, which are more sensitive and more resistant to STS than wild type, respectively (Castro et al., 2010). Fig. 2C shows additional strains that are clearly more sensitive (ΔNCU21652, previously called ΔNCU09974) or more resistant (ΔNCU03229, ΔNCU06419, ΔNCU04512) to STS than the wild type strain, indicating that the respective proteins play a significant role in the *N. crassa* response to the drug and pointing directions for future work. Taken together, our results also underline the general use of transcriptional profiling for the identification of novel proteins involved in the cellular reaction to death inducers.

Interestingly, the product of the *NCU21652* gene, which is located adjacent to *abc3* in the *N. crassa* genome, contains a domain present in transcription factors. Despite that it was not included in a previous characterization of transcription factor mutants (Colot et al., 2006), we hypothesized that *NCU21652* encodes a transcription factor involved in the genetic response to STS. Indeed, RT-PCR experiments demonstrate that the increased expression levels of *NCU09141* and *abc3* genes is impaired in the presence of STS in a NCU21652 deletion-mutant background (Fig. 1E). These data represent strong evidence that NCU21652 is a novel transcription factor required to set up a genetic response to STS and explain the high STS-sensitivity of the ΔNCU21652 strain.

3.2. The ABC3 protein has a role in staurosporine export

The predicted amino acid sequence of NCU09975 (ABC3) displays high homology with members of the superfamily of ABC transporters (Fig. S2A) and this type of proteins have been implicated in ATP-dependent drug efflux (Cannon et al., 2009). The high sensitivity of the abc3 mutant strain to STS led us to hypothesize that it is a STS exporter. In order to assess its function, we

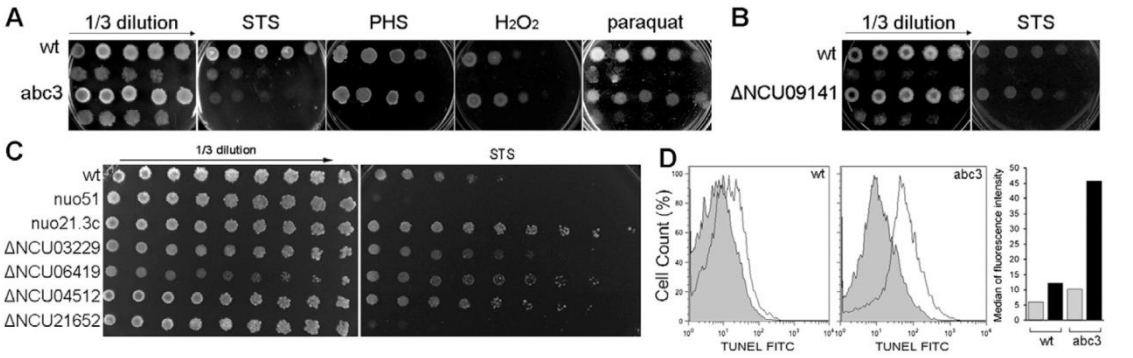

Fig. 2. Drug-sensitivity of different strains. (A–C) Serial dilutions of conidial suspensions of the designated strains were spotted and incubated in control medium (left panels of A, B and C) or medium containing 5 μM STS or 10 μg/ml phytosphingosine (PHS) or 1.5 mM hydrogen peroxide or 200 μM paraquat, as indicated. (D) TUNEL staining. Quantification by fluorescence-activated cell sorter analysis of DNA fragmented cells from wild type (wt) or abc3 mutant cells that were incubated for 3 h in the absence (gray shadow histogram) or presence (unshadow histogram) of 12.5 μM STS. FITC, fluorescein isothiocyanate. The median of the fluorescein isothiocyanate fluorescence in the absence (gray) or presence (black) of STS is indicated on the right graph.

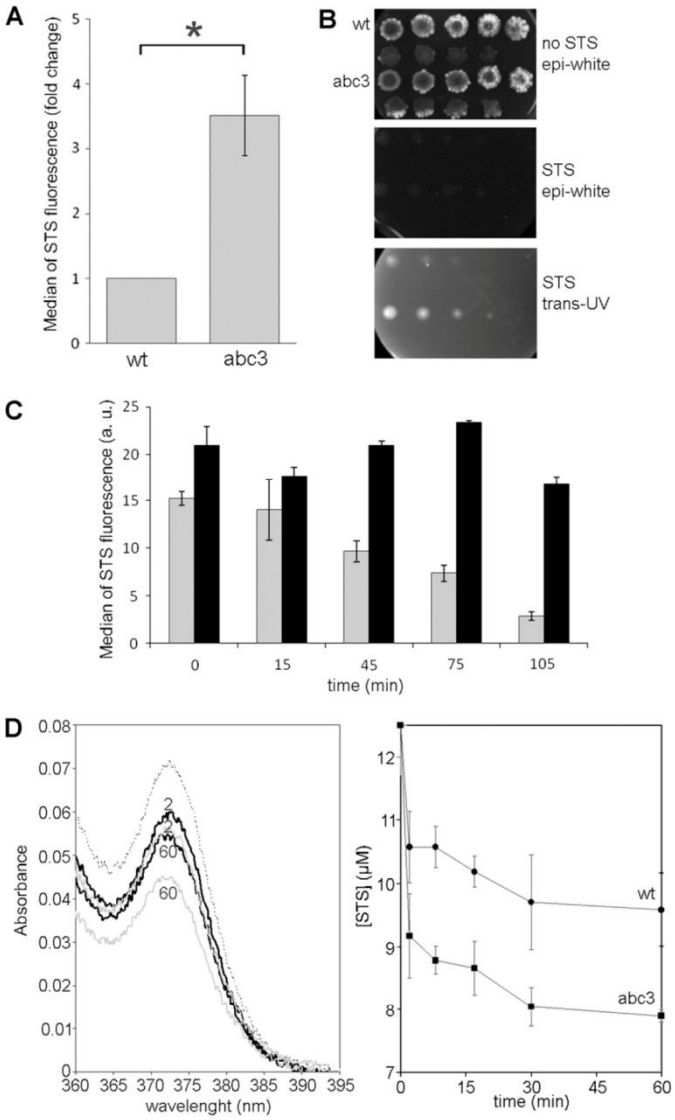

Fig. 3. Mutant abc3 cells accumulate high levels of STS as a result of defective drug extrusion. (A) Quantification of intracellular STS by flow cytometry in wild type (wt) and abc3 mutant strain after 1 h incubation with 25 μM STS. Bar graphs show average ± standard deviation of the median of STS fluorescence from three independent experiments. A Mann–Whitney test was performed (*$p < 0.05$). (B) Nine spots of serial 3-fold dilutions of conidial suspensions of wild type (wt) and abc3 strains were incubated in GFS medium in the absence (top) or presence of 7.5 μM STS. The plates were scanned in Gel Doc instrument (Bio Rad) in epi-white mode or trans-UV mode. (C) Wild type (gray) and abc3 mutant cells (black) were incubated in medium containing 25 μM STS, but devoid of sugars. After sucrose addition, samples were collected at the indicated time point and intracellular STS concentration was determined by flow cytometry. A representative experiment performed in triplicate is shown. PI-positive or dead cells monitored throughout the time-course were always <1.5%. (D) Visible absorption spectra of culture media from wild type (solid black lines) and abc3 cells (solid gray lines) after the indicated 2 or 60 min of incubation in 12.5 μM STS is shown in the left panel, with the dashed line representing the spectrum of control (media with 12.5 μM STS and no cells). The time-course concentration of staurosporine measured from visible absorption spectra of culture media of wild type (circles) and abc3 (squares) is shown in the right panel. The data represent the average ± standard deviation from three independent experiments.

compared the accumulation of STS in wild type and the abc3 mutant strain. Taking advantage of STS fluorescence (Iyer et al., 2008), we devised a flow cytometry methodology to measure its intracellular concentration. Conidial suspensions (5×10^6 cells/ml) were incubated for 1 h at room temperature in minimal medium containing 25 μM STS, after which cells were washed and their STS intracellular content measured. Fig. 3A shows that STS accumulation is ca 3.5 times higher in the mutant than in wild type cells. Since STS partially fluoresces in the visible region of the spectrum when excited with UV radiation, spots of cells loaded with STS should fluoresce in a trans-UV illuminator. Indeed, when spotted in GFS solid medium with a high STS concentration, in which growth is barely observed (middle panel in Fig. 3B), mutant cells exhibit much higher fluorescence over UV-transillumination than

wild type cells (Fig. 3B, lower panel), confirming a higher STS accumulation in the abc3 mutant cells.

We sought thus to test if the higher accumulation of STS in the mutant was due to a limited drug efflux capacity. Since drug transport by ABC proteins requires ATP (Cannon et al., 2009) and we did not observe higher intracellular accumulation of STS in the mutant *versus* wild type when cells are incubated in water instead of growth medium, we assessed the rate of STS extrusion between wild type and abc3 mutant strains. This was done by incubating conidia from both strains for 15 min at room temperature in minimal medium containing 25 μM STS and devoid of sugars to avoid active STS export. Afterwards, sucrose was added, aliquots were collected at different time points and the STS internal content was assessed. It was observed that, over a period of 100 min, the internal STS content of wild type cells decreases to ca 1/5 of the initial value, whereas in the abc3 mutant cells the STS content oscillates around the initial value (Fig. 3C). In accordance with higher intracellular STS concentration, the extracellular concentration of STS in the mutant liquid culture was smaller than in the wild type liquid culture (Fig. 3D). The higher STS accumulation in the mutant cells, together with lower extracellular concentrations and limited STS export capacity observed in the mutant strain, points to an essential role of ABC3 protein in the export of STS.

3.3. Targeted drug inhibitors modulate fungal sensitivity to staurosporine

Since the abc3 strain is highly sensitive to STS and the ABC3 protein plays a role in STS export, we reasoned that inhibiting the ABC3 protein would also make wild type cells much more sensitive to STS. Therefore, we searched the literature and tested the effects on *N. crassa* of a series of compounds targeting ABC-type proteins when used in combination with STS (Table S4). While some compounds revert the sensitivity of wild type to STS, others stimulate the effects of STS, indicating capability to modulate fungal sensitivity to STS. Fig. 4A shows that STS has a much stronger antifungal effect against wild type *N. crassa* cells when combined with either Verapamil or sodium orthovanadate. Orthovanadate is a universal inhibitor of ABC transporters, binding at the phosphate binding site and impairing ATP hydrolysis (Sarkadi et al., 2006). Verapamil has been described as a specific competitive inhibitor of human P-glycoprotein (Tsuruo et al., 1982). While these compounds have little if any effect on *N. crassa* when used alone, their combination with STS leads to a dramatic effect on fungal growth. This effect could be also observed in other *N. crassa* strains, such as the nuo78 complex I mutant that show a similar transcription of *abc3* as the wild type strain (not shown), corroborating the ability to modulate staurosporine sensitivity with inhibitors.

In order to confirm that Verapamil and orthovanadate were indeed inhibiting STS export, the intracellular accumulation of STS in the presence of each of these compounds was assessed in both wild type and abc3 mutant cells (Fig. 5C and D). After 1 h of incubation with STS together with either Verapamil or orthovanadate, the STS intracellular content of the wild type cells increases significantly, whereas in the *abc3* mutant the differences are not significant. Accordingly, extracellular levels of STS in wild type cells treated with Verapamil are lower than in untreated cells (Fig. 5A and B). These results provide an explanation for the enhanced antifungal effects of the combination of STS with either Verapamil or orthovanadate. By preventing STS elimination from fungal cells, these two inhibitors potentiate the cellular effects of STS treatment.

To determine whether the interaction of drug combinations on cell growth was specific for Neurospora or could be generalized to other fungi, we tested the effect of combining STS with an inhibitor of ABC transporters in two common human pathogens, *C. albicans* (Fig. 4B) and *A. fumigatus* (Fig. 4C). Like in *N. crassa*, the combination of STS and sodium orthovanadate results in an impressive effect on growth of both of the pathogenic species. These results unravel the potential of this type of drug combinations to be used as antifungal agents.

Despite the fact that the ΔNCU09141 mutant is not particularly sensitive to STS, the drug-induced expression of the respective gene observed in microarray hybridizations advocates that the encoded protein may play a role in the fungal response to STS. NCU09141 is classified as a "probable pyridoxine dehydrogenase", suggesting an interesting link between cell death and vitamin biosynthesis. However, we found that it also displays similarity to β-subunits (regulators) of the shaker-related family of voltage-gated potassium channels (Fig. S2B). These proteins have been implicated in programmed cell death including STS-induced apoptosis in mammalian cells (Szabo et al., 2008, 2010) and *NCU02887*

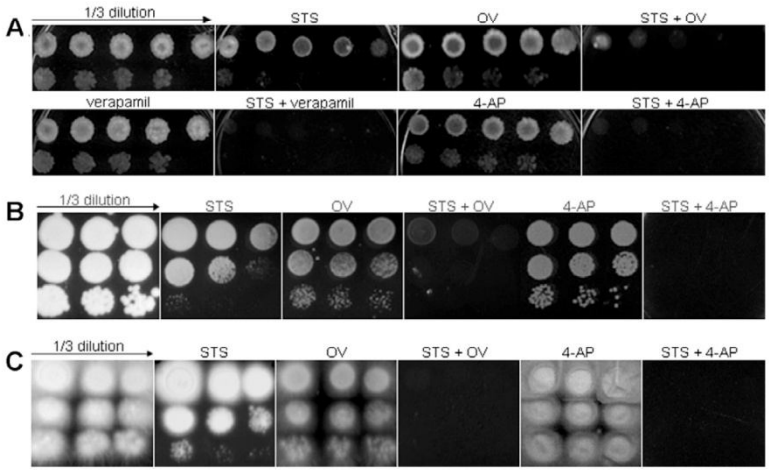

Fig. 4. Antifungal effects of drug combinations. Serial dilutions of cellular suspensions of *N. crassa* (A), *C. albicans* (B) and *A. fumigatus* (C) were spotted and incubated in control medium (first panels of A, B and C) or medium containing STS or sodium orthovanadate (OV) or Verapamil or 4-aminopyridine (4-AP), or combinations of drugs. Drug concentrations used were 5, 15 and 10 μM STS and 5, 1 and 1 mM OV (A, B and C, respectively), 5 mM 4-AP and 0.5 mM Verapamil.

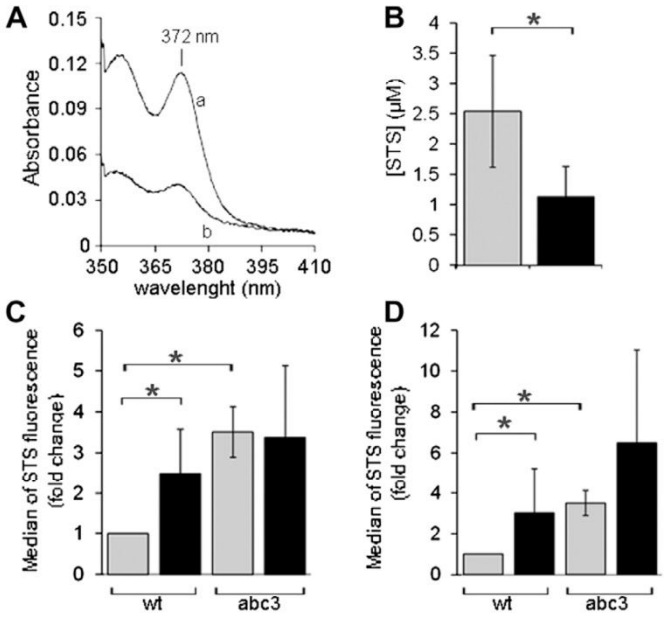

Fig. 5. Verapamil and orthovanadate increase STS intracellular accumulation and a concomitant decrease of extracellular STS concentration. (A) Visible absorption spectra of concentrated external media of 5 h-grown *N. crassa* (initial concentration 10^7 conidia/ml) in minimal medium at 30 °C followed by 30 min in the presence of 12.5 μM STS and in the absence (a) or presence of 0.5 mM Verapamil (b). (B) STS extracellular concentration in the absence (gray) or presence of Verapamil (black) calculated from the spectra in A. (C and D) Quantification by flow cytometry of relative intracellular STS concentration in the indicated strains in the absence (gray) or presence (black) of 5 mM Verapamil (C) or 5 mM orthovanadate (D). The data in B, C and D represent the average ± standard deviation of three independent experiments. Statistical significance was determined with the Mann–Whitney test (*$p \leqslant 0.05$).

(annotated as a voltage-gated potassium channel subunit) is also induced upon *N. crassa* exposure to STS (Table S1). Therefore, as rationalized for ABC transporters above, we tested the effects of combining compounds targeting voltage-gated potassium channels with STS on fungal growth (Table S4). Fig. 4A–C illustrates the strong enhancement effect of the combination between STS and 4-aminopyridine on growth of *N. crassa*, *C. albicans* and *A. fumigatus*. These results suggest that NCU09141 may indeed be associated with potassium channels and support their involvement in the response to STS. Altogether, our results point out the power of transcriptional profiling for identifying novel proteins with potential to become drug targets.

4. Discussion

The ability to modulate programmed cell death has broad implications in the medical field, from cancer treatment to fighting infectious diseases (Ramsdale, 2008; Reed, 2006; Sharon et al., 2009). Knowledge about its molecular basis is expectedly valuable for designing drugs targeting specific proteins that can be used to modulate programmed cell death. Our data support this assumption and prove the underlying principle. We analyzed time-course alterations in *N. crassa* gene expression resulting from exposure to the death-inducer STS. Novel proteins involved in the response to the drug were found as judged by alterations in gene expression profiles and/or altered sensitivity to the drug of specific null-mutant strains. Among these, an ABC transporter protein (NCU09975) and a protein with similarity to voltage-gated potassium channels subunits (NCU09141) were identified. Then, we showed that treating *N. crassa* with inhibitors of either of this type of proteins allows modulation of the fungal sensitivity to STS. In particular, some inhibitors extremely enhance the antifungal effect of STS, namely the general ABC transporter inhibitor orthovanadate (Sarkadi et al., 2006), the competitive inhibitor of mammalian p-glycoprotein Verapamil (Aller et al., 2009) and the 4-aminopyridine inhibitor of voltage-gated potassium channels (Chin et al., 1997). This effect is observed not only against *N. crassa*, but also against common fungal pathogens, such as *A. fumigatus* and *C. albicans*. Thus, these drug combinations have potential applications as antifungals and, possibly, anticancer agents.

While NCU09141 is assigned as a probable pyridoxine dehydrogenase, we noticed its similarities to regulatory subunits of voltage-gated potassium channels of the shaker-related subfamily Kvβ2 (Xu and Li, 1997). While this remains to be proved, our data clearly associate voltage-gated potassium channels with the response to STS. *NCU09141* and another gene (*NCU02887*, annotated as a voltage-gated potassium channel subunit) are induced upon *N. crassa* exposure to STS. In addition, the inhibitor of voltage-gated potassium channels 4-aminopyridine (Chin et al., 1997) reinforces the antifungal properties of STS. These channels are involved in apoptosis, although it remains controversial whether their activation leads to or protects from apoptosis (Szabo et al., 2010). The action of β2 subunits on the regulation of voltage-gated K^+ channels is not clear, but its proposed role in channel activation (Xu and Li, 1997) lead us to speculate that STS-driven overexpression of NCU09141 may protect against cell death by activating K^+ efflux.

The product of *NCU09975* (ABC3) displays high homology with members of the superfamily of ABC transporters. These proteins have been often implicated in conferring multidrug resistance to chemotherapy both to tumor cells and to infectious organisms (Cannon et al., 2009; Nascimento et al., 2003). The best human homolog of ABC3 is p-glycoprotein (33% identity and 54% similarity), a multiple drug exporter involved in apoptosis protection (Sarkadi et al., 2006). In a phylogenetic analysis of fungal ABC pro-

teins, *N. crassa* ABC3 was placed in Group III of the ABC-B subfamily (Kovalchuk and Driessen, 2010), but no clear functions have been attributed so far to members of this group. Expression of *A. fumigatus* AtrC, another member of the group, increases in the presence of various toxicants but the respective knockout mutant is not differentially sensitive to them (Andrade et al., 2000). The *Magnaporthe grisea* ABC3 homolog is required for host cell penetration and for protection from oxidative stress (Sun et al., 2006). By functional characterization, we show that an ABC3 deletion-mutant accumulates more STS than wild type *N. crassa* when exposed to the drug. In sharp contrast to the mutant, wild type is able to extrude STS upon energization of the cells indicating that ABC3 is involved in STS transport. This conclusion is further supported by the fact that STS accumulation in the wild type strain is enhanced by two inhibitors of p-glycoprotein, orthovanadate and Verapamil, while the same inhibitors did not affect significantly the STS content of the mutant strain. Despite the high accumulation of STS in the mutant, its sensitivity to STS observed from spot assays results from STS-induced PCD and not just through STS toxicity resulting from deficient efflux, as demonstrated by the TUNEL assay. ABC3 appears to have narrower substrate specificity than p-glycoprotein, which might reflect the fact that, facing changing environments, fungal genomes possess a higher density of ABC transporters than the human genome (Ren et al., 2007). To our knowledge, ABC3 is the first described transporter of the widely used death-inducer STS. The fact that ABC3 is highly induced in the presence of STS and the abc3 mutant is extremely sensitive to the drug and that inhibitors of ABC transporters enhance the effects of STS against *N. crassa* and pathogenic fungi illustrates common mechanisms of drug resistance among fungi and pinpoints a major role of ABC3 in these processes.

Multidrug resistance often arises from mutations in regulators of multidrug resistance genes like the ABC transporters (Akache et al., 2004). In this work, we also identified a novel transcription factor NCU21652 that can be elicited as a drug target. We showed that NCU21652 is required for the STS-dependent overexpression of the *NCU09141* and *NCU09975* genes, indicating that it has a pivotal role in the control of the genetic response of *N. crassa* to STS. It should be noticed that all these proteins seem to be also at least partially involved in the response to other death-inducers, since the respective genes are induced in *N. crassa* cells exposed to phytosphingosine (Videira et al., 2009). In summary, the identification of proteins responsible for drug response by transcriptional profiling, with subsequent protein targeted inhibition combined with drug insult revealed to be a powerful strategy to overcome drug resistance in fungi. These data stand as a basis for designing novel drugs/strategies for attacking tumor or pathogenic cells.

Acknowledgments

We acknowledge Paula Magalhães for help with Real-Time PCR, Dr Isabel Carvalho and Tânia Ribeiro for rat immunization and antiserum preparation, and Dr Paula Sampaio for help with immunofluorescence microscopy. This work was supported by a "Programa Ciência" fellowship financed by POPH-QREN (typology 4.2) with co-funding from ESF and MCTES to ASF, a Fundação Calouste Gulbenkian PhD fellowship to APG, NIH grant GM60468 to NLG, research grants from FCT Portugal and the European POCI program of QCAIII (co-participated by FEDER) and a sabbatical fellowship from Fundação Luso-Americana to AV.

Appendix A. Supplementary material

Supplementary data associated with this article can be found, in the online version, at doi:10.1016/j.fgb.2011.09.004.

References

Akache, B., MacPherson, S., Sylvain, M.A., Turcotte, B., 2004. Complex interplay among regulators of drug resistance genes in *Saccharomyces cerevisiae*. J. Biol. Chem. 279, 27855–27860.

Aller, S.G., Yu, J., Ward, A., Weng, Y., Chittaboina, S., Zhuo, R., Harrell, P.M., Trinh, Y.T., Zhang, Q., Urbatsch, I.L., Chang, G., 2009. Structure of P-glycoprotein reveals a molecular basis for poly-specific drug binding. Science 323, 1718–1722.

Andrade, A.C., Van Nistelrooy, J.G., Peery, R.B., Skatrud, P.L., De Waard, M.A., 2000. The role of ABC transporters from *Aspergillus nidulans* in protection against cytotoxic agents and in antibiotic production. Mol. Gen. Genet. 263, 966–977.

Cannon, R.D., Lamping, E., Holmes, A.R., Niimi, K., Baret, P.V., Keniya, M.V., Tanabe, K., Niimi, M., Goffeau, A., Monk, B.C., 2009. Efflux-mediated antifungal drug resistance. Clin. Microbiol. Rev. 22, 291–321.

Castro, A., Lemos, C., Falcao, A., Glass, N.L., Videira, A., 2008. Increased resistance of complex I mutants to phytosphingosine-induced programmed cell death. J. Biol. Chem. 283, 19314–19321.

Castro, A., Lemos, C., Falcao, A., Fernandes, A.S., Glass, N.L., Videira, A., 2010. Rotenone enhances the antifungal properties of staurosporine. Eukaryot. Cell 9, 906–914.

Chin, L.S., Park, C.C., Zitnay, K.M., Sinha, M., DiPatri Jr., A.J., Perillan, P., Simard, J.M., 1997. 4-Aminopyridine causes apoptosis and blocks an outward rectifier K^+ channel in malignant astrocytoma cell lines. J. Neurosci. Res. 48, 122–127.

Colot, H.V., Park, G., Turner, G.E., Ringelberg, C., Crew, C.M., Litvinkova, L., Weiss, R.L., Borkovich, K.A., Dunlap, J.C., 2006. A high-throughput gene knockout procedure for neurospora reveals functions for multiple transcription factors. Proc. Natl Acad. Sci. USA 103, 10352–10357.

Davis, R.H., de Serres, F.J., 1970. Genetic and microbiological research techniques for *Neurospora crassa*. Methods Enzymol. 17A, 79–143.

Davis, R.H., Perkins, D.D., 2002. Timeline: Neurospora: a model of model microbes. Nat. Rev. Genet. 3, 397–403.

Duarte, M., Sousa, R., Videira, A., 1995. Inactivation of genes encoding subunits of the peripheral and membrane arms of Neurospora mitochondrial complex I and effects on enzyme assembly. Genetics 139, 1211–1221.

Dunlap, J.C., Borkovich, K.A., Henn, M.R., Turner, G.E., Sachs, M.S., Glass, N.L., McCluskey, K., Plamann, M., Galagan, J.E., Birren, B.W., Weiss, R.L., Townsend, J.P., Loros, J.J., Nelson, M.A., Lambreghts, R., Colot, H.V., Park, G., Collopy, P., Ringelberg, C., Crew, C., Litvinkova, L., DeCaprio, D., Hood, H.M., Curilla, S., Shi, M., Crawford, M., Koerhsen, M., Montgomery, P., Larson, L., Pearson, M., Kasuga, T., Tian, C., Basturkmen, M., Altamirano, L., Xu, J., 2007. Enabling a community to dissect an organism: overview of the Neurospora functional genomics project. Adv. Genet. 57, 49–96.

Galagan, J.E., Calvo, S.E., Borkovich, K.A., Selker, E.U., Read, N.D., Jaffe, D., FitzHugh, W., Ma, L.-J., Smirnov, S., Purcell, S., Rehman, B., Elkins, T., Engels, R., Wang, S., Nielsen, C.B., Butler, J., Endrizzi, M., Qui, D., Ianakiev, P., Bell-Pedersen, D., Nelson, M.A., Werner-Washburne, M., Selitrennikoff, C.P., Kinsey, J.A., Braun, E.L., Zelter, A., Schulte, U., Kothe, G.O., Jedd, G., Mewes, W., Staben, C., Marcotte, E., Greenberg, D., Roy, A., Foley, K., Naylor, J., Stange-Thomann, N., Barrett, R., Gnerre, S., Kamal, M., Kamvysselis, M., Mauceli, E., Bielke, C., Rudd, S., Frishman, D., Krystofova, S., Rasmussen, C., Metzenberg, R.L., Perkins, D.D., Kroken, S., Cogoni, C., Macino, G., Catcheside, D., Li, W., Pratt, R.J., Osmani, S.A., DeSouza, C.P.C., Glass, L., Orbach, M.J., Berglund, J.A., Voelker, R., Yarden, O., Plamann, M., Seiler, S., Dunlap, J., Radford, A., Aramayo, R., Natvig, D.O., Alex, L.A., Mannhaupt, G., Ebbole, D.J., Freitag, M., Paulsen, I., Sachs, M.S., Lander, E.S., Nusbaum, C., Birren, B., 2003. The genome sequence of the filamentous fungus *Neurospora crassa*. Nature 422, 859–868.

Gescher, A., 2000. Staurosporine analogues – pharmacological toys or useful antitumour agents? Crit. Rev. Oncol. Hematol. 34, 127–135.

Glass, N.L., Dementhon, K., 2006. Non-self recognition and programmed cell death in filamentous fungi. Curr. Opin. Microbiol. 9, 553–558.

Iyer, G.H., Taslimi, P., Pazhanisamy, S., 2008. Staurosporine-based binding assay for testing the affinity of compounds to protein kinases. Anal. Biochem. 373, 197–206.

Jarvis, W.D., Turner, A.J., Povirk, L.F., Traylor, R.S., Grant, S., 1994. Induction of apoptotic DNA fragmentation and cell death in HL-60 human promyelocytic leukemia cells by pharmacological inhibitors of protein kinase C. Cancer Res. 54, 1707–1714.

Kasuga, T., Townsend, J.P., Tian, C., Gilbert, L.B., Mannhaupt, G., Taylor, J.W., Glass, N.L., 2005. Long-oligomer microarray profiling in *Neurospora crassa* reveals the transcriptional program underlying biochemical and physiological events of conidial germination. Nucleic Acids Res. 33, 6469–6485.

Kovalchuk, A., Driessen, A.J., 2010. Phylogenetic analysis of fungal ABC transporters. BMC Genomics 11, 177.

Livak, K.J., Schmittgen, T.D., 2001. Analysis of relative gene expression data using real-time quantitative PCR and the 2(-Delta Delta C(T)) Method. Methods 25, 402–408.

Madeo, F., Frohlich, E., Frohlich, K.U., 1997. A yeast mutant showing diagnostic markers of early and late apoptosis. J. Cell Biol. 139, 729–734.

Marques, I., Duarte, M., Assunção, J., Ushakova, A.V., Videira, A., 2005. Composition of complex I from *Neurospora crassa* and disruption of two "accessory" subunits. BBA-Bioenergetics 1707, 211–220.

McCluskey, K., 2003. The Fungal Genetics Stock Center: from molds to molecules. Adv. Appl. Microbiol. 52, 245–262.

Nascimento, A.M., Goldman, G.H., Park, S., Marras, S.A., Delmas, G., Oza, U., Lolans, K., Dudley, M.N., Mann, P.A., Perlin, D.S., 2003. Multiple resistance mechanisms among *Aspergillus fumigatus* mutants with high-level resistance to itraconazole. Antimicrob. Agents Chemother. 47, 1719–1726.

Omura, S., Iwai, Y., Firano, A., Nakagawa, A., Awaya, F., Tsuchiya, T., Masuma, R., 1977. A new alkaloid AM-2282 of Streptomyces origin taxonomy, fermentation isolation and preliminary characterization. J. Antibiot. 30, 275–282.

Osman, A.B., Gani, S.M., Engh, R.A., 2010. Protein kinase inhibition of clinically important staurosporine analogues. Nat. Prod. Rep. 27, 489–498.

Ramsdale, M., 2008. Programmed cell death in pathogenic fungi. Biochim. Biophys. Acta 1783, 1369–1380.

Reed, J.C., 2006. Drug insight: cancer therapy strategies based on restoration of endogenous cell death mechanisms. Nat. Clin. Pract. Oncol. 3, 388–398.

Ren, Q., Chen, K., Paulsen, I.T., 2007. TransportDB: a comprehensive database resource for cytoplasmic membrane transport systems and outer membrane channels. Nucleic Acids Res. 35, D274–279.

Ruepp, A., Zollner, A., Maier, D., Albermann, K., Hani, J., Mokrejs, M., Tetko, I., Guldener, U., Mannhaupt, G., Munsterkotter, M., Mewes, H.W., 2004. The FunCat, a functional annotation scheme for systematic classification of proteins from whole genomes. Nucleic Acids Res. 32, 5539–5545.

Sarkadi, B., Homolya, L., Szakacs, G., Varadi, A., 2006. Human multidrug resistance ABCB and ABCG transporters: participation in a chemoimmunity defense system. Physiol. Rev. 86, 1179–1236.

Schulte, T.H., Scarborough, G.A., 1975. Characterizati on of the glucose transport systems in *Neurospora crassa* sl. J. Bacteriol. 122, 1076–1080.

Sharon, A., Finkelstein, A., Shlezinger, N., Hatam, I., 2009. Fungal apoptosis: function, genes and gene function. FEMS Microbiol. Rev. 33, 833–854.

Sun, C.B., Suresh, A., Deng, Y.Z., Naqvi, N.I., 2006. A multidrug resistance transporter in Magnaporthe is required for host penetration and for survival during oxidative stress. Plant Cell 18, 3686–3705.

Szabo, I., Bock, J., Grassme, H., Soddemann, M., Wilker, B., Lang, F., Zoratti, M., Gulbins, E., 2008. Mitochondrial potassium channel Kv1.3 mediates Bax-induced apoptosis in lymphocytes. Proc. Natl Acad. Sci. USA 105, 14861–14866.

Szabo, I., Zoratti, M., Gulbins, E., 2010. Contribution of voltage-gated potassium channels to the regulation of apoptosis. FEBS Lett. 584, 2049–2056.

Townsend, J.P., 2003. Multifactorial experimental design and the transitivity of ratios with spotted DNA microarrays. BMC Genomics 4, 41.

Townsend, J.P., Hartl, D.L., 2002. Bayesian analysis of gene expression levels: statistical quantification of relative mRNA level across multiple strains or treatments. Genome Biol. 3, RESEARCH0071.

Tsuruo, T., Iida, H., Yamashiro, M., Tsukagoshi, S., Sakurai, Y., 1982. Enhancement of vincristine- and adriamycin-induced cytotoxicity by verapamil in P388 leukemia and its sublines resistant to vincristine and adriamycin. Biochem. Pharmacol. 31, 3138–3140.

Videira, A., Kasuga, T., Tian, C., Lemos, C., Castro, A., Glass, N.L., 2009. Transcriptional analysis of the response of *Neurospora crassa* to phytosphingosine reveals links to mitochondrial function. Microbiology 155, 3134–3141.

Xu, J., Li, M., 1997. Kvbeta2 inhibits the Kvbeta1-mediated inactivation of K^+ channels in transfected mammalian cells. J. Biol. Chem. 272, 11728–11735.

Zauner, R., Christner, J., Jung, G., Borchart, U., Machleidt, W., Videira, A., Werner, S., 1985. Identification of the polypeptide encoded by the URF-1 gene of *Neurospora crassa* mtDNA. Eur. J. Biochem. 150, 447–454.

Table S1 in the Supplemental material lists mRNA profiling results and functional annotations. Microarray data have been deposited at the NCBI gene expression and hybridization array data repository (GEO, http://www.ncbi.nlm.nih.gov/geo/, accession No. GSE32451).

Table S2. Oligonucleotide primers used in PCR amplifications.
Underlined sequences correspond to introduced *Bam* HI and *Nde* I restriction sites, respectively.

primers	nucleotide sequence
primers for Real-Time RT-PCR	
NCU09975 (abc3), forward	GACTCCTTCATTGCCTCGTTGCC
NCU09975 (abc3), reverse	CCATCTCCATCTGCTCCACCTTCG
NCU09141 , forward	CGTTCCCAATGTTGCTTCACTTCC
NCU09141 , reverse	GTCGCATCAATCTCGTCCATCTCC
NCU04173 (actin) , forward	GGCATCACACCTTCTACAACGAG
NCU04173 (actin), reverse	ATGTCAACACGGGCAATGGC
primers for expression of ABC3 C-terminus	
forward	CATATGATTACCAAGGCGCAGCAC
reverse	GGATCCTCATCTATCCAAAGACTGTCC

Table S3. List of deletion strains tested regarding their sensitivity to staurosporine.

Gene deleted	STS sensitivity (as compared to wild type)
NCU09974/NCU21652	More sensitive
NCU09975	More sensitive
NCU03229	More resistant
NCU04512	More resistant
NCU06419	More resistant
NCU00355	Similar sensitivity
NCU00605	Similar sensitivity
NCU01066	Similar sensitivity
NCU02193	Similar sensitivity
NCU02887	Similar sensitivity
NCU03639	Similar sensitivity
NCU03979	Similar sensitivity
NCU04276	Similar sensitivity
NCU04490	Similar sensitivity
NCU04521	Similar sensitivity
NCU04699	Similar sensitivity
NCU04987/NCU20410	Similar sensitivity
NCU05338	Similar sensitivity
NCU05832	Similar sensitivity
NCU06125	Similar sensitivity
NCU06230	Similar sensitivity
NCU06603	Similar sensitivity
NCU06783	Similar sensitivity
NCU06911	Similar sensitivity
NCU08948	Similar sensitivity
NCU09115	Similar sensitivity
NCU09141	Similar sensitivity
NCU09355	Similar sensitivity
NCU09648/NCU21494	Similar sensitivity
NCU09881	Similar sensitivity

Table S4. Inhibitors used in combination with staurosporine.

Inhibitor	Effect on STS antifungal activity	reference
ABC transporter inhibitors		
Sodium orthovanadate	enhances	Sarado *et al* . (2006) Physiol Rev 107:721
Verapamil	enhances	Tsuruo *et al.* (1982) Biochem Pharmacol 31:3138
Enniatin B	no effect	Hiraga *et al.* (2005) BBRC 328:1119
Probenecid	no effect	Dallas *et al* . (2003) JPET 307:282
Josamycin	no effect	Wang *et al.* (2000) CEPP 27:587
Reversin 205	no effect	Sharom *et al.* (1999) Biochem Pharmacol 58:571
PGP-4008	no effect	Lee *et al* . (2004) J Med Chem 47:1413
Tryprostatin A	no effect	Woehlecke *et al.* (2003) Int J Cancer 107:721
MK571	reverses effect	Dallas *et al* . (2003) JPET 307:282
JS-2190	reverses effect	Ivanina and Sokolova (2008) Aquatic Toxicol 88:19
Sipholenol A	reverses effect	Shi *et al.* (2007) Cancer Sci 98:1373
Reversin121	reverses effect	Sharom *et al.* (1999) Biochem Pharmacol 58:571
voltage-gated K^+ channel inhibitors		
4-Aminopyridine	enhances	Claydon *et al* . (2007) J Pharmacol Exp Ther 320:162
Chloride tetraethylammonium	no effect	Levina *et al.* (1995) J Cell Sci 108:3405

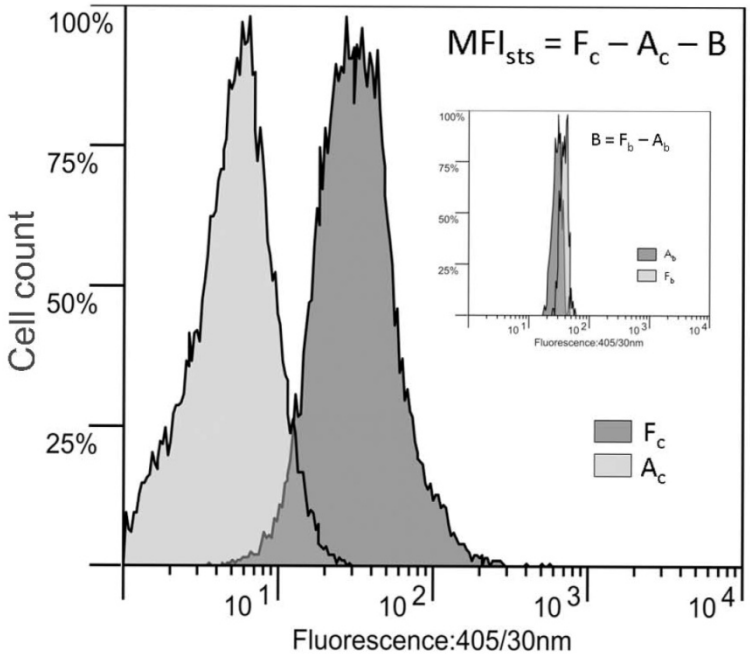

Fig. S1. Procedure for STS measurements by flow cytometry in a MoFlo (Beckman Coulter, Inc., Fort Collins, US). STS was excited with a multiline UV argon laser (330-360 nm, 40 mW), and a Sapphire blue laser (488 nm, 140 mW) was used to trigger, forward scatter measurements, and propidium iodide (PI) excitation. STS fluorescence emission was detected with a 405/30 band-pass filter, and PI with a 670/40 band-pass filter. Intracellular fluorescence (Median Fluorescence Intensity, MFI_{STS}) was determined by MFI_{STS}=Fc–Ac–B, where Fc is the median of total fluorescence in the sample (dark grey histogram), Ac is the autofluorescence signal obtained from a control sample without STS (light grey histogram), and B is the background or extracellular STS fluorescence. Inset - Background fluorescence was determined using fluorescent CaliBRITE beads (FITC-labeled, 6 µm in diameter, from Becton Dickinson) and calculated by B= Fb–Ab, where Fb is the fluorescence of beads in the 405/30 channel within the STS sample (ligh grey histogram), and Ab the fluorescence of the same beads in the same channel within the control sample without STS (dark grey histogram).To quantify dead cells, PI was added before reading in the cytometer at 5 µg/ml final concentration.

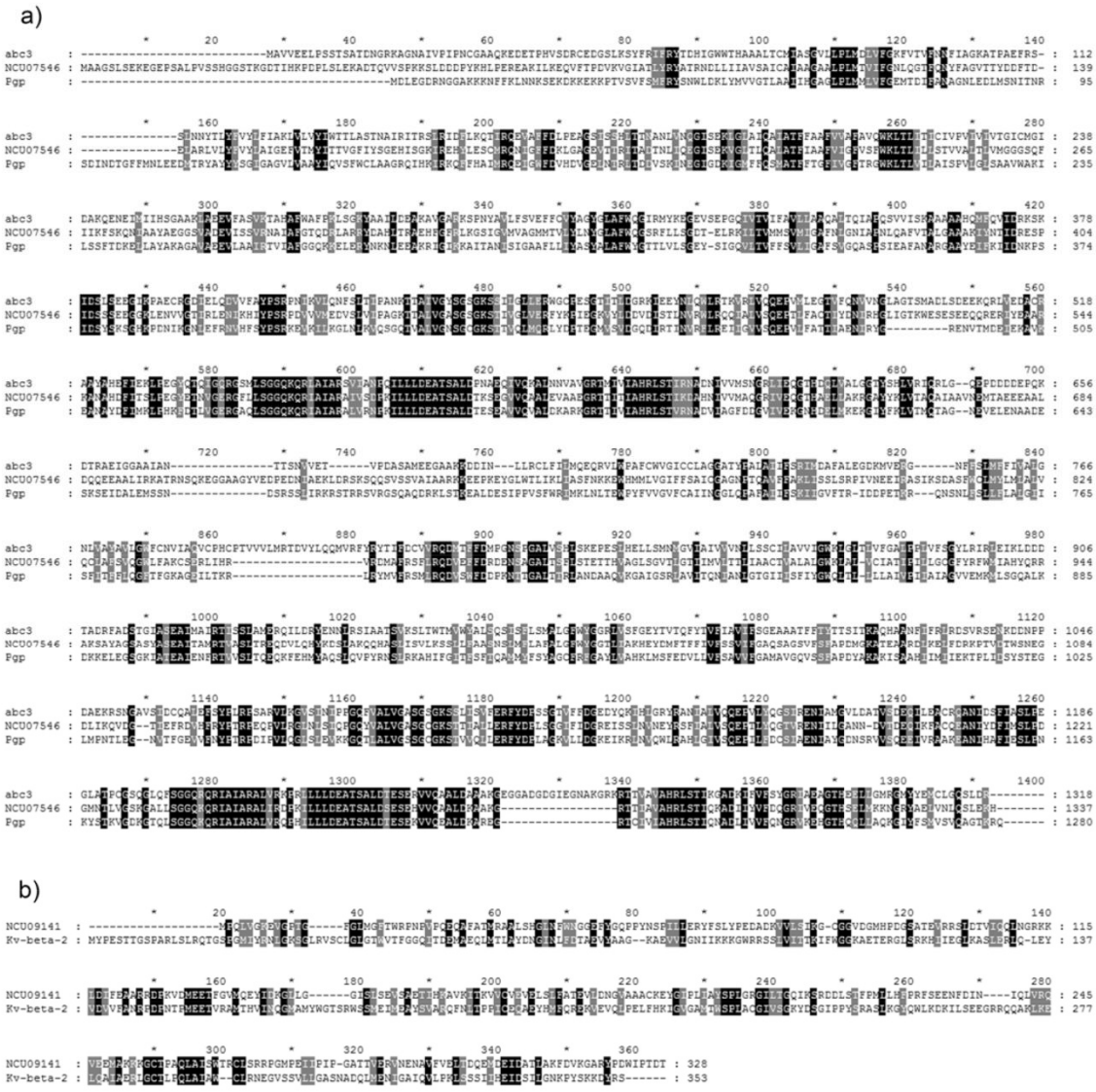

Fig. S2. Clustal alignment of protein sequences. Black and grey shadows indicate identical amino acid residues and conserved substitutions, respectively. Pgp is human P-glycoprotein (or MDR-1) (acc. no. AAA59575); Kv-beta-2 is the β-subunit of a human potassium voltage-gated channel, shaker related sub-family (acc. no. Q13303-2).

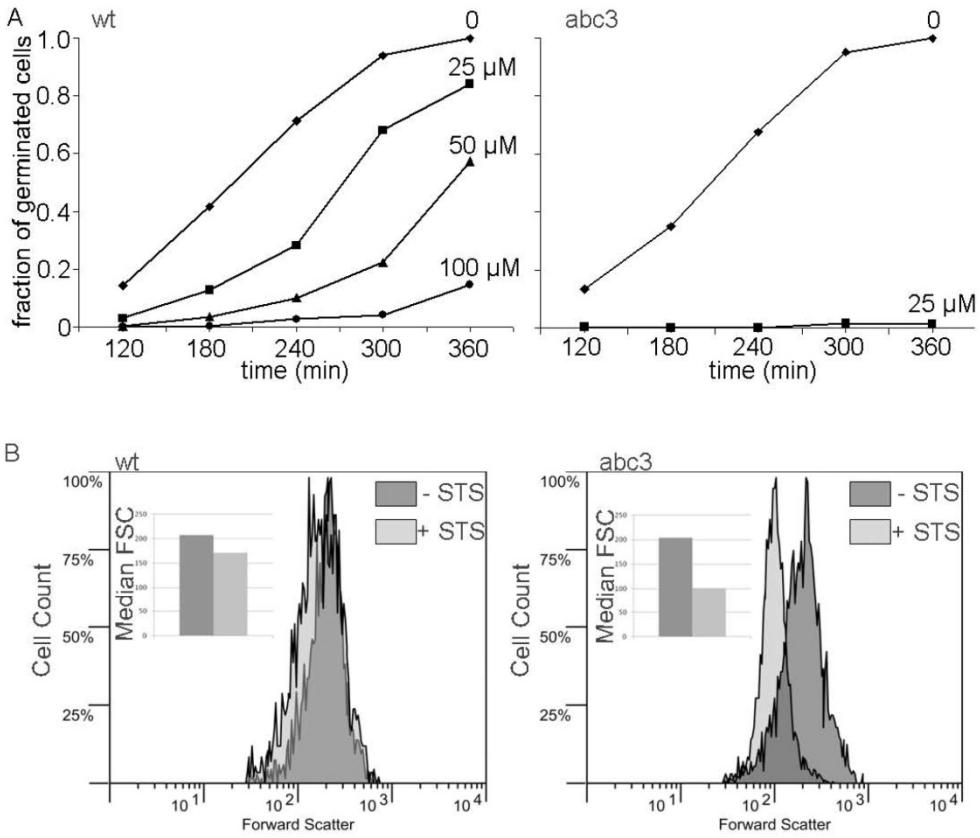

Fig. S3. STS severely impairs fungal germination. A) Fraction of wild type (left) or abc-3 conidia (right) germinating at different times in liquid minimal medium containing the indicated STS concentrations.B) Flow cytometry measurements of forward scatter parameter of wild type (left) and abc3 (right) cells after incubation in minimal medium for 4 h in the absence or presence of 12.5 µM STS, as indicated.

Programmed cell death in *Neurospora crassa*

A. Pedro Gonçalves, Arnaldo Videira

New Journal of Science (2014) Article ID 479015

Hindawi Publishing Corporation
New Journal of Science
Volume 2014, Article ID 479015, 7 pages
http://dx.doi.org/10.1155/2014/479015

Review Article

Programmed Cell Death in *Neurospora crassa*

A. Pedro Gonçalves[1,2] and Arnaldo Videira[1,2]

[1] *Instituto de Biologia Molecular e Celular (IBMC), Universidade do Porto, Rua do Campo Alegre 823, 4150-180 Porto, Portugal*
[2] *Instituto de Ciências Biomédicas de Abel Salazar (ICBAS), Universidade do Porto, Rua de Jorge Viterbo Ferreira 228, 4050-313 Porto, Portugal*

Correspondence should be addressed to A. Pedro Gonçalves; apgoncalves@ibmc.up.pt and Arnaldo Videira; avideira@ibmc.up.pt

Received 21 November 2013; Revised 29 January 2014; Accepted 30 January 2014; Published 2 March 2014

Academic Editor: Paula Ludovico

Programmed cell death has been studied for decades in mammalian cells, but simpler organisms, including prokaryotes, plants, and fungi, also undergo regulated forms of cell death. We highlight the usefulness of the filamentous fungus *Neurospora crassa* as a model organism for the study of programmed cell death. In *N. crassa*, cell death can be triggered genetically due to hyphal fusion between individuals with different allelic specificities at *het* loci, in a process called "heterokaryon incompatibility." Chemical induction of cell death can also be achieved upon exposure to death-inducing agents like staurosporine, phytosphingosine, or hydrogen peroxide. A summary of the recent advances made by our and other groups on the discovery of the mechanisms and mediators underlying the process of cell death in *N. crassa* is presented.

1. *Neurospora crassa* as a Model Organism

Neurospora crassa is a nonpathogenic filamentous fungus, very easy to maintain, grow, and manipulate. *N. crassa* enjoys modest nutritional requirements: the common minimal medium (Vogel's minimal medium) includes a sugar, a nitrogen source (ammonium and nitrate), phosphate, sulfate, potassium, magnesium, calcium, trace metals, and a small amount of the vitamin biotin [1]. Moreover, *N. crassa* is one of the fastest growing filamentous fungi (approximately 10 cm per day under optimal conditions), justifying its appearance among the first colonizers of recently burned vegetation [2]. It is prone to genetic experiments like the induction of mutations, genes, and mutants isolation, microscopic analysis, biochemical testing, and so on. Thus, *Neurospora* presents some features that turn it into a very attractive option to be used in the laboratory.

N. crassa is a multicellular ascomycete. It was initially documented in 1843, when several Parisian bakeries were infested by cultures of an orange sporulating mould [3]. A century later, mycologists Cornelius Shear and Bernard Dodge moved it to the *Neurospora* genus, based on the discovery that this fungus possesses a sexual morphological structure called perithecia [4]. Literally translated, "Neurospora" means "nerve" plus "spore" and the explanation for this name resides in the fact that the fungal spores display longitudinal striations resembling animal axons which belong to the nervous system. In its natural habitat, *Neurospora* is found essentially in tropical and subtropical regions but also in temperate climates [2]. Figure 1 shows spots of *N. crassa* colonization that can be easily observed following a forest fire. During the 20th century, this fungus was the basis of some breakthrough discoveries in the molecular genetics field. The Nobel Prize in Physiology and Medicine was awarded to George Wells Beadle and Edward Lawrie Tatum in 1958, because of their "one gene-one enzyme" pioneering hypothesis. The theory, which conceived the idea that particular portions of genetic material lead to the synthesis of specific proteins, was described in 1941 [5] and allowed the comprehension of one of the most basic aspects of Biology. In another work using *N. crassa* during the 1940s, Srb and Horowitz showed that metabolic pathways comprise a series of steps each of them catalysed by an enzyme [6].

The aforementioned works of renowned geneticists represent only a few examples of successful applications of *N. crassa* in the study of the molecular basis of biological processes. The fungus has also been used to study circadian

Figure 1: *N. crassa* in a natural habitat. In nature, *Neurospora* is commonly found as one of the first colonizers of burned vegetation. The picture depicts growth of *N. crassa* on a burned tree in Portugal (note the presence of the orange mould throughout the trunk, indicated with arrows).

rhythms, gene silencing, DNA repair, cell differentiation, and mitochondrial biology [7]. More recently, in 2003, the genome of *N. crassa* was fully sequenced [8]. Access to this information, together with the availability of valuable genetic tools such as a large collection of deletion strains and a rich assortment of plasmids for protein expression, provided by the Fungal Genetics Stock Center [9], makes *N. crassa* a great model organism to work with. Our group has focused on the mechanisms employed by the mitochondrial respiratory chain to produce energy in *N. crassa* for several years [10–12] and, more recently, became interested in the process of programmed cell death [13–22].

2. Programmed Cell Death-Controlled "Suicide" of Cells

Balance between cell division and cell death is of supreme importance for the development and maintenance of multicellular organisms. Deregulation of this equilibrium can lead to pathological conditions, namely, cancer and neurodegenerative disorders. Therefore, the balance between life and death is tightly controlled and abnormal elements can be effectively eliminated by a process called "programmed cell death" [23]. Decades ago, programmed cell death was held synonymous with apoptosis, and the concepts of apoptosis and necrosis were the only used to explain the death of cells. However, in recent years, it has become evident that this is an oversimplification of the highly sophisticated mechanisms guarding the organism against potentially harmful situations. Many reports have been published and many terms have been proposed to define dissimilar pathways of cell death. However, some of these distinct ways of dying might not be really different, because there are many overlapping features and the precise biochemical mechanisms are often unclear. To overcome this issue, the Nomenclature Committee on Cell Death has recently proposed unified criteria for the definition of cell death and its different morphologies and molecular signals [24]. Despite the advances made in the comprehension of the cell death subject, several mechanisms are still a matter of debate and new approaches might unravel new pathways and mediators.

Cell death studies have been carried out for decades using mammalian models. However, it has become clear that lower eukaryotes and even prokaryotes undergo programmed cell death when insulted with chemical agents and other stress signals. Humans, the nematode *Caenorhabditis elegans*, the fly *Drosophila melanogaster,* and the yeast *Saccharomyces cerevisiae* represent major organisms used to investigate programmed cell death. Because of the aforementioned advantages of using *N. crassa* as a model organism and because it was shown that it presents additional proteins with homology to cell death-related molecules of mammalian cells when compared with other models such as yeasts [25], we anticipated that it would be a good prototype to study the fundamentals of cell death. More specifically, *in silico* searches predict dozens of cell death-associated genes in filamentous species that seem to be absent in *S. cerevisiae* with a part of them being fungal-specific and related to heterokaryon incompatibility (please see the next section). Moreover, the similarity between mediators of cell death (like BIR1, AMID, CulA, and HtrA) in humans and filamentous fungi is higher than the similarity of the same proteins between yeasts and filamentous species [25].

3. Advances on the Understanding of Cell Death in *N. crassa*

To our knowledge, the first report of cell death in *N. crassa* was published back in the 1950s when Strauss described that unstable attempts of auxotrophic strains to grow in the absence of the required nutrient result in cell death [26]. Later, it was observed that other stimuli lead to cell death in *N. crassa*, particularly a combined stress of moderate heat shock (45°C) and carbohydrate deprivation [27] or the incubation with the polymer chitosan [28] or the small antifungal peptide PAF26 [29]. Interestingly, the two latter stimuli disturb intracellular calcium (Ca^{2+}) homeostasis during the process of cell death induction.

Filamentous ascomycetes, namely, *N. crassa*, possess a defense system for non-self-recognition that leads to programmed cell death and functions as a barrier to viral transfer between fungal individuals and to prevent resource plundering [30, 31]. This process occurs upon hyphal fusion between individuals that are genetically dissimilar at *het* loci (11 *het* loci have been identified so far). A cell death program on the fusion compartment and surrounding cells is triggered, leading to the rejection of heterokaryon formation. This was therefore termed "heterokaryon incompatibility." At the molecular level, heterokaryon incompatibility seems to be controlled by the transcriptional regulator VIB-1 [32], which is downstream of a negative regulation by the IME-2 kinase

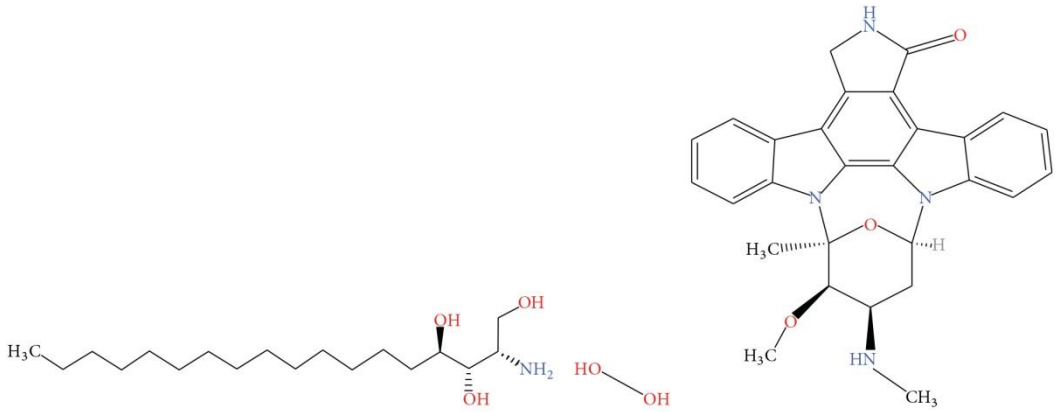

FIGURE 2: Chemical structures of cell death-inducing agents: phytosphingosine (a), hydrogen peroxide (b), and staurosporine (c). Chemical structures were obtained from http://www.chemspider.com/.

[33]. The production of reactive oxygen species (ROS) and the induction of genes involved in phosphatidylinositol and (Ca^{2+}) signaling pathways are also implicated in the phenomenon [34]. Heterokaryon incompatibility was also shown to be induced by the ectopic expression of the bacterial HET-C homologue from *Pseudomonas syringae*, phcA [35]. Cell death associated with heterokaryon incompatibility features several hallmarks of apoptosis such as DNA condensation and fragmentation, plasma membrane shrinkage, vesicle formation, and internalization of vital dyes [31, 34, 36].

Altogether, accumulating evidence shows that programmed cell death in *N. crassa* can be achieved chemically or genetically. During the last years, our group has focused on the study of the molecular basis of cell death using a chemical induction approach. The process has been mainly induced with either phytosphingosine, hydrogen peroxide, or staurosporine (Figure 2). Below we summarize the main findings from the work with these compounds.

3.1. Phytosphingosine (PHS) and Hydrogen Peroxide (H_2O_2). Phytosphingosine (PHS) is a natural long-chain sphingoid base [37]. The evidence that this sphingolipid has potent antifungal activity against *Aspergillus nidulans* with mitochondrial involvement [38] prompted us to investigate the effects of the drug in *N. crassa*. Treatment of conidia with PHS results in reduced viability, impairment of asexual spore germination, production of ROS, YO-PRO1 staining, and DNA condensation and fragmentation, suggesting the induction of an apoptosis-like cellular death [16, 17]. Analysis of gene expression during PHS-induced cell death by DNA microarrays revealed that most of the alterations at the transcriptional level correspond to upregulation of genes. However, there is a very strong enrichment of genes encoding mitochondrial proteins in the set of genes that are downregulated by the drug that likely explains its effects in the fungus [22]. This may be correlated with the fact that deletion of genes encoding subunits of the mitochondrial complex I, like NUO9.8, NUO14, NUO21, NUO21.3c, NUO30.4, NUO51, and NUO78 (but not the deletion of components of the other complexes of the respiratory chain) confers increased resistance to PHS. The same resistance profile is paralleled by the treatment of complex I mutants with H_2O_2, indicating shared intracellular mechanisms after the treatment with PHS and H_2O_2.

We observed that complex I mutant strains generate less ROS than wild type when exposed to PHS [16]. Transcriptional analyses of H_2O_2-treated wild type versus Δ*nuo14* cells showed that genes encoding mitochondrial proteins are the most enriched category among those with higher expression in the mutant in the presence of the insult [22]. Thus, absence of a functional complex I results in lowered production of ROS upon treatment with PHS and confers increased tolerance to some drug-induced transcriptional alterations and this may explain why these cells cope better with the growth insult elicited by PHS and H_2O_2. The involvement of the mitochondria during PHS-induced cell death is further stressed by the evidence that deletion mutants for subunit 4 of mitochondrial ATP synthase, for a mitochondrial aldehyde dehydrogenase, and for the homologue of the mammalian apoptosis-inducing factor (AIF) are more resistant to the drug than wild type. On the other hand, Δ*amid* cells, lacking a homologue of the mammalian apoptosis-inducing factor-homologous mitochondrion-associated inducer of death (AMID) are more sensitive to PHS than wild type [16]. Another group showed that deletion of the tRNA processing molecules TRANSLIN and TRAX confers increased resistance to PHS [39]. More recently, we observed that treatment with PHS, as well as staurosporine, causes the export of reduced glutathione (GSH) [17], although both drugs induce cell death through very distinct mechanisms (see below). Addition of exogenous GSH does not revert the effects of PHS, neither in *N. crassa* [17] nor in *A. nidulans* [38].

In *S. cerevisiae* there is evidence showing that response to distinct cellular stresses such as heat [40] and

nitrogen starvation [41] is correlated with the accumulation of phytosphingosine species. Additionally, yeast mutant cells defective in the addition of inositol phosphate to ceramide are particularly sensitive to treatment with PHS [42]. Exposure of *S. cerevisiae* to PHS also reduces the uptake of some amino acids by specific transporters, namely, tryptophan, leucine, histidine, and proline, leading to amino acid starvation [43].

3.2. Staurosporine (STS). Staurosporine (STS) is a bacterial alkaloid initially isolated from *Streptomyces staurosporeus* during a screening for protein kinase C inhibitors [44], which was later shown to display a broad kinase inhibitory activity [45]. The protein kinase C homologue Pkc1 of *S. cerevisiae* was validated as an essential target of STS [46]. This drug displays strong anticancer and antimicrobial activities and is widely used by the scientific community as a prototypical cell death-inducing agent. Importantly, some STS analogues displaying better selectivity profiles, such as UCN-01, CGP41251, or PKC412, are currently under evaluation in clinical trials for the treatment of different forms of cancer [47]. In *N. crassa*, STS induces loss of cell viability, marked impairment of conidial germination, chromatin fragmentation, YO-PRO1 staining, uptake of vital dyes, and early ROS production [15, 17, 18]. In contrast to the observations with PHS, deletion of some subunits of mitochondrial complex I such as NUO9.8, NUO14, NUO30.4, and NUO51 (but not others like NUO78) results in hypersensitivity to STS. Interestingly, complex I assembly status of these mutant strains cannot explain the increased susceptibility to STS because cells with similar assembly phenotypes display different sensitivity to the drug. Thus, it seems that some of the proteins play a specific role during intracellular cell death signaling or execution. This in line with observation that mammalian complex I subunits execute particular programmed cell death programs: GRIM-19 (NUO14 homologue) regulates cell death by binding a cytomegalovirus RNA [48] and is also involved in β-interferon- and retinoic acid-induced cancer cell death [49]; cleavage of NDUFS1 (NUO78 homologue) [50] by a caspase and cleavage of NDUFS3 (NUO30.4 homologue) by granzyme A [51] mediate cell death; downregulation of NDUFA6 (NUO14.8 homologue) induces apoptosis in HIV-1-infected cells [52]. STS and PHS definitively act by different mechanisms, but mitochondria and respiration are central for the cell death process induced by both drugs.

Because of the involvement of mitochondrial complex I during the fungal response to STS, we decided to combine STS with the classical complex I inhibitor rotenone. It was observed that the combination of the drugs displays synergistic activity against the growth of *N. crassa* and the clinically relevant fungi *Aspergillus fumigatus* and *Candida albicans* [15]. Surprisingly, this synergistic behavior is also observed in complex I mutant strains (in which the enzyme is already nonfunctional), suggesting a complex I-independent for the action of rotenone. Indeed, other complex I inhibitors (piericidin A and diphenyleneiodonium) do not act like rotenone in combination with staurosporine and the combination STS plus rotenone is synergistic even against *S. cerevisiae* cells which are devoid of complex I. This led us to study the mechanisms of rotenone activity. Using thyroid cancer cells as the model system, we observed that the drug acts as an antimitotic agent, causing cell death following cell cycle arrest and mitotic catastrophe with p53 being a pivotal player in the process [19]. Importantly, the combination of STS with rotenone is also synergistic in thyroid cancer cells [19, 20], validating *N. crassa* as a good model to study broad mechanisms of programmed cell death.

The exogenous addition of GSH or its precursor N-acetyl-cysteine (NAC) effectively blocks STS-induced cell death, pointing to the importance of ROS generation during the fungal response to STS [15]. We observed recently, for the first time in fungi, that the export of GSH is a crucial event during the cell death program driven by STS [17]. It seems that GSH efflux following treatment with STS (or PHS, with even faster kinetics) is an early and specific event of cell death rather than a secondary effect such as a detoxification mechanism. Thus, *N. crassa* exports GSH when exposed to STS causing a change in the intracellular environment to a more oxidative redox state. The consequent decrease of the internal GSH/GSSG ratio modulates intracellular redox signaling and may facilitate the oxidation of proteins or lipids. Antioxidants like β-carotene and ascorbic acid are ineffective in the modulation of the effects of STS and a combined treatment with STS and rotenone results in increased depletion of GSH [15].

Analysis of transcriptional alterations associated with treatment with STS by DNA microarrays revealed that the drug strongly induces high levels of expression of a gene encoding a member of the ABC (ATP-binding cassette)-transporter family, *abc3* [18]. This result was confirmed at the gene level by qRT-PCR and at the protein level by western blotting with a house-made specific antibody. This antibody allowed the localization of ABC3 at the cell surface. Interestingly, the deletion of *abc3* results in extreme sensitivity to STS. Because of the significant homology between ABC3 and the human P-glycoprotein, shown to mediate multidrug resistance in cancer cells [53], we measured the levels of intracellular and extracellular STS after treatment of *N. crassa* cells. To achieve this, a method that took advantage of the fact that STS fluoresces when excited with UV light was devised. We showed that ABC3 performs drug efflux to the extracellular space, describing for the first time a transporter of the broadly used STS [18]. In agreement with this, a combined treatment of STS and the P-glycoprotein inhibitors verapamil and sodium orthovanadate results in synergistic inhibition of growth in *N. crassa* as well as in the pathogenic *A. fumigatus* and *C. albicans*, likely due to blockage of STS efflux. Sodium orthovanadate is not selective and, in cancer cells, the drug causes dose-dependent and caspase-mediated cell death by interfering with the PI3K/Akt/mTOR signaling cascade [21].

Gene expression data obtained with microarrays was also used to identify other putative mediators of STS-induced cell death. We showed that two STS highly induced genes, NCU09141 and NCU02887, present homology with β-subunits of voltage-gated potassium channels. In line with a role for this proteins during the action of STS, an inhibitor of these potassium channels, 4-aminopyridine, enhances cell death elicited by STS in *N. crassa*, *A. fumigatus,* and *C.*

albicans [18]. In addition, microarray data also unraveled a novel transcription factor with a role on STS-induced cell death that we are currently characterizing.

The literature on the effects of STS in fungi other than *N. crassa* is scarce. In *S. cerevisiae*, a group of genes termed *stt* (for "staurosporine- and temperature-sensitive") were isolated. This set of genes whose respective deletion strains are particularly susceptible to STS includes protein kinases such as Pkc1, Pi4k, and Bck1, mediators of Golgi to vacuole protein sorting (Vps18, Vps34, Vps11, Vps45, and Vps33), a protein involved in glycophosphatidylinositol anchor synthesis (Gpi1), the acetoacetyl-CoA thiolase involved in ergosterol biosynthesis Erg10, vacuolar H^+-ATPase mutants (Vma1, Vma2, Vma3, Vma4, Vma11, Vma12, and Vma13), and a subunit of oligosaccharyltransferase [46, 54–56].

4. Concluding Remarks

The understanding of the molecular mechanisms of programmed cell death has benefited from the intensive research carried out in the last years, but it is still open to new approaches and discoveries. Ongoing projects in our group include, for example, the determination of the role of Ca^{2+} during STS-induced cell death. We observed that incubation with this drug (but not PHS) promotes a well-defined profile of alterations in cytosolic Ca^{2+} levels, similarly to what is observed when fungal cells are exposed to other cell death stimuli [57]. On the other hand, we are taking advantage of the recent developments on the transcriptomics field and employing high-throughput RNA sequencing (RNA-seq) to study the transcriptional profile of *N. crassa* cells submitted to different cell death conditions and identify novel cell death intervenients.

It is inevitable to stress that there are several important differences between filamentous fungi and yeast programmed cell death. Due to their multicellular nature, filamentous species require cell death to accomplish different developmental and defense processes, such as the aforementioned heterokaryon incompatibility. Another discrepant aspect resides in the characteristics of the electron respiratory chain in both types of fungi. Whereas complex I is undoubtedly involved in programmed cell death in *N. crassa* [15, 16, 22], it is absent in *S. cerevisiae*. However, in the latter, under certain nutritional conditions, the overexpression of the alternative NADH dehydrogenase NDI1, the first component of the yeast electron transport chain, results in programmed cell death [58]. Our group is also interested in unraveling links between cell death, oxidative stress, mitochondrial bioenergetics, and specific enzymes, such as NAD(P)H dehydrogenases [13, 14].

In summary, evidence points to the usefulness of using *N. crassa* as a model for the study of the mechanisms of programmed cell death although the available data is still limited. We anticipate that this fungus will be an invaluable tool for future investigations on the cell death field.

Conflict of Interests

The authors declare that there is no conflict of interests regarding the publication of this paper.

Acknowledgments

A. Pedro Gonçalves was recipient of a fellowship from Fundação Calouste Gulbenkian (104210). This work was supported by FCT Portugal (PEst-C/SAU/LA0002/2013 and FCOMP-01-0124-FEDER-037277 to Arnaldo Videira), the European POCI program of QCAIII co-participated by FEDER (NORTE-07-0124-FEDER-000003), and a Grant from the University of Porto (PP_IJUP2011-20).

References

[1] H. J. Vogel, "A convenient growth medium for *Neurospora* (medium N)," *Microbial Genetics Bulletin*, vol. 13, pp. 42–43, 1956.

[2] D. J. Jacobson, J. R. Dettman, R. I. Adams et al., "New findings of *Neurospora* in Europe and comparisons of diversity in temperate climates on continental scales," *Mycologia*, vol. 98, no. 4, pp. 550–559, 2006.

[3] A. Payen, "Extrain d'un rapport addressé à M. Le Maréchal Duc de Dalmatie, Ministre de la Guerre, Président du Conseil, sur une altération extraordinaire du pain de munition," *Annales de Chimie et de Physique*, vol. 9, pp. 5–21, 1843.

[4] C. L. Shear and B. O. Dodge, "Life histories and heterothallism of the red bread-mold fungi of the *Monilia sitophila* group," *Journal of Agricultural Research*, vol. 34, pp. 1019–1042, 1927.

[5] G. W. Beadle and E. L. Tatum, "Genetic control of biochemical reactions in *Neurospora*," *Proceedings of the National Academy of Sciences of the United States of America*, vol. 27, no. 11, pp. 499–506, 1941.

[6] A. M. Srb and N. H. Horowitz, "The ornithine cycle in *Neurospora* and its genetic control," *The Journal of Biological Chemistry*, vol. 154, no. 1, pp. 129–139, 1944.

[7] R. H. Davis and D. D. Perkins, "*Neurospora*: a model of model microbes," *Nature Reviews Genetics*, vol. 3, no. 5, pp. 397–403, 2002.

[8] J. E. Galagan, S. E. Calvo, K. A. Borkovich et al., "The genome sequence of the filamentous fungus *Neurospora crassa*," *Nature*, vol. 422, no. 6934, pp. 859–868, 2003.

[9] K. McCluskey, A. Wiest, and M. Plamann, "The Fungal Genetics Stock Center: a repository for 50 years of fungal genetics research," *Journal of Biosciences*, vol. 35, no. 1, pp. 119–126, 2010.

[10] A. Videira, "Complex I from the fungus *Neurospora crassa*," *Biochimica et Biophysica Acta*, vol. 1364, no. 2, pp. 89–100, 1998.

[11] A. Videira and M. Duarte, "On complex I and other NADH: ubiquinone reductases of *Neurospora crassa* mitochondria," *Journal of Bioenergetics and Biomembranes*, vol. 33, no. 3, pp. 197–203, 2001.

[12] A. Videira and M. Duarte, "From NADH to ubiquinone in *Neurospora* mitochondria," *Biochimica et Biophysica Acta*, vol. 1555, no. 1–3, pp. 187–191, 2002.

[13] P. Carneiro, M. Duarte, and A. Videira, "Characterization of apoptosis-related oxidoreductases from *Neurospora crassa*," *PLoS ONE*, vol. 7, no. 3, Article ID e34270, 2012.

[14] P. Carneiro, M. Duarte, and A. Videira, "Disruption of alternative NAD(P)H dehydrogenases leads to decreased mitochondrial ROS in *Neurospora crassa*," *Free Radical Biology and Medicine*, vol. 52, no. 2, pp. 402–409, 2012.

[15] A. Castro, C. Lemos, A. Falcão, A. S. Fernandes, N. Louise Glass, and A. Videira, "Rotenone enhances the antifungal properties of staurosporine," *Eukaryotic Cell*, vol. 9, no. 6, pp. 906–914, 2010.

[16] A. Castro, C. Lemos, A. Falcão, N. L. Glass, and A. Videira, "Increased resistance of complex I mutants to phytosphingosine-induced programmed cell death," *The Journal of Biological Chemistry*, vol. 283, no. 28, pp. 19314–19321, 2008.

[17] A. S. Fernandes, A. Castro, and A. Videira, "Reduced glutathione export during programmed cell death of *Neurospora crassa*," *Apoptosis*, vol. 18, no. 8, pp. 940–948, 2013.

[18] A. S. Fernandes, A. P. Gonçalves, A. Castro et al., "Modulation of fungal sensitivity to staurosporine by targeting proteins identified by transcriptional profiling," *Fungal Genetics and Biology*, vol. 48, no. 12, pp. 1130–1138, 2011.

[19] A. P. Gonçalves, V. Máximo, J. Lima, K. K. Singh, P. Soares, and A. Videira, "Involvement of p53 in cell death following cell cycle arrest and mitotic catastrophe induced by rotenone," *Biochimica et Biophysica Acta*, vol. 1813, no. 3, pp. 492–499, 2011.

[20] A. P. Gonçalves, A. Videira, V. Máximo, and P. Soares, "Synergistic growth inhibition of cancer cells harboring the *RET/PTC1* oncogene by staurosporine and rotenone involves enhanced cell death," *Journal of Biosciences*, vol. 36, no. 4, pp. 639–648, 2011.

[21] A. P. Gonçalves, A. Videira, P. Soares, and V. Máximo, "Orthovanadate-induced cell death in *RET/PTC1*-harboring cancer cells involves the activation of caspases and altered signaling through PI3K/Akt/mTOR," *Life Sciences*, vol. 89, no. 11-12, pp. 371–377, 2011.

[22] A. Videira, T. Kasuga, C. Tian, C. Lemos, A. Castro, and N. L. Glass, "Transcriptional analysis of the response of *Neurospora crassa* to phytosphingosine reveals links to mitochondrial function," *Microbiology*, vol. 155, no. 9, pp. 3134–3141, 2009.

[23] Y. Fuchs and H. Steller, "Programmed cell death in animal development and disease," *Cell*, vol. 147, no. 4, pp. 742–758, 2011.

[24] L. Galluzzi, I. Vitale, J. M. Abrams et al., "Molecular definitions of cell death subroutines: recommendations of the Nomenclature Committee on Cell Death 2012," *Cell Death and Differentiation*, vol. 19, no. 1, pp. 107–120, 2012.

[25] N. D. Fedorova, J. H. Badger, G. D. Robson, J. R. Wortman, and W. C. Nierman, "Comparative analysis of programmed cell death pathways in filamentous fungi," *BMC Genomics*, vol. 6, article 177, 2005.

[26] B. S. Strauss, "Cell death and 'unbalanced growth' in *Neurospora*," *Microbiology*, vol. 18, no. 3, pp. 658–669, 1958.

[27] N. S. Plesofsky, S. B. Levery, S. A. Castle, and R. Brambl, "Stress-induced cell death is mediated by ceramide synthesis in *Neurospora crassa*," *Eukaryotic Cell*, vol. 7, no. 12, pp. 2147–2159, 2008.

[28] J. Palma-Guerrero, I.-C. Huang, H.-B. Jansson, J. Salinas, L. V. Lopez-Llorca, and N. D. Read, "Chitosan permeabilizes the plasma membrane and kills cells of *Neurospora crassa* in an energy dependent manner," *Fungal Genetics and Biology*, vol. 46, no. 8, pp. 585–594, 2009.

[29] A. Munoz, J. F. Marcos, and N. D. Read, "Concentration-dependent mechanisms of cell penetration and killing by the *de novo* designed antifungal hexapeptide PAF26," *Molecular Microbiology*, vol. 85, no. 1, pp. 89–106, 2012.

[30] N. L. Glass and I. Kaneko, "Fatal attraction: nonself recognition and heterokaryon incompatibility in filamentous fungi," *Eukaryotic Cell*, vol. 2, no. 1, pp. 1–8, 2003.

[31] N. L. Glass and K. Dementhon, "Non-self recognition and programmed cell death in filamentous fungi," *Current Opinion in Microbiology*, vol. 9, no. 6, pp. 553–558, 2006.

[32] K. Dementhon, G. Iyer, and N. L. Glass, "VIB-1 is required for expression of genes necessary for programmed cell death in *Neurospora crassa*," *Eukaryotic Cell*, vol. 5, no. 12, pp. 2161–2173, 2006.

[33] E. A. Hutchison, J. A. Bueche, and N. L. Glass, "Diversification of a protein kinase cascade: IME-2 is involved in nonself recognition and programmed cell death in *Neurospora crassa*," *Genetics*, vol. 192, no. 2, pp. 467–482, 2012.

[34] E. Hutchison, S. Brown, C. Tian, and N. L. Glass, "Transcriptional profiling and functional analysis of heterokaryon incompatibility in *Neurospora crassa* reveals that reactive oxygen species, but not metacaspases, are associated with programmed cell death," *Microbiology*, vol. 155, no. 12, pp. 3957–3970, 2009.

[35] G. Wichmann, J. Sun, K. Dementhon, N. L. Glass, and S. E. Lindow, "A novel gene, *phcA* from *Pseudomonas syringae* induces programmed cell death in the filamentous fungus *Neurospora* crassa," *Molecular Microbiology*, vol. 68, no. 3, pp. 672–689, 2008.

[36] S. M. Marek, J. Wu, N. L. Glass, D. G. Gilchrist, and R. M. Bostock, "Nuclear DNA degradation during heterokaryon incompatibility in *Neurospora crassa*," *Fungal Genetics and Biology*, vol. 40, no. 2, pp. 126–137, 2003.

[37] A. Morales, H. Lee, F. M. Goñi, R. Kolesnick, and J. C. Fernandez-Checa, "Sphingolipids and cell death," *Apoptosis*, vol. 12, no. 5, pp. 923–939, 2007.

[38] J. Cheng, T.-S. Park, L.-C. Chio, A. S. Fischl, and X. S. Ye, "Induction of apoptosis by sphingoid long-chain bases in *Aspergillus nidulans*," *Molecular and Cellular Biology*, vol. 23, no. 1, pp. 163–177, 2003.

[39] L. Li, W. Gu, C. Liang, Q. Liu, C. C. Mello, and Y. Liu, "The translin-TRAX complex (C3PO) is a ribonuclease in tRNA processing," *Nature Structural & Molecular Biology*, vol. 19, no. 8, pp. 824–830, 2012.

[40] G. M. Jenkins, A. Richards, T. Wahl, C. Mao, L. Obeid, and Y. Hannun, "Involvement of yeast sphingolipids in the heat stress response of *Saccharomyces cerevisiae*," *The Journal of Biological Chemistry*, vol. 272, no. 51, pp. 32566–32572, 1997.

[41] M. Yamagata, K. Obara, and A. Kihara, "Unperverted synthesis of complex sphingolipids is essential for cell survival under nitrogen starvation," *Genes to Cells*, vol. 18, no. 8, pp. 650–659, 2013.

[42] M. M. Nagiec, E. E. Nagiec, J. A. Baltisberger, G. B. Wells, R. L. Lester, and R. C. Dickson, "Sphingolipid synthesis as a target for antifungal drugs: complementation of the inositol phosphorylceramide synthase defect in a mutant strain of *Saccharomyces cerevisiae* by the *AUR1* gene," *The Journal of Biological Chemistry*, vol. 272, no. 15, pp. 9809–9817, 1997.

[43] M. S. Skrzypek, M. M. Nagiec, R. L. Lester, and R. C. Dickson, "Inhibition of amino acid transport by sphingoid long chain bases in *Saccharomyces cerevisiae*," *The Journal of Biological Chemistry*, vol. 273, no. 5, pp. 2829–2834, 1998.

[44] S. Omura, Y. Iwai, A. Hirano et al., "A new alkaloid AM-2282 of *Streptomyces* origin taxonomy, fermentation, isolation and preliminary characterization," *The Journal of Antibiotics*, vol. 30, no. 4, pp. 275–282, 1977.

[45] M. W. Karaman, S. Herrgard, D. K. Treiber et al., "A quantitative analysis of kinase inhibitor selectivity," *Nature Biotechnology*, vol. 26, no. 1, pp. 127–132, 2008.

[46] S. Yoshida, E. Ikeda, I. Uno, and H. Mitsuzawa, "Characterization of a staurosporine- and temperature-sensitive mutant, *STT1*, of Saccharomyces cerevisiae: *STT1* is allelic to *PKC1*," *Molecular and General Genetics*, vol. 231, no. 3, pp. 337–344, 1992.

[47] O. A. Gani and R. A. Engh, "Protein kinase inhibition of clinically important staurosporine analogues," *Natural Product Reports*, vol. 27, no. 4, pp. 489–498, 2010.

[48] M. B. Reeves, A. A. Davies, B. P. McSharry, G. W. Wilkinson, and J. H. Sinclair, "Complex I binding by a virally encoded RNA regulates mitochondria-induced cell death," *Science*, vol. 316, no. 5829, pp. 1345–1348, 2007.

[49] G. Huang, Y. Chen, H. Lu, and X. Cao, "Coupling mitochondrial respiratory chain to cell death: an essential role of mitochondrial complex I in the interferon-β and retinoic acid-induced cancer cell death," *Cell Death and Differentiation*, vol. 14, no. 2, pp. 327–337, 2007.

[50] J.-E. Ricci, C. Muñoz-Pinedo, P. Fitzgerald et al., "Disruption of mitochondrial function during apoptosis is mediated by caspase cleavage of the p75 subunit of complex I of the electron transport chain," *Cell*, vol. 117, no. 6, pp. 773–786, 2004.

[51] D. Martinvalet, D. M. Dykxhoorn, R. Ferrini, and J. Lieberman, "Granzyme A cleaves a mitochondrial complex I protein to initiate caspase-independent cell death," *Cell*, vol. 133, no. 4, pp. 681–692, 2008.

[52] J. S. Ladha, M. K. Tripathy, and D. Mitra, "Mitochondrial complex I activity is impaired during HIV-1-induced T-cell apoptosis," *Cell Death and Differentiation*, vol. 12, no. 11, pp. 1417–1428, 2005.

[53] A. Breier, M. Barančík, Z. Sulová, and B. Uhrík, "P-glycoprotein—implications of metabolism of neoplastic cells and cancer therapy," *Current Cancer Drug Targets*, vol. 5, no. 6, pp. 457–468, 2005.

[54] S. Yoshida and Y. Anraku, "Characterization of staurosporine-sensitive mutants of *Saccharomyces cerevisiae*: vacuolar functions affect staurosporine sensitivity," *Molecular and General Genetics*, vol. 263, no. 5, pp. 877–888, 2000.

[55] S. Yoshida, Y. Ohya, A. Nakano, and Y. Anraku, "Genetic interactions among genes involved in the *STT4-PKC1* pathway of *Saccharomyces cerevisiae*," *Molecular and General Genetics*, vol. 242, no. 6, pp. 631–640, 1994.

[56] S. Yoshida, Y. Ohya, M. Goebl, A. Nakano, and Y. Anraku, "A novel gene, *STT4*, encodes a phosphatidylinositol 4-kinase in the *PKC1* protein kinase pathway of *Saccharomyces cerevisiae*," *The Journal of Biological Chemistry*, vol. 269, no. 2, pp. 1166–1172, 1994.

[57] Y. Zhang, S. Muend, and R. Rao, "Dysregulation of ion homeostasis by antifungal agents," *Frontiers in Microbiology*, vol. 3, article 133, 2012.

[58] W. Li, L. Sun, Q. Liang, J. Wang, W. Mo, and B. Zhou, "Yeast AMID homologue Ndi1p displays respiration-restricted apoptotic activity and is involved in chronological aging," *Molecular Biology of the Cell*, vol. 17, no. 4, pp. 1802–1811, 2006.